Justus Liebig University Giessen

Faculty 09 – Agricultural Sciences, Nutritional Sciences, and Environmental Management

Institute of Nutritional Science

Secondary metabolites of *Hericium erinaceus* against neurodegenerative diseases

Submitted by:

Bernhard Hellmann

09/2023

For the degree of *Doctor rerum naturalium (Dr. rer. nat.)*

Thesis reviewers

First reviewer: Prof. Dr. Gunter Eckert

Head of Department Nutrition in Prevention & Therapy, Institute of Nutritional Science,

Justus Liebig University Giessen

Second reviewer: Prof. Dr. Holger Zorn

Managing director of department of food chemistry and food biotechnology,

Justus Liebig University Giessen

“Que sais-je?

– Michel de Montaigne

Summary

Alzheimer's disease (AD) is increasing in prevalence, and the WHO estimates that more than 150 million people will be affected by 2050. The most significant factors influencing AD appear to be a combination of age-related changes in the brain, genetic predispositions, environmental influences, and lifestyle factors. On the molecular level, late-stage AD is characterized by mitochondrial dysfunction, increased reactive oxygen species (ROS) levels, amyloid-β (Aβ) protein aggregates, increased tau levels, and neurodegeneration. Currently, there are no existing treatments that can cure the disease; therefore, prevention and mitigation of symptoms are crucial.

Several compounds isolated from plants and mushrooms have shown beneficial effects in treating Alzheimer's disease (AD) by targeting different pathological mechanisms. Among these, erinacines, identified in the edible mushroom *Hericium erinaceus*, are particularly promising compounds that modulate disease progression. Extracts from this mushroom, rich in erinacines, have demonstrated potential to enhance mitochondrial function and promote neuronal health, suggesting a preventive approach against AD. Notably, studies have shown that erinacines stimulate Neuronal Growth Factor (NGF) production and neuritogenesis, indicating their key role in preventing the progression of AD. In particular, erinacine C has the strongest effects on NGF stimulation; however, it is scarce because it is produced only in the mycelium of the mushroom.

In the present work, erinacine C was produced through submerged cultivation of *Hericium erinaceus*, followed by isolation and characterization using HPLC-DAD, NMR, and HR-MS. Erinacine C was tested in SH-SY5Y, MOCK, and APP_{696} cells. Furthermore, an ethanolic mycelium extract of *Hericium erinaceus* was tested in the SH-SY5Y cell lines as well as in *Caenorhabditis elegans* CL2122 and GMC101 strains.

To test the hypothesis on the mitochondrial effects of erinacine C, experiments on cell viability, mitochondrial membrane potential, ATP levels, mitochondrial mRNA expression (SIRT1, CREB1, NRF1, TFAM, and ATP5D), respirometry, neurotoxicity, neuritogenesis, and Aβ levels were conducted. Results showed that erinacine C had positive effects in SH-SY5Y cells, including increased ATP levels, decreased oxidative stress, and elevated

expression of NRF1. Additionally, treatment activated genes related to axon guidance and actin binding, linking the genomic results with the in vitro data of positive neuronal outgrowth. Through RNA-seq analysis, the research scope expanded beyond just the mitochondria.

On the other hand, the *Hericium erinaceus* ethanolic extract showed increasing effects at low concentrations on the lifespan in GMC101 but not in CL2122. However, ATP levels in GMC101 were elevated after treatment. The extract was tested in SH-SY5Y cells to evaluate viability, ATP levels, and the expression of mitochondrial genes. Due to the unknown matrix components, no clear conclusion related to erinacine C could be drawn. Nevertheless, these findings underscore the potential of *Hericium erinaceus* to be used as part of a preventive strategy against AD, leveraging its mitochondrial and neuroprotective properties.

Altogether, the results presented here pave the way for more comprehensive studies to elucidate further the mechanisms through which *Hericium erinaceus* and its compounds, like erinacine C, confer neuroprotective benefits. The RNA-seq results suggest that erinacine C exhibits hormone-like effects on human neuronal cells. Future research should aim to better understand the mechanisms of action of these compounds and their potential in clinical settings.

Contents

List of abbreviations

AD	Alzheimer´s disease
ADP	adenosine diphosphate
AMPK	adenosine monophosphate-activated protein kinase
APP	amyloid precursor protein
ATP	adenosine triphosphate
A*β*	amyloid-*β*
BDNF	brain derived neurotrophic factor
CREB	cAMP response element binding protein
CS	citrate synthase
ctl	control
Da	Dalton
DMEM	Dulbecco´s Modified Eagle Medium
DMSO	dimethyl sulfoxide
DNA	desoxyribonucleic acid
EC	erinacine C
EtOH	ethanol
ETS	electron transport system
HBSS	Hank´s Balanced Salt Solution
HEM	*Hericum erinacues* mycelium
HEPES	4-(2-hydroxyethyl)-1-piperazineethanesulfonic acid
MMP	mitochondrial membrane potential
mtDNA	mitochondrial DNA
MTR	MitoTracker™ Red
NFT	neurofibrillary tangles
NGF	Nerve growth factor
NRF1	Nuclear respiratory factor 1
OXPHOS	oxidative phosphorylation
PBS	phosphate buffered saline

PCR	polymerase chain reaction
PGC-1*α*	peroxisome proliferator-activated receptor gamma coactivator 1- *α*
ROS	reactive oxygen species
mtRNA	Mitochondrial ribonucleic acid
SIRT	Sirtuin
SOD	superoxide dismutase
TFAM	mitochondrial transcription factor A
TIMM	translocase of the inner mitochondrial membrane
TOMM	translocase of the outer mitochondrial membrane
Tris	tris(hydroxymethyl)aminomethane
VDAC	voltage dependent anion channel

List of figures

List of tables

1 Introduction

1.1 Alzheimer's a disease with an epidemic proportion

Alzheimer's disease is increasing in prevalence, and currently, there is no cure available. The WHO estimates that in 2050, more than 150 million people will suffer from Alzheimer's disease (Martin Prince et al., 2015). In addition to developed countries, Alzheimer's disease is also on the rise in developing countries, such as China. Figure 1-1 shows the conservative estimations from the World Alzheimer's report. Even with conservative estimations, we can expect a sharp worldwide rise in Alzheimer's occurrence in the next thirty years. Current treatments reduce the symptoms but cannot cure the disease. The biggest contributors to this disease seem to be a combination of age-related changes in the brain, along with genetic, environmental, and lifestyle factors (Martin Prince et al., 2015). Figure 1-2 shows the median age of the worldwide populations in 2050. It is evident that the European population is aging. Therefore, it is important to find a cure for Alzheimer's disease.

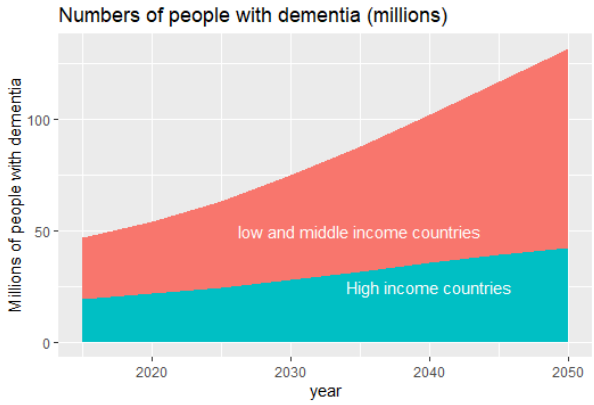

Figure 1-1 Conservative estimation of numbers of people with dementia (in millions) till 2050, own figure data provided by world Alzheimer report 2015.

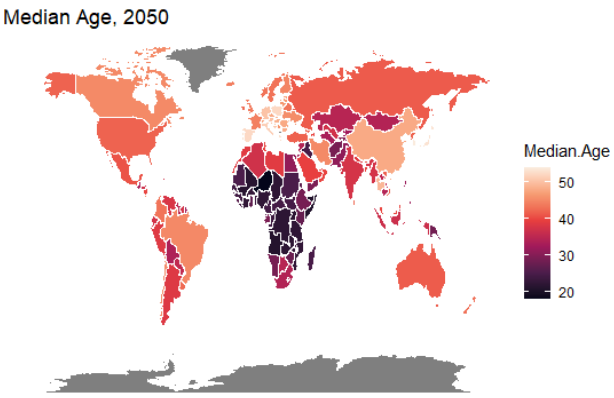

Figure 1-2 Estimated median age of worldwide populations in 2050, grey indicates no data, own figure data provided by https://ourworldindata.org/age-structure.

1.1.1 A biological definition of Alzheimer's disease

In 2018, the *National Institute on Aging* (NIA) and the Alzheimer's Association defined a research framework for Alzheimer's (Jack et al., 2018). The framework shifted from the symptom-based diagnosis and definition to a biological one. The authors stated that Alzheimer's disease (AD) is defined by its core pathologic processes that can be verified by post mortem examination or *in vivo* by biomarkers. The biomarkers are grouped into three categories: *β*-amyloid deposition (A), pathologic tau (T), neurodegeneration (N), and the combination of all three markers [AT(N)]. Although this framework is widely accepted, the underlying cause still lies in the realm of the unknown. Currently, there are four major hypotheses trying to explain the cause: the cholinergic, amyloid *β*, tau and inflammation hypotheses.

The cholinergic hypothesis was defined by Davies and Maloney (1976). They describe Alzheimer's disease as a deficiency in the production of the neurotransmitter acetylcholine due to the activity of the enzyme acetylcholinesterase (Francis et al., 1999). In Alzheimer's disease, acetylcholinesterase reduces cortical cholinergic innervation, which leads to alterations in the shift of tau to the hyperphosphorylated state – a precursor of neurofibrillary tangles – and an increased production of the amyloid *β* protein. Additionally, there is a negative alteration in corticocortical glutamatergic neurotransmission due to neuron or synapse loss, which can decrease glutamate production. These indirect processes can eventually lead to cognitive impairment (Francis et al., 1999).

While the cholinergic hypothesis describes a deficiency in neurotransmitters, the amyloid-*β* hypothesis refers to the cytotoxicity of mature aggregated amyloid fibrils and plaques. Glenner and Wong (1984) pioneered the amyloid-*β* theory in 1984, which was further supported by Goate et al. (1991), who discovered a mutation in the amyloid precursor protein gene (APP). Additional findings led to the identification of the *γ*-secretase proteins presenilin 1 (PSEN1) and presenilin 2 (PSEN2) (Scheuner et al., 1996). Mutations in APP support the production of longer variants of amyloid-*β*. This seeds the aggregation of amyloid-*β* into oligomers, insoluble fibrils, and eventually plaques. These plaques are characteristic of Alzheimer's disease and are believed to be the toxic form of the protein responsible for disrupting the cell's calcium ion homeostasis, depolarization of the synaptic membrane, and mitochondrial damage, thus inducing apoptosis and neurotoxicity (W. Chen et al., 2014; Polanco et al., 2018; Rhein et al., 2009). Although the A*β* theory is the most prominent, there are hints for other causes that lead to tau pathology. This is because a decade prior to the formation of A*β plaques,* tau pathology occurs (Arnsten et al., 2021). In contrast to A*β*, tau accumulates intracellularly, builds up neurofibrillary tangles (NFTs), and destroys neurons. In pathological conditions, tau may undergo post-translational modifications, e.g., hyperphosphorylation, that could lead to the detachment of tau

from microtubules, resulting in microtubule disintegration (Paspalas et al., 2018). This can trigger a vicious cycle of synaptic dysfunction to synaptic loss, eventually leading to a decline in neuronal function (Thies & Mandelkow, 2007). In the postsynaptic compartment, pathological tau strengthens the NMDA receptor. This supports the excitation of the neurotransmitter glutamate and thereby enhances Aβ toxicity (Ittner et al., 2010).

While Alzheimer's disease is defined as the occurrence of amyloid β deposition, pathologic tau, and neurodegeneration with intra- and extracellular disruptions, it seems that non-pathologies emerge alone. A fourth theory can provide a link to combine them. Despite extensive research, no treatment that effectively alters either pathology is available. Furthermore, even years before any observable AD symptoms or diagnosis are determinable, Aβ plaques and NFT tangles are detectable. This leads to a gap in understanding AD pathogenesis. Therefore, researchers assume a further factor as a driver for the disease: an increased inflammatory response (Akama & Van Eldik, 2000; Akiyama et al., 2000; Combs et al., 2000). The response is also called neuroinflammation and is attributed to activated microglial cells and the release of numerous cytokines, such as interleukin 1 (IL-1), IL-1β, and IL-6 (Das Sarma, 2014; Goldgaber et al., 1989; Quintanilla et al., 2004). Brain inflammation appears to be two-sided. In a healthy brain, it is neuroprotective but harmful when transitioning into a chronic state (Y. S. Kim & Joh, 2006). Increased levels of interleukin 1 (IL-1) are responsible for the increased APP production and Aβ burden. Additionally, a negative response cycle stimulates the activation of Cyclin-Dependent Kinases (CDK), which are known to hyperphosphorylate tau (Quintanilla et al., 2004). Microglia are involved in the phagocytosis of Aβ, but prolonged clearance further activates proinflammatory cytokines (Hickman et al., 2008). This leads to a forward loop in contribution to neurodegeneration and the combination of the core Alzheimer's pathologies.

1.1.2 Pathology of Alzheimer's disease

One can organize the decline within Alzheimer's on three levels: visible macroscopic features, microscopic features, and cellular features (Figure 1-3). However, the occurrence is mostly upside down – from cellular levels to macroscopic features.

To date, pathologic diagnosis remains the gold standard for AD diagnosis. Although certain features are typical for AD-affected brains, none of them are disease-specific. Macroscopic features that often appear in AD patients are brain atrophy, with the gyri as the most affected

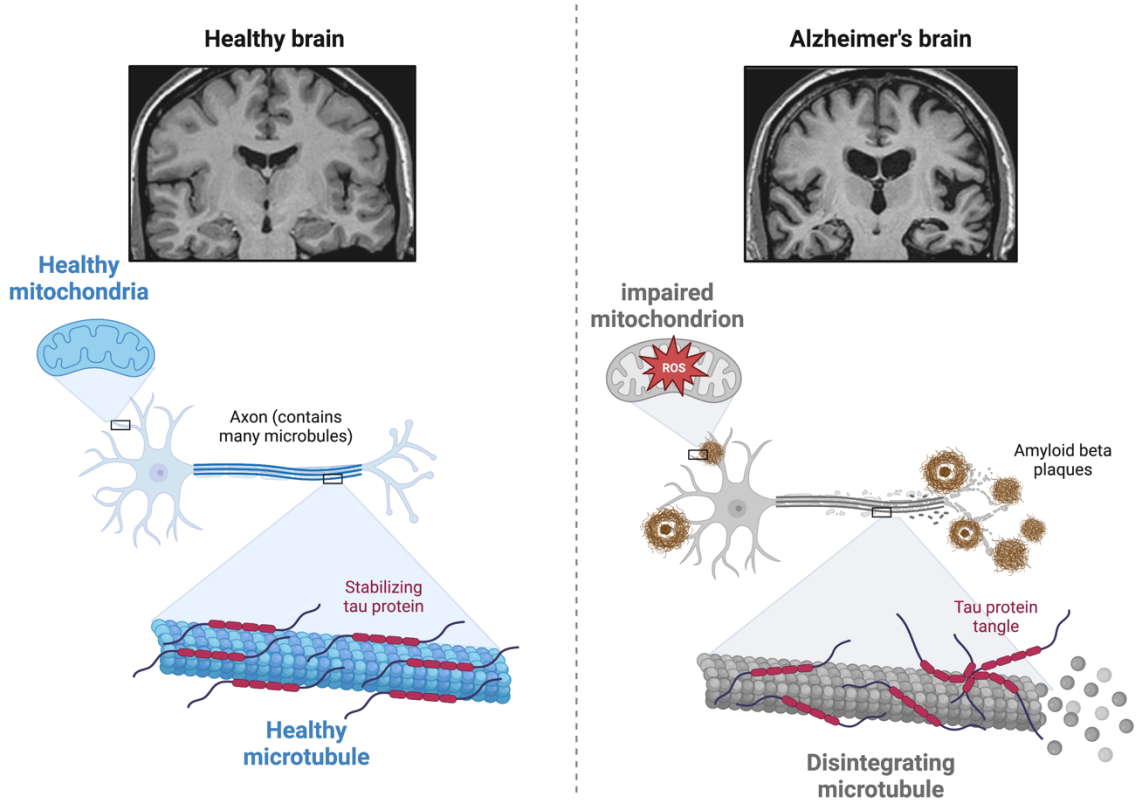

Figure 1-3 Differences between a healthy (left) and an Alzheimer's brain (right).
In an Alzheimer's brain are alterations on the macroscopic level (brain atrophy), the microscopic level (A beta alterations), as well as the cellular level (mitochondrial and tau alterations) visible. Created with BioRender.com

areas (Perl, 2010; Rami et al., 2012). Along comes an enlargement of the frontal and temporal horns of the lateral ventricles and a decreased brain weight (Piguet et al., 2009).

As observed by Alois Alzheimer over 100 years ago, the manifestation of extracellular amyloid plaques and intracellular neurofibrillary tangles is required for diagnosis (Ryan et al., 2015). These are microscopically smooth transitions to cellular features. Amyloid-β is a small peptide generated by proteolytic processing of amyloid precursor protein (APP). APP is a type-I transmembrane protein, and its encoding gene is located on chromosome 21 in humans. There are three major isoforms of APP (APP_{695}, APP_{751}, APP_{770}), and APP_{695} is predominantly expressed in neurons (Cam & Bu, 2006; U. C. Müller et al., 2017; Nhan et al., 2015; Y. W. Zhang et al., 2011; J. Zhao et al., 2020).

APP can be processed via two alternative pathways: amyloidogenic and nonamyloidogenic (Figure 1-4). In the nonamyloidogenic pathway, APP is cleaved by α-secretase, which releases a soluble fragment, sAPPα, from the cell surface and leaves an 83-amino-acid C-terminal APP fragment (C83). Further processing involves the intramembrane cleavage of α- and β-C-terminal fragments by γ-secretase, which liberates the P3 and Aβ peptides (Kahle & De Strooper,

2003). sAPPα may have a positive effect on neuronal activity because it can increase synaptogenesis (Haass et al., 1995). The amyloidogenic pathway of APP involves successive cleavage by β- and γ-secretase at the N and C termini of Aβ. The β-secretase generates a 99-amino-acid C-terminal fragment of APP (C99), which is further processed by γ-secretase at multiple sites, producing the final Aβ forms, the 40-amino-acid Aβ40 and the 42-amino-acid Aβ42, which are self-aggregating and toxic (Olsson et al., 2013; Takami et al., 2009). A dominant mutation in the APP, *PSEN1* and *PSEN2* genes can elevate the $A\beta_{42}/A\beta_{40}$ ratio or increase the self-aggregation propensity of subsequent Aβ peptides (W. Chen et al., 2014; De Jonghe et al., 2001; Selkoe, 2001).

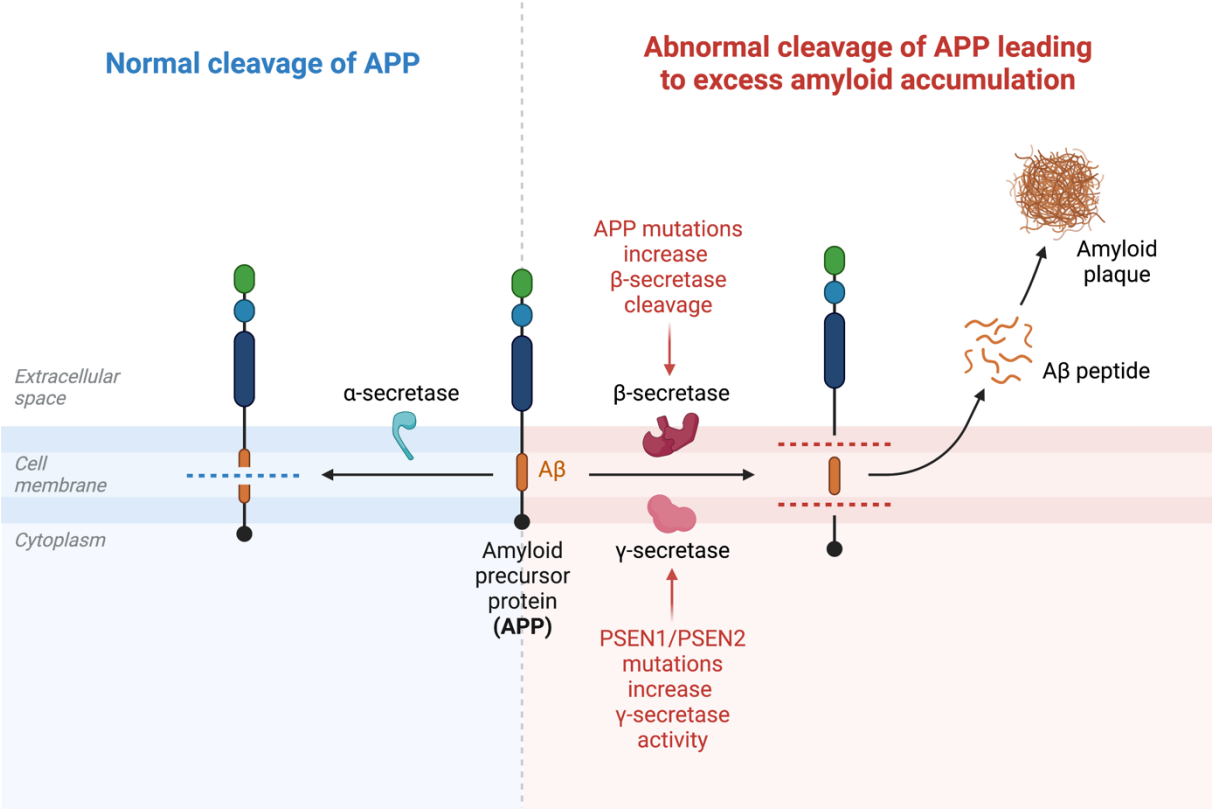

Figure 1-4 APP proteolysis in the nonamyloidogenic pathway and amyloidogenic pathway (modified from Chen et al., 2017).

The nonamyloidogenic pathway is initiated by α-secretase, which cleaves APP to generate C83 and the soluble N-terminal fragment sAPPα, whereas the release of Aβ is prevented. Amyloidogenic APP processing starts with β-secretase releasing the C-terminal fragment C99 and the N-terminal sAPPβ. C99 is subsequently cleaved by γ-secretase into Aβ. Created with BioRender.com

Aβ peptides can bind to the plasma membranes of neurons, microglia, and astrocytes, triggering transmembrane signalling and abnormal intracellular changes (Peters et al., 2009; Z. X. Wang et al., 2016). Aβ oligomers might alter neuronal function negatively by causing synaptic dysfunction,

inducing mitochondrial dysregulation, and affecting microglia (Polanco et al., 2018). Neurons exposed to Aβ oligomers are unable to form new synapses, resulting in learning deficits (Y. Zhao et al., 2017).

Tau was discovered by Weingarten et al. (1975). The group showed that the protein is microtubule-associated and plays an important role in microtubule assembly and stabilization. Generally, tau shows no aggregation behaviour, but aggregation into paired helical filaments and neurofibrillary tangles (NFTs) is a characteristic of Alzheimer's disease. It seems to be involved in amyloid-β-induced neurotoxicity (Roberson et al., 2007).

In normal physiology, tau has various functions. In adult neurons, where tau is mainly located at axons, it stabilizes microtubules, promotes microtubule assembly, and regulates the dynamic instability of microtubules that allows reorganization of the cytoskeleton (Feinstein & Wilson, 2005; Mandelkow & Mandelkow, 2012). In addition to axons, tau is also found in dendrites and the nuclei of neurons. Although the effects are not clear, there is evidence for the regulation of synaptic plasticity and maintenance of the integrity of genomic DNA (Frandemiche et al., 2014; Sultan et al., 2011).

Although over 80 mutations of tau have been identified in AD, the aggregations seem to be sporadic. In pathological conditions, tau may undergo posttranslational modifications such as hyperphosphorylation, which could lead to the detachment of tau from microtubules, resulting in microtubule disassembly in axons. Mislocalized tau in presynaptic terminals can induce synaptic dysfunction, a reduction in synaptic vesicles, and synapse loss (Decker et al., 2015). In addition, tau can also enter postsynaptic compartments and trigger postsynaptic dysfunction, which also leads to synaptic loss (Hoover et al., 2010; Thies & Mandelkow, 2007).

The brain utilizes 25% of total body glucose and 20% of body oxygen consumption while in a resting awake state (Mergenthaler et al., 2013). Therefore, the brain is especially vulnerable to a lack of energy. The mitochondrion, which marks the third stage: the cellular level, will be described in depth in the next section.

1.2 Mitochondria in health and Alzheimer's disease

The term mitochondrion was coined by Carl Benda and comes from the Greek words μίτος, *mitos*, "thread", and χονδρίον, *chondrion*, "granule" (Ernster & Schatz, 1981). Warburg and Keilin linked its function to respiration in the 1920s (Koppenol et al., 2011). Mitochondria are organelles within cells but have their own DNA. This leads to a theory of endosymbiosis (Sagan, 1967). It stated that mitochondria descended from free-living prokaryotes, which were taken up by eukaryotic cells. Depending on the cell type or physiological state, mitochondria range in size from 0.75 to 3 μm in diameter (Wiemerslage & Lee, 2016). Their distribution varies widely by cell type and tissue (Frazier et al., 2006). The unique structure of the mitochondrion is composed of the outer membrane, intermembrane space, inner membrane, cristae (a fold in the inner membrane) and matrix. The outer membrane is porous and therefore traversable for ions and small, uncharged molecules. The voltage-dependent anion channel (VDAC) and pore-forming membrane proteins (porins) support this transfer (Bayrhuber et al., 2008). Molecules larger than 5000 Da, such as proteins, are shuttled through the outer membrane (TOM) translocase and the inner membrane (TIM) translocase. In contrast to the outer membrane, the inner membrane is a tight diffusion barrier to all ions and molecules. An outcome of this selectivity is an electrochemical membrane potential across the inner mitochondrial membrane. The establishment of the electrochemical gradient is used for oxidative phosphorylation and ATP synthesis. In addition, mitochondria are involved in other tasks, such as signalling, differentiation, and apoptosis, as well as maintaining control of the cell cycle and cell growth (McBride et al., 2006).

1.2.1 The mitochondrial respiratory chain and OXPHOS system

The main function of mitochondria is to provide the energy required for the synthesis of ATP by the electron transport chain (ETC) and oxidative phosphorylation (OXPHOS). The electron transport chain contains five complexes. These complexes are complex I (ubiquinone oxidoreductase), complex II (succinate dehydrogenase), complex III (cytochrome C oxidoreductase), complex IV (cytochrome oxidase), and complex V (ATP synthase) (Napolitano et al., 2021; Swerdlow, 2020). Complex I –IV create a proton gradient across the inner mitochondrial membrane, which is used to produce ATP from ADP via complex V. Here, NADH and $FADH_2$, which are derived from the Krebs cycle, are oxidized. Electrons transfer from NADH and succinate to Complex I and Complex II, respectively. Subsequently, complexes I and II transfer

electrons to ubiquinone. Electrons pass from ubiquinone through Complex III to cytochrome c (Cytc). In turn, cytochrome c reduces complex IV (Figure 1-5) (Shimada et al., 2017).
The energy released by reducing the redox potential of the electrons passing through the respiratory complexes is used to pump protons from the mitochondrial matrix into the intermembrane space. In this way, a proton motor force consisting of an electric ($\Delta\Psi m$) and proton (ΔpH) gradient is created (Mitchell & Moyle, 1965). Similar to gravity in a hydroelectric power station, this force brings protons back into the matrix via Complex V, resulting in the synthesis of ATP. This final process is called oxidative phosphorylation (OXPHOS).

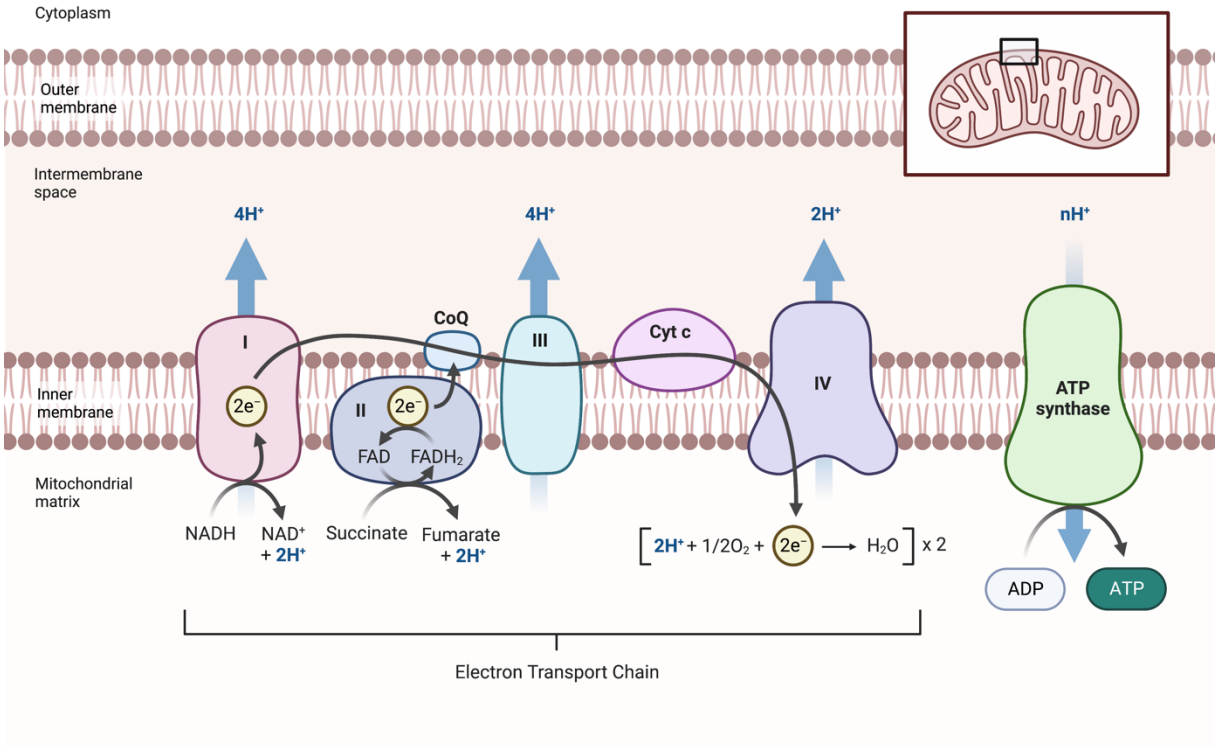

Figure 1-5 Overview of the respiratory chain and the ATP synthase (modified from (Kishi et al, 2018)
Arrows show the transfer of two electrons from oxidation of NADH or succinate of complex I or complex II. These electrons are then transferred to complex IV via cytochrome c oxidase, which catalyses the electron transfer to the final electron acceptor oxygen. Simultaneously, a proton motive force is generated by complex I, III and IV resulting in a negative charge in the inner side of the membrane and a positive charge on the outer side, which generates the mitochondrial membrane potential. Created with BioRender.com

As described above, mitochondria are the major energy source for cells. In addition, mitochondria are involved in intracellular signalling cascades, generate reactive oxygen species (ROS), execute fatty acid β oxidation, participate in amino acid metabolism, pyridine synthesis, phospholipid modifications, calcium regulation, and cell survival, senescence, and death. These dynamic processes require “quality control” to regulate mitochondrial mass and function. Mitochondrial homeostasis is controlled via fusion and fission, or more precisely, via the generation

of new mitochondria, mitochondrial biogenesis, and the removal of impaired mitochondria, mitophagy (Golpich et al., 2017; Ploumi et al., 2017).

Mitochondrial biogenesis involves mtDNA transcription and translation and nDNA-encoded synthesis, import, and assembly of mitochondrial proteins. PGC-1α, which is considered the master regulator of mitochondrial biogenesis, activates mtDNA transcription. Phosphorylation or deacetylation activates PGC-1α, which stimulates nuclear transcription factors such as nuclear respiratory factor-1 (NRF-1) and NRF-2. NRF1 regulates neuronal health and neuronal outgrowth (Kiyama et al., 2018). NRF1 and NRF2 activate mitochondrial transcription factor A (TFAM), which encodes subunits of the five complexes in the mitochondrial electron transport chain (ETC), thereby increasing the assembly of the respiratory apparatus (Uittenbogaard & Chiaramello, 2014). The activation of this PGC-1α-NRF-TFAM pathway leads to the synthesis of mitochondrial DNA and proteins and the generation of new mitochondria (Figure 1-6).

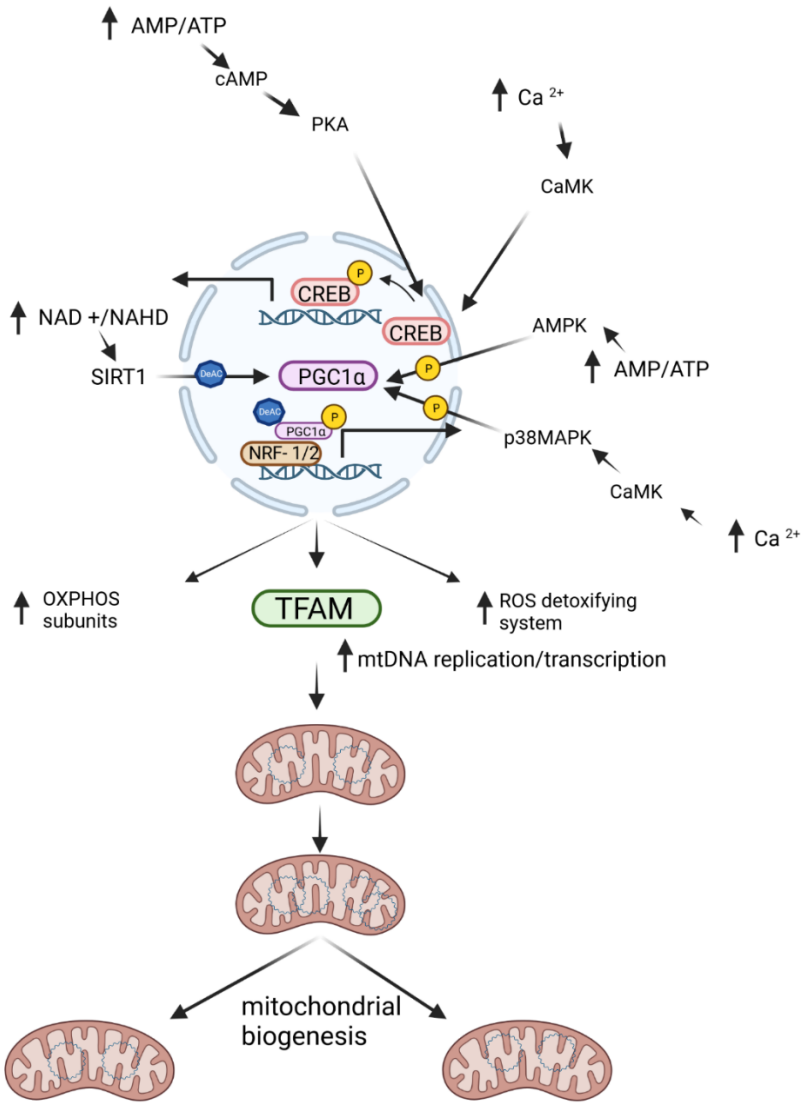

Figure 1-6 Signalling cascades of mitochondrial biogenesis.
Ca^{2+} and AMP/ATP are the main stimuli of mitochondrial biogenesis. Increased Ca^{2+} and AMP levels activate various kinases. These either phosphorylate CREB, which promotes PGC-1α expression, or phosphorylate PGC-1α directly. An increased NAD^{+}/NADH ratio also leads to the activation of PGC-1α via deacetylation by SIRT1. Following its activation, PGC-1α binds to NRF1/2 and promotes the expression of several mitochondrial proteins, including TFAM, resulting in increased mitochondrial biogenesis (modified from Cardanho-Ramos and Morais 2021). Created with BioRender.com

The transcription factor cAMP response element-binding protein (CREB) also mediates the activation of the PGC-1α signalling pathway. CREB plays a role in neuronal plasticity and long-

term memory formation in the brain (P. Sharma et al., 2019). The downregulation of CREB is associated with the pathology of Alzheimer's disease (Pugazhenthi et al., 2011).

It has also been reported that silent information regulator-1 (SIRT1) stimulates the PGC-1α-mediated transcription of nuclear and mitochondrial genes encoding proteins during mitochondrial proliferation, oxidative phosphorylation, energy production, and mitophagy (Gurd, 2011; Lan et al., 2008; Yoshii & Mizushima, 2015).

1.2.2 Mitochondrial dysfunction in Alzheimer's disease

Mitochondria are a critical source of energy in cells. The mitochondrial cascade hypothesis links the dysfunctional aspects of mitochondria with Alzheimer's disease (Swerdlow, 2020). The first evidence for mitochondrial dysfunction in Alzheimer's disease emerged in cerebral blood flow studies, where the cerebral metabolic rates of oxygen, CO_2 and lactate were examined (Hoyer, 1991). Furthermore, it has been confirmed that AD individuals show a reduction in brain glucose metabolism using fluorodeoxyglucose PET (FDG-PET) (Mosconi et al., 2010). It is assumed that the reduction is initiated by synaptic dysfunction and neuronal loss. Although this can be compensated by shifting to alternative energy sources (Toledo et al., 2017), it seems to be a indication for mitochondrial dysfunction.

A further sign for mitochondrial dysfunction is increased oxidative stress and ROS damage in the brains of AD subjects in the early stages. Compared with non-AD controls, cells with mtDNA from AD subjects show increased ROS and free radical production (Swerdlow et al., 1997.

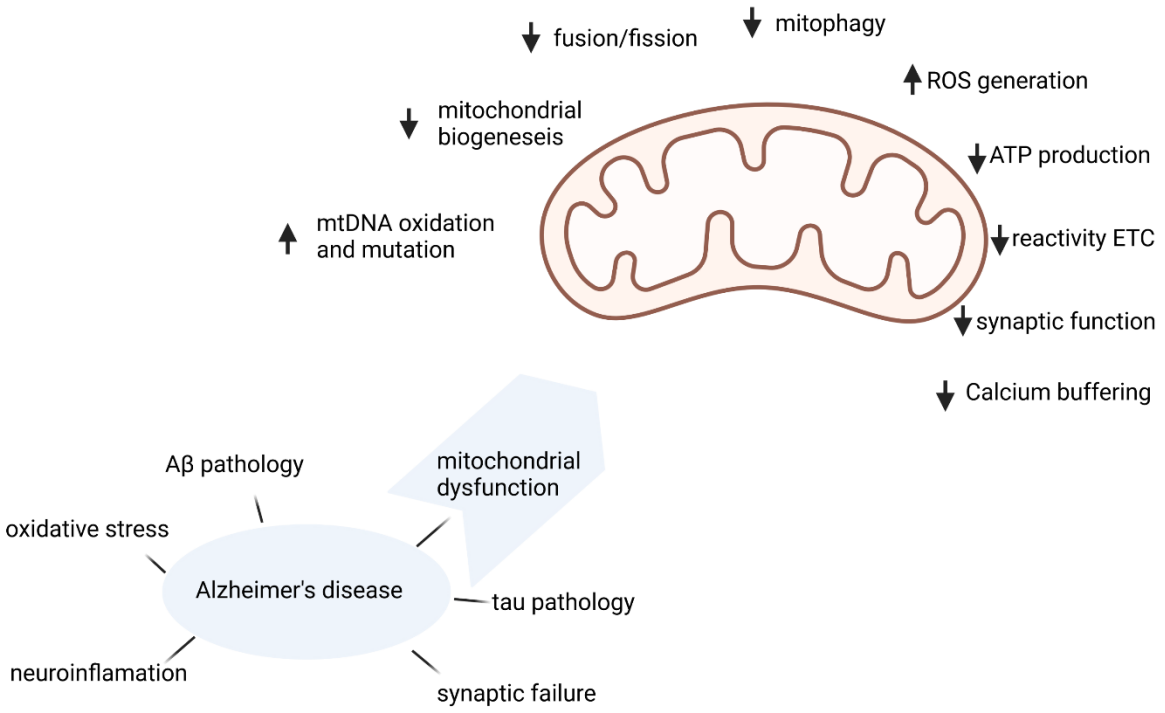

Figure 1-7 Effects in AD pathology and mitochondrial dysfunction in AD (modified fromCenini and Voos 2019). Created with BioRender.com

Moreover, mitochondrial function in AD brains is attributed to compromised mitochondrial enzymes such as cytochrome c oxidase, pyruvate dehydrogenase complex and α-ketoglutarate dehydrogenase (Gibson et al., 2010). Subunits of these enzymes, which are encoded by mtDNA, are degraded (Swerdlow et al., 1997).

Additionally, it has been documented that Aβ and hyperphosphorylated tau can accumulate in the late stages of AD (W. E. Müller et al., 2010; Stockburger et al., 2018). Aβ is able to translocate into mitochondria (Anandatheerthavarada & Devi, 2007). The accumulation of Aβ in mitochondria causes inhibition of complexes II and IV of the respiratory chain, resulting in reduced OXPHOS and increased production of ROS (Rhein et al., 2009). This can lead to a vicious cycle in which mitochondrial dysfunction and Aβ accumulation influence each other. Perturbed OXPHOS leads to an inhibition of ATP production, which induces higher levels of BACE-1, a β-secretase, and elevates ROS-induced Aβ production (Busciglio et al., 2002). In the end, Aβ accumulation leads to impaired mitochondrial dynamics, causing reduced clearance of impaired mitochondria, which further enhances mitochondrial dysfunction Figure 1-7) (Manczak et al., 2011).

Tau pathology affects mitochondrial dysfunction in a similar way. Overexpression of tau inhibits mitochondrial function by decreasing the activity of the ETC and antioxidant enzymes (A. Eckert et al., 2011; X. C. Li et al., 2016). Tau localized in the mitochondrial membrane can further impair ATP synthesis and mitochondrial membrane potential (Atlante et al., 2008). Brains of P301L tau transgenic mice showed that the activity of complexes I and V was significantly reduced. Additionally, ATP synthesis and the mitochondrial membrane were disturbed along with increased ROS levels (David et al., 2005).
Although it is not clear what causes mitochondrial dysfunction, it is apparent that AD patients have negative changes in their mitochondrial power supply compared to healthy subjects (W. E. Müller et al., 2010; Stockburger et al., 2018).

1.3 Current treatment therapies against Alzheimer's disease

Currently, there is no cure for Alzheimer's disease. Modern therapies can provide people with reassurance and dignity and reduce symptoms. Therapies are divided into two categories: disease-modifying therapies and symptomatic treatments. Presently, treatments target the breakdown of acetylcholine and block excess glutamate release. A newly approved treatment removes abnormal accumulation of amyloid beta.
As described above, the cholinergic hypothesis describes the disorder in the cholinergic system as a cause for Alzheimer's disease. Therefore, one of the therapeutic strategies is to increase cholinergic levels by inhibiting acetylcholinesterase (AChE). The inhibition results in continuous accumulation of ACh and activation of cholinergic receptors. Currently in use for the symptomatic treatment of AD are donepezil, rivastigmine, and galantamine (K. Sharma, 2019).
N-methyl d-aspartate (NMDA) receptors are thought to have a central role in the pathophysiology of AD. NMDA receptors activate signal transduction through Ca^{2+} influx. This initiates gene transcription, which is essential for the formation of long-term potentiation. It is essential for synaptic neurotransmission, plasticity, and memory formation. Overactivation of NMDA receptors causes an abnormal level of Ca^{2+} signalling and overstimulation of glutamate release. Glutamate is the primary excitatory amino acid in the CNS, which results in synaptic dysfunction, neuronal cell death, and a decline in cognitive functions (Y.-J. Huang et al., 2012; Liu et al., 2019). NMDA antagonists such as memantine block overactivation and therefore decrease abnormal glutamate release (Williams & Buvanendran, 2021).
Aducanumab targets the underlying causes of the disease; therefore, it is called a disease-modifying drug. Sevigny et al. showed that treatment with aducanumab reduces brain Aβ plaques.

In June 2021, the Food and Drug Administration (FDA) granted its first accelerated approval to this antibody-based immunotherapeutic approach. (FDA, 2021). In 2023, the FDA granted approvals for new medications, including lecanemab (FDA, 2023). Others, like donanemab, are likely to follow. Table 1-1 presents a comprehensive list of drugs used in Alzheimer's treatment, along with their respective therapeutic targets.

Table 1-1 List of Alzheimer drugs and therapeutic targets.

Drug name	**Drug type**	**Therapeutic target**
Aducanumab	Disease-modifying immuno-therapy	Removes abnormal Aβ
Donepezil	Cholinesterase inhibitor	Blocks breakdown of acetyl-choline in the brain
Rivastigmine	Cholinesterase inhibitor	Blocks breakdown of acetyl-choline and butyrylcholine in the brain
Memantine	N-methyl D-aspartate (NMDA) antagonist	Blocks excess glutamate and regulates glutamate activa-tion
Galantamine	Cholinesterase inhibitor	Blocks breakdown of acetyl-choline in the brain

Despite extensive research on this disease, only a few drugs that can delay the progression of the disease are currently available. A major setback for all current drugs is side effects. Treatment with Alzheimer’s drugs can lead to adverse gastrological, cardiovascular, neurological, psychological, respiratory, and dermatological effects. Acetylcholinesterase inhibitors increase gastric acid secretion and internal propulsion, which can lead to gastrointestinal ulceration and bleeding (Lewin, 1999). Furthermore, abdominal pain, nausea, vomiting, diarrhea, and poor appetite have been reported (CC et al., 2014; Hansen et al., 2008). The most common side effects for memantine are dizziness, headache, confusion, diarrhoea, and constipation (Williams & Buvanendran, 2021). Although aducanumab reduces Aβ, it shows a tendency toward brain edema, which can be deadly (Khanna et al., 2022). This concern led the European Medicines Agency (EMA) to withhold approval for its marketing as an Alzheimer's remedy (EMA, 2022). However, it seems that newly approved medications, like lecanemab, present a reduced risk of disease progression, as shown by van Dyck et al. (2023)

In recent years, several compounds with pharmacological activities isolated from plants and mushrooms have been revealed to have beneficial effects for the treatment of AD, targeting different pathological mechanisms. Thus, a wide range of natural compounds may play a relevant role in the prevention of AD in the future.

1.4 The fungus *Hericium erinaceus* and its metabolites

Fungi have enormous biotechnological potential. As opposed to plants, fungi have the great advantage that they can be grown in large bioreactors. Growing fungi at an industrial scale makes fermentation cost-efficient. Fungal biotechnological research has led to pharmaceuticals, such as beta-lactam antibiotics, statins and cyclosporine (Hyde et al., 2019). Although fungi have already shown their capabilities, research on their potential applications is still limited. More interdisciplinary efforts are needed to prove the full power of fungal applications. In particular, the fungus *Hericium erinaceus* is a noteworthy object in neurodegenerative research (H.-T. Huang et al., 2021; Kawagishi & Zhuang, 2008; I.-C. Li et al., 2018; Tsai-Teng et al., 2016; Tzeng et al., 2018).

Figure 1-8 Fruiting body of Hericium erinaceus, Picture with courtesy from Alison Harrington.

Hericium erinaceus (Bull.) Pers. 1797 belongs to the family Hericiaceae, order Russulales and class Agaricomycetes under the phylum Basidiomycota (Figure 1-8) (Ainsworth et al., 2008). Erinaceus literally means “hedgehog” in Latin. Its appearance also explains its trivial names: “Lion’s Mane”, “Igel-Stachelbart” (German) “Monkey’s Mushroom”, “Pom Pom”, “Yamabushitake” (Japanese), and “猴頭菇” (Houtou, Chinese), which means "monkey head". *Hericium erinaceus* is considered a saprotroph or weak parasite. It most often occurs on dead wood, but sometimes its fruiting bodies may spring from knotholes or cracks of living hardwoods. In China, *Hericium erinaceus* is a highly valued culinary ingredient due to its distinct taste and texture profile. The mushroom possesses a tender, somewhat elastic texture, and its flavor exhibits seafood-like characteristics, often comparedto lobster or shrimp. This unique combination renders it well-suited for

traditional Chinese dishes, such as stir-fries or hot pots. It is also a primary ingredient in Chinese snacks such as mushroom chips and crisps, offering a healthier alternative to traditional snack foods. The versatility of *Hericium erinaceus* in culinary and food industry applications highlights its growing popularity and potential for continued innovation in the food sector. As with other edible mushrooms *Hericium erinaceus* is rich in proteins, vitamins, fiber, and minerals, has comparatively low levels of carbohydrates and lipids, and represents a valuable food source with nutritional therapeutic significance (Chaturvedi et al., 2018; Cohen et al., 2014). The mycelium and the fruiting body differ in the composition of the main nutrients (see Table 1-2 according to Cohen et al., 2014)

Table 1-2 Macronutrient composition of the mycelium and fruiting body of Hericium erinaceus.

	Protein [%]	Lipids [%]	Carbohydrates [%]	Ash [%]	Energy [kcal/100 g]
Fruiting body	20.8 ± 0.43	5.1 ± 0.11	61.1 ± 3.6	6.8 ± 0.22	374 ± 14
Mycelium	42.5 ± 0.18	6.3 ± 0.32	42.9 ± 2.8	3.9 ± 0.08	398 ± 18

In addition to its nutritional value, *Hericium erinaceus* fruiting bodies and mycelia contain exceptionally large amounts of structurally different bioactive and potentially bioactive components (Figure 1-9). There are bioactive secondary metabolites that can be obtained from submerged cultures, which may not be produced in fruiting bodies and *vice versa*. However, high yields of mycelial biomass are only achieved with submerged cultivation.

Figure 1-9 Fruiting body and mycelium of Hericium erinaceus, Picture with courtesy from Alison Harrington.

In general, the bioactive metabolites from *Hericium erinaceus* can be classified into two categories: high molecular mass compounds and low molecular mass compounds. Polysaccharides are high molecular mass compounds, whereas polyketides, amino acids and terpenoids represent low molecular mass compounds (Kawagishi et al., 1994; Ma et al., 2010; Mizuno et al., 1992).

Polysaccharides are found mainly in the cell walls of fungi and make up approximately 20% of the biomass (François, 2007). Those are, for example, xylans, glucoxylans, heteroxyloglucans, and galacto-xyloglucans, which show antitumour activity and antioxidative properties (Mizuno et al., 1992; Ren et al., 2018). Ergothioneine is an L-histidine derivative that naturally occurs in bacteria and fungi (Figure 1-10) (Borodina et al., 2020). In addition to its antioxidative properties, it has the ability to protect against amyloid-β-induced cell death (Cheah et al., 2019; Paul & Snyder, 2009)

Terpenoids have special properties for various applications. *Hericium erinaceus* contains a special group of cyathane-type diterpenoids called erinacines (Figure 1-10). Erinacines were first described by Kawagishi et al. (1994) who pointed out their special NGF activating

properties.Erinacines are hard to isolate because of their massive use of organic solvents and their rare occurrence. Shen et al. (2015) showed that a special medium containing oatmeal and Edamin ^{K} can enhance erinacine C production in submerged mycelial cultures to 275 mg/L.

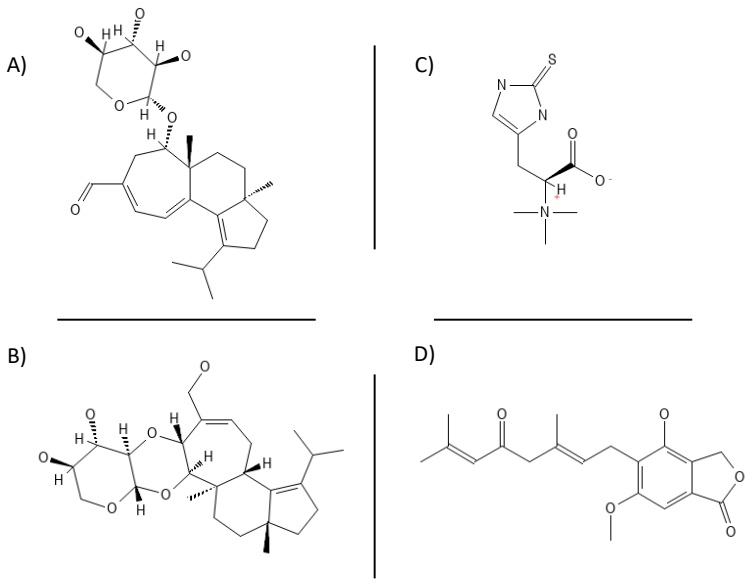

Figure 1-10 Bioactive compounds of Hericium erinaceus.
Structures of A) Erinacine C, B) Erinacine A, C) Ergothionine and D) Hericenone A.

1.4.1 Biotechnological production, isolation and characterization of erinacines

Erinacines are in general hard to isolate because of the massive use of organic solvents and their rare occurrence. The studies of Wolters et al. (2015), Shen et al. (2015) and Bhandari et al. (2014) contributed a huge body of research on the understanding of the production, distribution, and isolation of erinacines, and especially erinacine C. Shen et al. (2015) showed with high-resolution MALDI MS imaging the distribution and occurrence of secondary metabolites, including erinacines, in the *Hericium erinaceus* fungus. Most erinacines and metabolites are homogeneously distributed between the fruiting body and the mycelium. However, erinacine C was exclusively found in the mycelium (submerged culture) (Bhandari et al., 2014). This leads to the search for optimized parameters for the production of erinacines, especially erinacine C. It is generally known that the carbon to nitrogen (C/N) ratio is important for the biosynthesis of many secondary metabolites in fungal cultures (Lin & Chen, 2007). High production of erinacines in submerged cultures of *Hericium erinaceus* could allow the use of this fungus for therapeutic purposes, as well as a promising ingredient as a functional food. Shen et al. first optimized the production of erinacine C in submerged cultures using an optimized adjustment of the C/N ratio. She mainly used oatmeal and sugars as a carbon source and the peptide

Edamin® K as a nitrogen source. This pushed the maximum concentration of erinacine C to 257 mg/L after the 9th culture day (Shen, 2013; Shen et al., 2015). Furthermore, she developed a highly sensitive and specific ELISA for the qualitative and quantitative detection of cyathane diterpenoids in complex mixtures (Shen et al., 2014). Wolters et al. (2015) stabilized the pH value in the submerged culture of *Hericium erinaceus* with 100 mM HEPES buffer and reached concentrations of 273 mg/L. In addition to HPLC-DAD, HPTLC-UV/vis/FLD-*Aliivibrio fischeri* analysis may also be used to directly detect cyathane diterpenoids in crude extracts (Shen et al., 2015).

Chen et al. paved the way for future research with his study on the genomic and transcriptomic regulation of terpenoid production in *Hericium erinaceus* (J. Chen et al., 2017). Since erinacines are synthesized via the mevalonate pathway and the associated genes are known, biotechnological production via genetically modified microorganisms (e.g., *E. coli*) could be used to achieve high yields (J. Chen et al., 2017; Y. L. Yang et al., 2017).

1.4.2 Therapeutic applications of Hericium erinaceus

The therapeutic applications of medicinal mushrooms have been mostly in the field of diabetes prevention and supporting anticancer treatments (Venturella et al., 2021). However, *Hericium erinaceus* is a traditional medicinal mushroom in Eastern Asia for treating lack of concentration and stress (Ying, 1987). Modern scientific research is now providing answers regarding how *Hericium erinaceus* positively impacts brain health. Polysaccharides derived from submerged mycelial cultures and fruiting bodies of *Hericium erinaceus* showed immunomodulatory effects (Han et al., 2013; J. S. Lee & Hong, 2010). The negative effects of ROS on mitochondria and Alzheimer's have already been described above. Many studies have shown the antioxidant properties of *Hericium erinaceus* (Abdullah et al., 2012; Kushairi et al., 2019; Malinowska et al., 2009; Z. Zhang et al., 2012). Valu et al. (2021) showed antioxidative activities of an ethanolic extract in a zebrafish model of cognitive impairment through the elevation of glutathione levels. Lee et al. demonstrated that erinacine A could prevent the cytotoxicity of neuronal cells and the production of ROS *in vitro* and *in vivo* (K.-F. Lee et al., 2020).

Rita Levi-Montalcini and Stanley Cohen discovered an important biological effect of neuronal growth factor (NGF) on neuronal cells and explained the possible mechanism of NGF on cells of the immune system (Levi-Montalcini et al., 1996). In 1986, they were awarded the Nobel Prize in Physiology/Medicine for their research. NGF prevents neuronal death, promotes neurite outgrowth, supports synapse formation, and enhances memory function. Furthermore, it is essential in maintaining and organizing neuron function (Yutaro & Norimichi, 2002). In

Alzheimer's disease, the decline in neurons and synapses is progressive, and neurotrophic factors are essential for the maintenance and organization of neurons. Therefore, neurotrophic factor-like substances or their inducers are expected to soon be a treatment against neurodegenerative diseases. Implantation of NGF-releasing cells into the basal forebrain resulted in reduced brain atrophy in responders in a 12-month trial (Ferreira et al., 2015). A 10-year trial Tuszynski et al. (2015) showed that degenerated neurons in the AD brain respond to NGF. This was indicated by axonal sprouting, cell hypertrophy and the existence of neuronal markers. This is especially interesting because NGF cannot penetrate the blood–brain barrier *in vivo*. However, erinacine S can pass the blood–brain barrier (J. H. Hu et al., 2019). Furthermore, they show a wide range of positive effects on neuronal health. Shimbo et al. (2005) treated rats with erinacine A, which led to increased levels of NGF in the locus coeruleus and hippocampus. (Tsai-Teng et al., 2016) showed similar results in an Alzheimer's disease model using APPswe/PS1dE9 transgenic mice. Furthermore, the group showed increased hippocampal neurogenesis.

Since *Hericium erinaceus* and its secondary metabolites, such as erinacines, show promising neuroprotective, antioxidative, and neurogenesis effects, it is important to investigate their effects on Alzheimer's disease and its effect on mitochondrial function. As a part of a balanced diet, consuming *Hericium erinaceus* may serve as a natural strategy to support brain health and potentially prevent or delay the onset of Alzheimer's disease.

1.5 Models of Alzheimer's research

Alzheimer's is a complex disease, and current models cannot portray all its aspects. The complexity can be noted in the limited efficacy of available drugs. In addition to aging, environmental and genetic factors contribute to the disease. Ethical concerns of animal experiments and failures of several clinical trials targeting neurodegenerative diseases complicate the matter even further. Therefore, more work is required to identify the underlying molecular mechanisms and corresponding pharmacological targets. The identification of mechanisms of action with *in vitro* testing reduces the time and costs of research. Although cellular and invertebrate models have some limitations, such as that they cannot recapitulate all cellular functions of an organ, the advantages outweigh the shortcomings (Drummond & Wisniewski, 2017).

SH-SY5Y cells are a common *in vitro* model used in AD research. SH-SY5Y cells are a neuroblastoma cell line that was originally derived from a metastatic bone tumor biopsy. June Biedler described the cells and deposited them at ATCC® (ATCC number: CRL-2266). They have three major characteristics: they are adherent and floating, they contain neuroblast-like and epithel-like cells, and they can be differentiated into a more mature neuron-like phenotype (Kovalevich & Langford, 2013).

Two variants of this cell line were used in this work: SH-SY5Y MOCK and SH-SY5Y APP_{695}. SH-SY5Y APP_{695} cells are based on SH-SY5Y amyloid precursor protein wild type (APPwt), which is suitable to conduct investigations within the framework of the mitochondrial cascade hypothesis but misses Aβ overexpression. For this purpose, an additional copy of human AβPP (AβPP_{695}) was transfected, resulting in a twofold increased level of Aβ compared to the control cells SH-SY5Y MOCK, which possess a corresponding empty vector (pCEP4) instead of the additionally inserted copy of APP (Peraus et al., 1997). APP and Aβ are thus present in higher amounts, but the deposits typical in later stages do not yet take place.

The overexpression and increased levels of $A\beta_{1\text{-}40}$ and $A\beta_{1\text{-}42}$ result in mitochondrial dysfunction characterized by altered mitochondrial membrane potential (MMP) and decreased mitochondrial respiration. As a result, the synthesis of ATP is reduced. The cells compensate for this by an increased rate of glycolysis, as has also been demonstrated in this phase of Alzheimer's disease in humans. In addition, a change in the dynamics of the mitochondria towards more fission and fragmentation of the organelles was shown. Surprisingly, neurite growth is increased in the APP type, which the authors attribute to increased levels of sAβPPα (Stockburger et al., 2014).

Despite having many advantages, they suffer from drawbacks, such as having a cancerous cell nature, withstanding high oxidative stress, expressing high levels of oxidative stress response

genes in similar forms and high rates of glycolysis, which may alter the experimental outcomes (Forster et al., 2016; Krishna et al., 2014).

Sydney Brenner introduced 1963 *Caenorhabditis elegans* as a model organism (Brenner, 1974). *Caenorhabditis elegans* is a small (1 mm in length), transparent roundworm and has a short life cycle of 3 days from egg to adult at 25°C (Brenner, 1974). Under suitable growing conditions, hatched animals develop in four larval stages (L1–L4). They mature as adult hermaphrodites, with a lifespan between 2 and 3 weeks and 959 somatic cells (Sulston & Horvitz, 1977). Its genome was sequenced in 1998 (The C. elegans Sequencing Consortium, 1998). Furthermore, it has been demonstrated that approximately 38% of worm genes have human orthologues, such as APP and tau (Shaye & Greenwald, 2011). Therefore, *C. elegans* has many advantages as an *in vivo* model for the study of AD and other neurodegenerative diseases.

To fully exploit this system for drug discovery, a model expressing and accumulating full-length A$\beta_{1\text{-}42}$ is needed. The *C. elegans* strain GMC101 was engineered to express full-length Aβ1-42. An extra Asp-Ala (DA) was inserted N-terminally into the human-Aβ sequence in the expression vector pCL12(unc-54:A$\beta_{1\text{-}42}$). This results in A$\beta_{1\text{-}42}$ expression in body wall muscle cells, where it aggregates, which leads to severe and fully penetrant age-progressive paralysis at 25°C. This model is a better model than CL2120, which expresses A$\beta_{3\text{-}42}$. Compared to A$\beta_{1\text{-}42}$, the A$\beta_{3\text{-}42}$ peptide has different physicochemical properties. A$\beta_{3\text{-}42}$ is more hydrophobic and aggregates more rapidly *in vitro*. In the human AD brain, A$\beta_{1\text{-}42}$ is a predominant Aβ species (Portelius et al., 2010). The strain CL2122 is a control strain for GMC101 because it has no expression of Aβ under the same vector.

In recent years, the GMC 101 model has helped to understand mitochondrial metabolism, such as mitochondrial iron metabolism and mitochondrial proteasis (J. Huang et al., 2018; Sorrentino et al., 2017). Furthermore, GMC101 was used to investigate the effects of vitamin B_{12} deficiency-induced oxidative stress. The deficiency might promote Aβ1-42 stabilization and toxic oligomerization (Koseki et al., 2021).

1.6 Objective of the work and hypothesis

Alzheimer's disease is an increasing burden on societies and healthcare systems nationally and globally (Lane et al., 2018). In the absence of sustainable curative treatment options, other approaches are increasingly coming to the fore. These include influencing mitochondria because metabolic energy deficits, including mitochondrial dysfunction and increased generation of reactive oxygen species, are among the early events of AD (Swerdlow, 2020). The use of traditionally used medicinal plants and mushrooms and their bioactive constituents has gained more importance as preventive and curative treatment options (Elkhateeb et al., 2019).

Small neurotrophic components that cross the blood–brain barrier and could have a positive effect on the maintenance and regeneration of neurons have been intensively researched. These components include EC, which is synthesized in the mycelium of *Hericium erinaceus*. It has already been demonstrated that EC and several other structurally similar erinacines mediate various neuroprotective effects and consequently have preventive or therapeutic potential with regard to the treatment of neurodegenerative diseases such as AD (Kawagishi & Zhuang, 2008; Phan et al., 2017). In particular, erinacine C has been shown to have strong effects on neuronal outgrowth and stimulate NGF synthesis (Kawagishi et al., 1994; Kawagishi & Zhuang, 2008; Rascher et al., 2020; Tzeng et al., 2018).

This work serves to investigate the effects of an ethanolic extract of the edible mushroom *Hericium erinaceus* and the metabolite erinacine C on mitochondrial function in a preclinical cell and invertebrate model of AD. Since electrochemical signal transduction in neurons is an energy intensive process, it is hypothesized that an ethanolic extract of *Hericium erinaceus* and erinacine C has a positive effect on mitochondrial parameters.

For this, the results of Shen et al. (2015) were replicated to produce, isolate and characterize erinacine C in a submersed liquid culture and optimized the extraction method. The molecule was analysed and characterized using HPLC, NMR and HR-MS.

The ethanolic extracts of *Hericium erinaceus* and pure erinacine C were then used in invertebrate and cellular models of AD. Two strains of *C. elegans*, GMC101 and CL2122, were used. Here, the ethanolic mycelial extract of *Hericium erinaceus* was investigated for its effects on lifespan under heat stress, ATP levels and ROS levels.

In SY5Y-MOCK and SY5Y-APP cells, a broad concentration spectrum of the ethanolic extract was investigated. Effects on metabolic activity and ATP synthesis were tested. Based on these findings, the ethanolic extract was analysed on effects on gene expression of various mitochondrial genes, such as ATP5D, NRF1 and TFAM, or the longevity genes CREB-1 and SIRT-1.

In the next step, the effects of erinacine C were explored further. A broad concentration spectrum of erinacine C was investigated. First, the effects on metabolic activity and ATP synthesis were tested. Based on these findings, erinacine C was analysed on effects on the respiratory chain, Aβ levels, and the gene expression of mitochondrial genes such as ATP5D, MAP1LC3B, SOD-2 and TFAM, CREB-1 and SIRT-1. To investigate the antioxidative and anti-inflammatory effects, the cells were additionally treated with H_2O_2. Furthermore, the neuritogenic effects of erinacine C were tested and a potential mechanism through the TrkB receptor was tested applying molecular modelling. To link the *in vivo* data with genomic data and to broaden the view on the effects of erinacine c, an RNAseq analysis was performed. A graphical overview of the work performed can be found in the graphic abstract below (Figure 1-11).

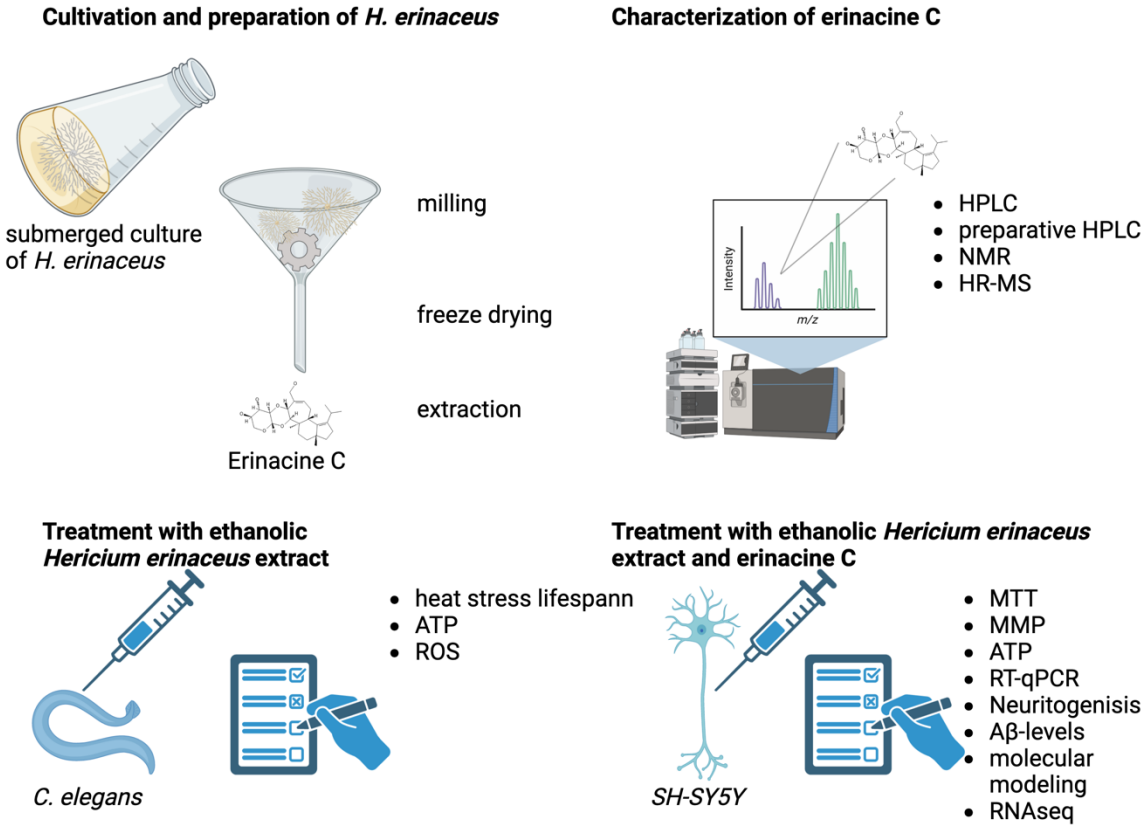

Figure 1-11 Graphical abstract of the work performed in this thesis.
Hericium erinaceus mycelium was cultivated in submerged cultures and then processed by milling, freeze drying and extraction. Erinacine C was analyzed using HPLC, preparative HPLC, NMR and HR-MS. The model organisms C. elegans was treated with an ethanolic extract of Hericium erinaceus and SH-SY5Y with the ethanolic extract and erinacine C. Created with BioRender.com

2 Results

The following section sheds light on the results produced for this work. The first part will describe the isolation and characterization of erinacine C, followed by the experimental results of the ethanolic mycelium extract of *Hericium erinaceus*. For the extract, effects are described for the invertebrate models CL2122 and GMC 101 and the cellular models SH-SY5Y MOCK and SH-SY5Y-APP$_{695}$. The result section will close with the effects of erinacine C on and the cellular models of SH-SY5Y MOCK and SH-SY5Y-APP$_{695}$. The experiments in this thesis came to realization with the help of four master's students: Katharina Appel, Lea Schüssler, Leonie Wach and Nathalie Grimm. A list of experiments, conducted with the assistance of master's students, can be found in Chapter 8.3.

2.1 Isolation and characterization of erinacine C from *Hericium erinaceus*

Erinacine C was biotechnologically produced in submerged cultures of *Hericium erinaceus* in the laboratory of Prof. Holger Zorn at the department of food chemistry and food biotechnology at JLU Giessen using a special growth medium (Chapter 5.1.6) (Shen et al., 2015). After extraction (Chapter 5.2.5), the collected sample was analysed using HPLC, preparative HPLC, NMR, and HR-Mass spectrometry.

2.1.1 HPLC Analysis of Erinacine C

Erinacine C was extracted using ethyl acetate from a liquid culture of *Hericium erinaceus* and analysed using an analytical HPLC-DAD system. Figure 2-1 (left) shows a chromatogram directly after extraction without further processing. Successive lyophilization resulted in a clearer chromatogram (Figure 2-1 right). Chapter 5.2.6 lists the column, solvents and parameters used. HPLC can also be used preparatively.

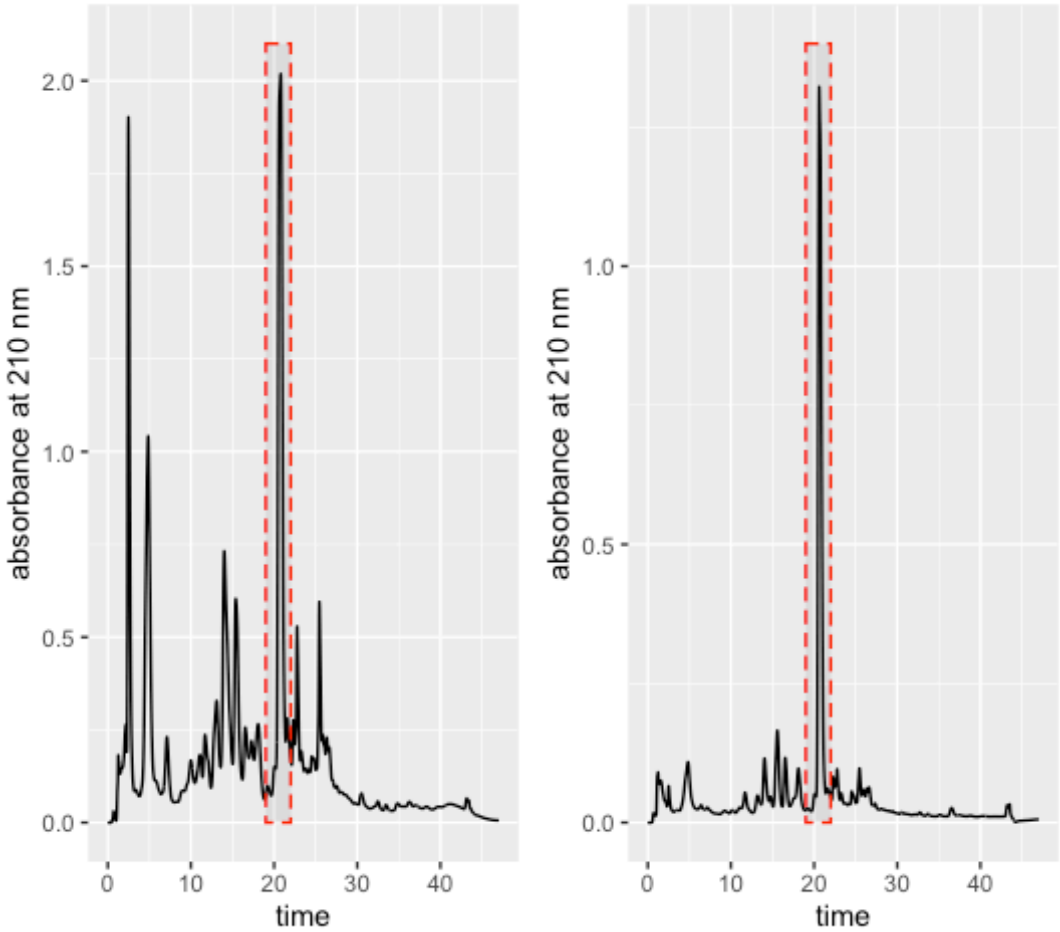

Figure 2-1 Showing erinacine C on an analytical HPLC-DAD.
MERCK HPLC (guard column: CC 8/3 Nucleosil® 100-5 C18 ; column: CC 125/3 Nucleosil® 100-5 C18) at 210 nm with the solvents acetonitrile and water and elution time of 21 minutes (left) after extraction without lyophilization, (right) after extraction with lyophilization. The extraction was carried out using ethyl acetate. The peak for erinacine C is marked in a red rectangle in both graphs. Detailed parameters are found in chapter 5.2.6.

2.1.2 Isolation of Erinacine C Using Preparative HPLC

Erinacine C was collected using a preparative HPLC system (
Figure 2-2). Figure 2-2 shows a chromatogram of a preparative HPLC separation, and the collected peak for erinacine C is marked in a red rectangle. Chapter 5.2.7 lists the column, solvents and parameters used.

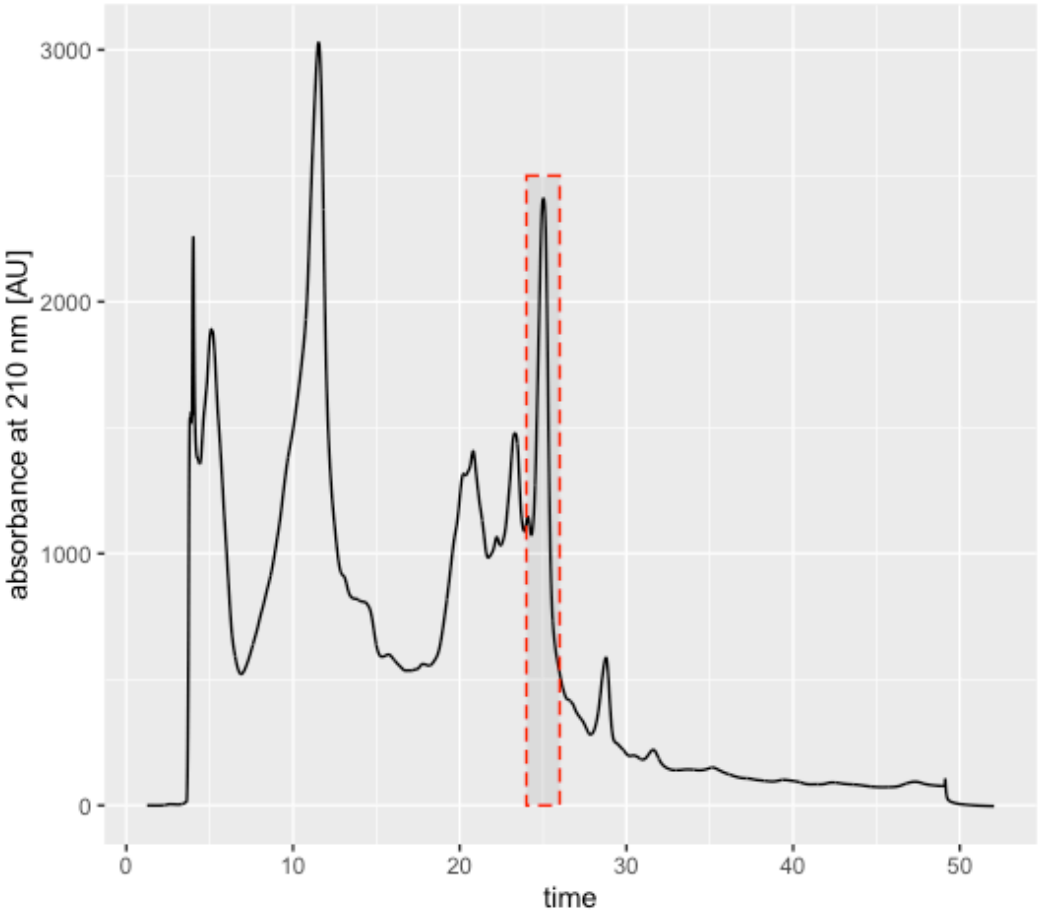

Figure 2-2 Chromatogram of erinacine C collected with preparative HPLC.
Guard column: CC 50/20 mm Nucleosil®, 100 C18, 7 µm; column CC 250/20 Nucleosil® 100-7 C18 at 26 minutes (changes in elution times are due to column volume and solvent velocity). A gradient with acetonitrile and water was used to elute erinacine C (detection at 210 nm). The peak for erinacine C is marked in a red rectangle. Detailed parameters are found in chapter 5.2.7.

2.1.3 *Erinacine C 2D HETCOR NMR Characterization*

To assess erinacine C correctly, 2D HETCOR NMR spectroscopy was carried out. The structure of erinacine C has been proven by DEPT, COSY, NOESY, HSQC and HMBC analyses and comparisons with the data published by Kawagishi et al. (1994) (Figure 2-3). Carbon atoms are labelled with letters a-t, hydrogen atoms with numbers 1-20.

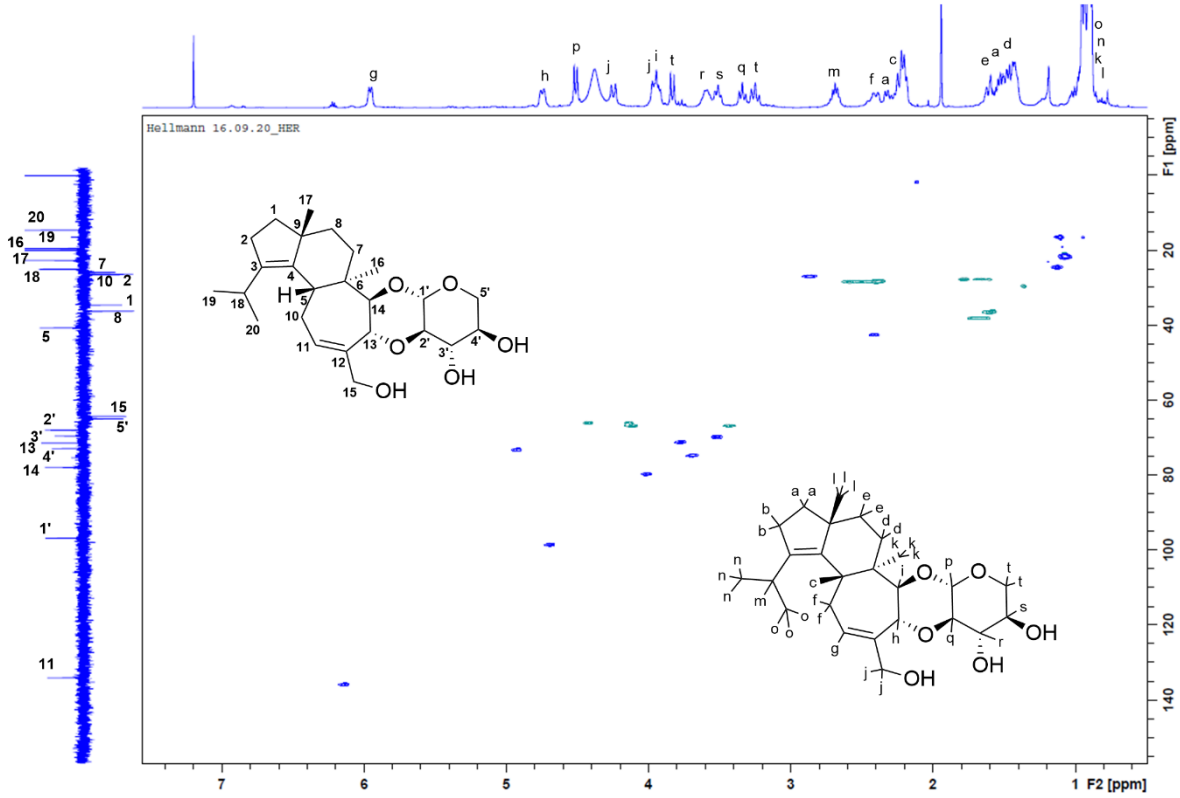

Figure 2-3 2D HETCOR NMR of the collected sample.
Device: Bruker Avance II 400 MHz NMR Spectrometer. Carbon atoms are labelled with letters a-t, hydrogen atoms with numbers 1-20.

Erinacine C: ^{1}H NMR (400 MHz, $CDCl_3$, ppm): δ = 6.01 (br. d, J=7.3 Hz, 1H), 4.81 (br. d, J= 9.7 Hz, 1H), 4.58 (dd, J= 8.6 Hz, 1H), 4.31 (d, J= 11.9 Hz, 2H), 4.OO (d, J = 11.9 Hz, 2H), 3.99 (dd, J= 10.6 Hz, J = 5.4 Hz, 1H), 3.89 (d, J= 9.7 Hz, 1H), 3.63 (m, 1H), 3.56 (dd, J= 8.9 Hz, J= 8.6 Hz, 1H), 3.41 (dd, J= 8. 6 Hz, J= 8.9 Hz, 1H), 3.3l (dd, J= 10.6 Hz, J= 10.9 Hz, 2H), 2.75 (heptet, J= 6.6 Hz, 1H), 2.48 (m, 1H, 2.41(m, 1H), 2.32 (m, 1H), 2.27 (m, 2H), 1.66 (m, 2H), 1.63 (m, 2H), 1.52 (m, 2H), 1.50 (m, 2H), 1.02 (s, 3H), l.00 (s, 2H), 0,97 (d, J= 6.6 Hz, 3H), 0.96 (d, J= 6.6 Hz, 3H)

2.1.4 ESI-MS Micro TOF Characterization of Erinacine C

Using a time-of-flight mass spectrometer HR-MS TOF, the exact mass of m/z = 457.2563 could be determined (Figure 2-4). This is consistent with the theoretically calculated mass of m/z = 457.2650 (Bhandari et al., 2014). This confirmed that the isolated substance is erinacine C.

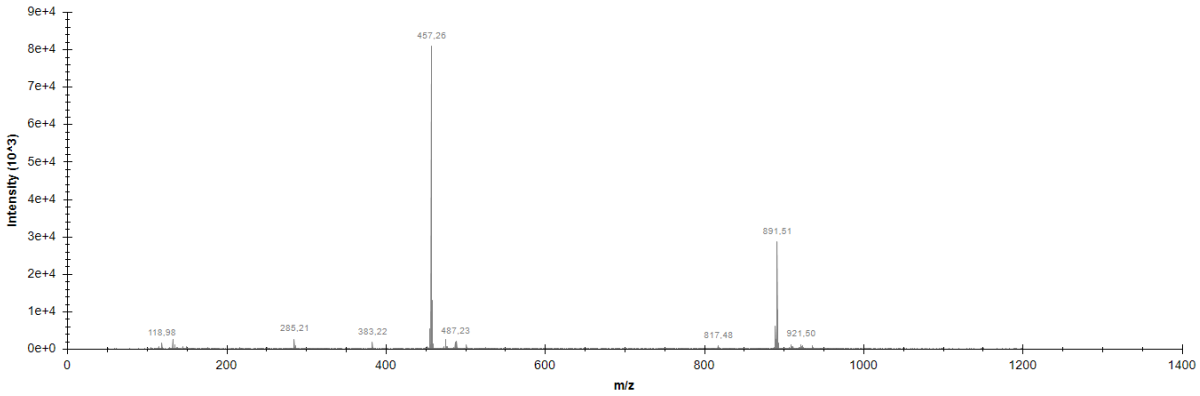

Figure 2-4 High-resolution mass spectrum of erinacine C.

The exact mass of 457.2563 m/z matches the theoretically determined mass of 457.2560. (Instrument: ESI-MS Bruker micro-TOF).

2.2 Effects of erinacine C on metabolic activity in SH-SY5Y cells

The following shows the results of the effect of erinacine C (EC) on viability and metabolic activity in SH-SY5Y cells. Erinacine C was isolated using ethyl acetate, collected using preparative HPLC and characterized using NMR and hr-MS (chapter 2.1). Cells were incubated with erinacine C (0.01 µM, 0.1 µM, 1 µM, 10 µM, 100 µM, 1000 µM) for 24 h. DSMO served as the solvent control. Subsequently, the viability was determined by the reduction of MTT to formazan via absorption (Chapter 5.2.12.1). As described above, the MTT assay generally reflects metabolic and mitochondrial activity based on a mitochondrial NAD(P)H-dependent oxidoreductase. Chapter 2.2.1 shows the effects of erinacine C in SH-SY5Y-MOCK cells, while chapter 2.2.2 shows the effects in SH-SY5Y-APP_{695} cells. The results reveal a model-specific response after treatment with erinacine C. This might also be due to the general viability of the two cell models.

2.2.1 Effects of erinacine C on metabolic activity in SH-SY5Y-MOCK cells

Figure 2-5 shows the effect of different EC concentrations (0.01 µM, 0.1 µM, 1 µM, 10 µM, 100 µM, 1000 µM) on metabolic activity in MOCK cells. Exposure to 10 µM, 100 µM and 1000 µM EC resulted in a strong decrease in the metabolic activity of the cells with statistical relevance ($p < 0.0001$). Lower concentrations showed no effect compared to the control group.

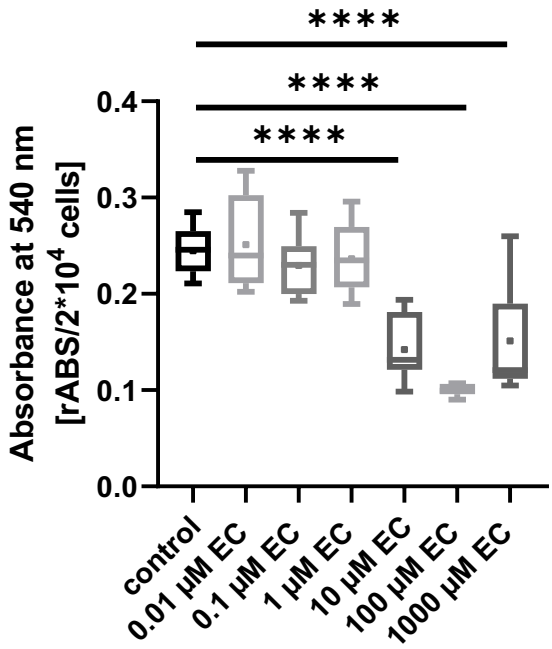

Figure 2-5: Effects of erinacine C on metabolic activity in SH-SY5Y-MOCK cells.
*Metabolic activity in SH-SY5Y-MOCK cells after 24 h incubation with EC (0.01 µM, 0.1 µM, 1 µM, 10 µM, 100 µM, 1000 µM) compared to the control group (DMSO), n = 10. Whiskers indicate minimal and maximal values. The +- sign indicates the mean values. Significance was determined by means of analysis of variance (one-way ANOVA) and Dunnett's multiple comparison post hoc test (****p < 0.0001).*

2.2.2 Effects of erinacine C on metabolic activity in SH-SY5Y-APP$_{695}$ cells

Furthermore, the effect of different EC concentrations on metabolic activity in APP$_{695}$ cells was determined. It is clearly visible that the relative absorbance of the SH-SY5Y-APP$_{695}$-cells is approximately 50% less for the control group compared to the SH-SY5Y-MOCK cells. This reflects the lower viability due to the higher expression of Aβ. Treatment with EC cannot reverse the effect. Here, the higher concentrations also showed a negative impact. However, only 100 µM was statistically significant (p value = 0.0391). The lower concentrations showed a positive trend regarding the median and mean (~22%), but the effect was not significant.

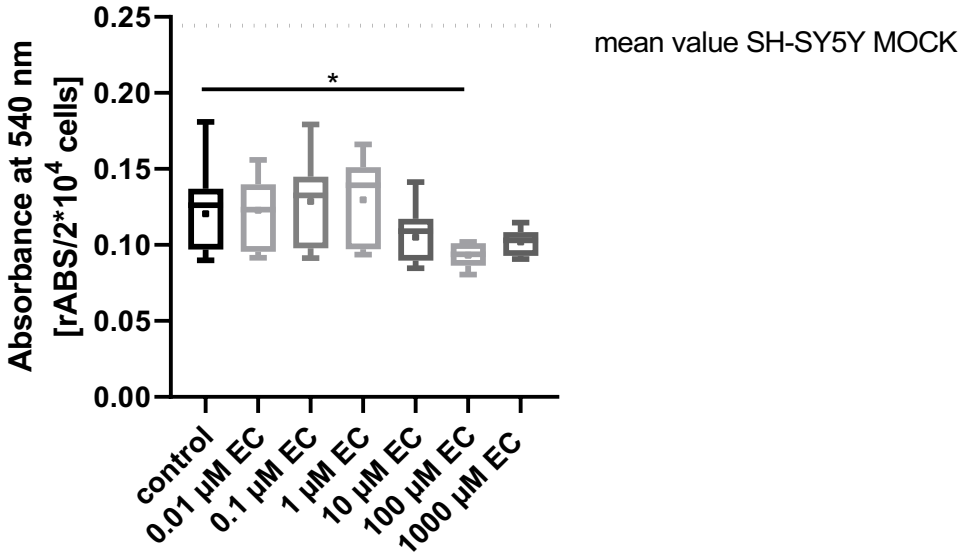

Figure 2-6 Effects of erinacine C on cell viability and proliferation in SH-SY5Y-APP$_{695}$ cells.
Metabolic activity in SH-SY5Y-APP$_{695}$ cells after 24 h incubation with EC (0.01 µM, 0.1 µM, 1 µM, 10 µM, 100 µM, 1000 µM) compared to the control group (DMSO), n = 11. Whiskers indicate minimal and maximal values. The +- sign indicates the mean values. The dotted line shows the mean value of the control group of SH-SY5Y cells (0.2442). Significance was determined by analysis of variance (one-way ANOVA) and Dunnett's multiple comparison post hoc test (* $p < 0.05$).

2.3 Effects of erinacine C on mitochondrial membrane potential in SH-SY5Y cells

The following discusses the results of the effect of EC on MMP in SH-SY5Y cells. The MMP, which drives the generation of ATP, is a key factor for evaluating mitochondrial function. Mitochondrial function is impaired in AD individuals (Swerdlow, 2020). Cells were incubated with EC (0.01 µM, 0.1 µM, 1 µM, 10 µM, 1000 µM) for 24 h. Rotenone was used as an impairment model and was administered 1 hour after EC incubation. DSMO served as the solvent control. Subsequently, the MMP was determined by use of R123 fluorescence as described in Chapter 5.2.12.2. Chapter 2.3.1 shows the effects of erinacine C in SH-SY5Y-MOCK cells, while chapter 2.3.2 shows the effects in SH-SY5Y-APP$_{695}$ cells. Additionally, a potential interaction between EC (1000 µM) and R123 was evaluated by co-incubating both substances in a cell-free medium. Subsequent measurements, based on the MMP protocol, yielded high values, suggesting an interaction between the two substances (data not shown). The effects at 1000 µM

can be visually observed in the provided graphs, offering a comprehensive view of the entire spectrum of effects.

2.3.1 Effects of erinacine C on mitochondrial membrane potential in SH-SY5Y-MOCK cells

Figure 2-7 shows the effects of EC on MMP compared to the control group in MOCK cells without (A) and with (B) rotenone. Only treatment with 100 µM resulted in a significant decrease in MMP ($p = 0.0162$). Treatment with 1000 µM tended to increase MMP ($p = 0.3150$). For treatment with the other concentrations, no effect on the MMP could be recorded (Figure 2-7 A). In the impairment model, incubation with 1000 µM EC caused a significant improvement in MMP ($p < 0.0001$). For treatment with 1 µM EC, a slight increase in MMP tended to be recorded after rotenone impairment ($p = 0.1239$). All other concentrations showed no influence on the MMP in the impairment model compared to the control group (Figure 2-7 B).

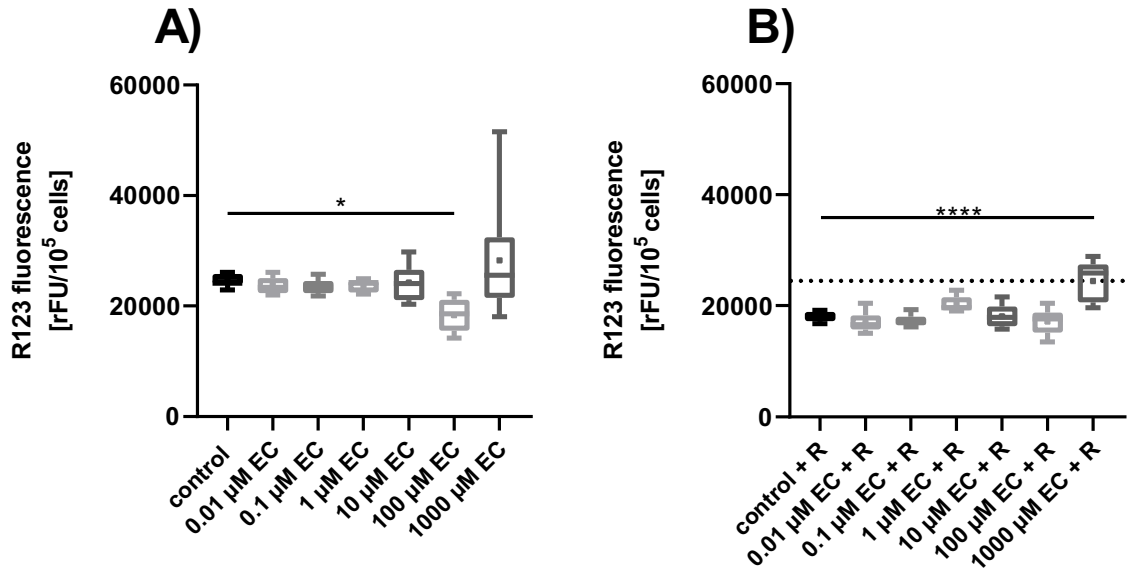

Figure 2-7 Relative MMP fluorescence in SH-SY5Y-MOCK cells after treatment with erinacine C.
*MMP in SH-SY5Y-MOCK cells after 24 h incubation with EC (0.01 µM, 0.1 µM, 1 µM, 10 µM, 100 µM, 1000 µM) compared to the control group (DMSO). Rotenone was administered 1 hour after EC incubation. A) Without rotenone impairment. B) After rotenone impairment. n = 9. Whiskers indicate minimal and maximal values. The +-sign indicates the mean values of each group. The dotted line shows the mean value of the control group without rotenone impairment (24670 rFU/10^5 cells). Significance was determined by analysis of variance (one-way ANOVA) and Dunnett's multiple comparison post hoc test (*p < 0.05; ****p < 0.0001).*

2.3.2 *Effects of erinacine C on mitochondrial membrane potential in SH-SY5Y-APP$_{695}$ cells*

Figure 2-8 shows the effects of EC on MMP compared to the control group in APP$_{695}$ cells without (A) and with (B) rotenone damage. Only treatment with 100 µM resulted in a significant decrease in MMP (p = 0,0215). Treatment with 1000 µM tended to increase MMP (p = 0,3069). Regarding the treatment with the other concentrations, no effect on the MMP could be recorded (Figure 2-8 A). In the impairment model, incubation with 1000 µM EC caused a significant improvement in MMP (p < 0.0001). All other concentrations showed no influence on the MMP in the impairment model compared to the control group (Figure 2-8 B).

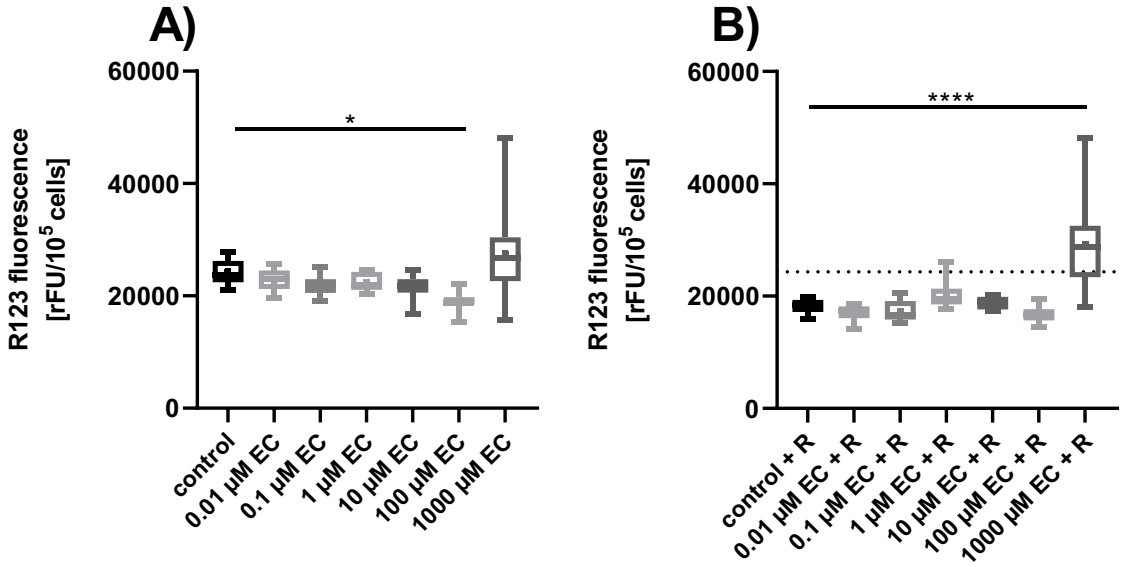

Figure 2-8 Effects of erinacine C on MMP in SH-SY5Y-APP$_{695}$ cells.
*MMP in SH-SY5Y-APP$_{695}$ cells after 24 h incubation with EC (0.01 µM, 0.1 µM, 1 µM, 10 µM, 100 µM, 1000 µM) compared to the control group (DMSO). Rotenone was administered 1 hour after EC incubation. A) Without rotenone impairment. B) After rotenone impairment. n = 9. Whiskers indicate minimal and maximal values. The +-sign indicates the mean values of each group. The dotted line shows the mean value of the control group without rotenone impairment (24332s rFU/10^5 cells). Significance was determined by analysis of variance (one-way ANOVA) and Dunnett's multiple comparison post hoc test (*p < 0.05; ****p < 0.0001).*

2.4 Effects of erinacine C on ATP levels in SH-SY5Y cells

Mitochondria generate the major energy source of neurons: ATP. Nevertheless, mitochondria in AD patients and models are affected by increased oxidative stress. This leads to a reduction in ATP production and to a lack of energy for neurons. To evaluate the effect of EC on ATP levels in SH-SY5Y cells, they were incubated for 24 h with EC (0.1 µM, 1 µM, 10 µM, 100 µM, 1000 µM) or the solvent control (DMSO). Additional impairment was induced with rotenone. It inhibits complex I of the mitochondrial electron transport chain, leading to increased oxidative stress, impaired energy metabolism, and altered calcium homeostasis. By inducing mitochondrial dysfunction, rotenone can mimic many features of AD, helping to investigate the relationship between mitochondrial impairment and AD progression (Stockburger et al., 2014). Subsequently, bioluminescence was measured as described in Chapter 5.2.12.3. Chapter 2.4.1 shows the effects of erinacine C in SH-SY5Y-MOCK cells, while chapter 2.4.2 displays the effects in SH-SY5Y-APP_{695} cells.

2.4.1 Effects of erinacine C on ATP levels in SH-SY5Y-MOCK cells

Figure 2-9 shows the effect of treatment with EC in MOCK cells without (A) and with (B) rotenone impairment compared to the control group (DMSO). Treatment with 100 µM and 1000 µM EC resulted in a significant strong decrease in ATP levels almost to the zero level (0 µM) in both cases ($p < 0.0001$). However, incubation with 0.1 µM ($p = 0.0483$) and 1 µM EC ($p = 0.0128$) resulted in a significant increase in ATP levels (Figure 2-9 A). This effect was also observed in the impairment model (0.1 µM EC: $p = 0.0217$, 1 µM EC ($p = 0.0215$) (Figure 2-9 B). Treatment with 10 µM EC had no effect on ATP concentrations both without and under rotenone impairment.

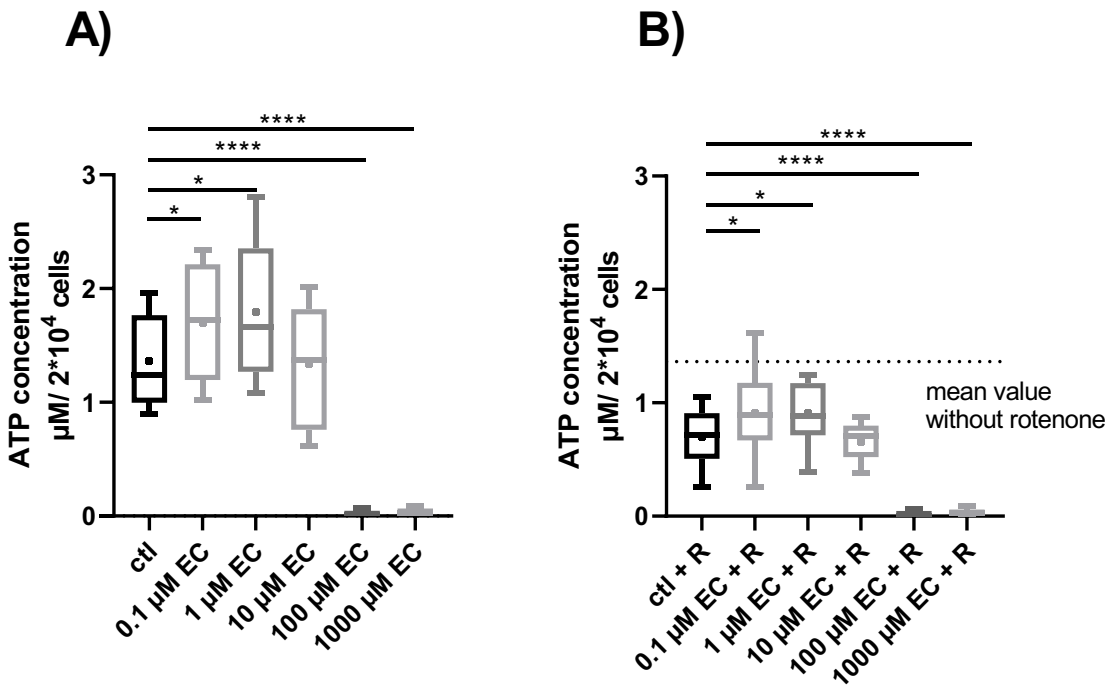

Figure 2-9 Effects of erinacine C on ATP levels in SH-SY5Y-MOCK cells.
ATP levels in SH-SY5Y-MOCK cells after 24 h incubation with EC (0.1 µM, 1 µM, 10 µM, 100 µM, 1000 µM) compared to the control group (DMSO). Rotenone was administered 1 hour after EC incubation. A) Without rotenone impairment. B) After rotenone impairment. Control: n = 13; 0.1 µM EC: n = 13; 1 µM EC: n=13; 10 µM EC: n=10; 100 µM EC: n=10; 1000 µM EC: n= 10. Whiskers indicate minimal and maximal values. The +- sign indicates the mean values of each group. The dotted line shows the mean value of the control group without rotenone impairment (1.363 µM $^{ATP/2*104}$ cells). Significance was determined by analysis of variance (one-way ANOVA) with FDR adjustment ($p < 0.05$. **** $p < 0.0001$).*

2.4.2 Effects of erinacine C on ATP levels in SH-SY5Y-APP$_{695}$ cells

The decrease in ATP levels recorded in MOCK cells after treatment with 100 and 1000 µM EC was also confirmed in APP$_{695}$ cells. As shown in Figure 2-10, exposure of the cells to these concentrations both without (A) and under (B) rotenone impairment also resulted in a significant sharp drop in ATP levels (0 µM) ($p < 0.0001$). In addition, treatment with 10 µM EC resulted in a significant decrease in ATP levels in the impairment model ($p < 0.0001$). This significance was lacking in the absence of rotenone impairment, but a trend of reduction was evident ($p = 0.1300$). In contrast, treatment with 0.1 µM ($p = 0.0225$) and 1 µM ($p = 0.0026$) EC caused a significant increase in ATP levels compared to the control group (see Figure 2-10 A). Even under rotenone impairment, these concentrations tended to lead to slightly increased

ATP concentrations without statistical relevance (0.01 µM EC + R: p = 0.0986, 1 µM EC + R: p = 0.1433) (Figure 2-10 B).

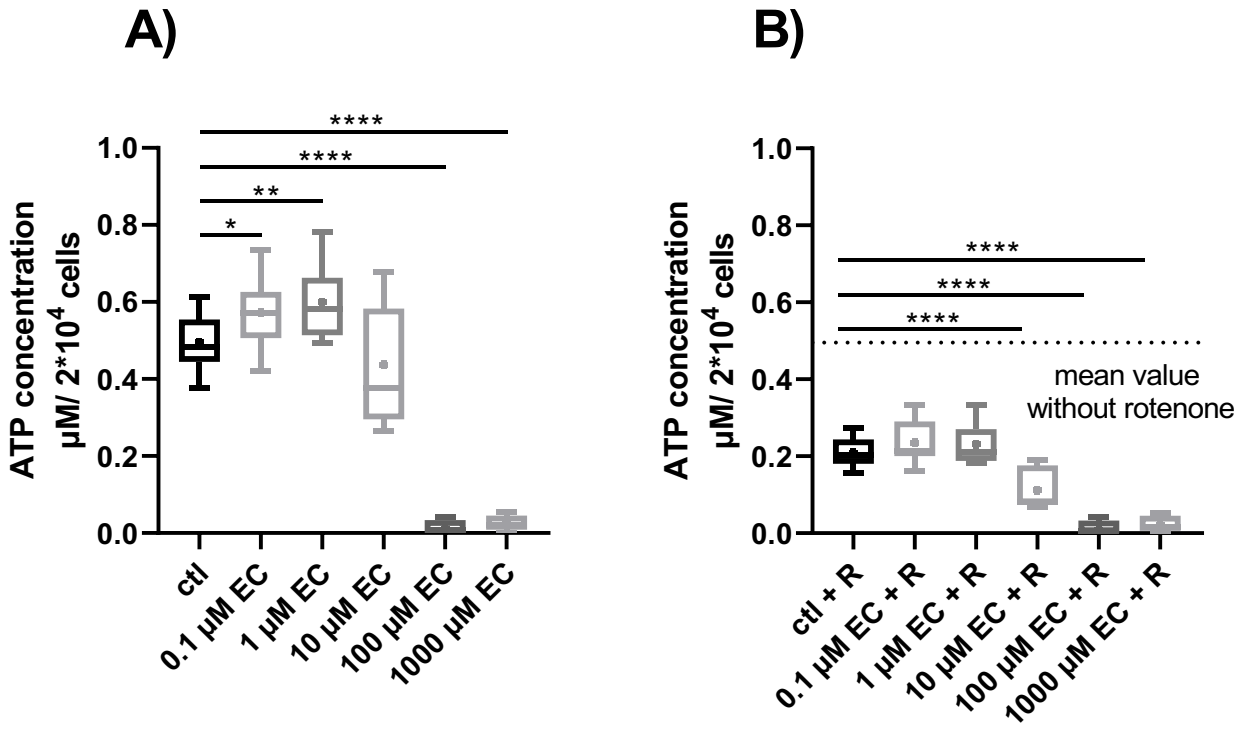

Figure 2-10 Effects of erinacine C on ATP levels in SH-SY5Y-APP$_{695}$ cells.
*ATP levels in SH-SY5Y-APP$_{695}$ cells after 24 h incubation with EC (0.1 µM, 1 µM, 10 µM, 100 µM, 1000 µM) compared to the control group (DMSO). Rotenone was administered 1 hour after EC incubation. A) Without rotenone impairment. B) After rotenone impairment. Control (n = 15), 0.1 µM EC (n = 15); 1 µM EC (n = 15); 10 µM EC (n = 9); 100 µM EC (n = 9); 1000 µM EC (n = 9). Whiskers indicate minimal and maximal values. The +- sign indicates the mean values of each group. The dotted line shows the mean value of the control group without rotenone impairment (0.4951 µM ATP/2*104 cells). Significance was determined by analysis of variance (one-way ANOVA) with FDR adjustment (* p < 0.05. ** p < 0.01. **** p < 0.0001).*

2.5 Effects of erinacine C on mitochondrial respiration

Given the increase in ATP levels, the next step involved investigating the endogenous respiration and the respiratory capacity of the individual complexes of the respiratory chain. This was accomplished in real time using an O_2 oxygen electrode. Mitochondrial respiration was assessed after 24 h incubation with 1 µM erinacine C, this concentration was chosen due to the highest

effect on the ATP-level. Figure 2-11 shows the effect on SH-SY5Y-MOCK and Figure 2-12 the effect on SH-SY5Y-APP_{695} with incubation of 1 µM erinacine C compared against the control group. For both cell lines, there were no significant differences detectable. However, both cell lines show higher O_2 consumption in the mean values.

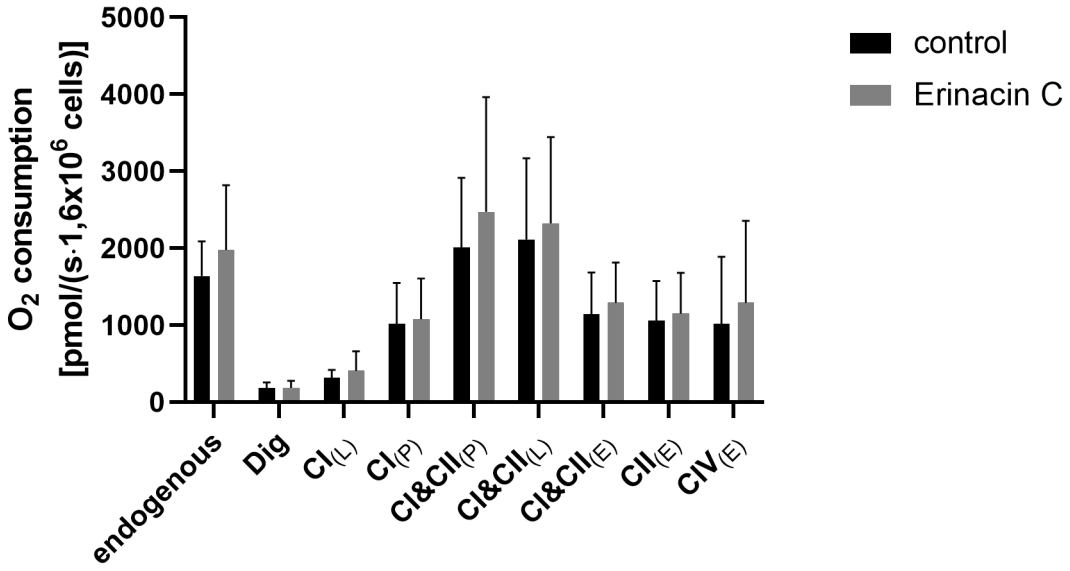

Figure 2-11 Effects of 1 µM erinacine C on mitochondrial respiration in SH-SY5Y-MOCK cells.
O_2 consumption of SH-SY5Y-MOCK cells with 1 µM erinacine C and solvent control (DMSO); values were normalized to cell number; all values are displayed as the mean ± SD, control n = 9, 1 µM erinacine C n = 9; endogenous cell respiration (endogenous), respiration of permeabilized cells after digitonin addition (Dig), leak respiration of complex I (CI(L)), activity of complex I (CI(P)), activities of complex I + II (CI&CII(P)), leak respiration of complex I + II (CI&CII(L)), decoupled activity of complexes I + II (CI&CII(E)), decoupled activity of complex II (CII(E)), decoupled activity of complex IV (CIV(E)).

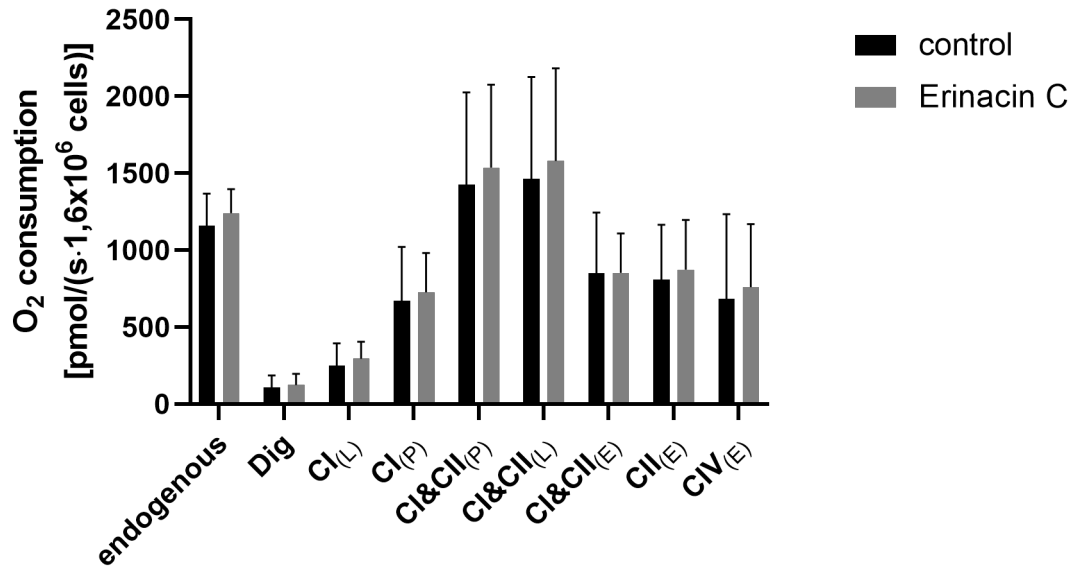

Figure 2-12 Effects of 1 µM erinacine C on mitochondrial respiration in SH-SY5Y-APP$_{695}$ cells.
O_2 consumption of SH-SY5Y-MOCK cells with 1 µM erinacine C and solvent control (DMSO); values were normalized to cell number; all values are displayed as the mean ± SD, control n = 9, 1 µM erinacine C, n = 9; endogenous cell respiration (endogenous), respiration of permeabilized cells after digitonin addition (Dig), leak respiration of complex I (CI(L)), activity of complex I (CI(P)), activities of complex I + II (CI&CII(P)), leak respiration of complex I + II (CI&CII(L)), decoupled activity of complexes I + II (CI&CII(E)), decoupled activity of complex II (CII(E)), decoupled activity of complex IV (CIV(E)).

2.6 Oxidative stress in SH-SY5Y cells

To assess the oxidative stress effects of H_2O_2, a range of concentrations was tested. SH-SY5Y-cells were incubated with H_2O_2 (10 µM, 25 µM, 50 µM, 75 µM. 100 µM, 150 µM, 200 µM, 250 µM) for 24 h. H_2O served as the solvent control. The response to oxidative stress was assessed using an MTT assay (Chapter 5.2.12.1).

2.6.1 Effects of H_2O_2 in SH-SY5Y-MOCK cells

Figure 2-13 shows the effect of H_2O_2 on the viability of SH-SY5Y-MOCK cells. Ranging from 75 µM to 250 µM, the viability decreased significantly. The values decreased by 30% to 60% compared to the control group.

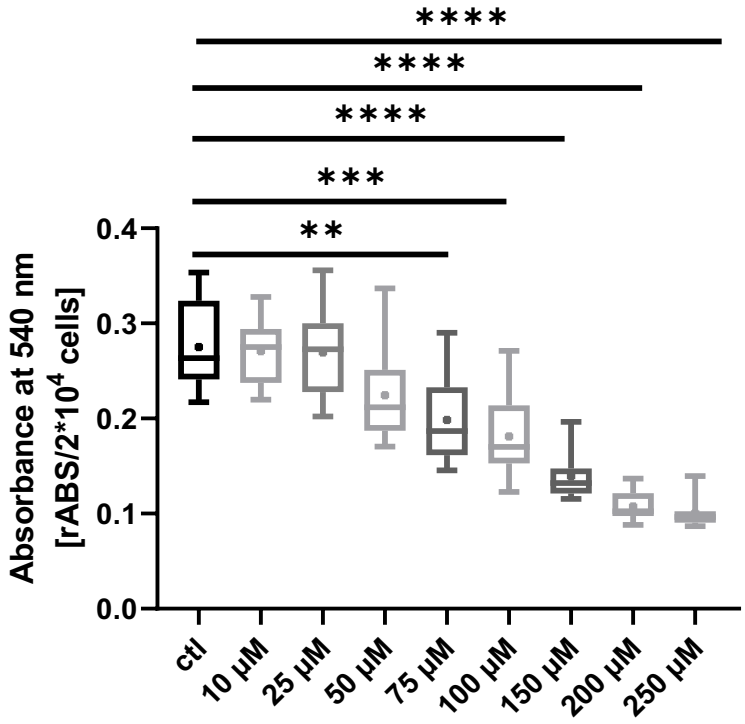

Figure 2-13 Effects of H_2O_2 on cell viability and proliferation in SH-SY5Y-MOCK cells.
Metabolic activity in SH-SY5Y-MOCK cells after 24 h incubation with H_2O_2 (10 µM, 25 µM, 50 µM, 100 µM, 150 µM, 200 µM, 250 µM) compared to the control group (H_20), n = 8. Whiskers indicate minimal and maximal values. The +- sign indicates the mean values. Significance was determined by analysis of variance (one-way ANOVA) and Dunnett's multiple comparison post hoc test ($p < 0.05$).*

2.6.2 Effects of H2O2 on SH-SY5Y-APP$_{695}$ cells

Figure 2-14 shows the effect of H_2O_2 on the viability of SH-SY5Y-APP$_{695}$ cells. Ranging from 50 µM to 250 µM, the viability decreased significantly. The values decreased by 20% to 50% compared to the control.

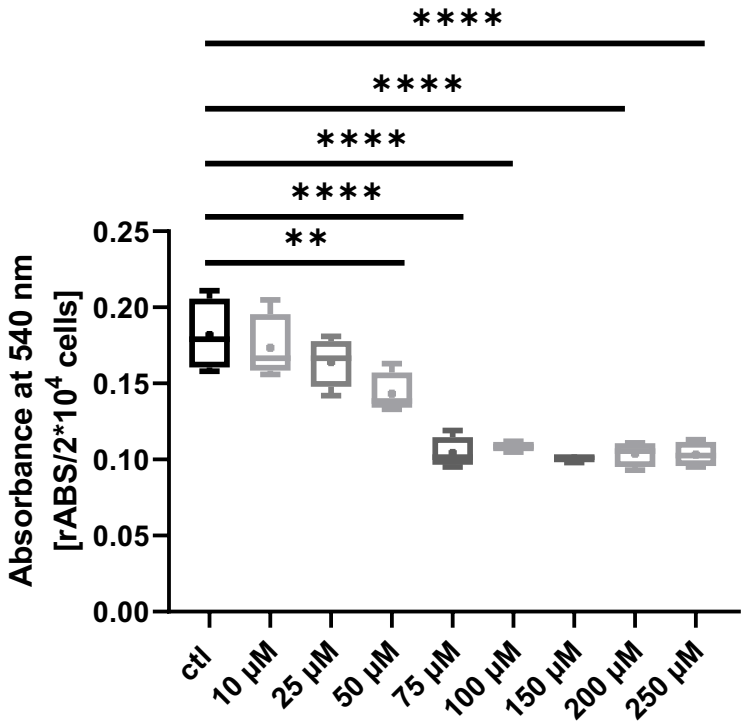

Figure 2-14 Effects of H_2O_2 on cell viability and proliferation in SH-SY5Y-APP_{695} cells.
Metabolic activity in SH-SY5Y-APP_{695} cells after 24 h incubation with H_2O_2 (10 µM, 25 µM, 50 µM, 100 µM, 150 µM, 200 µM, 250 µM) compared to the control group (H_20), n = 8. Whiskers indicate minimal and maximal values. The +- sign indicates the mean values. Significance was determined by analysis of variance (one-way ANOVA) and Dunnett's multiple comparison post hoc test ($p < 0.05$).*

2.6.3 Effects of erinacine C in SH-SY5Y-MOCK cells under oxidative stress

To assess the effects of erinacine C under oxidative stress, concentrations of 50 and 75 µM H_2O_2 were tested with cotreatment of erinacine C (0.1 µM, 1 µM and 10 µM). The previous experiment showed a decrease of 20 – 30% of viability for 50 and 75 µM H_2O_2 (Figure 2-13). Cotreatment did not significantly improve viability, but treatment with 1 µM erinacine improved viability by up to 16% (p value = 0.0940). Treatment with 10 µM cotreatment was statistically significant (p value < 0.0001) and further decreased viability (Figure 2-15).

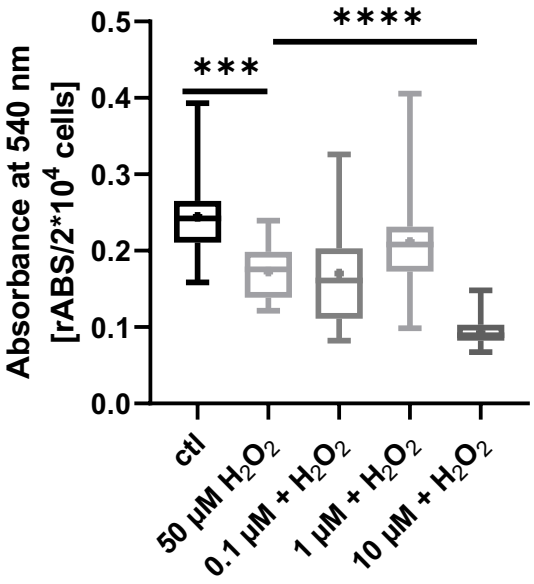

*Figure 2-15 Effects of H_2O_2 and erinacine C on cell viability and proliferation in SH-SY5Y-MOCK cells. Metabolic activity in SH-SY5Y-MOCK cells after 24 h incubation with H_2O_2 (50 µM) and erinacine C (0.1 µM, 1 µM, 10 µM) compared to the control group (DMSO), ctl n = 19, 0 n = 17, 0.1 µM n = 18, 1 µM n = 19, 10 µM n = 19. Whiskers indicate minimal and maximal values. The +- sign indicates the mean values. Significance was determined by analysis of variance (one-way ANOVA) and Dunnett's multiple comparison post hoc test (*** p < 0.001, **** p < 0.0001).*

Figure 2-16 shows the effect of 75 µM H_2O_2 with erinacine C cotreatment. Erinacine C (0.1 µM and 1 µM) ameliorated the effects of 75 µM H_2O_2 by 10 and 15%, respectively. 1 µM was statistically significant positive (p value = 0.0247), whereas 10 µM further statistically significant decreased (p value = 0.0036) the viability.

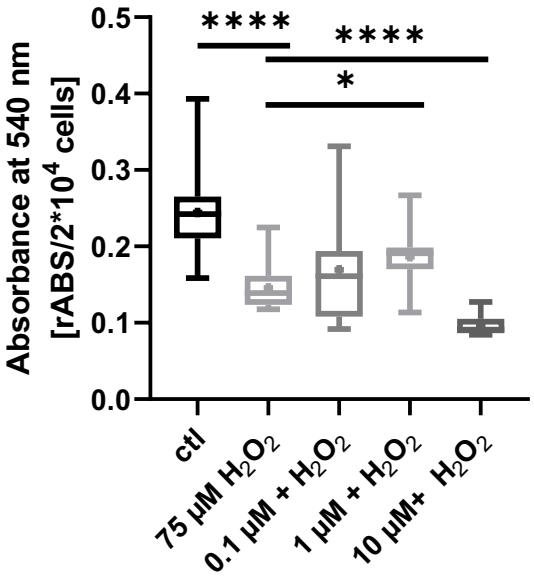

Figure 2-16 Effects of H_2O_2 and erinacine C on cell viability and proliferation in SH-SY5Y-MOCK cells. Metabolic activity in SH-SY5Y-MOCK cells after 24 h incubation with H_2O_2 (75 µM) and erinacine C (0.1 µM, 1 µM, 10 µM) compared to the control group (DMSO), ctl n = 19, 0 n = 17, 0.1 µM n = 19, 1 µM n = 18, 10 µM n = 18. Whiskers indicate minimal and maximal values. Significance was determined by analysis of variance (one-way ANOVA) and Dunnett's multiple comparison post hoc test (p < 0.05, **** p < 0.0001).*

2.6.4 Effects of erinacine C on SH-SY5Y-APP$_{695}$ cells under oxidative stress

To evaluate the effects of erinacine C under oxidative stress, concentrations of 50 and 75 µM H_2O_2 were tested with cotreatment of erinacine C (0.1 µM, 1 µM and 10 µM) in SH-SY5Y-APP$_{695}$ cells. The previous experiment showed a decrease to 79 – 57% viability for 50 and 75 µM H_2O_2 (Figure 2-14). The cotreatment could not improve the viability compared to the group with 50 µM H_2O_2. All groups showed a statistically significant decrease in viability. Figure 2-17 shows a further decrease in viability of 10 to 20% compared to treatment with 50 µM H_2O_2.

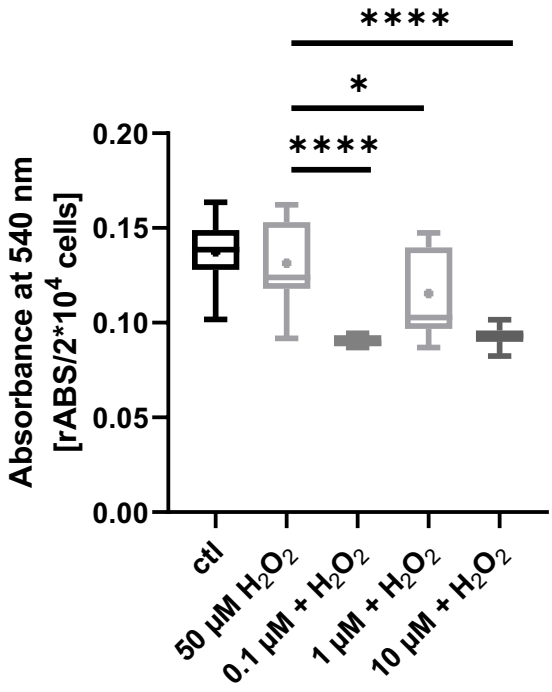

Figure 2-17 Effects of H_2O_2 and erinacine C on cell viability and proliferation in SH-SY5Y-APP$_{695}$ cells. Metabolic activity in SH-SY5Y-APP$_{695}$ cells after 24 h incubation with H_2O_2 (50 µM) and erinacine C (0.1 µM, 1 µM, 10 µM) compared to the control group (DMSO), n = 15. Whiskers indicate minimal and maximal values. Significance was determined by analysis of variance (one-way ANOVA) and Dunnett's multiple comparison post hoc test ($p < 0.05$, **** $p < 0.0001$).*

Figure 2-18 shows the effect of 75 µM H_2O_2 with erinacine C cotreatment. Erinacine C (0.1 µM and 10 µM) further decreased the effects of 75 µM H_2O_2 by 18 and 16%, respectively. 1 µM showed no effect.

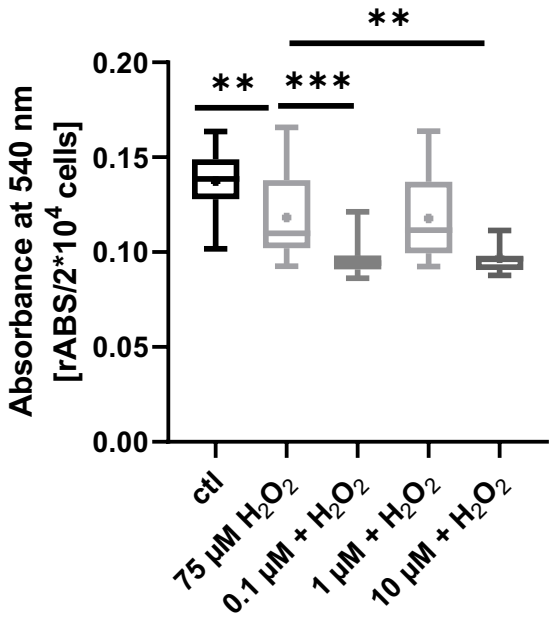

*Figure 2-18 Effects of H_2O_2 and erinacine C on cell viability and proliferation in SH-SY5Y-APP$_{695}$ cells. Metabolic activity in SH-SY5Y-APP$_{695}$ cells after 24 h incubation with H_2O_2 (75 µM) and erinacine C (0.1 µM, 1 µM, 10 µM) compared to the control group (DMSO), n = 15. Whiskers indicate minimal and maximal values. Significance was determined by analysis of variance (one-way ANOVA) and Dunnett's multiple comparison post hoc test (** $p < 0.01$, *** $p < 0.001$).*

2.7 Effects of erinacine C on mRNA Expression in SH-SY5Y cells

The effect of EC on the expression of specific AD-associated genes in SH-SY5Y cells was also investigated in this work. Based on the results regarding ATP levels and cell viability, concentrations of 0.1 µM and 1 µM EC were used for this purpose. DMSO was used as a solvent control. SH-SY5Y cells were incubated for 24 h with the listed EC concentrations or DMSO. This was followed by isolation of RNA, synthesis of cDNA and finally the actual RT–qPCRqPCR (Chapter 5.2.12.4). The genes examined included ATP5D, NRF1, SIRT1, TFAM, and CREB1.

2.7.1 Effects of erinacine C on ATP5D in SH-SY5Y cells

ATP5D encodes a subunit of the mitochondrial ATP synthase and is related to the respiratory electron transport system (Oláhová et al., 2018). Given the observed elevation in ATP levels, it

would be worthwhile to investigate the mRNA expression levels of ATP5D, a key subunit of ATP synthase, to elucidate the underlying molecular mechanisms.

In SH-SY5Y-MOCK cells, ATP5D was significantly reduced at 0.1 µM (p value = 0.0408) and 1 µM (p value < 0.0001). 1 µM reduced the expression of ATP5D even more than 0.1 µM (~50%). Similar results were observed in SH-SY5Y-APP$_{695}$ cells. 0.1 µM (p value < 0.0001) and 1 µM (p value < 0.0001) also had a significant adverse effect on ATP5D expression (Figure 2-19).

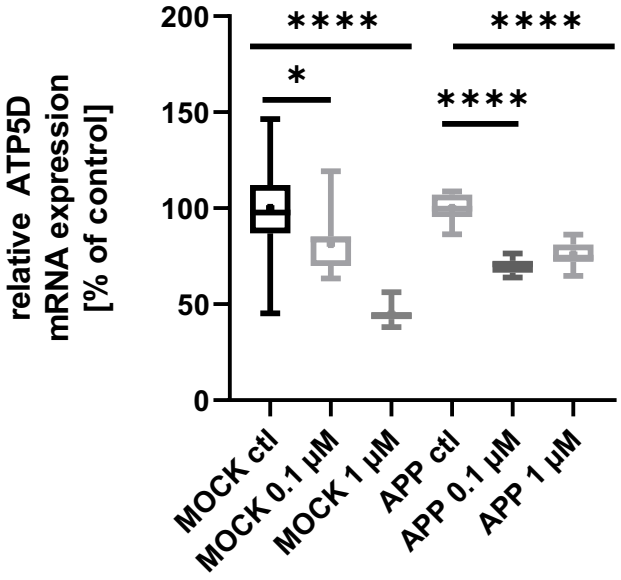

Figure 2-19 Relative ATP5D mRNA levels after treatment with erinacine C in SH-SY5Y-MOCK cells and SH-SY5Y-APP$_{695}$ cells.

Relative mRNA expression after 24 h of incubation with 0.01 µM and 1 µM erinacine C in SH-SY5Y-MOCK cells and SH-SY5Y-APP$_{695}$ cells. n = 1; Whiskers indicate minimal and maximal values. The +- sign indicates the mean values. The results were normalized to the mRNA expression levels of three housekeeping genes (beta-actin (ACTβ), glyceraldehyde 3-phosphate dehydrogenase (GAPDH) and phosphoglycerate kinase 1 (PGK1) according to the MIQE guidelines. Significance was determined by analysis of variance (one-way ANOVA) and Dunnett's multiple comparison post hoc test (∗p < 0.05, ∗∗p < 0.01, ∗∗∗∗p < 0.0001).

2.7.2 Effects of erinacine C on NRF1 in SH-SY5Y cells

Nuclear respiratory factor 1 (NRF1) encodes a protein that activates the expression of some key metabolic genes regulating cellular growth and nuclear genes required for respiration and mitochondrial DNA transcription. It is also associated with the regulation of neurite outgrowth. Furthermore, it is related to pathways connected to mitochondrial gene expression and organelle biogenesis and maintenance (Kiyama et al., 2018). Considering the positive changes observed

in the vitality parameters and the reduction in oxidative stress, it would be valuable to explore the role of NRF1.

In SH-SY5Y-MOCK cells, 1 µM erinacine C revealed a statistically positive effect (p value = 0.0015). For SH-SY5Y-APP$_{695}$, both concentrations, 0.1 µM (p value =0.0002) and 1 µM (p value = 0.0104), significantly elevated the expression of NRF1. However, 0.1 µM was stronger in its effect (Figure 2-20).

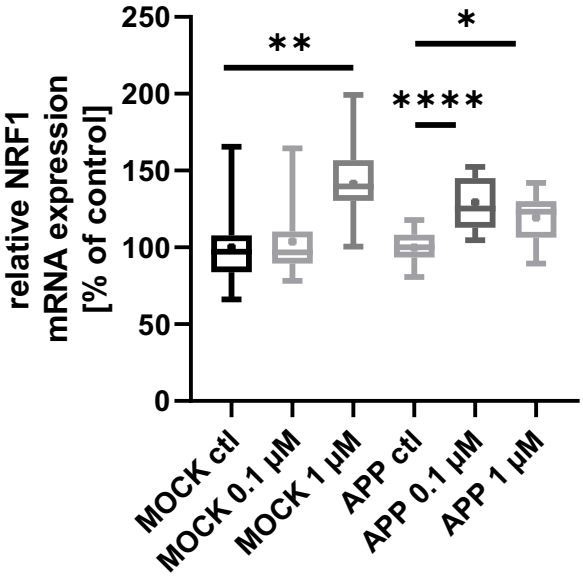

Figure 2-20 Relative NRF1 mRNA levels after treatment with erinacine C in SH-SY5Y-MOCK cells and SH-SY5Y-APP$_{695}$ cells.

Relative mRNA expression after 24 h of incubation with 0.01 µM and 1 µM erinacine C in SH-SY5Y-MOCK cells and SH-SY5Y-APP$_{695}$ cells. n = 11; whiskers indicate minimal and maximal values. The results were normalized to the mRNA expression levels of three housekeeping genes (beta-actin (ACTβ), glyceraldehyde 3-phosphate dehydrogenase (GAPDH) and phosphoglycerate kinase 1 (PGK1)) according to the MIQE guidelines. Significance was determined by analysis of variance (one-way ANOVA) and Dunnett's multiple comparison post hoc test (∗p < 0.05, ∗∗p < 0.01, ∗∗∗∗p < 0.0001).

2.7.3 Effects of erinacine C on SIRT1 in SH-SY5Y cells

NAD-dependent protein deacetylase sirtuin-1 (SIRT1) encodes a member of the sirtuin family of proteins. Although their effect is not clear in humans, in yeast, sirtuins are known to regulate gene silencing. It is associated with the longevity regulating pathway and AMP-activated protein kinase (AMPK) signalling (Autiero et al., 2009). In light of the improvements in vitality parameters and the attenuation of oxidative stress, it is intriguing to investigate the involvement of SIRT1. In SH-SY5Y-MOCK cells, treatment with 1 µM erinacine C significantly elevated (p value < 0.0001) the levels of SIRT1. The effect was profound and 85% above the control

group. For SH-SY5Y-APP$_{695,}$ the opposite was detected. The expression was significantly lower for 0.1 µM (p value < 0.0001) and 1 µM (p value < 0.0001) compared to the control group (Figure 2-21).

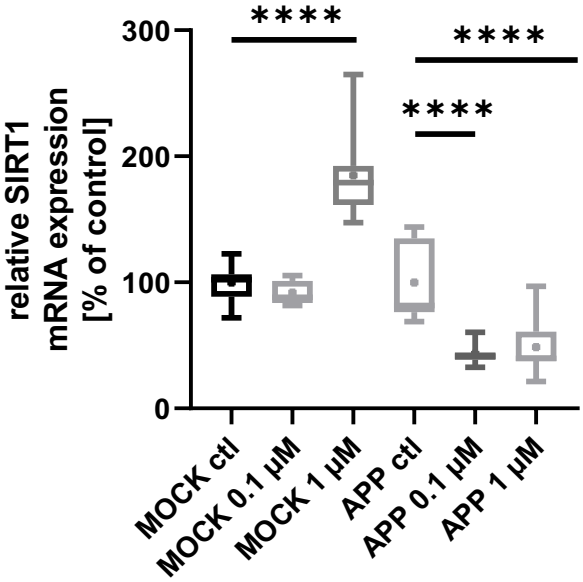

Figure 2-21 Relative SIRT1 mRNA levels after treatment with erinacine C in SH-SY5Y-MOCK cells and SH-SY5Y-APP$_{695}$ cells.

*Relative mRNA expression after 24 h of incubation with 0.01 µM and 1 µM erinacine C in SH-SY5Y-MOCK cells and SH-SY5Y-APP$_{695}$ cells; n = 11. Whiskers indicate minimal and maximal values. The +- sign indicates the mean values. The results were normalized to the mRNA expression levels of three housekeeping genes (beta-actin (ACTβ), glyceraldehyde 3-phosphate dehydrogenase (GAPDH) and phosphoglycerate kinase 1 (PGK1)) according to the MIQE guidelines. Significance was determined by analysis of variance (one-way ANOVA) and Dunnett's multiple comparison post hoc test (**** p < 0.0001); n = 11.*

2.7.4 Effects of erinacine C on TFAM in SH-SY5Y cells

Mitochondrial transcription factor 1 (TFAM) encodes proteins that function in mitochondrial DNA replication and repair. It is associated with mitochondrial gene expression and organelle biogenesis and maintenance (Kang et al., 2018). Observing the increased ATP levels, coupled with enhancements in vitality parameters and a decrease in oxidative stress, it would be valuable to investigate the involvement of TFAM (mitochondrial transcription factor A) in order to further comprehend the underlying molecular mechanisms at play. For SH-SY5Y-MOCK, 1 µM erinacine C significantly elevated (p value = 0.0003) the levels of TFAM. The reverse was observed in SH-SY5Y-APP$_{695}$ cells. 0.1 µM (p value < 0.0001) and 1 µM (p value < 0.0001) significantly decreased the expression (Figure 2-22).

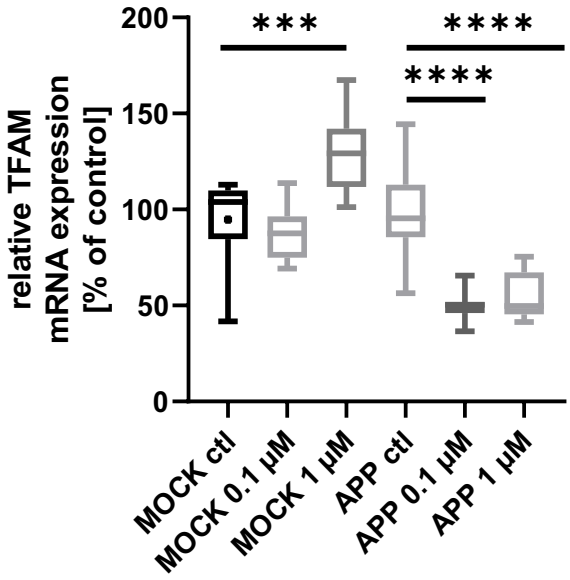

Figure 2-22 Relative TFAM mRNA levels after treatment with erinacine C in SH-SY5Y-MOCK cells and SH-SY5Y-APP$_{695}$ cells.

*Relative mRNA expression after 24 h of incubation with 0.01 µM and 1 µM erinacine C in SH-SY5Y-MOCK cells and SH-SY5Y-APP$_{695}$ cells; n = 11. Whiskers indicate minimal and maximal values. The +- sign indicates the mean values. The results were normalized to the mRNA expression levels of three housekeeping genes (beta-actin (ACTβ), glyceraldehyde 3-phosphate dehydrogenase (GAPDH) and phosphoglycerate kinase 1 (PGK1)) according to the MIQE guidelines. Significance was determined by analysis of variance (one-way ANOVA) and Dunnett's multiple comparison post hoc test (**** p < 0.0001); n = 11.*

2.7.5 Effects of erinacine C on CREB1 in SH-SY5Y cells

Cyclic AMP-Responsive Element-Binding Protein 1 is a phosphorylation-dependent transcription factor that promotes transcription upon binding to the DNA cAMP response element (CRE). PI3K/AKT activation is relevant to the related pathways (H. Wang et al., 2018). In the context of increased ATP levels, enhanced vitality parameters, and reduced oxidative stress are noteworthy for several reasons. Investigating the role of CREB1 in these circumstances could provide insights into the molecular mechanisms responsible for the observed improvements. Erinacine C showed no effect in SH-SY5Y-MOCK cells. For SH-SY5Y-APP$_{695,}$ an adverse effect was identified for 0.1 µM (p value < 0.0001) and 1 µM (p value < 0.0001) (Figure 2-23).

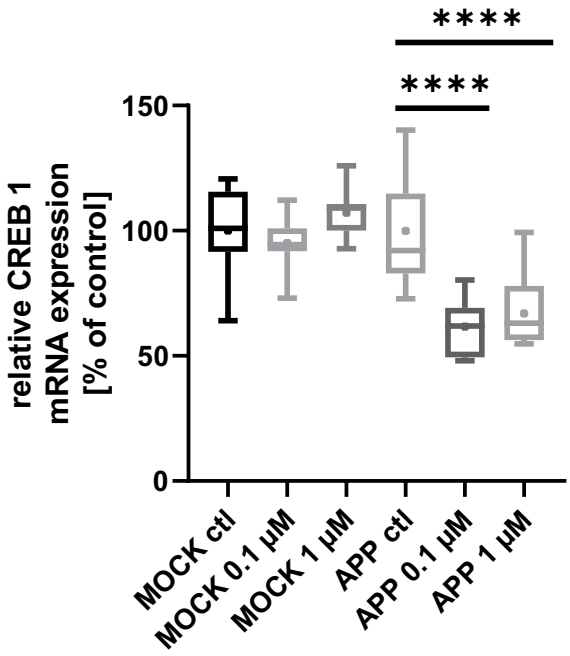

Figure 2-23 Relative CREB1 mRNA levels after treatment with erinacine C in SH-SY5Y-MOCK cells and SH-SY5Y-APP$_{695}$ cells.

Relative mRNA expression after 24 h of incubation with 0.01 µM and 1 µM erinacine C in SH-SY5Y-MOCK cells and SH-SY5Y-APP$_{695}$ cells; n = 11. Whiskers indicate minimal and maximal values. The +- sign indicates the mean values. The results were normalized to the mRNA expression levels of three housekeeping genes (beta-actin (ACTβ), glyceraldehyde 3-phosphate dehydrogenase (GAPDH) and phosphoglycerate kinase 1 (PGK1)) according to the MIQE guidelines. Significance was determined by analysis of variance (one-way ANOVA) and Dunnett's multiple comparison post hoc test (∗p < 0.05, ∗∗p < 0.01, ∗∗∗p < 0.001).

2.8 Effects of erinacine C on neurite growth in SH-SY5Y cells

Based on the results of RT qPCR, the effect of EC on neurite growth in SH-SY5Y cells was investigated in the present research work. For this purpose, concentrations of 0.1 µM and 1 µM EC were used. To assess the effect on neuritogenesis, SH-SY5Y cells were stimulated to differentiate with retinoic acid and then incubated with EC or the solvent control. Following haematoxylin-eosin staining, light microscopy images were used to determine the average neurite length (Chapter 5.2.12.7). Since Alzheimer's disease primarily affects the health and resilience of neuronal neurons, the outgrowth and bearing of new neuronal connections can reduce the symptoms of Alzheimer's and can reduce the progression of the disease.

The effect of EC on average neurite length compared to the control group in SH-SY5Y-MOCK is shown in Figure 2-24 (A). Treatment with 0.1 µM EC tended to increase the average neurite

length compared to the control group, but this did not reach statistical relevance (p = 0.0952). In contrast, the influence of treatment with 1 µM EC was statistically significant (p < 0.0001). For this treatment group, a prolongation of the average neurite length to approximately 200% of the control was recorded. Using the ROUT outlier test, two outliers were excluded (Q= 1%). Although the treatment with 1 µM shows a statistically relevant effect, one must note here that the data show a huge range in variation. The minimal value of the treatment group is even below the median and mean of the control group.

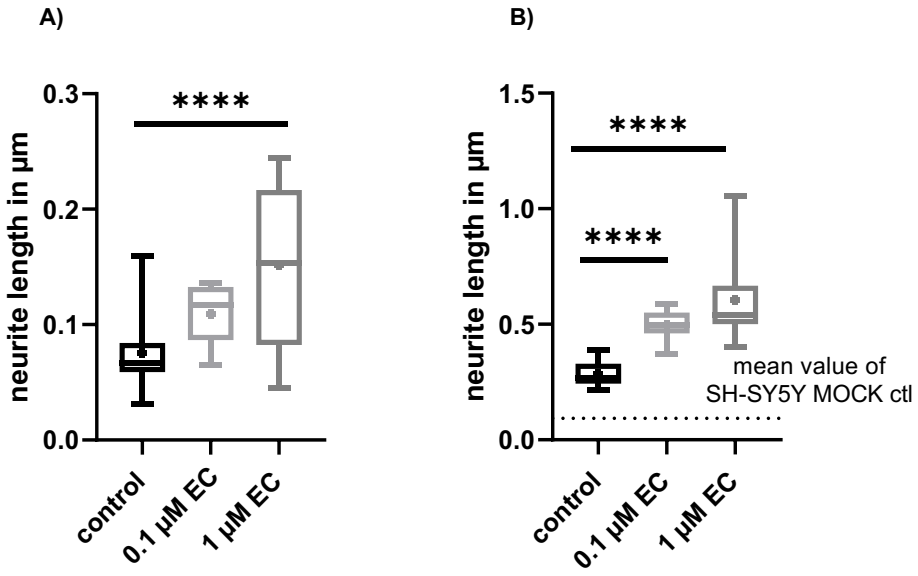

Figure 2-24 Effects of erinacine C on neuritogenesis in SH-SY5Y cells.
*Average neurite length in SH-SY5Y-MOCK (A) cells after incubation with EC (0.1 µM, 1 µM) compared to the control group (DMSO). control: n = 15; 0.1 µM EC: n = 15; 1 µM EC: n = 16. Whiskers indicate minimal and maximal values. Significance was determined by analysis of variance (one-way ANOVA) and Dunnett's multiple comparison post hoc test. **** p < 0.0001. Average neurite length in SH-SY5Y-APP$_{695}$ (B) cells after incubation with EC (0.1 µM, 1 µM) compared to the control group (DMSO). Control: n = 17; 0.1 µM EC: n = 17; 1 µM EC: n = 15. Whiskers indicate minimal and maximal values. The +- sign indicates the mean values. The dotted line shows the mean value of the control group of SH-SY5Y MOCK (0,09354 µM). Significance was determined using analysis of variance (one-way ANOVA) and Dunnett's multiple comparison post hoc test. **** p < 0.0001.*

Figure 2-24 (B) shows that treatment with both EC concentrations for SH-SY5Y-APP$_{695}$ resulted in a significant increase in average neurite length compared to the solvent control (p < 0.0001). For treatment with 1 µM EC, an increase to approximately two times that of the control was recorded, analogous to MOCK cells.

Figure 2-25 shows a representative collection of pictures of SH-SY5Y-APP$_{695}$ cells treated with erinacine C (0.1 µM and 1 µM). The length of neurites increases from left to right.

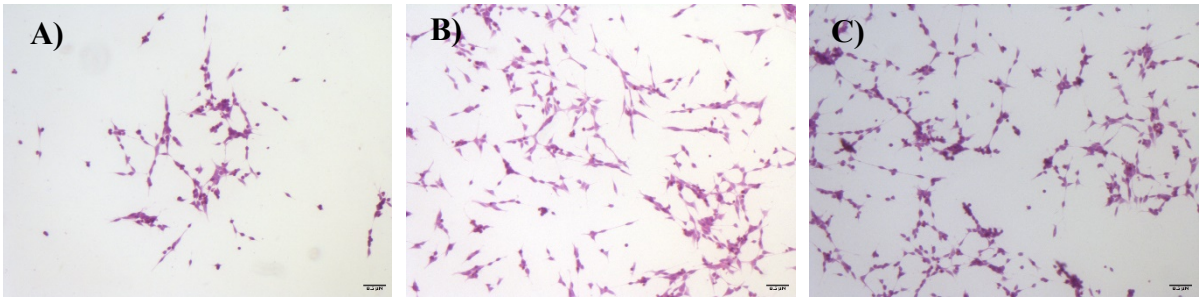

Figure 2-25 Representative pictures of the effects of erinacine C on neuritogenesis in SH-SY5Y-APP$_{695}$ cells. A) control group, B) treatment with 0.1 µM erinacine C; C) treatment with 1 µM erinacine C; scale bar indicates a size of 0.5 µM.

2.9 Effects of erinacine C on A$\beta_{1\text{-}40}$ levels

Increased levels of Aβ plaques are hallmarks of Alzheimer's disease. Tzeng et al. (2018) demonstrated that an erinacine A-enriched mycelium of *Hericium erinaceus* affects on Aβ levels. Elevated Aβ levels have been associated with an increased risk of mitochondrial dysfunction (Swerdlow, 2020). To assess the effects of erinacine C on Aβ levels, an HTRF assay was performed (Chapter 5.2.12.10). Figure 2-26 shows the evaluation of A$\beta_{1\text{-}40}$ levels in SH-SY5Y-APP$_{695}$ cells after treatment with erinacine C (0.1 µM, 1 µM and 10 µM) against the control group. No significant difference for all treatment groups of erinacine C was detected.

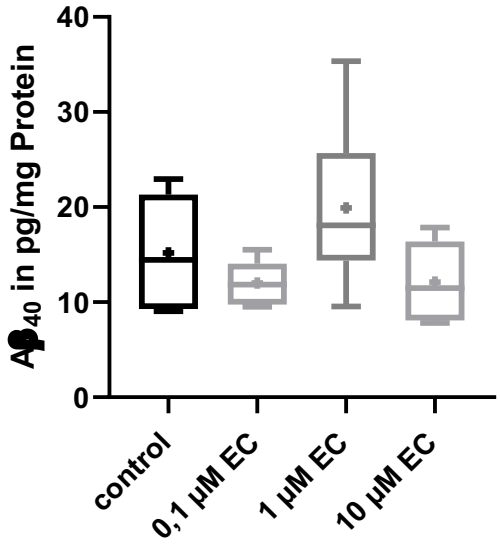

Figure 2-26 $A\beta_{1-40}$ levels in SH-SY5Y-APP_{695} cells after treatment with erinacine C.
Control cells (n = 6) were treated with DMSO at erinacine C concentrations of 0.1 µM, 1 µM and 10 µM. Whiskers indicate minimal and maximal values. The +- sign indicates the mean values. Significance was determined using analysis of variance (one-way ANOVA) and Dunnett's multiple comparison post hoc test.

2.10 Molecular modelling of TrkB-receptor interaction

To date, only biological parameters were investigated in this work to explore the effect of EC on mitochondrial parameters in Alzheimer's disease. Due to the effects of EC on the mRNA expression levels of TFAM and the positive effects on neuronal outgrowth, it is hypothesized that EC has an effect on the tropomyosin receptor kinase B (TrkB) receptor. TrkB, which is stimulated by neurotrophins such as BDNF, is an important factor for neuronal differentiation and synaptic plasticity. Molecular modelling models help to test and simulate potential interactions between proteins and ligands. To model the potential mechanism of action of erinacine C, an *in silico* experiment was performed. Table 2-1 Scoring output of AutoDock Vina. The scoring from Table 2-1 shows nine different conformations, which were tested for protein–ligand interactions. The higher the affinity, the more likely is a protein–ligand interaction. Figure 2-27 shows the erinacine C in the cavity of TrkB with the highest calculated affinity. For the surface structure, it is visible how neatly EC fits in the cavity of TrkB and could activate the TrkB receptor. In Figure 2-28, the interaction at the binding site is displayed. The hydrophobic part

sits in the cavity, and the hydrophilic head sticks out. The simulation shows a hydrogen bond between EC and aspartic acid in TrkB.

Table 2-1 Scoring output of AutoDock Vina.
The scoring output describes the affinity of the ligand to the receptor. The lower the affinity is, the stronger the protein–ligand interaction. The root-mean-square deviation of atomic positions (RMSD) describes the comparison of the atom type and distance compared to the other configurations.

mode	Affinity (kcal/mol)	dist from rmsd l.b.	best mode rmsd u.b.
1	-7.9	0.000	0.000
2	-7.6	3.040	7.778
3	-7.2	2.416	3.519
4	-7.0	1.473	3.808
5	-7.0	3.959	6.750
6	-6.8	2.851	7.874
7	-6.7	3.356	8.740
8	-6.6	3.502	8.740
9	-6.6	3.027	7.879

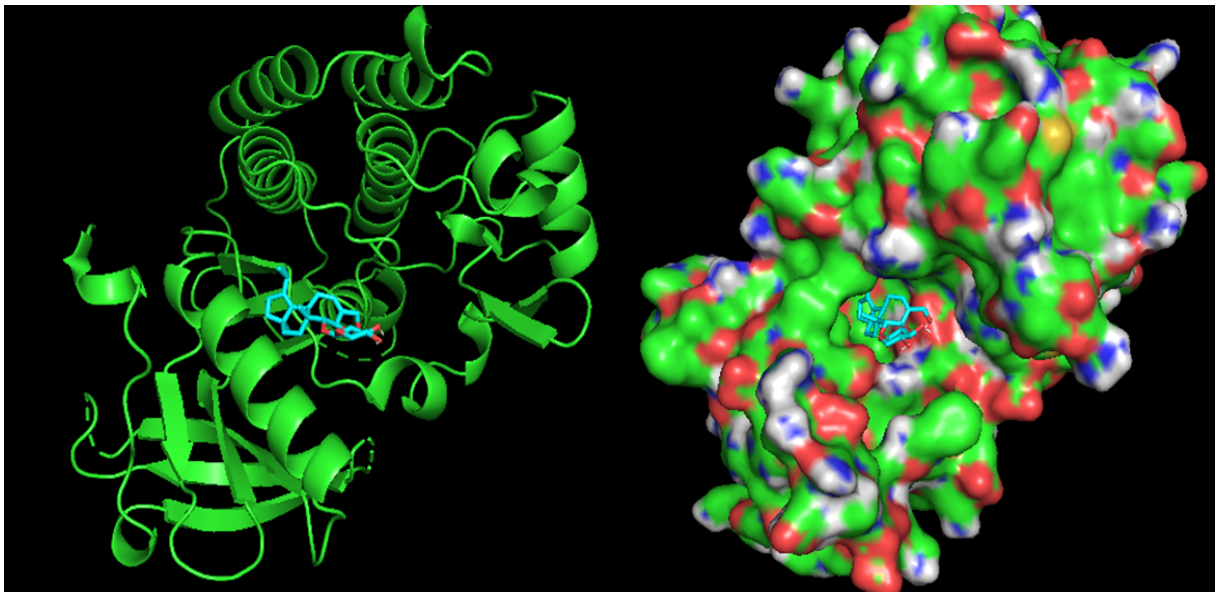

Figure 2-27: Ribbon structure (left) and surface structure (right) of TrkB with erinacine C in its best calculated affinity mode after Table 2-1 displayed with PyMOL.

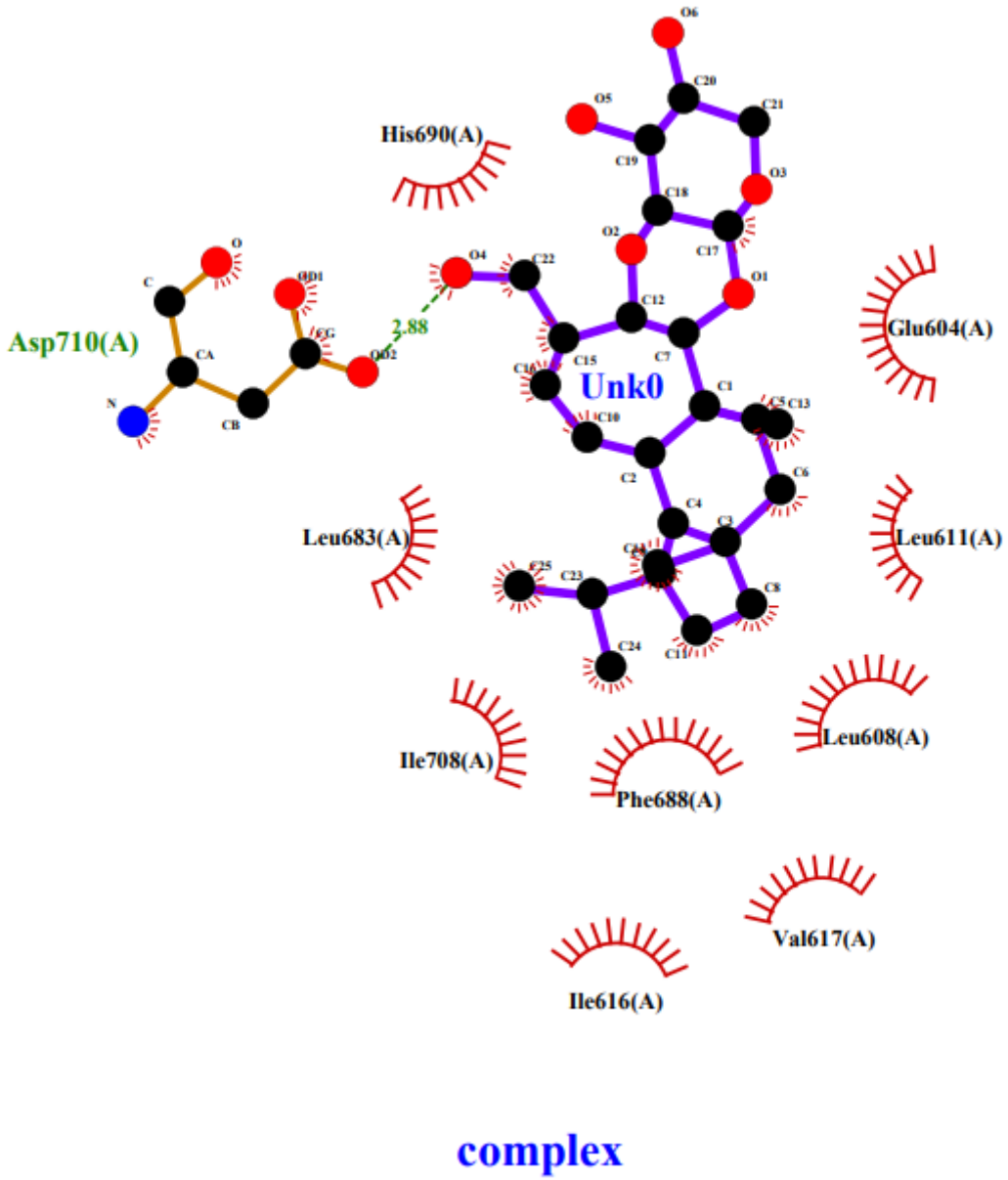

Figure 2-28 shows the modelled interaction of erinacine C with TrkB.
The simulated hydrogen bond interaction of erinacine C with aspartic acid (Asp710A) in the cavity of the TrkB receptor is displayed using LigPlot+. The red dots represent oxygen atoms, black dots carbon atoms and blue dots nitrogen atoms.

2.11 RNAseq ShinyGo enrichment analysis

RNAseq is a high-throughput deep-sequencing technology to gain insights into the transcriptome of cells. This helps to analyse the whole RNA of a biological sample at a given moment to understand the effect of erinacine C treatment in the context of the complete cell. This

approach was driven by previous results from RNA expression as well as molecular modelling. An *in silico* interaction of erinacine C with TrkB was found, which was based on previous RNA expression and neuronal outgrowth experiments. To better understand the underlying biological processes and the effects of erinacine C, an RNAseq analysis was performed using ShinyGO. ShinyGO (Ge et al., 2020) uses the Shiny framework of R, connects it with various databases and allows it to be visualized. ShinyGo was used to detect pathways or functional categories. Gene Ontology (GO) stands for a genome-wide study, where with the help of enrichment, it is possible to test the gene set for certain pathways or functional categories. The following datasets were analysed: MOCK-DMSO *vs* MOCK HER and APP-DMSO *vs* APP HER. Here, the gene sets were filtered using p value $p \leq 0.05$ and just protein coding genes, leaving small nucleolar RNA (snoRNA), long noncoding RNA (lncRNA), uncategorized genes, and pseudogenes out. The kits used for the analysis are described in chapter 5.2.12.9.

2.11.1 RNAseq analysis MOCK-DMSO vs MOCK-EC

For the analysis, the gene set was described as above using the filter p value $p \leq 0.05$ and protein-coding genes. Hereby, 1292 protein-coding genes and a background of 1421 protein-coding genes were found. Gene Ontology (GO) for biological process gene sets produces an enrichment result, as shown in Figure 2-29. The most significant groups of terms were related to nervous system development (295 genes, FDR < 1.3×10^{-18}) and regulation of cellular component organization (284 genes, FDR < 5.4×10^{-15}). In addition, there was a cluster of neurogenesis (209 genes, FDR < 6.5×10^{-12}), neuron differentiation (177 genes, FDR < 3.1×10^{-10}) and generation of neurons (197 genes, FDR < 1.2×10^{-11}). When switching to GO cellular component (Figure 2-30), the most significant process is cell junction (266 genes, FDR < 1.6×10^{-17}). In addition, processes for axons (96 genes, FDR < 2.1×10^{-8}), postsynapse (88 genes, FDR < 7.8×10^{-7}), synapses (169 genes, FDR < 2.3×10^{-10}) and neuron projection (163 genes, FDR < 1.4×10^{-8}) were detected. Together, they are represented by 516 protein-coding genes (40%). Using GO molecular function (Figure 2-31), ShinyGO revealed that most genes were activated in processes such as RNA binding (251 genes, FDR < 2.1×10^{-18}), enzyme binding (233 genes, FDR < 1.6×10^{-7}) and carbohydrate derivative binding (227, FDR < 3.1×10^{-5}). This list contains many transcription factors, such as MAP3K9, BTK, REV3L, and PIK3C2A.

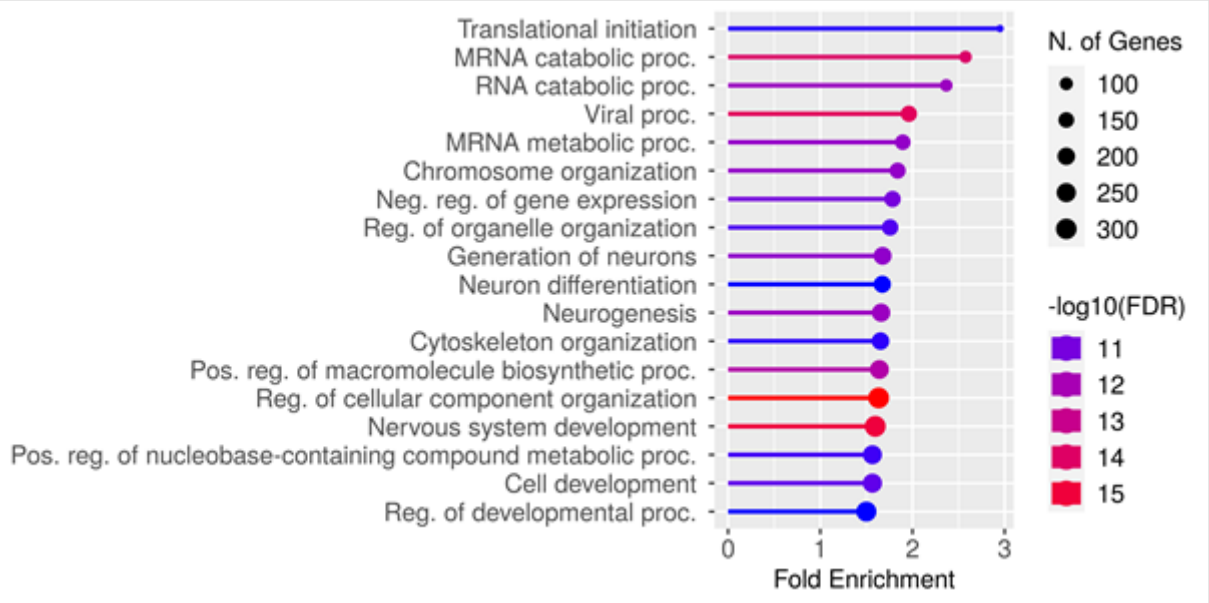

Figure 2-29 Gene Ontology for biological process enrichment in SH-SY5Y MOCK DMSO vs SH-SY5Y MOCK HER.

Genes for nervous system development were the most significant regulated along with genes for regulation of cellular component organization, neurogenesis, neuron differentiation and generation of neurons.

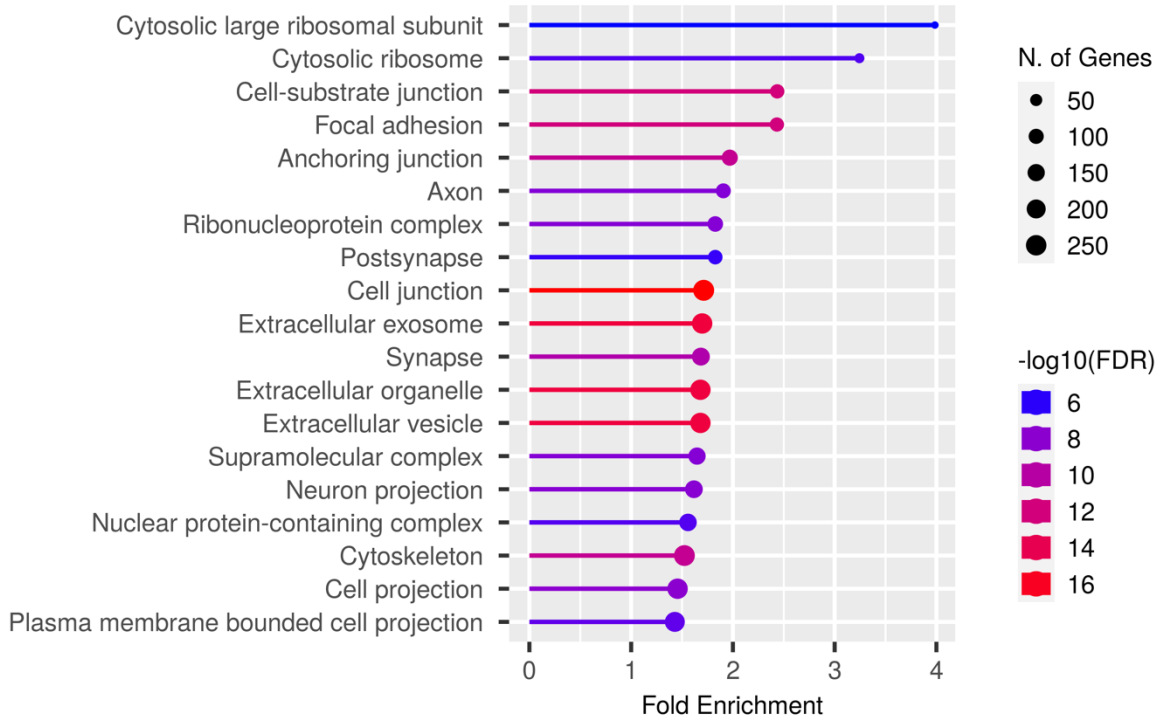

Figure 2-30 Gene Ontology for cellular component enrichment in SH-SY5Y MOCK DMSO vs SH-SY5Y MOCK HER.

Genes for cell junction process were the most significant regulated. Along with processes for axons, postsynapse, synapses and neuron projection.

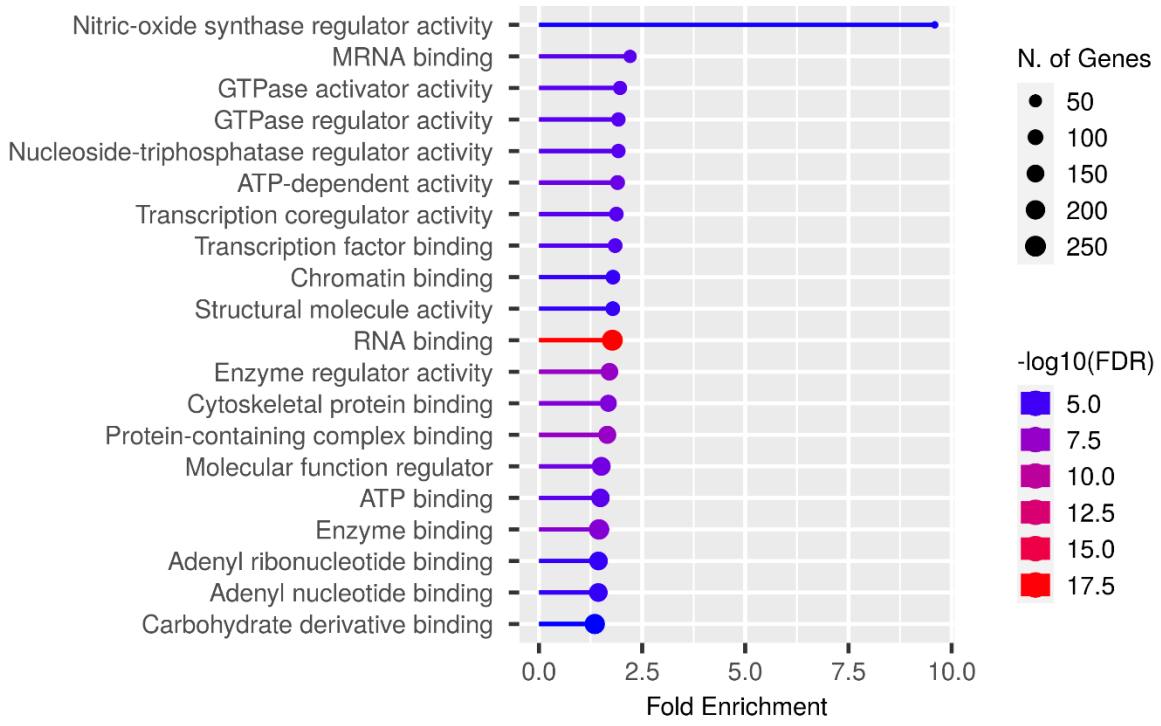

Figure 2-31 Gene Ontology for molecular function enrichment in SH-SY5Y MOCK DMSO vs SH-SY5Y MOCK HER.

Genes were mostly activated in processes such as RNA binding, enzyme binding and carbohydrate derivative binding.

With KEGG pathway analysis, the most significant changes were detected in ribosome pathways (32 genes, FDR < 1.9×10^{-5}) and the estrogen signalling pathway (23 genes, FDR < 8.2×10^{-4}). Most genes were found in pathways of neurodegeneration (65 genes, FDR < 3.6×10^{-4}), including amyotrophic lateral sclerosis (52 genes, FDR < 8.2×10^{-4}), Huntington's disease (48 genes, FDR < 3.6×10^{-4}), Alzheimer's disease (48 genes, FDR < 9.3×10^{-3}), and Parkinson's disease (41 genes, FDR < 1×10^{-3}). Unsurprisingly, axon guidance pathways (30 genes, FDR < 3.5×10^{-3}) were also activated. The KEGG annotation related to Alzheimer's disease has been provided, with the corresponding figures available in the supplemental section (chapter 8.1).

2.11.2 RNAseq analysis APP-DMSO vs APP-EC

For the analysis, the gene set was described as above using the filter p value $p \leq 0.05$ and protein-coding genes. Hereby, 52 protein-coding genes and a background of 14070 protein-coding genes were found. Compared to the MOCK cells, significantly fewer genes were activated. Gene Ontology (GO) for biological process gene sets produces an enrichment result, as shown

in Figure 2-32. The most significant groups of terms were related to cell-substrate junction assembly (5 genes, FDR < 1.7×10^{-2}), central nervous system development (12 genes, FDR < 1.7×10^{-2}), glial cell development (5 genes, FDR < 1.7×10^{-2}), and cell development (17 genes, FDR < 1.7×10^{-2}). Additionally, the terms neurogenesis (15 genes, FDR < 2.3×10^{-2}), positive regulation of axon extension (3 genes, FDR < 3.9×10^{-2}) and oligodendrocyte development (3 genes, FDR < 3.8×10^{-2}) were enriched. Looking into GO cellular component (Figure 2-33), the most significant processes are intermediate filament cytoskeleton (5 genes, FDR < 7.2×10^{-3}), Apical part of cell (7 genes, FDR < 8.7×10^{-3}), Hemidesmosome (2 genes, FDR < 1.3×10^{-2}), and unconventional myosin complex (2 genes, FDR < 3.4×10^{-2}). For GO molecular function (Figure 2-34), the analysis with ShinyGO revealed that only actin binding was activated (8 genes, FDR < 1.5×10^{-2}). For KEGG, no pathways could be visualized.

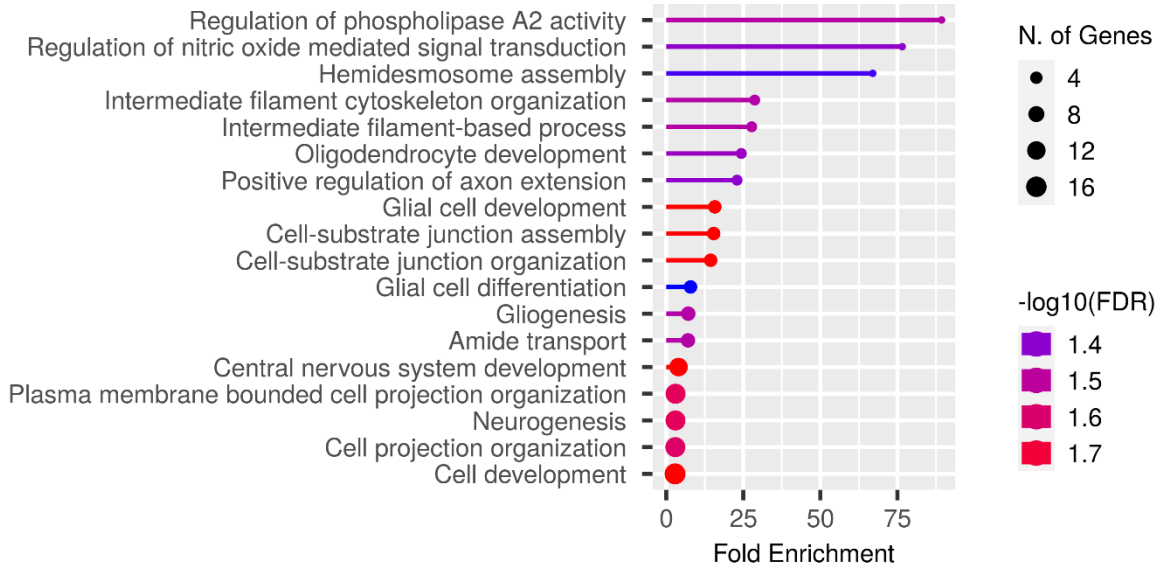

Figure 2-32 Gene Ontology for biological process enrichment in SH-SY5Y APP$_{695}$ DMSO vs SH-SY5Y APP$_{695}$ HER cells.

Genes for cell-substrate junction assembly, central nervous system development, glial cell development, and cell development were mostly regulated. Genes for neurogenesis, positive regulation of axon extension and oligodendrocyte development were also regulated.

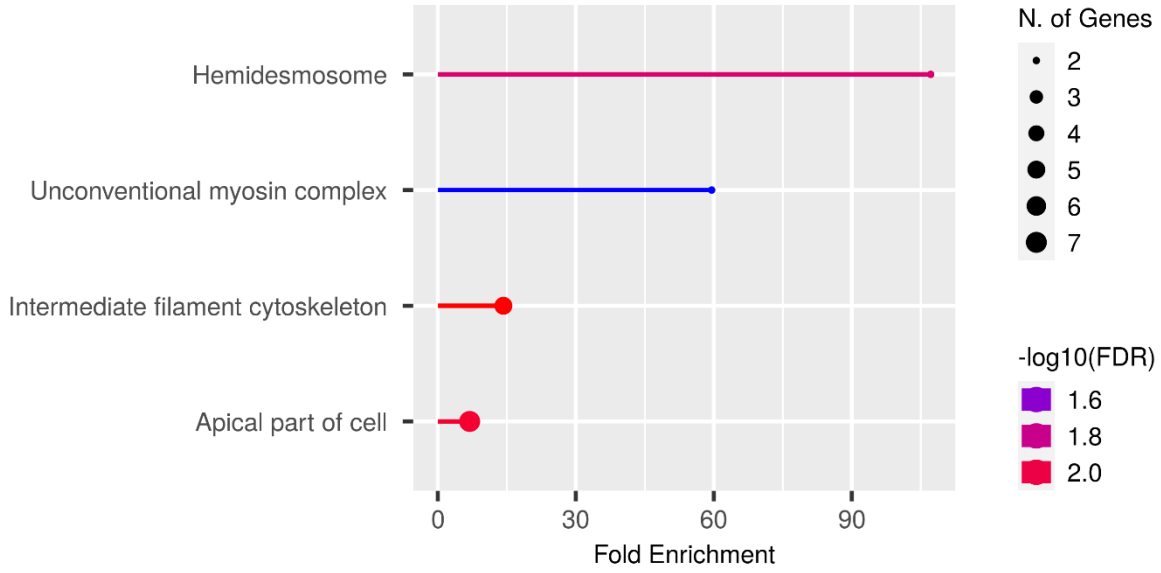

Figure 2-33 Gene Ontology for cellular component enrichment in SH-SY5Y APP_{695} DMSO vs SH-SY5Y APP_{695} HER cells.

The most significant regulated gens processes are intermediate filament, apical part of cell, hemidesmosome, and unconventional myosin complex.

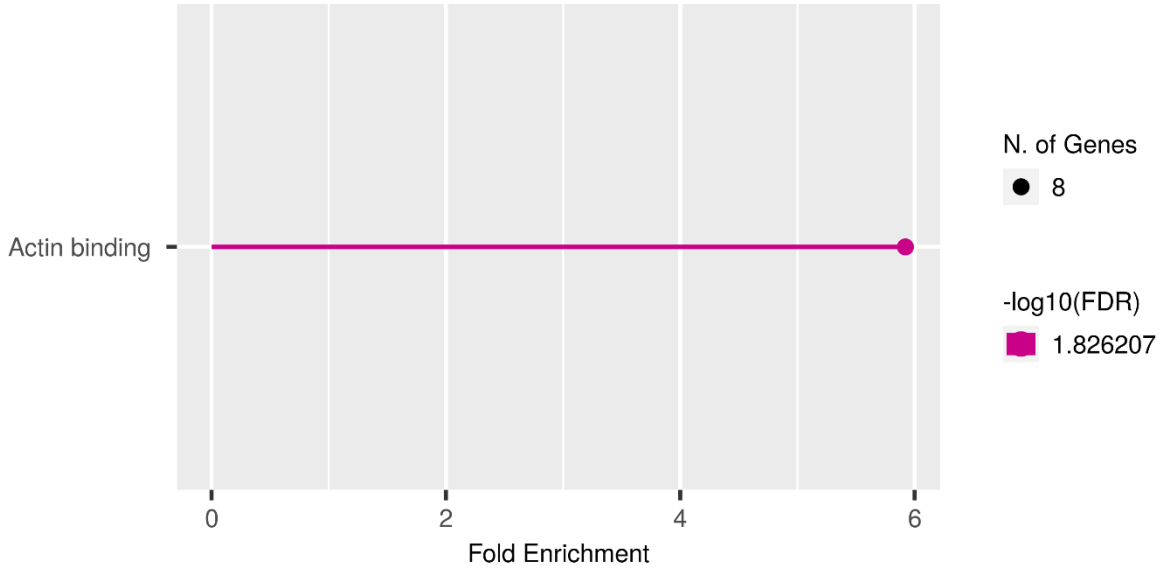

Figure 2-34 Gene Ontology for molecular function enrichment in SH-SY5Y APP_{695} DMSO vs SH-SY5Y APP_{695} HER. Here only Actin binding genes were regulated.

2.12 Effects of ethanolic mycelium extract in *Caenorhabditis elegans*

Since *Hericium erinaceus* contains valuable pharmacological molecules such as polysaccharides, ergothionein and polyketides, there was interest in the effects of the whole extract. An ethanolic extract of *Hericium erinaceus* mycelium (HEM) was produced to test its effects in a higher organism, since ethanolic extracts showed promising effects on cells, fish and rats (Kushairi et al., 2019; Sun et al., 2021; Valu et al., 2021; Yi et al., 2015). *Caenorhabditis elegans* is an excellent model organism for investigating complex molecular mechanisms. To date, the effects of *Hericium erinaceus* have never been investigated in *Caenorhabditis elegans*. Two strains equivalent to the cell models - CL2122 and GMC101 - were used. CL2122 serves here as the control for the Alzheimer-related GMC101 strain (chapter 1.5). Here, four concentrations: 0.1, 1, 10 and 100 µg/mL ethanolic *Hericium erinaceus* mycelium extract (HEM), were tested. Erinacine C was not detected in the sample extract using HPLC-DAD analysis. Refer to chapter 8.2 to view the chromatogram. DMSO was used as a solvent control.

2.12.1 Effects of ethanolic mycelium extract on lifespan after heat stress in CL2122

C. elegans is a well-established model system to study longevity and mitochondrial stress resilience. The heat stress assay at 37 °C simulates increased stress and provides information about the stress response. The heat shock assay was used to define a concentration range for HEM. In CL2122, the treatment with 0.1 µg/mL HEM showed no difference in the heat stress experiment compared to the control group (p value = 0.5534), although the median survival was 30 minutes longer than the control group (median survival control group 7 h; 0.1 µg/mL HEM 7.5 h) (Figure 2-35).

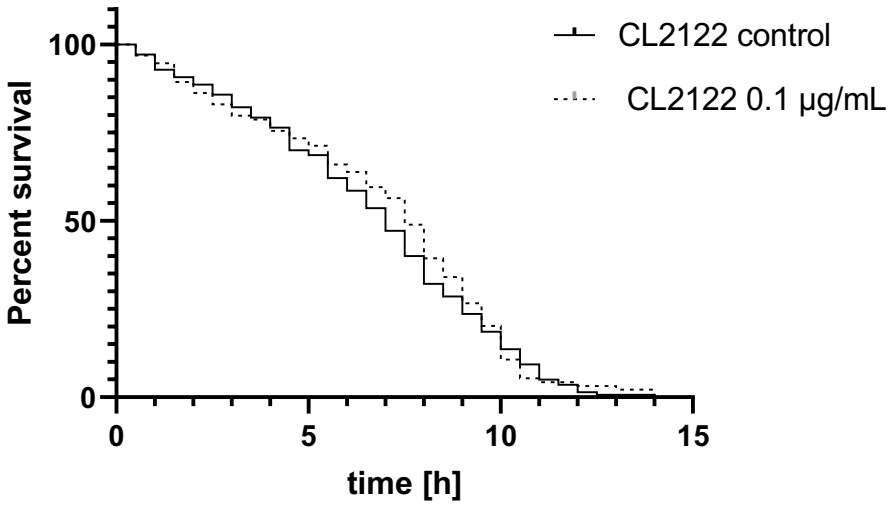

Figure 2-35 Heat stress survival curve in CL2122 with 0.1 µg/mL HEM.
The percentage survival of C. elegance per time is shown. Median survival control group 7 h 0.1 µg/mL HEM 7.5 h, comparison of survival with Mantel–Cox test, (control n = 140, 0.1 µg/mL n = 94).

In CL2122, the treatment with 1 µg/mL of HEM showed no difference in the heat stress experiment compared to the control group (p value = 0.7763), although the median survival was one hour less than the control group (Median survival control group 7 h; 0.1 µg/mL HEM 7.5 h) (Figure 2-36).

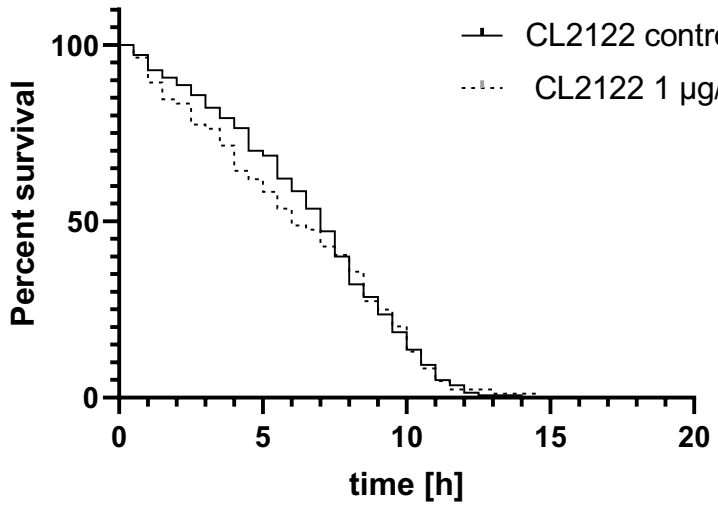

Figure 2-36 Heat stress survival curve in CL2122 with 1 µg/mL HEM.
The percentage survival of C. elegance per time is shown. Median survival control group 7 h 1 µg/mL HEM 6 h; comparison of survival with Mantel–Cox test, (control n = 140, 1 µg/mL n = 84).

In CL2122, the treatment with 10 µg/mL HEM showed no difference in the heat stress experiment compared to the control group (p value = 0.9387), although the median survival was 1 hour less than the control group (Figure 2-37).

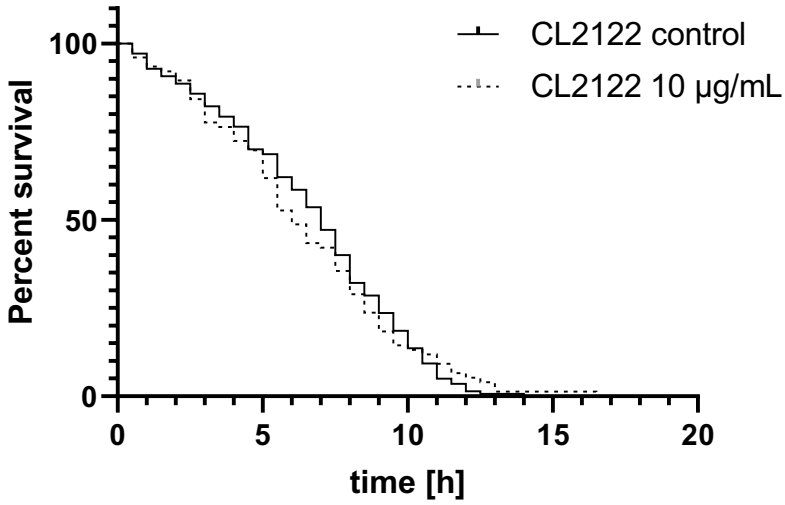

Figure 2-37 Heat stress survival curve in CL2122 with 10 µg/mL HEM.
The percentage survival of C. elegance per time is shown. Median survival control group 7 h 10 µg/mL HEM 6 h, comparison of survival with Mantel–Cox test, (control n = 140, 10 µg/mL n = 76).

In CL2122, the treatment with 100 µg/mL HEM showed no difference in the heat stress experiment (p value = 0.7018) compared to the control group, although the median survival was 30 minutes less than the control group (Figure 2-38).

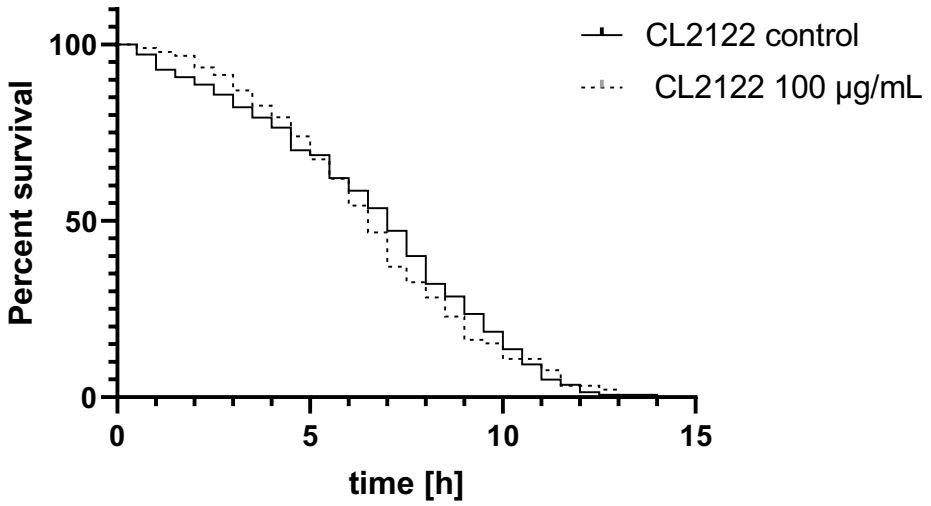

Figure 2-38 Heat stress survival curve in CL2122 with 100 µg/mL HEM.
The percentage survival of C. elegance per time is shown. Median survival control group 7 h 100 µg/mL HEM 6.5 h, comparison of survival with Mantel–Cox test, (control n = 140, 100 µg/mL n = 92).

In summary the results in CL2122 show no statistically significant effect, neither positive nor negative. Therefore, was CL2122 not further tested on ATP and ROS levels.

2.12.2 Effects of ethanolic mycelium extract on lifespan in GMC101

As described above, the heat stress assay was used to investigate the potential protective effects of HEM. The strain GMC 101, with the expression of Aβ_{1-42}, generally shows a lower median survival than CL2122. Treatment with 0.1 µg/mL HEM showed a statistically positive effect (p value <0.0001) on *C. elegans* GMC 101. The median survival increased from 5 to 7 hours. Furthermore, a higher survival is clearly visible within the Kaplan–Meier curve (Figure 2-39).

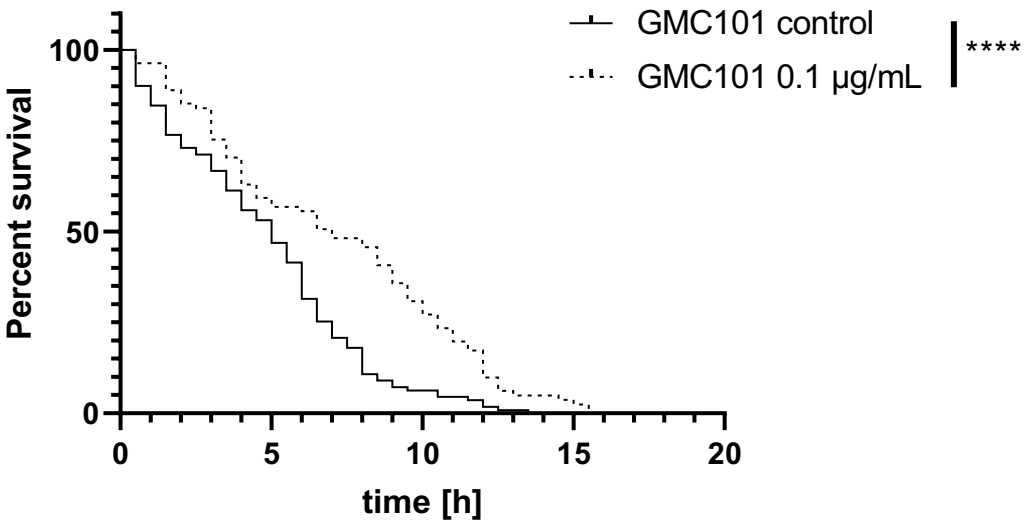

Figure 2-39 Heat stress survival curve in GMC101 with 0.1 µg/mL HEM.
*The percentage survival of C. elegance per time is shown. Median survival control group 5 h 0.1 µg/mL HEM 7 h, comparison of survival with Mantel–Cox test, (control n = 111, 100 µg/mL n = 81); **** p < 0.0001.*

The same is visible for the treatment with 1 µg/mL. The survival curve showed a clear trend towards longer survival. In addition, the median survival increased from 5 to 6.5 h. This marked a statistically significant effect for the treatment with 1 µg/mL HEM (p value <0.0001) (Figure 2-40).

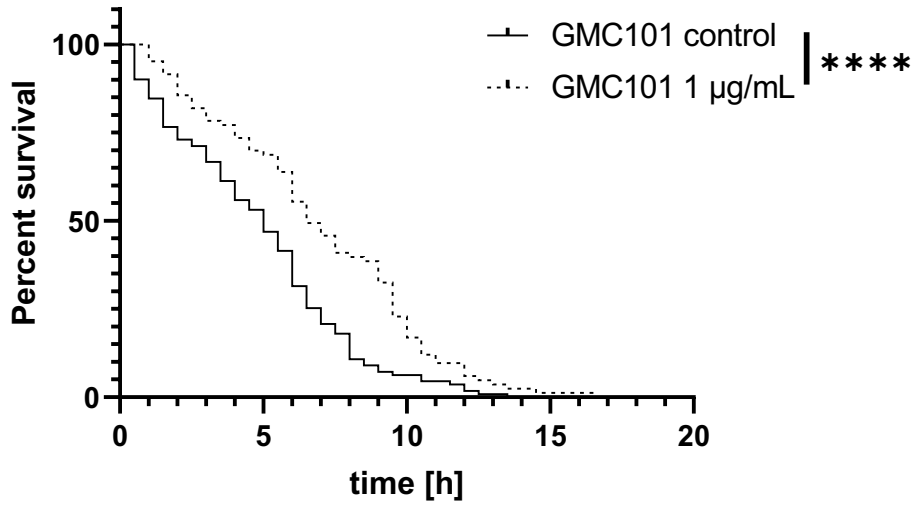

Figure 2-40 Heat stress survival curve in GMC101 with 1 µg/mL HEM.
*The percentage survival of C. elegance per time is shown. Median survival control group 5 h 1 µg HEM 6.5 h, comparison of survival with Mantel–Cox test, (control n = 111, 100 µg/mL n = 83); **** p < 0.0001.*

However, the median for the treatment with 10 µg/mL did not differ between the two groups. There was a statistically significant difference (p value = 0.0326) between the two groups toward treatment with HEM (Figure 2-41).

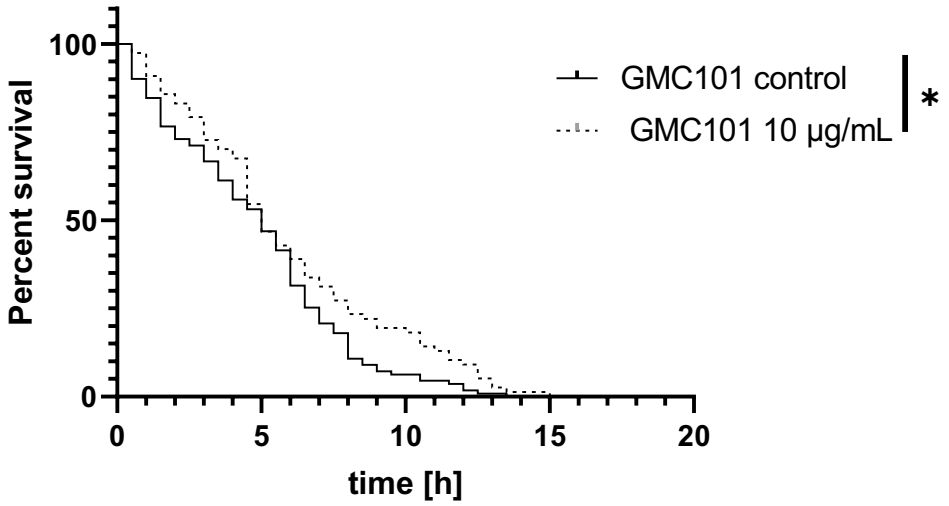

Figure 2-41 Heat stress survival curve in GMC101 with 10 µg/mL HEM.
*The percentage survival of C. elegance per time is shown. Median survival control group 5 h 10 µg/mL HEM 5 h, comparison of survival with Mantel–Cox test, (control n = 111, 100 µg/mL n = 77); * p < 0.05.*

For 100 µg/mL, the effect was also statistically positive (p value = 0.0160). The median survival increased from 5 to 6.5 h (Figure 2-42).

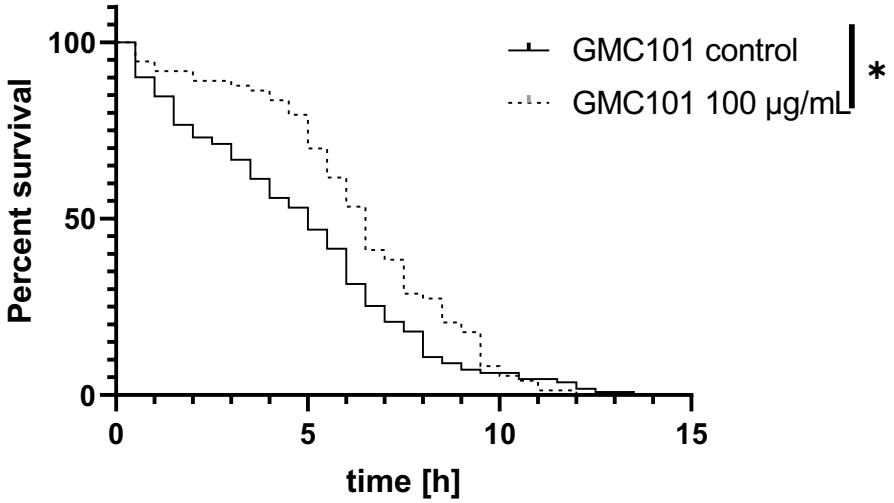

Figure 2-42 Heat stress survival curve in GMC101 with 100 µg/mL HEM.
*The percentage survival of C. elegance per time is shown. Median survival control group 5 h 10 µg/mL HEM 6.5 h, comparison of survival with Mantel–Cox test, (control n = 111, 100 µg/mL n = 73); * p < 0.05.*

To summarize the results, all four concentrations of the mycelium extract (0.1 µg/mL, 1 µg/mL, 10 µg/mL and 100 µg/mL) showed a statistically positive effect in increasing the probability for longer survival in GMC101. This can indicate an adjusted stress response due to the treatment with HEM. To further investigate the effects of HEM on longevity and mitochondrial stress resilience, ATP and ROS levels were investigated.

2.13 Comparative Analysis of ATP levels in CL2122 and GMC101

ATP serves as the primary energy source in mitochondria. In Alzheimer's disease, ATP levels have been observed to decline as the disease progresses (Swerdlow, 2020). By comparing the basal ATP levels between CL2122 and GMC101, it is possible to differentiate disease-specific effects in the utilized models and potentially elucidate any unspecific effects observed in the heat stress lifespan experiment.

Figure 2-43 illustrates the basal ATP concentration in µmol ATP/(mg/mL) protein for the Alzheimer's disease cell model GMC101 and the control strain CL2122 under standard laboratory conditions without any effector treatment. The GMC101 strain exhibits a lower average ATP concentration (19.17 µmol ATP/(mg/mL) protein) compared to the CL2122 strain (25.51 µmol ATP/(mg/mL) protein), with a statistically significant difference ($p < 0.01$). The observed difference in ATP concentrations between the two strains highlights the potential metabolic alterations occurring in the Alzheimer's disease model.

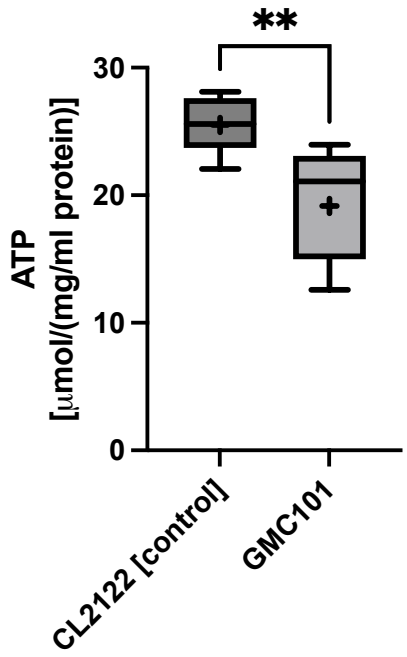

Figure 2-43 Basal ATP levels in CL2122 and GMC101.
*CL2122 n= 8, GMC101 n= 7; ATP levels [µmol ATP/(mg/mL) protein] of GMC101 and CL2122 without effector treatment. Mean (+) of CL2122: 25.51 ± SD 2.129; Mean (+) of GMC101: 19.17 ± SD 4.444. Whiskers indicate minimal and maximal values. The +- sign indicates the mean values. ** $p < 0.01$*

In the following the effect of HEM on ATP levels in the AD model GMC101 will be further investigated.

2.13.1 Effects of ethanolic mycelium extract on ATP levels in GMC101

ATP is the most important energy source in mitochondria. In Alzheimer's disease, the levels of ATP decrease with disease progression (Swerdlow, 2020). The change in ATP levels in the AD model GMC 101 can help to better understand the effects of HEM. If levels are increased, a improved stress response and resilience to the toxic effects of Aβ accumulation can be assumed. To assess the ATP levels, a luminescence assay was used (Chapter 5.2.14.2). GMC101 was administered at concentrations ranging from 0.1 to 100 mg/mL (HEM 0.1 µg/mL, 1 µg/mL, 10 µg/mL, 100 µg/mL). DMSO was used as a solvent control. Incubation with the mycelium extract showed a concentration-dependent increase in ATP level per µmol/(mg/mL protein). Although a dose-dependent trend was visible, only 10 µg/mL (p value <0.0001 showed a positive effect compared to the control group.) The deleterious effect of 100 µg/mL (p value = 0.0322) was statistically significant (Figure 2-44).

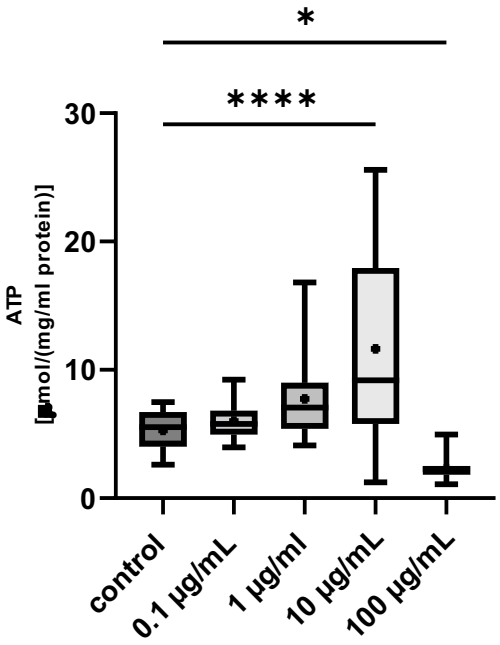

Figure 2-44 ATP levels in GMC101.

*ATP levels of GMC101 with and without treatment with HEM for 24 h compared against the control group (DMSO); n=24; whiskers indicate minimal and maximal values. The +- sign indicates the mean values. One-way ANOVA with Dunnett's multiple comparison test * p < 0.05, **** p < 0.0001.*

2.14 Comparative Analysis of ROS levels in CL2122 and GMC101

Reactive oxygen species (ROS) are linked to neuronal damage in Alzheimer's Disease (AD) due to an imbalance between their production and the body's ability to neutralize them, leading to oxidative stress (G. P. Eckert et al., 2012; Swerdlow, 2020). Here, ROS levels in two C. elegans strains: the control strain CL2122 and GMC101 were compared. GMC10, which expresses human amyloid-beta (Aβ1-42) in muscle cells is modelling some aspects of AD. As shown in Figure 2-45, ROS levels in GMC101 were significantly higher than in CL2122 (p-value < 0.0001), reinforcing the association between elevated ROS and AD.

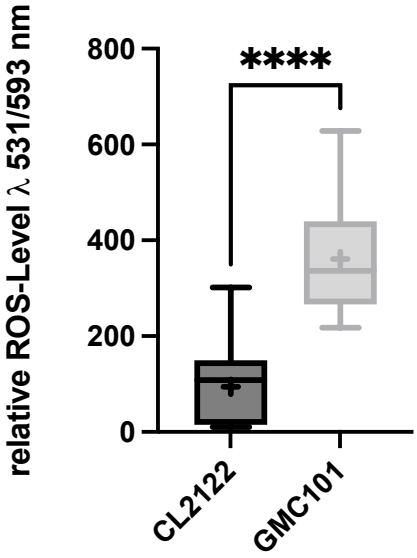

Figure 2-45 Comparative analysis of ROS levels in CL2122 and GMC101.
*CL2122 n = 26, mean value = 94.5 ± SD 78.9; GMC101 n = 22, mean value 360.8 ± SD 104.7; whiskers indicate minimal and maximal values. The +- sign indicates the mean of each group. The analysis was performed using an unpaired t-test **** p < 0.0001*

This sets the stage for exploring potential ROS-reducing effects of mycelium extract on GMC101 in the subsequent section.

2.15 Effects of ethanolic mycelium extract on ROS levels in GMC101

Reactive oxygen species are a marker for mitochondrial dysfunction and late-onset Alzheimer's disease (LOAD). Increased ROS formation leads to oxidative damage to lipids, proteins, and nucleic acids and can increase inflammation and the progression of AD (Swerdlow, 2020). The following showcases the results of GMC101 treated with HEM (0.1 µg/mL, 1 µg/mL, 10 µg/mL, 100 µg/mL). DMSO was used as a solvent. To measure ROS levels, the fluorescent dye MitoTracker™ red was used at λ 531/593 nm. The results were performed on three different days to control for statistical variation. If at least two out of three experiments pointed in the same direction, a conclusion was drawn. Figure 2-46 shows the treatment with HEM in GMC 101.

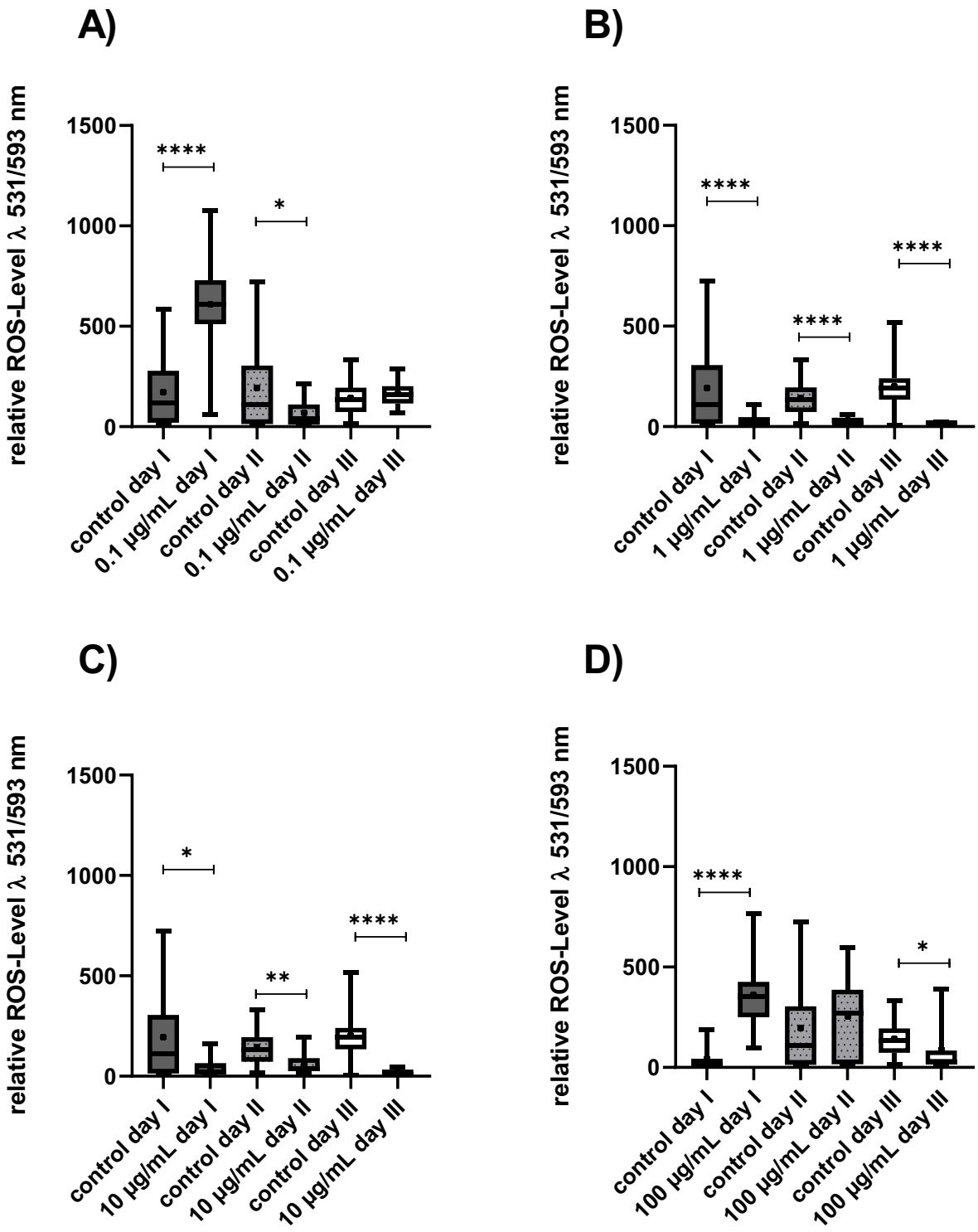

Figure 2-46 Relative ROS levels in GMC101 cells after treatment with HEM.

*A) 0.1 µg/mL; B) 1 µg/mL; C) 10 µg/mL; D) 100 µg/mL for 24 h compared against the control group (DMSO), n = 30; whiskers indicate minimal and maximal values. The +- sign indicates the mean of each group. Each day was compared with a nonparametric Mann–Whitney U test; * $p < 0.05$ ** $p < 0.01$, **** $p < 0.0001$.*

Although the heat stress assay showed a positive effect for all four concentrations in GMC101 (chapter 2.12.2), the experiment to assess ROS levels did not show clear results. However, a positive effect for all four treatment groups could be expected. For the treatment with 0.1 µg/mL (A), no distinct statement can be made because the results of day I and day II show different interactions, whereas day III shows no effect on ROS levels (Figure 2-46). Treatment with 100 µg/mL (D) showed the same inconclusive effect. 1 µg/mL (B) and 10 µg/mL (C) show the same decreasing effect (Figure 2-46). The treatment reduced the measured ROS level very strongly, which was statistically significant on three different days. A representative picture of ROS measured in GMC 101 is depicted in Figure 2-47. Figure 2-47 A shows GMC 101 with treatment of 1 µg/mL, compared to the control group (Figure 2-47 B). The reduced ROS levels can be observed visually.

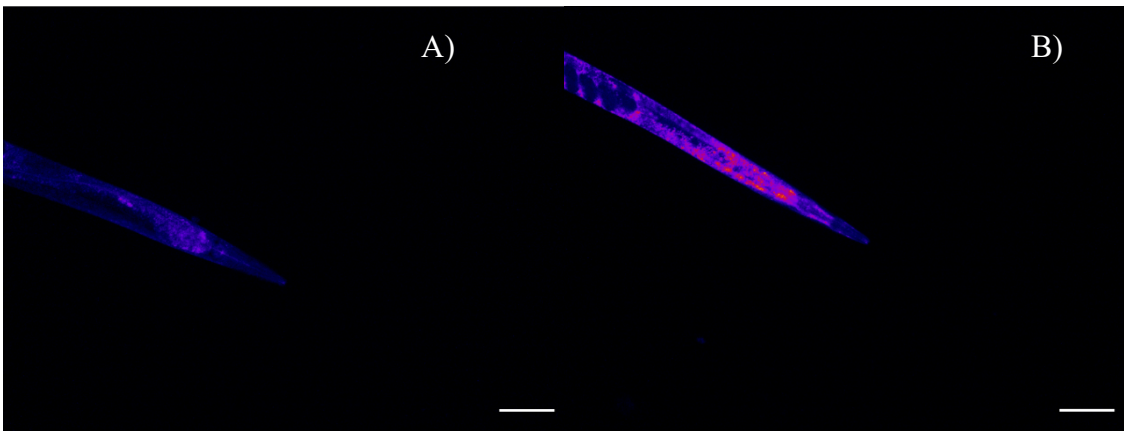

Figure 2-47 Representative fluorescent picture of GMC 101.
Quantitative ROS measurement using the fluorescent dye MitoTracker™ red, A) shows treatment in GMC101 with 1 µg/mL HEM compared to B) the control group, scale indicates 100 µm.

2.16 Effects of ethanolic mycelium extract on viability in SH-SY5Y cells

To narrow down the effects of the ethanolic extract, it was tested in a neuronal cell model. SH-SY5Y cells are a neuroblastoma cell line that is a widely used *in vitro* model for AD research (Kovalevich & Langford, 2013). SH-SY5Y-MOCK serves here as the control group. SH-SY5Y-APP_{695} cells show characteristics of mitochondrial dysfunction and elevated Aβ levels, which are typical for AD (chapter 1.5). The following are the results of the effect of HEM on viability in SH-SY5Y cells. The viability assay using MTT generally reflects metabolic and mitochondrial activity since tetrazolium dye reduction is based on a mitochondrial NAD(P)H-dependent oxidoreductase (Stockert et al., 2018). Cells were incubated with HEM (0.01 µg/mL, 1 µg/mL, 10 µg/mL, 100 µg/mL) for 24 h. DSMO was used as a solvent control. Subsequently, the viability was determined by reduction of MTT to formazan via absorption (Chapter 5.2.12.1). Chapter 2.16.1describes the effect of the extract on SH-SY5Y-MOCK cells, and chapter 2.16.2 describes the effect on SH-SY5Y-APP_{695} cells. Although the effect is different, both models show increased viability after treatment with the extract.

2.16.1 Effects of ethanolic mycelium extract on viability in SH-SY5Y-MOCK cells

Figure 2-48 shows the viability effect of various HEM concentrations in SH-SY5Y-MOCK-cells. Treatment with 0.01 µg/mL (p value = 0.0144) and 0.1 µg/mL (p value = 0.0500) showed statistically significant positive effects. 0.1 µg/mL also had the highest effect. The viability seemed to decrease with concentrations ranging from 1 µg/mL to 100 µg/mL, although the effects were not statistically significant.

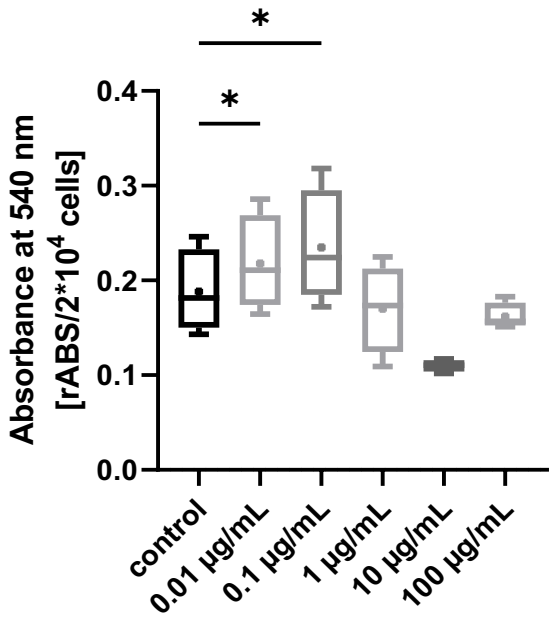

Figure 2-48 Effects of HEM on viability in SH-SY5Y-MOCK cells.
*Viability of SH-SY5Y-MOCK cells treated with HEM (0.01 µg/mL, 0.1 µg/mL, 1 µg/mL, 10 µg/mL, 100 µg/mL) for 24 h compared against the control group (DMSO); n=4; whiskers indicate minimal and maximal values. The +- sign indicates the mean value. One-way ANOVA with Dunnett's multiple comparison test * p < 0.05.*

2.16.2 Effects of ethanolic mycelium extract on the viability of SH-SY5Y-APP$_{695}$ cells

Figure 2-49 shows the viability effect of various HEM concentrations in SH-SY5Y-APP$_{695}$-cells. In general, it is clearly visible that the relative absorbance of the SH-SY5Y-APP695-cells is approximately 30% less for the control group compared to the SH-SY5Y-MOCK cells. This reflects the lower viability due to the higher expression of Aβ. Treatment with 0.01 µg/mL (p value = 0.0420) and 100 µg/mL (p value = 0.0007) showed statistically significant positive effects. 0.1 µg/mL and 1 µg/mL were not statistically significant but had a p value of 0.07. Although a p-value of 0.07 is not as strong evidence as a p-value of 0.05, it still can point on the possible effect. Interestingly, treatment with 10 µg/mL showed no effect, whereas 100 µg/mL was highly statistically significant and showed the largest effect compared to the control.

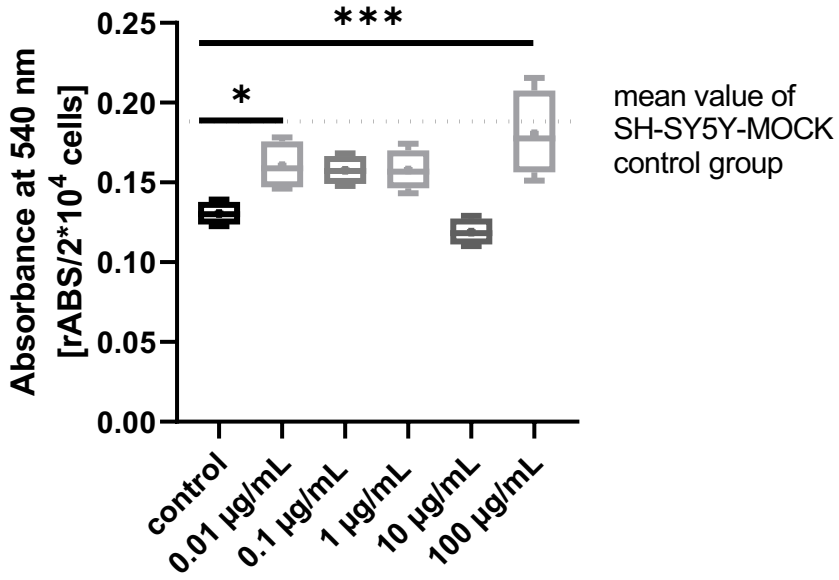

Figure 2-49 Effects of HEM on viability in SH-SY5Y-APP$_{695}$ cells.
*Viability of SH-SY5Y-APP$_{695}$ cells treated with HEM (0.01 µg/mL, 0.1 µg/mL, 1 µg/mL, 10 µg/mL, 100 µg/mL) for 24 h compared with the control group (DMSO); n=4; the dotted line shows the mean value of SH-SY5Y MOCK (0,1882 rABS/2*10^4 cells) whiskers indicate minimal and maximal values. The +- sign indicates the mean value. One-way ANOVA with Dunnett's multiple comparison test* $p < 0.05$, *** $p < 0.01$.*

2.17 Effects of ethanolic mycelium extract on ATP levels in SH-SY5Y cells

To investigate the effects of the ethanolic extract on ATP levels, a luminescence-based assay (Chapter 5.2.12.3) was used. ATP levels are an indicator of mitochondrial function and resilience. The higher the ATP levels, the higher the energy levels and the resilience of the cells against stressors. Furthermore, it can indicate a higher ATP production the OXPHOS (Swerdlow, 2020). The following are the results of the effect of HEM on ATP levels in SH-SY5Y cells. Cells were incubated with HEM (0.01 µg/mL, 1 µg/mL, 10 µg/mL, 100 µg/mL) for 24 h. DSMO served as the solvent control.

2.17.1 Effects of ethanolic mycelium extract on ATP levels in SH-SY5Y-MOCK cells

Figure 2-50 shows the effect of HEM (0.001 µg/mL, 0.01 µg/mL, 0.1 µg/mL, 1 µg/mL, 10 µg/mL) compared to the control group (DMSO) in SH-SY5Y-MOCK cells. No effects were visible for concentrations ranging from 0.001 to 0.1 µg/mL. 1 µg/mL and 10 µg/mL were statistically significant and showed ATP levels of 0 µmol/10^6 cells.

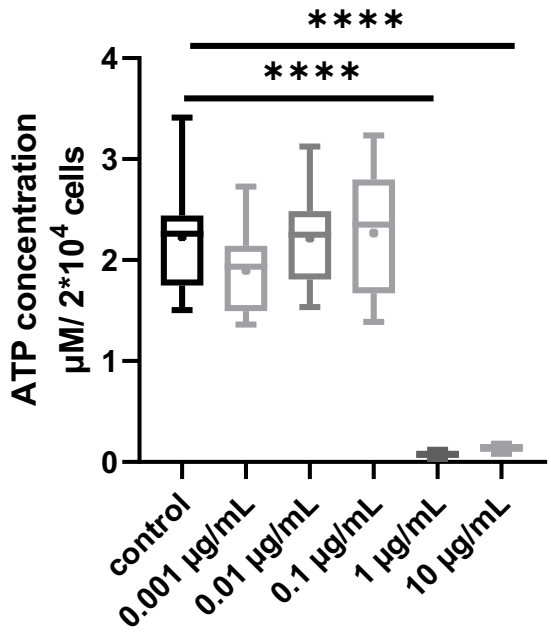

Figure 2-50 Effects of HEM on ATP levels in SH-SY5Y-MOCK cells.
*Viability of SH-SY5Y-MOCK cells treated with HEM (0.01 µg/mL, 0.1 µg/mL, 1 µg/mL, 10 µg/mL, 100 µg/mL) for 24 h compared against the control group (DMSO); n=8; whiskers indicate minimal and maximal values. The +- sign indicates the mean value. One-way ANOVA with Dunnett's multiple comparison test **** $p < 0.001$.*

2.17.2 Effects of ethanolic mycelium extract on ATP levels in SH-SY5Y-APP$_{695}$ cells

Figure 2-51 shows the effect of HEM (0.001 µg/mL, 0.01 µg/mL, 0.1 µg/mL, 1 µg/mL, 10 µg/mL) compared to the control group (DMSO) in SH-SY5Y-APP$_{695}$ cells. 0.001 µg/mL showed a statistically negative effect (p value = 0.0005), whereas 0.01 µg/mL showed a statistically positive effect (p value = 0.0385). 1 µg/mL (p value < 0.0001) and 10 µg/mL (p value < 0,0001) were statistically significant but were similar to the SH-SY5Y-MOCK ATP levels of 0 µmol/10^6 cells.

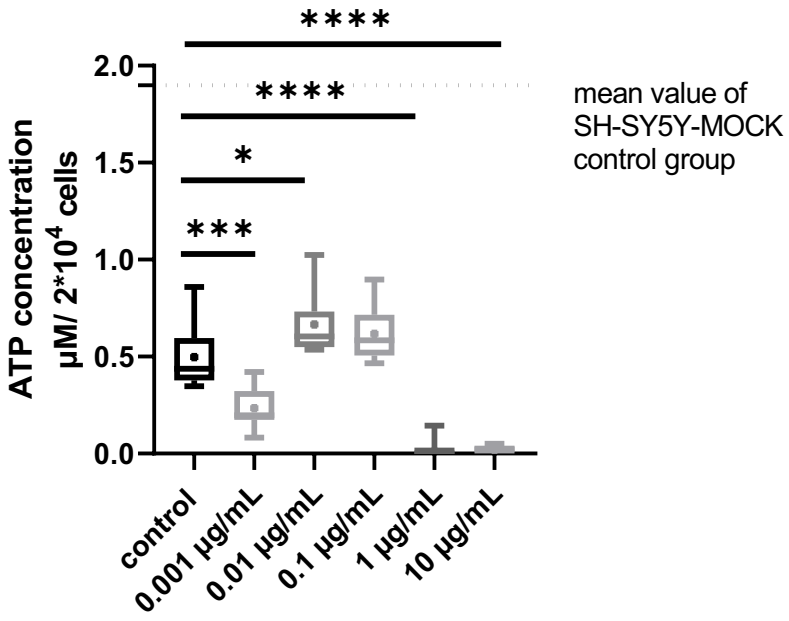

Figure 2-51 Effects of HEM on ATP levels in SH-SY5Y-APP$_{695}$ cells.
*Viability of SH-SY5Y-APP$_{695}$ cells treated with HEM (0.01 µg/mL, 0.1 µg/mL, 1 µg/mL, 10 µg/mL, 100 µg/mL) for 24 h compared with the control group (DMSO); n=8; the dotted line shows the mean value of SH-SY5Y MOCK (0,1882 rABS/2*10^4 cells); whiskers indicate minimal and maximal values. The +- sign indicates the mean value. One-way ANOVA Dunnett's multiple comparison post hoc test * p < 0.05, *** p < 0.001, **** p < 0.0001.*

2.18 Effects of ethanolic mycelium extract on mRNA expression

To assess the effects on mitochondrial genes, RT–qPCR was carried out as described in 5.2.12.4. The mitochondrial genes ATP5D, TFAM, SIRT1, CREB1 and NRF1 are markers for longevity, mitochondrial biogenesis, neuronal outgrowth and antioxidative stress response. The expression of mRNA in SH-SY5Y-MOCK and SH-SY5Y-APP_{695} cells showed miscellaneous effects after treatment with 0.01 mg/mL and 0.1 mg/mL HEM.

ATP5D was reduced in both treatments compared to the control. The concentration of 0.1 mg/mL significantly reduced ATP5D expression ($p = 0.0129$) (Figure 2-52 A). For SH-SY5Y-APP_{695}, the results were found to be different. HEM (0.01 mg/mL) significantly increased ATP5D expression ($p = 0.0052$), whereas HEM (0.1 mg/mL) significantly reduced ATP5D expression ($p < 0.0001$) (Figure 2-52 A).

For CREB1, the results for both cell lines were similar. The concentration of 0.01 mg/mL showed no effect in both cell lines, while 0.1 mg/mL showed a significant positive effect (SH-SY5Y-MOCK $p = 0.0012$; SH-SY5Y-APP_{695} $p = 0.0048$). For both cell lines, the increase was approximately 60% compared to the control (Figure 2-52 B).

Figure 2-52 C shows the effects of HEM on NRF1. Only SH-SY5Y-APP_{695} displayed a visible effect. 0.1 mg/mL significantly reduced the NRF1 expression levels by 30% ($p = 0.0207$).

In SH-SY5Y-MOCK and SH-SY5Y-APP_{695} cells, the results for TFAM were similar to each other (Figure 2-52 D). The concentration of 0.01 mg/mL had no effect in either cell line; however, the directions were opposite. For SH-SY5Y-MOCK cells, treatment with 0.01 mg/mL increased mean TFAM levels by 35%. In SH-SY5Y-APP_{695} cells, the mean levels were decreased by approximately 22%. The concentration of 0.1 mg/mL significantly and strongly increased the expression levels of TFAM in both cell lines. In SH-SY5Y-MOCK cells, the mean levels were 90% increased ($p= 0.0024$). In SH-SY5Y-APP_{695} cells, the mean levels were 4 times higher than those in the control cells ($p= 0.0007$).

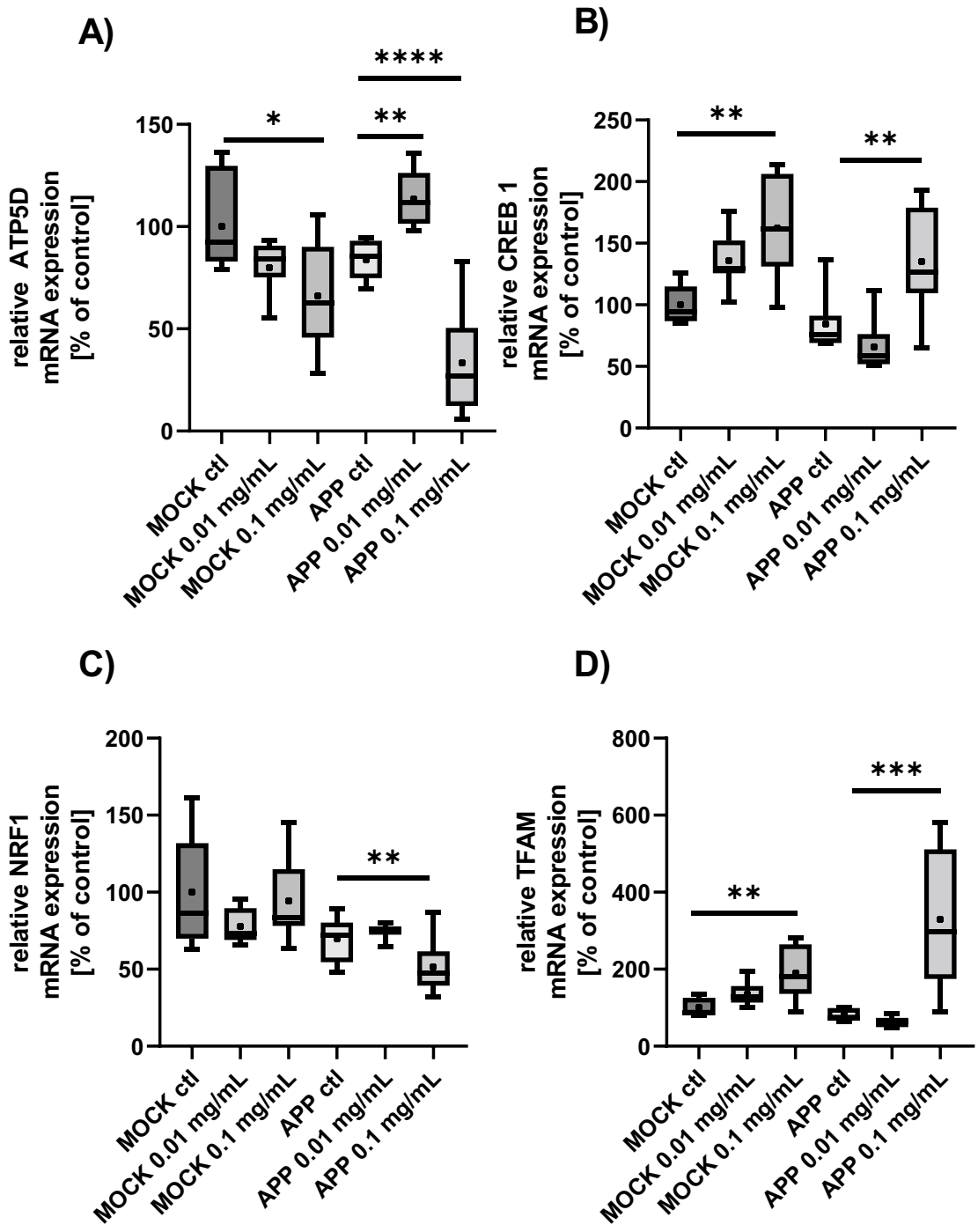

Figure 2-52 Relative normalized mRNA expression after treatment with HEM in SH-SY5Y-MOCK cells and SH-SY5Y-APP$_{695}$ cells.

Relative mRNA expression after 24 h incubation with 0.01 mg/mL and 0.1 mg/mL mycelium extract (HEM) in SH-SY5Y-MOCK cells and SH-SY5Y-APP$_{695}$ cells; A) mRNA expression of ATP5D, B) mRNA expression of CREB1, C) mRNA expression of NRF1, D) mRNA expression of TFAM, n = 8. Whiskers indicate minimal and maximal values. The +- sign indicates the mean values. The results were normalized to the mRNA expression levels of three housekeeping genes (beta-actin (ACTβ), glyceraldehyde 3-phosphate dehydrogenase (GAPDH) and phospho-glycerate kinase 1 (PGK1) according to the MIQE guidelines. Significance was determined by analysis of variance (one-way ANOVA) and Dunnett's multiple comparison post hoc test (∗p < 0.05, ∗∗p < 0.01, ∗∗∗∗p < 0.0001).

3 Discussion

In this work, the effects of the isolated metabolite erinacine C and a mycelium extract from the edible mushroom *Hericium erinaceus* on mitochondrial parameters in a preclinical cell and invertebrate model of AD were investigated. Therefore, *Hericium erinaceus* was cultivated in a submerged culture using an optimized medium. After 9 days, the ethanolic extract was extracted and erinacine C was isolated from the main culture. The results show that the ethanolic mycelium extract and erinacine C have a positive effect on mitochondrial parameters. However, it appears that the positive effects of erinacine C extend beyond altering mitochondrial dynamics. In the following sections, first, the effects of erinacine C and then of the ethanolic extract will be explained, compared and evaluated regarding the scientific literature.

3.1 *Hericium erinaceus* cultivation and erinacine C production

The original work done by Shen et al. (2015) was replicated. The authors first published the use of oatmeal and Edamin ^{K} as a special additive to increase the amount of erinacine C in a submerged culture of *Hericium erinaceus*. In this work, this could be successfully repeated. The analytical results of HPLC, NMR and HR-MS clearly show that erinacine C was purely isolated. Furthermore, the application of an additional lyophilization step led to a purer HPLC chromatogram. It is assumed that lyophilization reduced the number of volatile compounds in the extracted matrix. Although Wolters et al. (2015) reported the use of a buffer to increase yields of erinacine C, it is thought this subject needs further and even more systematic investigation using, for example, a design of analysis (DOE) experiment, which was beyond the scope of this work. To assure a cost–benefit production of erinacines and erinacine C, the independent and dependent variables must be examined. Dependent variables are presumably as reported: carbon and nitrogen sources as well as the pH value (Bhandari et al., 2014; Shen et al., 2015; Wolters et al., 2015). Furthermore, it is reported by Paul Stamets that beginning a submerged culture with primordial colonies from the agar plate is recommended (Stamets, 2000). This fact is rarely mentioned in the scientific literature and helps to accelerate the growth of mycelial cultures.

Alternative paths can include genetically modified fungi or the production of erinacines in *E. coli*. J. Chen et al. (2017) described the genes involved in the mevalonate pathway. Based on this work, one can imagine a heterologous expression of the involved genes, such as geranylgeranyl pyrophosphate synthase (EC 2.5.1.29), which is responsible for the biosynthesis of the

common precursor geranylgeranyl pyrophosphate for diterpene compound production in *Hericium erinaceus*. It is economically beneficial to start a precursor step since raw materials such as geranylgeranyl pyrophosphate are currently very expensive. The carbon skeletons of diterpenes are shaped by diterpene cyclases, which are described by Y. L. Yang et al. (2017). This may help to produce erinacines in sufficient quantities to apply them in animal or studies.

3.2 Effects of erinacine C on SH-SY5Y cells

In this work, the effects of erinacine C on mitochondrial parameters such as viability, mitochondrial membrane potential, ATP levels, respiration, mitochondrial gene expression, neurotoxicity and neuronal outgrowth were tested. Initially, a range was tested (0.1 µM, 1 µM, 10 µM, 100 µM, 1000 µM) to evaluate the effective dose. Subsequently, the concentration range was reduced since the highest concentrations showed no effect in various experiments. The first set of experiments was primarily focused on mitochondrial parameters, and the following set of experiments was developed out of the previous experiments and results regarding the mitochondrial genes. For the RNAseq analysis, the goal was to generate new questions, given that the mitochondrial effects were only moderate. Effects on viability, MMP, ATP, and mitochondrial respiration.

The hypothesis was built on the basis that erinacines, especially erinacine C, improve neuronal viability. Therefore, it is assumed that erinacine C can improve mitochondrial parameters, since activated neuronal cells and increased neuronal activity need more energy. Therefore, mitochondrial parameters were systematically examined. The experiments started with a simple MTT assay to evaluate the effects of erinacine C (EC) on viability. The MTT assay is primarily used to determine cell viability. More active mitochondria (indicative of healthy cells) will convert more MTT, yielding a stronger color. However, it's worth noting that while the MTT assay is widely used, it has its limitations, including its inability to differentiate between cells that are truly dead and those that are just not metabolically active (Ghasemi et al., 2021). Here, it could be seen that the highest concentrations (10 µM, 100 µM and 1000 µM) show adverse effects on viability in both cell lines, indicating cytotoxic properties of the compound above a certain threshold concentration. Incubation with lower EC concentrations (≤ 1 µM) did not affect metabolic activity in either cell model. Wang et al. examined the effect of EC (0.1, 0.5, 1, 2.5, 5, 10 µM) on cell viability in BV2 microglial cells. Incubation with 0.1 - 2.5 µM EC showed no

effect on cell viability, while treatment with 5 µM and 10 µM EC significantly affected cell viability (L.-Y. Wang et al., 2019). These results are consistent with the effects of EC on metabolic activity in SH-SY5Y cells collected in this work. EC concentrations ≤ 1 µM analogously did not affect cell viability, whereas EC concentrations ≥ 10 µM did.

The MMP is directly correlated with ATP synthesis and is essential for its regulation. Even small deviations can indicate disturbances in ATP synthesis (Connolly et al., 2018). For this reason, it is considered as a key parameter of mitochondrial function (Sakamuru et al., 2016). Depolarization of the MMP is associated with mitochondrial dysfunction as well as apoptosis and is frequently present in neurodegenerative diseases, such as AD (Sakamuru et al., 2016). APP_{695} cells exhibit decreased MMP compared to MOCK cells (Grewal et al., 2020). No effect on the mitochondrial membrane potential was observed. However, it seems that 1 µM seems to increase MMP in the impairment model. However, the effect was not statistically significant. The significant increase for 1000 µM was due to pan assay interference, as indicated in 2.3.
One of the main mitochondrial tasks is ATP synthesis via the proton gradient established in the respiratory chain across the inner mitochondrial membrane (Nunnari & Suomalainen, 2012). In AD, mitochondrial dysfunction leads to an impaired ATP synthesis capacity (Oliver & Reddy, 2019; X. Wang et al., 2014). This is associated with decreased activity of some mitochondrial energy production enzymes, such as ATP synthase and complex IV, which impairs MMP maintenance and thus potentially ATP synthesis. ROS generation and antioxidant capacity dysfunction are also associated with AD and negatively affect the cellular energy status (Cenini et al., 2019). These impairments are manifested in a reduced availability of the energy substrate ATP in AD models (Oliver & Reddy, 2019). It has already been shown that APP_{695} cells have significantly reduced ATP levels compared to SH-SY5Y-MOCK cells (Grewal et al., 2020).

The effects of EC on ATP levels in SH-SY5Y cells were determined after incubation with EC (0.1 µM, 1 µM, 10 µM, 100 µM and 1000 µM) or the solvent control. In the impairment model, the specific inhibition of complex I of the respiratory chain was carried out with rotenone, which resulted in a decrease in ATP levels. Incubation with 0.1 µM and 1 µM EC resulted in a statistically significant increase in ATP levels in both cell lines compared to the control group. In "healthy" neuronal cells (SH-SY5Y MOCK cells), a protective effect under rotenone damage could also be demonstrated for treatment with these concentrations. Exposure to higher EC concentrations (≥ 100 µM), on the other hand, resulted in a statistically significant drop in ATP levels to zero (0 µM) in SH-SY5Y cells. This result is in contrast with the results in the MTT assay and the MMP measurements. In the MTT assay, it became clear that metabolic activity

in SH-SY5Y cells was severely impaired but existed after incubation with the listed concentrations. The MMP showed only a slight statistically significant impairment after treatment with 100 µM EC. Consequently, a reduction in ATP levels but not a complete inhibition of ATP synthesis would be expected. To analyse this contradiction in more detail, it was further checked whether EC (0.1 - 1000 µM) interacts with the ATP assay. An interaction was excluded for all concentrations (data not shown).

To evaluate whether EC is able to compensate or increase the global defect of the mitochondrial respiratory capacity in SH-SY5Y- cells, the activities of the respiratory system complexes after 24-h incubation with 1 µM EC were measured. In accordance with the results of ATP production, an increase in mitochondrial respiration could be expected. However, the results from the respirometry showed an increase in the mean values for both cell lines, but the increase was not statistically significant. This outcome may indicate a shift of metabolism towards upregulated glycolytic ATP production to compensate for declining mitochondrial respiration and OXPHOS energy production. It was aimed to investigate the effects of EC on oxidative stress simulated by exposure to H_2O_2 (50 µM and 75 µM), as previous experiments had shown potential benefits of EC in mitigating stress in cells. Specifically, this work suggests that EC may enhance cell viability. Remarkably, it was observed that treatment with 1 µM EC led to an increase in viability levels in SH-SY5Y-MOCK cells under conditions of oxidative stress. To the best of our knowledge, this study is the first to demonstrate this particular effect of EC. The findings add to the growing body of evidence supporting the antioxidative, antiaging, and longevity-promoting properties of EC. While low concentrations of EC did not affect cell viability, a 1 µM concentration of EC improved viability levels under oxidative stress in SH-SY5Y-MOCK cells. Previous research by Wang et al., Diling et al., and Kushairi et al. (discussed in chapter 3.4.1) has shown positive influences on ATP levels from substances extracted from *Hericium erinaceus*. Damaged cells were restored to higher ATP levels by these various metabolites. These findings align with the observations of elevated ATP levels after rotenone impairment. The measurements also indicated an increase in ATP levels in cells not damaged by rotenone, compared to untreated cells. This increase may be due to improvements in the respiratory chain complexes. However, increased activity of these complexes can also lead to heightened oxidative stress, as the main producers of ROS in the Electron Transport System are complexes I and III. The production of ROS can negatively affect these complexes and downstream Complex IV (Nickel et al., 2014). A possible explanation for the increased ATP levels could be the protective effects of EC observed during both rotenone and hydrogen peroxide treatments. These protective effects could be mediated by different mechanisms, such as antioxidant-mediated defence in peroxide-treated cells. Such defence mechanisms could function either

directly or through enzymatic systems. Rotenone-damaged cells could also benefit from enhanced antioxidant protection. Increased expression of enzymes like SIRT-1 and subsequent downstream processes could also positively influence these effects.

3.2.1 Effects on mRNA expression, oxidative stress, neuronal outgrowth, and Aβ levels

Furthermore, the effect of a 24-hour incubation with EC compared to the solvent control on the expression of various mitochondrial and Alzheimer's-associated genes (SIRT1, CREB1, NRF1, TFAM, ATP5D) was determined in the present work in SH-SY5Y cells. Based on the findings of the ATP and MTT assays, concentrations of 0.1 µM and 1 µM EC were used for this purpose as these showed the strongest effects in the assays measured up to this point. To our current knowledge, this has not been investigated before.

SH-SY5Y-MOCK cells show a positive effect after treatment with 1 µM EC on NRF1, TFAM and SIRT1. However, in SH-SY5Y-APP_{695} cells, only NRF1 was significantly increased.

Mitochondrial biogenesis is considered an important parameter that is impaired in the progression of AD (Cenini et al., 2019). Hirai et al. (2001) were able to show in brain tissue samples of the human hippocampus that the number of mitochondria is statistically significantly reduced in AD patients compared to the control group. Moreover, Reddy et al. (2018) demonstrated significantly decreased PGC-1α (2.1-fold), NRF1 (1.8-fold) and TFAM (2.5-fold) mRNA levels in mAPP-HTT2 cells transfected with an APP mutation vector compared to the nontransfected control group. In their study, Sheng et al. analysed the extent to which alterations in the PGC-1α/NRF/TFAM pathway contribute to mitochondrial dysfunction in AD. It was shown that the expression of PGC-1α, NRF1 and -2 as well as TFAM was statistically significantly downregulated in the hippocampal tissue of AD patients as well as in APPswe M17 cells, a model of EOAD, compared to the control group. Decreased expression of PGC-1α as a master regulator of mitochondrial biogenesis and the other downstream transcription factors suggests interference with this signalling pathway in AD. In the cerebellum of AD patients, these changes were absent, suggesting a restriction of mitochondrial biogenesis in AD-specific brain regions. In APPswe M17 cells, transfection of the cells with a PGC-1α plasmid, which led to overexpression of the gene, promoted expression of the downstream proteins NRF1 and TFAM and thus mitochondrial biogenesis (Sheng et al., 2012). These findings indicate that increased

expression of these transcription factors could stimulate mitochondrial biogenesis and counteract AD-associated mitochondrial dysfunction.

In APP_{695} cells, treatment with EC caused an impairment of the investigated upstream elements of PGC-1α, which does not indicate an increase in the expression of the master regulator of mitochondrial biogenesis. In addition, the expression of TFAM, a downstream protein of NRF1, was decreased despite increased expression of NRF1 after EC exposure. In the context of the functions of the various up- and downstream regulators, the data collected do not indicate an influence of EC on the PGC-1α/NRF/TFAM signalling pathway in the AD model. For this reason, it can be postulated that EC in this AD model does not exert a positive influence on the mitochondrial transcription factors studied at the gene level and does not influence the associated reduced mitochondrial biogenesis via increased activation of the PGC-1α/NRF/TFAM signalling pathway. In contrast to the results in APP_{695} cells, treatment with 1 µM EC in SH-SY5Y-MOCK cells resulted in a statistically significant upregulation of SIRT1, NRF1 and TFAM. Increased expression of SIRT1 could result in increased expression of PGC-1α and associated downstream elements, thus positively affecting mitochondrial biogenesis. This could indicate a concentration-dependent positive effect of EC on biological aging and should be further explored in this context. Comparable studies regarding the influence of mitochondrial biogenesis on the gene level after treatment of neuronal cells with EC are rare. To confirm the listed assumptions, the expression of the genes at the protein level should also be considered. The gene expression analysis of further regulators of mitochondrial biogenesis, such as PGC-1α and AMPK, could allow additional conclusions on an influence of EC on the listed signalling pathway. Furthermore, it would be interesting to look at the average number of mitochondria and their distribution in this context.

SIRT1 is known for its function as a longevity regulator, acting as a key molecule for neuronal plasticity, cognitive function, and protection against age-related neurodegeneration and cognitive decline. Studies have shown that overexpression of SIRT1 in the brain, especially in mice, is associated with an increase in lifespan and other anti-ageing effects (Roda et al., 2021). In their study, I.-C. Li et al. (2019) demonstrated for the first time that treatment with 5 mg/g erinacine A-enriched HE myeloid solution resulted in a dose-dependent statistically significant increase in the lifespan of Drosophila melanogaster (+ 32 %) and senescence-accelerated P8 mice (+ 23 %). In this research, a statistically significant positive effect on SIRT1 expression could only be observed in SH-SY5Y MOCK cells after treatment with 1 µM EC, which could

have a favourable effect on biological ageing and the antioxidative stress response. In this context, further studies are needed.

Since a high response for SIRT1 was observed, the effects of EC on a previous impairment with H_2O_2 (50 µM and 75 µM) to simulate oxidative stress were investigated. From previous experiments, one should expect some positive effects of EC on stressed cells. As expected, 1 µM EC improved the viability levels under oxidative stress in SH-SY5Y-MOCK cells. This has never been carried out before and supports the antioxidative, antiaging and longevity effects of EC.
Degeneration of neurons is already present in the early stages of AD (Mufson et al., 2019). Increasing the functionality and connectivity of neurons is therefore a promising approach to treating AD.
Gene expression analysis of NRF1 by RT–qPCR showed statistically significant upregulation of the gene after treatment with EC in both APP_{695} (0.1 µM, 1 µM) and MOCK cells (1 µM). Since NRF1, in addition to its role as a downstream protein in the PGC1-α/NRF/TFAM pathway, also plays an important role in the regulation of neuritogenesis (J. L. Wang et al., 2013), the effect of EC (0.1 µM, 1 µM) on neurite growth in SH-SY5Y cells was also investigated in this research. Treatment with EC or DMSO alone failed to induce the differentiation of SH-SY5Y cells. Since retinoic acid plays a role in inducing neural differentiation, only the groups treated with it were evaluated (Maden, 2007).. Coincubation with EC resulted in a statistically significant increase in average neurite length in both cell variants. After treatment with 1 µM EC, the average neurite length was increased to approximately twice that of the control group. These effects were also clearly visible in the light microscope images.
This is consistent with the *in vivo* studies of Tzeng et al. (2018), who investigated the effects of erinacine A in 5-month-old female APPswe/PS1dE9 mice. To study the effect of dried, 5-month-old APP/PS1 mice were fed with erinacine A and erinacine S (30 mg/kg/day) for 30 days. The group showed that the treatment supported the growth of neurons in the hippocampus and cerebral cortex (Tzeng et al., 2018).

In hippocampal neurons, impaired NGF signalling resulted in activation of the amyloidogenic pathway, resulting in increased Aβ levels and increased intra- and extracellular Aβ aggregation and ultimately neuronal cell death (Matrone et al., 2008). In the experiments, no effects of EC on $A\beta_{1\text{-}42}$ levels in SH-SY5Y-APP_{695} cells were found. This is contrary to previous experiments by Tzeng et al. The group showed that treatment with erinacine A alleviates the burden of Aβ plaques in APPswe/PS1dE9 mice. However, one must note that they investigated a

noncompacted Aβ form. Therefore, a further comparison is not possible. Additionally, the effects of EC on Aβ plaques have not been further investigated in the scientific literature.

3.2.2 RNAseq analysis and molecular modelling of TrkB binding

In addition to NGF, brain-derived neurotrophic factor activates signalling pathways by binding to TrkB, which promotes neuronal survival, differentiation, synaptic plasticity and neurogenesis. Jang et al. (2010) demonstrated that 7,8-dihydroxyflavone (7,8-DHF) acts as a high-affinity TrkB receptor agonist and initiates dimerization and autophosphorylation of the receptor, which in turn activates downstream signalling pathways. Accordingly, 7,8-DHF protected wild-type but not TrkB-deficient neurons from apoptosis and had a neuroprotective effect in an animal model of Parkinson's disease (Jang et al., 2010). Ötzkan et al. (2021) reported that 21 days of oral supplementation of male C57BL/6 mice with 100 mg/kg body weight 7,8-DHF restored decreased levels of the Rho proteins Rac1 and Rab3A in membrane preparations from the brains of the treatment group. Rho proteins are considered key regulators of neuronal morphogenesis and support synaptic plasticity. 7,8-DHF had no effect on BDNF and TrkB levels but positively influenced T lymphoma invasion and metastasis-inducing protein 1 (TIAM1) levels, which were reduced in the brains of old mice. Tiam1 is associated with numerous neuronal processes, including neurite growth. Therefore, it can be postulated that 7,8-DHF counteracts age-related cognitive dysfunction(Ötzkan et al., 2021). Molecular docking analyses revealed in silico that EC binds to TrkB with a higher affinity than 7,8-DHF (data not shown in this work). This can explain the neuritogenesis effects presented in this work (chapter 2.8).

Regarding this array of noncohesive effects of EC in the literature and our own results, one should investigate the effects more broadly. Erinacines are synthesized in *Hericium erinaceus* at the mevalonate pathway. The pathway is also called the isoprenoid pathway, which is also the building block of cholesterol and steroid hormones, both of which are fat soluble and can pass through membranes. Since erinacine C is also synthesized in the mevalonate pathway and shows a wide array of effects, it is interesting to check its effects in an RNAseq analysis.

Erinacines were first discovered 28 years ago and show a wide array of effects (Kawagishi et al., 1994, 1996; Kawagishi & Zhuang, 2008). Erinacines, especially erinacine C, are able to induce nerve growth factor β (NGF) and brain-derived neurotrophic factor (BDNF) expression in astrocytes (Chiu et al., 2018; H.-T. Huang et al., 2021; Kawagishi et al., 1994). Despite inducing neurotrophic expression, it has also been reported that erinacines act as antidepressants (Chiu et al., 2018), neuroprotective agents (K.-F. Lee et al., 2014, 2020), and anti-inflammatory

agents (Bailly & Gao, 2020; Tsai-Teng et al., 2016) and stimulate neurogenesis (Rascher et al., 2020; Shimbo et al., 2005). Rascher et al. (2020) proposed TrkA receptor activation as the underlying mechanism for neurogenesis.
In their experimental setup, they investigated expression changes in astrocytic cells induced by erinacine C. They found that erinacine C induces NGF expression, subsequently stimulating PC12 differentiation by binding and activating TrkA. Furthermore, they tested transcriptional processes activated by erinacine C. Here, the group found several reporter constructs reflecting particular signalling pathways upregulated. However, only binding sites for estrogen receptors (ERE) and E26 transformation specific (ETS) were statistically significant. Since their results could not support their hypothesis that NGF secretion is not activated alone via ETS, they offered a pleiotropic transcriptional response as an explanation.

Unfortunately, PC12 cells do not express TrkB receptors, which are activated by BDNF and can activate neurotrophic effects in neuronal cells such as SH-SH5Y cells. Our own research gave us the hint to investigate TrkB, which shows in silico a higher affinity than an already known agonist 7,8-DHF (data not shown). This is also already supported by *in vivo* data. Chiu et al. (2018) tested the antidepressant effects of an erinacine A-enriched mycelium in ICR mice. Although the group used a versatile mouse model, one can suspect the broad effect of erinacines, the mechanism of which is rarely discussed in the scientific literature.

The discoverer of erinacines, Prof. Hirokazu Kawagishi, asked in his latest paper “Chemical studies on bioactive compounds related to higher fungi” the question of whether erinacines are similar to gibberellins and therefore plant hormones (Kawagishi, 2021). Plant hormones are involved in a range of activities, such as plant growth and development, pathogen defence (Bürger & Chory, 2019) and stress tolerance (Ku et al., 2018). Furthermore, they are lipophile and can pass through membranes. Could this explain the extensive effect of erinacines?

Gene Ontology (GO) enrichment analysis was performed for both cell lines treated with 1 µM erinacine C. To our knowledge, this is the first transcriptomic profiling in SH-SY5Y cells after treatment with erinacine C. Here, interesting discoveries were made that smoothly link the genomic data with the *in vitro* data. Based on existing scientific literature and our own RT–qPCR results at activating NRF1, it was rightly assumed that erinacine C stimulates neurogenesis (chapter 2.8). With the GO of biological processes, a clear activation of neurogenesis, neuronal differentiation and generation of neuron-related genes after treatment with 1 µM erinacine C could be seen. Similar activations were found in the GO Cellular Component enrichment. Here,

processes for axons, postsynapse, synapses and neuron projection were the most activated processes. This clearly demonstrates the neurogenesis effects of erinacine C. Furthermore, it also shows that those processes are not exclusively activated. Rascher et al. (2020) claimed a pleiotropic effect regarding the effect of erinacine C. The claim could be expanded, supporting the hypothesis by Kawagishi et al. (2021) that erinacines exert a hormone-like effect. This hypothesis finds support in the KEGG pathway analysis, which shows that 1 µM erinacine activates a wide range of genes in various pathways. However, most importantly, it activated the estrogen signalling pathway with 97 pathway genes. Here, genes such as GNAI3, HSP90AA1, NCOA1, and MMP2 are activated. GNAI3 and MMP2 are guanine nucleotide-binding proteins and metalloproteinases, which are two different classes of genes. However, both are activated on the cell membrane and are transducers in transmembrane signalling pathways (Baldini et al., 2022; Toyama et al., 2017). NCOA1 encodes proteins that act as transcriptional coactivators for steroid and nuclear hormone receptors (Wu et al., 2002). HSP90AA1 encodes heat shock proteins that act as chaperones. Chaperones promote the maturation, structural maintenance and regulation of specific target proteins involved in cell cycle control and signal transduction. HSP90AA1 plays a critical role in mitochondrial import. It delivers preproteins to the mitochondrial import receptor TOMM70 (Young et al., 2003). This is interesting because the translocase of outer mitochondrial membrane 70 (TOMM70) is related to mitophagy pathways and therefore to mitochondrial viability. Furthermore, many genes in the insulin signalling pathway were activated. This makes sense because the oestrogen and insulin signalling pathways are often correlated in their mechanism of action. The insulin signalling pathway is building the bridge for mitochondrial viability via an alternative production of ATP via beta oxidation. With GO a regulation of acetyl-CoA carboxylase 2 (ACACB), was found. ACACB is a complex multifunctional enzyme system that catalyzes the carboxylation of acetyl-CoA to malonyl-CoA, the rate-limiting step in fatty acid synthesis (Cheng et al., 2007; Colbert et al., 2010; Kaushik et al., 2009; C. W. Kim et al., 2010).

Malonyl-CoA inhibits CPT1, which is the shuttle for fatty acids into the mitochondrial matrix. In Alzheimer's, mitochondria are in a substrate undersupply for energy production (Grewal et al., 2020; Swerdlow, 2020). To maintain energy production, other substrates can be used. In this research, it was found that ACACB is downregulated, which leads to higher levels of acetyl-CoA and reduces the probability of malonyl-CoA inhibiting CPT1 and therefore increases the availability of alternative substrates for the Krebs cycle and subsequently for OXPHOS. ACACB is also a drug target in clinical research (L. Chen et al., 2019).

An extensive effect of erinacine C has already been demonstrated, which is by far not exhaustive. To further support the hypothesis of a hormone-like effect of erinacines and erinacine C,

the last part will generally and briefly discuss the GO in neurodegenerative pathways. Solute carrier family 25 member 5 (SLC25A5) encodes a gated pore that translocates ADP from the cytoplasm into the mitochondrial matrix and ATP from the mitochondrial matrix into the cytoplasm. This antiporter also plays crucial roles in mitochondrial uncoupling and mitochondrial permeability transition pore (mPTP) activity. It has been suggested that it is the master regulator of mitochondrial energy output by maintaining a subtle balance between ATP production and thermogenesis (Ito et al., 2010; Namba et al., 2020).

In chapters 0 and 3.2.1, discrepancies between the results achieved by the ATP assay and the downregulation of ATP5D (also named ATP5F1D) were identified. This subunit of mitochondrial ATP synthase catalyzes ATP synthesis using an electrochemical gradient of protons during oxidative phosphorylation. ATP synthase is composed of two linked complexes with multiple subunits: the soluble catalytic core, F_1, and the membrane-spanning component, F_O, including the proton channel. The catalytic section of mitochondrial ATP synthase is made of 5 different subunits (alpha, beta, gamma, delta, and epsilon) assembled with a stoichiometry of 3 alpha, 3 beta, and a single representative of the other 3 (Fernandez-Vizarra & Zeviani, 2021; Nirody et al., 2020; Watanabe & Noji, 2013). The RNAseq data show a significant upregulation of the subunits ATP5F1A, ATP5F1B and ATP5F1E. ATP5F1C and ATP5F1D are upregulated but not statistically significant. Therefore, as indicated in chapter 3.2.1, downregulation is presumed to be negligible given the positive regulation of mitochondrial parameters and increased ATP levels detected using a luminescence assay.

3.3 Effects of ethanolic *Hericium erinaceus* mycelium extract on *C. elegans*

To our knowledge, the effects of *Hericium erinaceus* on mitochondria in an AD model of *C. elegans* have not yet been investigated. To compare the effects, two strains, CL2122 and GMC101 were used. CL2122 was utilized here as a control strain because it expresses no $A\beta_{1\text{-}42}$. In Alzheimer's disease, mitochondrial function, as indicated by ATP production, is known to be impaired (Swerdlow, 2020). It was observed that ATP levels in GMC101 (mean = 19.17 ± SD 4.444) are significantly lower than those in the control strain CL2122 (mean = 25.51 ± SD 2.129). This finding supports the initial assumption and aligns with the documented mitochondrial dysfunction in Alzheimer's disease. Erinacine C was not detected in the sample, as evidenced by the chromatogram in chapter 8.2. There could be several reasons for its absence,

including but not limited to degradation during processing, stability issues, or shelf-life concerns. As of 2023, there is no information in the scientific literature that addresses these speculations. The ethanolic mycelium extract of *Hericium erinaceus* showed no effect on the lifespan of all concentrations on CL2122. This result is divergent from the result of Chuang et al. The group described protective effects of a *Hericium erinaceus* extract in the wild-type N2 strain (Chuang et al., 2009). Therefore life-prolonging results in CL2122 would have been expected. However, the authors here presumably used a water extraction from a crude extract containing fruiting bodies and not mycelium. Nevertheless, the effects of GMC101 on the lifespan assay were positive and statistically significant at all concentrations (0.01 mg/mL, 1 µg/mL, 10 µg/mL, 100 µg/mL). ATP levels showed a stepwise increase at concentrations of 0.01 mg/mL, 1 µg/mL, and 10 µg/mL and were statistically significant at 10 µg/mL. At 100 µg/mL, the ATP levels decreased. The results are not sufficient enough to compare or correlate the ATP levels with lifespan outcomes. However, higher concentrations might be toxic and not further support antioxidative and longevity effects.

Currently, there is no literature available discussing the effects of an ethanolic extract of *Hericium erinaceus* mycelium in an AD model of *C. elegans*. However, the ethanolic extract contains a wide array of molecules, such as polysaccharides, heteropolysaccharides, polyphenols, phenolic compounds, lipid compounds and ergothioneine (Khan et al., 2013). Therefore, only an assumption regarding the effects and components of the extract is possible. Valu et al. (2021) tested the effects of an ethanolic *Hericium erinaceus* mycelium extract (0.5 µg/mL, 1 µg/mL, 3 µg/mL) containing erinacine A on cognitive function using the scopolamine (SCOP)-induced zebrafish (*Danio rerio*) model of memory impairment. The results indicate that *Hericium erinaceus* extract has positive effects in managing memory deficits and brain oxidative stress in zebrafish with memory impairment. Although the paper primarily tested cognitive functions, they also tested antioxidative markers. Here, markers such as acetylcholinesterase activity, superoxide dismutase, catalase, glutathione peroxidase, glutathione, malondialdehyde and carbonylated proteins were investigated. The overall effect of those markers was positive after treatment (Valu et al., 2021). Along with the study of Valu et al. (2021), Sun et al. (2021) tested the effects of water and ethanol extracts from *Hericium erinaceus* (200 ppm) solid-state fermentation containing erinacine A on the effects in brain cells in zebra fish embryos. The authors showed that treatment with different concentrations of an ethanol and water extract of the *Hericium erinaceus* extract could reverse the toxic effects of 1 % ethanol treatment. While the neural mechanisms and lifespans of zebrafish and *C. elegans* differ significantly, both organisms serve as crucial pieces of a larger puzzle in understanding the intricacies of neurological health. Observations from zebrafish illuminate vertebrate neural function, while findings

in *C. elegans* offer windows into cellular processes, including oxidative stress. Making direct comparisons remains a challenge; however, solving this puzzle requires connecting these distinct pieces. Together, the insights from both organisms may suggest that optimal neurological health could be linked to longevity and reduced oxidative stress across different species. Oxidative stress, or the overproduction of reactive oxygen species (ROS), has been linked to the progression of Alzheimer's disease. ROS are also involved in various cellular functions, including gene transcription and signal transduction(Wilson et al., 2018). However, overproduction of ROS and free radicals leads to a deterioration of cellular antioxidant defence mechanisms (Murphy, 2009; Swerdlow, 2020). Intracellular ROS are generated from various endogenous and exogenous sources. For example, 90 % of cellular ROS are generated by mitochondria. The mitochondrial electron transport chain is considered the primary endogenous source of ROS, including superoxide ($O^{2-}\bullet$), hydrogen peroxide (H_2O_2), singlet oxygen ($^1O^2$), nitric oxide (NO) and hydroxyl radical (OH•), which are involved in cellular function and signalling (Murphy, 2009).

The metabolic reduction of oxygen can lead to the production of potentially harmful ROS (Z. Chen & Zhong, 2014; Swerdlow, 2020). Mutations and metabolic imbalances can lead to a significant shift in redox balance and mitochondrial dysfunction, which inhibit enzyme and protein synthesis and result in excessive ROS production. In the brains of Alzheimer's patients, elevated oxygen consumption, increased polyunsaturated lipid content and impaired antioxidant defence systems lead to further ROS formation. Neurons and glial cells are sensitive to oxidative stress, and the accumulation of excess ROS alters the function of key biomolecules, including nucleic acids (DNA, RNA), proteins and lipids. In addition, alterations in the activity of antioxidant enzymes (e.g., glutathione peroxidase and superoxide dismutase) have been shown to reduce the proliferation rate of neuronal cells in AD (Z. Chen & Zhong, 2014). The observations indicate that ROS levels in the GMC101 strain (mean = 360.8 ± SD 104) are significantly higher than those in the control strain CL2122 (mean = 94.5 ± SD 78.9) ($p < 0.0001$). This increase in ROS aligns with the recognized phenomenon of oxidative stress resulting from mitochondrial dysfunction, a prominent characteristic seen in Alzheimer's disease. However, in the fluorescence microscope-based quantification of ROS levels in GMC101 cells, a clear reduction in ROS levels after treatment with 1 µg/mL and 10 µg/mL was found. This is consistent with the improved longevity effects under heat stress. As described above, Valu et al. showed an increase in antioxidative enzymes (Valu et al., 2021). In the *C. elegans* model, the effects of antioxidative enzymes were not further investigated. However, in the mRNA experiments, an increase in TFAM in both cell lines was observed, which was even higher in the SH-SY5Y-APP_{695} AD model. This could explain the decreased ROS levels. Zhao et al. showed that

increased mtROS and mitochondrial dysfunction affect TFAM-mediated mtDNA maintenance (M. Zhao et al., 2021). Conversely, increased TFAM levels reduce oxidative stress. The effects of HEM could reduce ROS through upregulation of antioxidative enzymes and TFAM.
The results of the cellular experiments show a more in-depth analysis of its effects and mechanisms. It is suggested that further investigations with the invertebrate model will reveal more positive and in-depth effects. A definitive limitation of the experiments is that the compounds present in the mycelium were not analysed – a known mixture would be better, but characterizing compounds in a matrix is time and labour intensive. Furthermore, references and standards are limited.

3.4 Effects of ethanolic *Hericium erinaceus* mycelium extract on SH-SY5Y cells

In the present work, the effect of an ethanolic *Hericium erinaceus* mycelium extract (HEM) on ATP levels in SH-SY5Y cells was investigated for the first time. SH-SY5Y-MOCK cells are used here as a control cell line compared to the early onset Alzheimer's model SH-SY5Y-APP_{695}. Both cell lines show similarities in morphology, but due to the additionally transfected coding region of human AβPP (AβPP_{695}) or a corresponding empty vector (pCEP4), they can be used as different models.
Currently, only a few studies have been published on the effect of *Hericium erinaceus* (HE) extracts or other bioactive HE metabolites on mitochondrial parameters such as ATP concentration and mRNA expression. A limitation of this work is that the HEM matrix was not thoroughly analysed. Therefore, the derived effects are only speculative. Since the same parameters were also investigated for erinacine C, a more in-depth discussion will be found in chapter 3.2.

3.4.1 Effects on viability, ATP levels and mRNA expression

The effects of the extract differed between the two cell models. SH-SY5Y-MOCK showed a positive and gradual increase in viability with the MTT assay after treatment with 0.01 µg/mL and 0.1 µg/mL HEM. The higher concentrations showed a decreasing effect that was not statistically significant. However, in SH-SY5Y-APP_{695} cells, treatment with 0.01 µg/mL and 100 µg/mL showed a positive effect. The concentrations in between showed no statistically significant effect. SH-SY5Y-MOCK showed a stronger effect than the impairment model. This may be because APP_{695} generally has lower viability. What seems odd is that the concentration of 100 µg/mL shows a positive effect for the impairment model. A general problem is the

comparability of the results with the scientific literature. This is due to the different growing parameters, use of different parts from the fungi and different extraction methods. P. P. Yang et al. (2020) tested the effect of crude extracts of *Hericium erinaceus* mycelium on the viability of SH-SY5Y cells. In their assay, they found that the extract did not affect the viability of human SH-SY5Y cells at concentrations below 10 µg/mL. Higher concentrations (25 µg/mL, 50 µg/mL and 100 µg/mL) did not decrease the viability statistically but at least showed a downwards trend. Kushairi et al. (2019) tested the effect of an ethanolic basidocarp extract of *Hericium erinaceus* on BV2 microglia and HT22 neuron cells. They showed that the extract was neither neurotoxic nor stimulated the growth of BV2 microglia and HT22 neurons at concentrations ranging from 100 – 400 µg/mL. However, the ethanolic extract protected HT22 cells against H_2O_2-induced neurotoxicity at concentrations of 100 µg/mL, 200 µg/mL, and 400 µg/mL. The results of Kushairi et al. (2019) cannot confirm the positive viability results but also show no adverse effects.

The effects on the ATP levels unexpectedly showed a decrease in ATP for the two highest concentrations (1 µg/mL and 10 µg/mL). This is contradictory because this sharp decrease cannot be assumed from the viability experiments.

The results are even more paradoxical for APP_{695}. Treatment with 0.001 µg/mL led to a decrease of ~ 50 %, whereas 0.01 µg/mL showed a positive effect, increasing the levels by approximately 20 %. Amara et al. (2020) tested the effects of *Hericium erinaceus* biomass containing mycelium and primordia on PC12 cells. The cells were treated with 1 µM of the extract to test its effects against oxidative stress and apoptosis induced by di(2-ethylhexyl)phthalate (DEHP). In addition to other positive effects, the treatment could reverse the dissipation of the mitochondrial membrane potential (MMP). However, the treatment alone could not increase the MMP levels compared to the control group (Amara et al., 2020). In the experiments, an increase in ATP levels was observed, which was not shown by Amara et al. (2020) regarding the MMP values.

D. Wang et al. (2019) investigated the preventive effect of treatment with EP-1, a polysaccharide from HE mycelium, on ATP levels in Caco2 cells. Treatment with H_2O_2 resulted in a statistically significant decrease in ATP levels (-22.6 %) compared to the untreated control group. The decreased ATP levels could be increased 4.5- and 5.2-fold by preincubation with 100 µg/mL and 500 µg/mL EP-1, respectively, suggesting an improvement of mitochondrial function by the metabolite (D. Wang et al., 2019). Similar results were obtained in a study by Diling et al. (2017) In this study, it was shown that 3-hydroxyhericenone F (3-HF) (1 µg/mL, 1.5 µg/mL) isolated from the HE fruiting body also had a preventive effect on ATP levels and ATP

synthase activity in sodium azide (NaN3)-injured PC12 cells (Diling et al., 2017). Furthermore, coincubation with an ethanolic extract from the basidiocarp of HE (400 µg/mL) in mouse hippocampal neurons (HT22) significantly counteracted an H_2O_2 (250 µM)-induced decrease in ATP concentration (~ +21 %) (Kushairi et al., 2019).

Due to the absence of standardized effectors or matrices and the employment of different cell culture lines, a direct comparability of the results from the listed studies with the data collected in this work is not assured. This variability underscores the necessity for increased research efforts to investigate and standardize the extract. However, the current literature indicates a positive effect of *Hericium erinaceus* or various *Hericium erinaceus* metabolites on ATP levels after different types of impairment in various cell models.

As already described, the results from RT–qPCR show miscellaneous effects on ATP5D, CREB1, NRF1 and TFAM. The results cannot easily be explained within the previous results from this work and may lead to new questions being raised. A more detailed discussion can be found in chapter 3.2.1. Additionally, a comparison to scientific literature is difficult, since mitochondrial parameters regarding *Hericium erinaceus* extracts are rarely investigated ATP5D was decreased for SH-SY5Y-MOCK for the concentrations 0.01 µg/mL and 0.1 µg/mL. Interestingly, 0.1 mg/mL showed an increasing effect compared to 0.01 µg/mL in SH-SY5Y-APP_{695} cells. This is also in accordance with the results from the ATP levels, where 0.01 µg/mL increased the values. However, 0.1 µg/mL showed a decreasing effect. This finding can be explained by the viability assay or by the ATP levels.
The extract showed a positive effect on CREB1 expression in both cell lines at 0.1 mg/mL. However, the trend for the lower concentration diverges.
NRF1 showed no effect in SH-SY5Y-MOCK cells and had a negative effect at 0.1 µg/mL in SH-SY5Y-APP_{695} cells. TFAM showed a strong response for both cell lines at a concentration of 0.1 µg/mL. One can speculate about the implications and mechanism of the results presented, but a conclusion about the effects of the extract cannot be drawn. This is due to the unknown matrix and the lack of further experiments to pinpoint the effects of the extract on mitochondrial parameters. A better approach is the investigation of a single compound such as erinacine C, which is described in the following chapters.

3.5 Effects of *Hericium erinaceus* and erinacine C on neurodegenerative diseases

Research on *Hericium erinaceus*, also known as Lion's Mane mushroom, has shown promising potential for its use in Alzheimer's research. Alzheimer's disease is a progressive neurological disorder that affects cognitive function and memory, and there is currently no cure for the disease. The current drugs available for Alzheimer's disease have several shortcomings.

First, these drugs do not provide a cure for the disease. They can only help manage symptoms and slow down the progression of the disease in some cases. Furthermore, the drugs have side effects that can be significant, such as nausea, vomiting, diarrhea, and loss of appetite. Third, the drugs only address some of the symptoms of Alzheimer's disease, such as memory loss and cognitive impairment. Fourth, the cost of Alzheimer's drugs can be a significant burden for patients and their families, especially since the disease is often associated with other health problems that require expensive treatments. Overall, current drugs do not address the underlying causes of the disease, such as the accumulation of β-amyloid plaques, neurofibrillary tangles in brain neuron loss and loss of mitochondrial functionality (Cummings et al., 2019; Frozza et al., 2018; Kinney et al., 2018; Mehta et al., 2017).

Hericium erinaceus is a natural supplement that has been found to have neurotrophic, anti-inflammatory, and antioxidant properties, which may help protect the brain from damage and inflammation that can contribute to the development and progression of Alzheimer's disease (Cordaro et al., 2021; I.-C. Li et al., 2018; Yanshree et al., 2022). In addition, *Hericium erinaceus* has been shown to improve cognitive function and memory in patients with mild cognitive impairment and Alzheimer's disease, which suggests that it may have therapeutic potential for the disease (I.-C. Li et al., 2020; Mori et al., 2009; Saitsu et al., 2019).

The use of natural supplements such as *Hericium erinaceus* as part of a broader strategy of lifestyle and nutrition interventions is an area of active research in Alzheimer's disease. There is evidence to suggest that a healthy diet and lifestyle can help reduce the risk of developing Alzheimer's disease and may also help slow the progression of the disease in people who have already been diagnosed. Several components in *Hericium erinaceus* may have potential therapeutic benefits for Alzheimer’s disease.

Beta-glucans are complex carbohydrates that are found in the cell walls of *Hericium erinaceus*. Beta-glucans have been shown to have immune-boosting properties and may also help reduce

inflammation in the brain, which is thought to contribute to the development and progression of Alzheimer's disease (Hagl et al., 2015; W. S. Lee et al., 2022; Shi et al., 2020). Ergothioneine is a naturally occurring amino acid that is found in high levels in *Hericium erinaceus* (Cohen et al., 2014; Roda et al., 2021). Ergothioneine has been found to have antioxidant properties, which may help protect the brain from oxidative damage and inflammation (Cheah et al., 2017; Song et al., 2014). Hericenones are also bioactive compounds that are unique to *Hericium erinaceus*. Hericenones and hericerin have been found to have anti-inflammatory and antioxidant properties, which may help protect the brain from damage and inflammation that can contribute to the development and progression of Alzheimer's disease (Martínez-Mármol et al., 2023; Mori et al., 2008). Erinacines are bioactive compounds that are unique to *Hericium erinaceus*. Erinacines have been found to stimulate the production of nerve growth factor (NGF), which is important for the growth and survival of nerve cells in the brain (Rascher et al., 2020; C.-C. Zhang et al., 2017). NGF also promotes the formation of new synapses, which are critical for learning and memory (Kopach et al., 2020; S. H. Wang et al., 2012). Furthermore, it has been shown that erinacines can pass the blood–brain barrier (J. H. Hu et al., 2019). The compounds alone and in combination could help to ameliorate AD.

The experiments performed in this thesis revealed that an ethanolic mycelium extract of *Hericium erinaceus* improved the lifespan under heat stress in the invertebrate AD model GMC101. Furthermore, ATP levels increased, and ROS levels partly decreased. This could be due to the synergistic effect of all components in the HER. Cheah et al. aimed to investigate the uptake, metabolism, and effects of ergothioneine, a natural antioxidant, on biomarkers of oxidative damage and inflammation in healthy human subjects. In the study, 20 healthy subjects were given 5 mg/kg ergothioneine daily for 28 days. Blood and urine samples were collected before and after supplementation to assess the uptake and metabolism of ergothioneine and its effects on biomarkers of oxidative damage and inflammation. The results showed that ergothioneine was well tolerated by the subjects and had high uptake and bioavailability. The levels of ergothioneine in the blood and urine of the subjects increased significantly after supplementation. The study also showed a significant reduction in biomarkers of oxidative damage and inflammation in the blood samples of the subjects after ergothioneine supplementation (Cheah et al., 2017). Beta glucans also have a valuable effect. Hu et al. (2022) investigated the effects of three different types of *β*-glucans, a type of soluble fibre, on cognition in rats and humans, with a focus on the role of the gut-brain axis. The results showed that all three types of *β*-glucans improved cognitive performance in both rats and humans, with the greatest effect observed with a particular type of *β*-glucan derived from oats. The study also found that the beneficial effects

of *β*-glucans on cognition were mediated by changes in gut microbiota composition, increased production of short-chain fatty acids, and reduced inflammation in the brain. Overall, the findings suggest that *β*-glucans may have potential as a dietary intervention to improve cognitive function and that the gut-brain axis may play an important role in this process (M. Hu et al., 2022). This is consistent with the study of Li et al., which aimed to investigate the potential lifespan-extending effects of erinacine A-enriched *Hericium erinaceus* mycelia (EAHE) on Drosophila melanogaster and aged mice. In Drosophila, the study found that feeding the mycleia to adult flies significantly extended their lifespan compared to a control group, while also improving their climbing ability and reducing oxidative stress. In aged mice, a study found that daily oral administration of EAHE improved cognitive function and extended the lifespan of mice (I.-C. Li et al., 2019). In the cell model, the effects of the ethanolic mycelium extract were diverse. Overall, a positive effect for both cell lines, the control and the AD group, is visible, but the effects are not always coherent. The viability test showed a higher effect in SH-SY5Y-MOCK cells than in SH-SY5Y APP_{695} cells, although the range was denser in SH-SY5Y APP_{695} cells. This means that the effect is more likely to occur in the AD group. The ATP levels also varied in both cell lines. In SH-SY5Y MOCK cells, no positive effects were found, whereas SH-SY5Y APP_{695} cells showed a positive effect at 0.01 µg/mL. Furthermore, 1 and 10 µg/mL HEM led to ATP levels of 0 µM. A hypothesis to clarify this result could be that a toxic level was reached. However, this seems unlikely since the viability showed no decline at those concentrations. Additionally, a pan interference assay could be ruled out. The only indication for a toxicity effect could be the mRNA results. In SH-SY5Y MOCK cells, ATP5D expression levels decreased at 0.1 mg/mL. This could suggest that higher concentrations further decrease ATP5D activity and therefore decrease ATP levels. However, the effect cannot be explained coherently because the levels of CREB1 and TFAM were elevated in both cell lines and therefore in line with the viability experiments in cellular and invertebrate models.

Overall, studies suggest that *Hericium erinaceus* has potential therapeutic effects on Alzheimer's disease in mice and rats and may have neurotrophic and neuroprotective properties that could be beneficial in the prevention and treatment of AD. While there is no direct link between beta-glucans and Alzheimer's disease, some research suggests that beta-glucans may have potential neuroprotective effects that could be beneficial for Alzheimer's patients. Shi et al. investigated the effects of *β*-glucan on cognitive function in mice with obesity induced by a high-fat, fibre-deficient diet (HFFD). The objective was to determine whether *β*-glucan could impact the gut-brain axis and alleviate cognitive impairment associated with Western-style dietary patterns. After 15 weeks of *β*-glucan supplementation, the mice showed improvements in cognitive

performance as assessed by object location, novel object recognition, and nesting building tests. *β*-glucan also reduced microglial activation, engulfment of synaptic puncta, and proinflammatory cytokine expression (TNF-*α*, IL-1*β*, and IL-6) in the hippocampus. Furthermore, *β*-glucan enhanced PTP1B-IRS-pAKT-pGSK3*β*-pTau signalling for synaptogenesis, improved synaptic ultrastructure, and increased both pre- and postsynaptic protein levels. In conclusion, the study provides evidence that *β*-glucan improves cognition and brain function by exerting beneficial effects on the gut microbiota-brain axis. The findings suggest that increasing the consumption of *β*-glucan-rich foods could be a viable nutritional strategy for preventing neurodegenerative diseases.(Shi et al., 2020). Q. Zhang et al. (2023) investigated the effects of *β*-glucan derived from *Saccharomyces cerevisiae* on cognitive impairment in a mouse model of Alzheimer's disease (APP/PS1 mice) by examining its influence on intestinal flora and their metabolites. The results showed that *β*-glucan treatment improved cognitive function in APP/PS1 mice, as assessed by various behavioural tests. In addition, *β*-glucan altered the composition of the intestinal flora in these mice, reducing the abundance of harmful bacteria and increasing the abundance of beneficial bacteria. The changes in gut microbiota were accompanied by alterations in their metabolites, such as short-chain fatty acids (SCFAs) and bile acids, which are known to be involved in maintaining gut health and modulating brain function. Furthermore, the study found that *β*-glucan treatment reduced A*β* plaque deposition and tau hyperphosphorylation in the brains of APP/PS1 mice, two key pathological features of Alzheimer's disease. This was accompanied by reduced neuroinflammation, as evidenced by decreased levels of proinflammatory cytokines and increased levels of anti-inflammatory cytokines in the brain (Q. Zhang et al., 2023). Trovato et al. (2016). investigated the effect of *Hericium erinaceus* on oxidative stress and inflammation in the brains of rats with Alzheimer's disease. The researchers found that treatment containing mycelium and primordia reduced oxidative stress and inflammation and increased the expression of lipoxin A4, a molecule with anti-inflammatory properties. They suggest that *Hericium erinaceus* may have potential as a therapeutic agent for AD and that its effects may be due to its ability to modulate the cellular stress response and promote lipoxin A4 expression (Trovato et al., 2016).

The study by Mori et al. (2009) was a randomized, double-blind, placebo-controlled trial investigating the effects of *Hericium erinaceus* mushroom on cognitive function in elderly Japanese individuals with mild cognitive impairment (MCI). A total of 30 participants were randomly assigned to either the *Hericium erinaceus* group or the placebo group and consumed tablets containing *Hericium erinaceus* extract or a placebo for 16 weeks. The results showed that the *Hericium erinaceus* group had significantly increased scores on a cognitive function scale

compared to the placebo group. The *Hericium erinaceus* group also showed improvement in their scores on a quality-of-life scale. The authors concluded that *Hericium erinaceus* may be effective in improving cognitive function in individuals with MCI, but further studies with larger sample sizes are needed to confirm these findings (Mori et al., 2009). Nagano et al. investigated the potential effects of *Hericium erinaceus* intake on depression and anxiety levels in adult humans. The study involved 30 female participants who consumed *Hericium erinaceus* powder daily for 4 weeks. The results showed a significant reduction in depression and anxiety scores after the 4-week intervention compared to the baseline scores. The authors suggest that the intake of *Hericium erinaceus* may have potential antidepressant and anxiolytic effects in humans. However, it should be noted that this study had a small sample size, and further research is needed to confirm these findings. However, the authors noted that a different mechanism from the NGF-enhancing action of *Hericium erinaceus* could also be an explanation for the effect (Nagano et al., 2010). The results reflect and support the positive effects, although the underlying mechanism is still unknown. In a pilot double-blind placebo-controlled study, I.-C. Li et al. (2020) explored the potential of erinacine A-enriched *Hericium erinaceus* mycelia as a preventive measure against early Alzheimer's disease. The researchers conducted a trial with participants who had a family history of AD or mild cognitive impairment (MCI) and were at risk of developing AD. Participants were divided into two groups, receiving either an erinacine A-enriched *Hericium erinaceus* mycelia supplement or a placebo for six months. Cognitive function was assessed using the Mini-Mental State Examination (MMSE), while mood, sleep quality, and daily living activities were evaluated through questionnaires. The results demonstrated that the group receiving the erinacine A-enriched *Hericium erinaceus* mycelia supplement showed significant improvements in cognitive function compared to the placebo group. In addition, the supplemented group exhibited improvements in mood, sleep quality, and daily living activities (I.-C. Li et al., 2020). Although the interfering effects of *Hericium erinaceus* have been reported, the mechanism of action and effect on mitochondrial levels remain to be revealed.

Limited studies of erinacine C at the mitochondrial level have been published thus far. Therefore, it is difficult to compare and discuss the results from this work in depth regarding the effect on mitochondrial parameters in AD. The data for erinacine C is again versatile and gives and fails to support strong mitochondrial effects of erinacine C in SH-SY5Y MOCK or SH-SY5Y APP_{695}. However, it can be noted that the results in this work are in line with data published thus far. Erinacine C shows an effect on ATP levels in both cell lines at 0.1 and 1 µM. Although the effect is not statistically strong due to high variance, the levels were increased by

at least 30 %. Even under additional rotenone stress, a significant positive effect on SH-SY5Y MOCK was visible. However, these results are not conclusive to hypothesize the impact on people with cognitive decline. Measuring mitochondrial respiration and mRNA levels did not fully support the positive effects. Although respiration was higher for every complex in both cell lines, the effect was due to the high standard deviation, which was not statistically positive. Furthermore, the mRNA results for both cell lines showed a decrease. This is embedded in the fact that the MMP shows no difference for all concentrations. This leads to an incomplete regarding the effects of erinacine C on mitochondrial parameters. An explanation for this could offer a paper by Zhou et al. (2018). Although it is crucial to mention that the paper was retracted and they did not clarify which erinacine was used. The authors stated that within cancerous Hep-G2 cells, erinacines open the mitochondrial permeability transition pore (Zhou et al., 2018). This could at least hypothetically explain the negative effect for 100 and 1000 µM. It can also lead to the question of whether other models, such as primary cells, should be used in the future to investigate the effects of erinacine C in neuronal models.

The mRNA results were also not clear regarding the effects on mitochondrial parameters. NRF1 shows a positive effect on both cell lines. NRF1 regulates cellular growth and is associated with neuronal growth (Kiyama et al., 2018). This finding is consistent with the positive effects on neuronal outgrowth after erinacine C treatment in both cell lines and the molecular modelling results. Additionally, this could explain the increasing ATP levels. SIRT1, CREB1 and TFAM regulate mitochondrial DNA integrity (Kang et al., 2018; J. Lee et al., 2005; Majeed et al., 2021). SIRT1 and TFAM showed a positive effect on SH-SY5Y cells but a negative effect on SH-SY5Y APP_{695}. CREB1 was only negative for SH-SY5Y APP_{695}. This could again indicate that at the mitochondrial level for SH-SY5Y APP_{695}, there is no or only a limited effect regarding erinacine C. However, the neuroplasticity- or neuronal growth-inducing effect of erinacine C may still be positive for elderly individuals and people suffering MCI. In particular, erinacines can pass the blood brain barrier (J. H. Hu et al., 2019). Finally, the results from the RNAseq analysis showed an overall positive effect on the cellular health of erinacine C, especially in neuronal differentiation axonal and synaptic sprouting. The effects are stronger and more versatile in SH-SY5Y MOCK. However, in SH-SY5Y cells, APP_{695} at the molecular level activated genes for actin binding. These proteins are important regulators of the cytoskeleton and further mitochondrial and cell integrity (Illescas et al., 2021; Svitkina, 2018). The generally versatile upregulation of genes is in accordance with the study of Rascher et al. The researchers found that erinacine C activates the transcription of genes involved in the promotion of neuronal growth and differentiation, including NGF, via the ETS family of transcription factors.

Specifically, they identified a consensus ETS DNA-binding site that is activated by erinacine C in astrocytic cells (Rascher et al., 2020). Nevertheless, the study failed to explain other effects triggered by erinacine C and suggested pleiotropic effects. Martínez-Mármol et al. (2023) investigated the effects of hericerin derivatives on spatial memory in rats. They found that treatment with hericerin derivatives improved spatial memory performance in the Morris water maze test, a commonly used test for assessing spatial learning and memory. The researchers also investigated the mechanism underlying the effects of hericerin derivatives and found that they activated a pan-neurotrophic pathway in central hippocampal neurons, leading to the enhancement of ERK1/2 signalling (Martínez-Mármol et al., 2023). Although this can also explain the neuroplasticity effect that is proposed for hericenones and erinacines, it cannot explain the overall effects. Therefore, it is suggested extending the pleiotropic effect of erinacines to a hormone-like effect. Erinacines and specifically erinacine C could activate the hormone like effect via direct impact on steroid hormones, stimulation of hormone synthesis enzymes or regulation of neuroendocrine cells. This is driven by the versatile activation of genes and pathways but also due to the upregulation of proteins encoding hormone receptors. This hypothesis could be further proven with a combined approach of RNAseq, Western blot analysis, ELISA and pharmacological inhibition. Testing this activity would be difficult in a human trial. However, *Hericium erinaceus* can be used safely as a food supplement to support healthy aging (I.-C. Li et al., 2020; Mori et al., 2009; Nagano et al., 2010; Saitsu et al., 2019). In the future, food supplements enriched with erinacines could have a further nutritional impact.

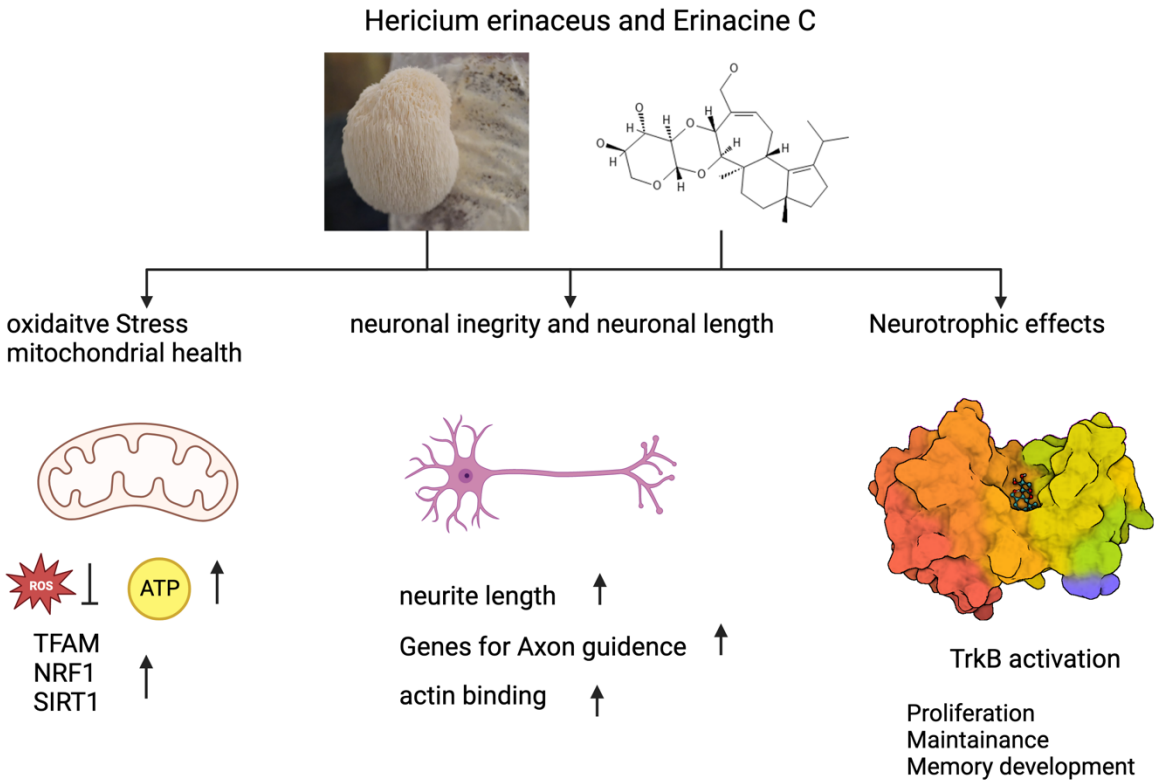

Figure 3-1 illustrates the effects of Hericium erinaceus and erinacine C on neurodegenerative diseases, such as Alzheimer's.

Both Hericium erinaceus mycelium extract and erinacine C can reduce oxidative stress and enhance mitochondrial health. Moreover, erinacine C has a positive impact on neuronal outgrowth and promotes neuronal integrity. A proposed mechanism involves the activation of TrkB, which leads to neuronal outgrowth and helps maintain and increase neuronal plasticity. Overall, these various effects could be triggered through a hormone-like mechanism. Created with BioRender.com

4 Conclusion

In conclusion, this study successfully isolated and characterized erinacine C from *Hericium erinaceus* mycelium using a submerged culture and optimized the process through lyophilization, resulting in clearer chromatograms. This suggests a potential pathway for further refining the yield of erinacine C through techniques such as buffering with HEPES. Although upscaling of erinacine C production has yet to be explored, the findings lay a foundation for future research in this direction. Additionally, this investigation has broken new ground in the examination of erinacine C's effects on mitochondrial, viability, and neuronal parameters in SH-SY5Y cells in an AD cell model. This is particularly significant given the lack of extensive previous research in this area. The development of quicker and more sensitive identification methods may enhance the ability to facilitate both *in vitro* and *in vivo* research, contributing to the broader understanding of erinacine C's properties and effects.

These findings might stimulate further studies to contribute to and broaden the existing understanding. However, it seems that the overall effect of erinacine C on various mitochondrial and neuronal parameters in SH-SY5Y cells are not overall specific. Therefore, new avenues of research have been opened with the RNAseq analysis, adding credence to the hypothesis of hormone-like effects of erinacine C. However, these results should be taken as a stepping stone rather than a conclusion. The proposed effects of erinacine C on the TrkB receptor and its potential to stimulate neuritogenesis still require in vitro validation. Future research may consider using a knockout model to further explore this hypothesis. Despite the rigorous methodological approach and high sample size used to ensure normalized results, the limitations of this study are recognized. The MTT assay, while providing indications of metabolic activity and viability, may benefit from additional, more sensitive assays such as BrdU. Unexpected findings like the decreased ATP levels at higher concentrations of erinacine C highlight areas for further investigation, perhaps employing tools like HPLC, NMR, or a seahorse assay to cross-check ATP levels.

The RNAseq analysis and mitochondrial gene investigation, while contributing valuable data, do not yet allow for concrete statements about the underlying mechanisms of erinacine C's effects. More in-depth mechanistic study, such as the application of Western blot methods to confirm protein expression corresponding to gene activity, is recommended.

One of the key limitations we encountered was the undefined matrix of the mycelium extract, which could potentially be responsible for observed longevity effects, increased ATP levels, and decreased ROS levels. Future research could employ LC-MS-MS investigation to examine the constituent molecules of this matrix more thoroughly. Though there is speculation around the general effectiveness of erinacine C in humans, the question remains open for empirical study. Existing research has indicated some positive effects of *Hericium erinaceus* extracts on small groups of individuals with dementia, though these effects have been marginal and are not yet thoroughly understood. However, our findings suggest that erinacines, particularly erinacine C, in *Hericium erinaceus* might function in a hormone-like manner, impacting a wide variety of genes, pathways, and hormone receptor proteins. To explore this hypothesis further, we recommend employing a blend of sophisticated methodologies, including RNA sequencing, Western blot analysis, and pharmacological inhibition.

Despite potential challenges in human trials, the safety profile of *Hericium erinaceus* lends itself to usage as a dietary supplement, potentially providing benefits for healthy aging and overall well-being. Essentially, this work contributes to the evolving understanding of erinacine C and its potential therapeutic applications in AD treatment and paving the way for future studies in this promising field.

In summary, despite certain limitations and areas for further research, the present study provides a comprehensive investigation into erinacine C's effects on mitochondrial parameters, neuroprotective properties, transcriptomic effects, and potential mechanisms. These findings are hoped to inspire further study to better understand and harness the potential of erinacine C.

5 Experimental Part

5.1 Materials

5.1.1 Devices

Table 5-1 lists all devices used.

Table 5-1 List of devices.

Description	Model	Company
Agitator ball mill	DYNO®-MILL Research LAB	Wiley A. Bachofen AG
Autoclave	LABOKLAV 25 Basic	SHP Steriltechnik AG
Autoclave	LABOKLAV 160 MSL	SHP Steriltechnik AG
Autoclave	LABOKLAV 160 MSL	SHP Steriltechnik AG
Autoclave	LABOKLAV 25 Basic	SHP Steriltechnik AG
Bunsen Burner	Fuego SCS basic	WLD-TEC GmbH
Cell counting chamber	Neubauer- counting chamber	Labor Optik
Cell counting chamber	Nageotte - counting chamber	Brand GmbH + Co. KG
Cell culture workbench	MSC Advantage	Thermo Scientific
Cell Homogeniser	Balch Cell Homogeniser	Isobiotech
centrifuge	Heraeus Megafuge 16 R	Thermo Scientific
centrifuge	Heraeus Fresco 21 Centrifuge	Thermo Scientific
centrifuge	GS-6R Centrifuge	Beckman Coulter GmbH
centrifuge	Microfuge® 22R	BECKMAN COULTER™
centrifuge	Allegra® X-15R	BECKMAN COULTER™
chiller	Minichiller MKR	Huber
Chiller	Minichiller	Huber
Clean bench	HERA safe KS18	Thermo Scientific
Drying cabinet	Heraeus T6	Thermo Scientific
Evaporator	Rotavapor® R-300	BÜCHI Labortechnik GmbH
Fluorescence microscope	EVOS M5000	Thermo Fisher Scientific
Freezer (-20 °C)	GNP 5255 Index 20A/001	Liebherr International Deutsch-land GmbH
Freezer (-80 °C)	TSX SERIES with V-DRIVE	Thermo Fisher Scientific
Freezing Container	Nalgene®, Mr. Frosty	Thermo Fisher Scientific
Fridge	LIEBHERR RBa4250 Prime	Liebherr International Deutsch-land GmbH

Hamilton-Syringe	Hamilton-Spritze gastight, #1701, #1702, # 1705, #1725	Hamilton
Heating bath	IKA® HB10 basic	IKA®-Werke GmbH
High resulution Mass spetrometre (hr-MS)	ESI-MS Mikro-TOF	Bruker Corporation
HPLC-system		
HPLC Autosampler	L-7200	MERCK HITACHI
HPLC DAD	L-7455	MERCK HITACHI
HPLC Interface	D-7000	MERCK HITACHI
HPLC Pump	L-7100	MERCK HITACHI
Ice machine	AF 80 Scotsman	Frimont
Incubator	Midi 40 CO_2 Incubator	Thermo Fisher Scientific
Incubator	INE 500	Memmert
Laminar air flow work bench	MSC Advantage	Thermo Fisher Scientific
Magnetic stirrer	IKA® RH basic 2	IKA®-Werke GmbH
Multichannel pipette	Xplorer 300 µL	Eppendorf
NanoDrop Microvolume Spectrophotometers and Fluorometer	Nanodrop One	Thermo Fisher Scientific
Nuclear magnetic resonance spectroscopy (NMR)	Bruker Avance III 400 MHz	Bruker Corporation
Oxygraph	Oxygraph-2K	Oroboros
PCR-Cycler	T100™ Thermal Cycler	Bio-Rad
PCR-Workstation	PCR-Workstation	Fisher Scientific
pH-Meter	pH Meter HI2210	Hanna Instruments Deutschland GmbH
pH-Meter	Seven Easy	Mettler Toledo GmbH (Schweiz)
Pipette	Finnpipette® 300 µL	Thermo Electron Corporation (Thermo Scientific)
Pipette	Research Plus 100-1000 µL	Eppendorf
Pipette	Pipetman P2, P20, P200, P1000	Gilson
Pipette Boy	accu-jet® pro	Brand
plate reader	CLARIOstar	BMG Labtech
Plate Stirrer	VARIOMAG MONO	H+P Labortechnik
precision balance	Präzisionswaage AEJ200-5CM	Kern&Sohn GmbH

Precision balance (d = 0,01 mg)	BP211D	Sartorius
Precision balance (d = 0.01 g)	Atilon Aculab	Sartorius Group
Preperative HPLC-system		
Preperative HPLC Fraction Collector	Foxy R1	KNAUER Wissenschaftliche Geräte GmbH
Preperative HPLC Pump	P 4.1S	KNAUER Wissenschaftliche Geräte GmbH
Preperative HPLC UV-Detector	UVD 2.1S	KNAUER Wissenschaftliche Geräte GmbH
Pure water device	Milli-Q Academic	Millipore
Pyrolysis furnace	HCE 8544.0	Bosch
Real-time-PCR-System	CFX Connect™ Real-Time System	Bio-Rad
Refrigerator (4 °C)	3130 Index 20B/001	Liebherr International Deutschland GmbH
Shaker	Multitron	Infors AG
SpeedVac	Christ Alpha RVC 2	Martin Christ GmbH
Thermomixer	PSC24N Thermo-Shaker	Grant-bio
Time-of-flight mass spectrometer	MicroTOF Agilent	Bruker Daltonics®
Ultrasonic bath	Elma T710DH	OMNILAB
Ultra-Turrax	IKA® T18 basic	IKA®-Werke GmbH
Vacuum pump	Diaphragm vacuum pump	Vaccubrand GmbH & Co
Vacuum Pump	Millivac-Mini Vacuum Pump, XF5423050	Merck KGaA
Vortex	Vortex-Genie 2®	Scientific Industries
Waterbath	WNB22	Memmert

5.1.2 Consumables

Table 5-2 lists all consumables used.

Table 5-2 List of consumables.

Description	Model	Company
12-Well-Plates	12 Well Cell Culture Plate	Greiner Bio-One
24-Well-Plates	24 Well Cell Culture Plate	Greiner Bio-One
6-Well-Plates	6 Well Cell Culture Plate	Greiner Bio-One
96-Well-Plates	96 Well Cell Culture Plate	Greiner Bio-One
96-Well-Plates (PCR)	Hard-Shell® PCR Plates 96-well, thin wall	Bio-Rad
Centrifuge tubes	Cellstar® tubes 50 mL, 15 mL	Greiner Bio-One
Coverslips	Menzel Coverglasses 24 x 46 mm	Thermo Fisher Scientific
Glas Pasteur pipettes	Glas Pasteur pipettes	Carl ROTH GmbH & Co. KG
Gloves	Vasco® Nitril white	B. Braun SE
PCR foil	Microseal® B-Adhesive Sealer MSB-1001	Bio-Rad
PCR tube	Saphire PCR- Reaction tubes 0,2 mL	Greiner Bio-One
Pipette tips	Ultratip 1000 µL, 200 µL, 10 µL	Greiner Bio-One
Pipette tips	Finntip® 1000 µL, 300 µL, 200 µL, 10 µL	Thermo Scientific
Plastic Pasteur pipettes	Pasteur pipettes	VWR
Precision Wipes	Kimtech Science tissue	Kimberley-Clark® Professional
Reaction tubes	Reaction Tubes 2 mL, 1 mL, 0,5 mL	Greiner Bio-One
Sealing film	PARAFILM® M	Sigma–Aldrich
Serological pipettes	Cellstar® 50 mL, 25 mL, 10 mL, 5 mL	Greiner Bio-One
Single use cannula	Fine-ject® 21Gx1 ½“ Nr.2 0,8x40 mm TW/LB	Henke Sass Wolf
Syringes	Injekt® Luer Solo 20 mL, 10 mL, 5 mL	B. Braun SE

5.1.3 Chemicals

Table 5-3 lists all chemicals and solutions used.

Table 5-3 List of chemicals

Description	Company
β-Mercaptoethanol (78,13 g/mol)	ITW Reagents
100% Ethanol (EtOH)	Carl ROTH GmbH & Co. KG
2xYT-Medium	Carl Roth GmbH + Co. KG
4-(2-hydroxyethyl)-1-piperazineethanesulfonic acid (HEPES)	Merck KGaA
70% EtOH	self-prepared
Aceton	Applichem
Acetonitril, Chromasolv, for HPLC, Gradient Gr.	Sigma–Aldrich
Acetyl-Coenzyme A	AppliChem
Adenosindiphosphat (ADP)	Sigma–Aldrich
Agar Agar SERVA Kobe I	SERVA Electrophoresis GmbH
Ammonium sulfate, ≥ 99,5 %, p.a., ACS, ISO	Carl Roth GmbH + Co. KG
Ampicillin sodium salt	Carl Roth GmbH + Co. KG
Antimycin A	Sigma–Aldrich
Apoprotinin	Sigma–Aldrich
Aqua double-distilled (Aqua dd)	Self-prepared with Milli-Q Academic
Biocoll Separating Solution	Biochrom
Bovine serum albumine, essentially fatty acid free (BSA)	Sigma–Aldrich
Calciumcarbonat, powder, 99 % A.C.S. pure	Sigma–Aldrich
Calciumcholrid-Dihydrat ($CaCl_2 \cdot 2\ H_2O$)	Merck KGaA
Carbenicillin disodium salt	AppliChem GmbH
Chloroform-d_1 + 0.03 % TMS	Acros Organics
Cholesterol	Sigma–Aldrich
D-(+)-Glucose-Monohydrat	Carl Roth GmbH + Co. KG
D(+)-Saccharose; ≥ 99,5 %, p.a.	Carl Roth GmbH + Co. KG
Digitonine	Merck KGaA
Dimethylsulfoxid (DMSO)	Merck KGaA
Dithionitrobenzoic acid (DTNB)	Sigma–Aldrich
D-Mannitol; ≥ 98 %	Sigma–Aldrich
Dulbecco's Modified Eagle Medium (DMEM)	Invitrogen by Thermo Fisher Scientific Inc.
Dulbecco's Phosphate Buffered Saline (DPBS) (10x)	Gibco (Thermo Scientific)

Edamin® K (Lactalbumin Enzymatic Hydrolysate)	Sigma Sigma–Aldrich
Ethanol (>99 %)	Merck KGaA
Ethanol (70 %)	Carl Roth GmbH + Co. KG
Ethyl acetate HPLC grade, 99.8 %	Carl Roth GmbH + Co. KG
Ethylene glycol tetraacetic acid (EGTA)	Sigma–Aldrich
Ethylenediaminetetraacetic acid (EDTA)	Merck KGaA
FCCP	Sigma–Aldrich
Fetal calf serum (FCS)	Sigma–Aldrich
Glucose	Merck KGaA
Glutamate	Sigma–Aldrich
Hanks' balanced salts	Sigma–Aldrich
Hanks' balanced salts	Sigma–Aldrich
Hydrochloric acid (HCl), 1 N; 0,1 N	Merck KGaA
Hydrochloric acid (HCl), 37 %	Merck KGaA
Hygromycin B (50 mg/mL)	Invitrogen by Thermo Fisher Scientific Inc.
iTaq™ Universal SYBR® Green Supermix	Bio-Rad
K-lactobionate	Sigma–Aldrich
Leupeptin	Sigma–Aldrich
Magnesium chloride hexahydrate	Merck KGaA
Magnesium sulfate heptahydrate	Merck KGaA
Magnesium sulfate heptahydrate	Merck KGaA
Malat	Sigma–Aldrich
Malt extract	Fluka
MEM vitamin solution 100x	Gibco by Thermo Fisher Scientific Inc.
Minimun Essential Media (MEM) Non-Essential Amino Acids (NEAA) 100x	Gibco by Thermo Fisher Scientific Inc.
MitoTracker™ Red CM-H_2Xros	Thermo Fischer Scientific
Molasses	Südzucker
N,N,N',N'-Tetramethyl-p-phenylendiamin-Dihydrochlorid	Sigma–Aldrich
Nystatin Suspension	Sigma–Aldrich
Oatmeal, organic	Bauck GmbH
Oligomycin	Sigma–Aldrich
Oxalacetate	Sigma–Aldrich
Penicillin/Streptomycin (PenStrep)	Invitrogen
Pepstatin	Sigma–Aldrich
Peptone from casein	Merck KGaA
Phenylmethylsulfonylfluorid (PMSF)	Merck KGaA

Potassium chloride	Merck KGaA
Potassium hydroxide (KOH), 5 N	Merck KGaA
Pyruvat	Sigma–Aldrich
Rhodamine-123	Sigma–Aldrich
RNAprotect® Cell Reagent	Qiagen
RNAse free water	Thermo Fisher Scientific
Rotenone	Sigma–Aldrich
Sodium azide	Sigma–Aldrich
Sodium Chloride	Merck KGaA
Sodium chloride (NaCl)	Sigma–Aldrich
Sodium deoxycholate	Merck KGaA
Sodium fluoride (NaF)	Sigma–Aldrich
Sodium hydroxide (NaOH), 1 N; 0,1 N	Merck KGaA
Sodium hydroxide pellets	Merck KGaA
Sodium hypochlorite solution	Carl Roth GmbH + Co. KG
Sodium orthovanadate	Sigma–Aldrich
Sodium pyruvate	Sigma–Aldrich
Sodiumhydrogencarbonat NaHCO3	Merck KGaA
Succinate	Sigma–Aldrich
Sucrose	Carl Roth GmbH + Co. KG
SYTOX™ Green acid stain (5 mM)	Thermo Fisher Scientific Inc.
Taurine	Sigma–Aldrich
Triethanolamine	Sigma–Aldrich
Tris(hydroxymethyl)-aminomethan	Merck KGaA
Triton X-100	Merck KGaA
Trypan blue	Sigma–Aldrich
Trypsin-EDTA (0.05%)	Gibco by Thermo Fisher Scientific Inc
TWEEN® 20	ChemCruz Bio-Connect B.V.
Urea	Merck KGaA
Yeast extract	OXOID Limited

5.1.4 Columns

Table 5-4 lists all columns used for HPLC and preparative HPLC.

Table 5-4 Columns for HPLC and preparative HPLC.

Name	**Supplier**
Kromasil 100 C18, 7 µm, 250 x 20 mm	MZ Analysentechnik

Nucleosil® C18, 100-5, 125 x 3 mm	Macherey Nage
guard-column Kromasil 50x20 mm, 100 C18, 7 µm	MZ Analysentechnik
guard-column Nucleosil® C18, 100-5, 8 x 3 mm	Macherey Nage

5.1.5 List of Kits

Table 5-5 lists all kits used.

Table 5-5 Kits used.

Description	**Company**
iScript™ cDNA-Synthesis Kit	Invitrogen (Thermo Scientific)
RNeasy Mini Kit (250)	Qiagen
Turbo DNA-free TM-Kit	Thermo Scientific

5.1.6 Media for fungi

Malt extract agar (MEA)

Table 5-6 Malt extract agar.

Component	Medium **Concentration** (g L^{-1})
D-(+)-glucose monohydrate	4.0
malt extract	10.0
yeast extract	4.0
Agar-Agar	15 g
dd H_2O	1 L

The medium was autoclaved at 121 °C for 20 min prior to use and then poured into Petri dishes.

YMG 6.3

Table 5-7 YMG-6.3.

Component	**Medium concentration (g L^{-1})**
D-(+)-glucose monohydrate	4.0
malt extract	10.0
yeast extract	4.0
dd H_2O	1 L

The pH was adjusted to 6.3, and the medium was autoclaved at 121 °C for 20 min prior to use.

ZM ½ medium

Table 5-8 ZM ½ medium

Component	Medium concentration (g L $^{-1}$)
water-soluble components	
Molasses	5
D-(+)-glucose monohydrate	1.5
Sucrose	4
d-mannitol	4
Ammonium sulfate	0.5
The water-insoluble components were weighed separately into the respective Erlenmeyer flasks and then filled up with water-soluble components.	
water-insoluble components	
Edamin® K	0.5
Oatmeal	5
Calcium carbonate	1.5

The medium was autoclaved at 121 °C for 20 min prior to use. The water-insoluble components were weighed separately into the respective Erlenmeyer flasks and then filled with water-soluble components.

5.1.7 Buffers, solutions, and media for cell culture and experiments

Ultrapure water was used for the preparation of all buffers, solutions and media (Milli-Q, Millipore, Billerica, USA), which will be referred to as H_2O below.

Tris buffer

Table 5-9 Tris buffer.

Chemical	**concentration (g L $^{-1}$)**
Tris	2.42
H_2O	1 L

The pH was adjusted to 7.4 at 4 °C with HCl (1 N).

Phosphate buffer saline (PBS)

Table 5-10 PBS

Chemical	Amount for 1 L
DPBS (10x)	100 mL
H_2O.	900 mL

HBSS buffer

Table 5-11 HBSS buffer.

Chemical	**concentration (g L $^{-1}$)**
HBSS	9.5
HEPES	2.4
$CaCl_2 \cdot 2H_2O$	0.147
$CgSO_4 \cdot 7H_2O$	0.246

The substances were dissolved in 1.0 L H_2O and adjusted to pH 7.4 at 37 °C using HCl (1 N) and NaOH (1 N).

Trypan blue solution (0.4 %)

Table 5-12 Trypan blue solution.

Chemical	**Concentration (g 0.1 L $^{-1}$)**
Trypan blue	0.1
PBS (1x)	100 mL

Trypan blue was dissolved in 100 mL of PBS (1x).

Cell culture medium for SH-SY5Y-MOCK and SH-SY5Y-APP$_{695}$ cells

Table 5-13 Cell culture medium.

Chemical	concentration
DMEM	500 mL
FCS	10 %
Hygromycin B	0.3 mg/mL
Sodium pyruvate	5 mL
NEAA	5 mL
Pen/Strep	60 U/mL
Vitamins	5 mL

The indicated volumes are required to produce full cell culture medium. For the production of reduced cell culture medium, the FCS content was lowered to 2 %. The cell culture medium was stored at 4 °C.

Freezing medium

Table 5-14 Freezing medium.

Chemical	
FCS	50 %
DMSO (sterile filtered)	10 %

Freezing medium was stored at -20 °C.

Buffers for the determination of citrate synthase activity

Tris HCl buffer (1.0 M)

Table 5-15 Tris HCl buffer (1.0 M).

Chemical	Concentration (g 0.1 L $^{-1}$)
Tris	12.114 g
H_2O	100 mL

The pH was adjusted to 8.1 with HCl (37 %)

Triethanolamine HCl buffer (0.5 M)

Table 5-16 Triethanolamine HCl buffer (0.5 M).

Chemical	
Triethanolamine	8.06 g
H_2O	100 mL
EDTA	186.1 mg

The pH was adjusted to 8.0 with HCl (37 %)

Triton X 100 (10 %)

Table 5-17 Triton X 100 (10 %).

Chemical	
Triton X-100	10 g
H_2O	90 mL

Oxalacetate solution (10 mM)

Table 5-18 Oxalacetate solution (10 mM).

Chemical	**concentration**
Oxalacetate	5.94 mg
Triethanolamine HCl buffer (0.1 M)	4.5 mL

DTNB solution (1.01 mM)

Table 5-19 DTNB solution (1.01 mM).

Chemical	
DTNB	3.6 mg
Tris buffer	9 mL

Citrate synthase reaction medium

Table 5-20 Citrate synthase reaction medium.

Chemical	
DTNB	0.1 mM
Triton-X-100	10 %
Oxalacetic acid	10 mM
Acetyl coenzyme A	12.2 mM

K-Lactobionat stock solution

Table 5-21 K-Lactobionat stock solution

Chemical	
K-Lactobionat	35.83 g
H_2O ad	200 mL

The pH was adjusted to 7.0 with KOH.

MIR05

Table 5-22 MIR05.

Chemical	
EGTA	0.5 mM
$MgCl_2 \cdot 6$ H2O	3 mM
K-Lactobionat	60 mM
Taurine	20 mM
Sucrose	100 mM
BSA	1 g/l
H_2O ad	1 l

The pH was adjusted to 7.1 at 30 °C with KOH (5 N), and MIR05 was stored at -20 °C.

Lysis buffer

Table 5-23 Lysis buffer 1.

Chemical	
EDTA	1 nM
Triton X-100	0.5 %
NaF	5 mM
PBS (1x) ad	250 mL

Table 5-24 Lysis buffer 2.

Chemical	
Urea	6 M
Sodium pyrophosphat	2.5 mM
Sodium orthovanadate	1 mM
Sodium deoxycholat	0.5 %
Sodium dodecylsulfate	0.5 %
Buffer 1 ad	100 mL
To the appropriate amount of buffer 2 shortly before use, following substances were added:	
Aprotinin	1.7 mg/mL
Leupeptin	5 mg/mL
Pepstatin	100 mM

5.1.8 Buffers, media and solutions for Caenorhabditis elegans cultivation and experiments

Stock solutions

Table 5-25 Stock solutions for C. elegans cultivation and experiments.

Component	concentration	solvent
$CaCl_2$	1 M	dd H_2O
Carbenicillin	25 mg/mL	50% Ethanol
Cholesterol	5 mg/mL	≥ 99,5% Ethanol
$MgSO_4$	1 M	dd H_2O
KH_2PO_4	1 M	dd H_2O
KOH	5 M	dd H_2O

Bleach solution

Table 5-26 Bleach solution.

Component	Weighing-in for 1.5 mL total volume
dd H_2O	0.5 mL
NaClO (12% Cl)	0.5 mL
NaOH (5 N)	0.5 mL

Ethanol:TWEEN® 20 (92:8 v/v)

Table 5-27 Ethanol:TWEEN® 20 (92:8 v/v) solution.

Component	Weighing-in for 100 mL total volume
Ethanol (≥99,5%)	92 mL
TWEEN® 20	8 mL

NaCl-Pepton

Table 5-28 NaCl-Pepton solution.

Component	Weighing-in for 400 mL total volume
Pepton from Casein	0.5 g
NaCl	0.6 g
dd H_2O	ad 400 mL

2x yeast extract tryptone (YT)-medium

Table 5-29 2x Yeast Extract Tryptone (YT)-Medium.

Component	Weighing-in for 200 mL total volume
2x YT-Medium (pulver)	6.2 g
dd H_2O	ad 200 mL

Nematode Growth Medium (NGM)

Table 5-30 Nematode growth medium.

Component	Weighing-in for 10 mL total volume
$CaCl_2$ (1 M)	10 µL
Cholesterol (5 mg/mL in Ethanol)	10 µL
Carbenicillin	10 µL
KH_2PO_4 (1 M, pH=6,0)	250 µL
$MgSO_4$ (1 M)	10 µL
NaCl-Pepton-Solution	9.72 mL

NGM-agar

Component	Weighing-in for 375 mL total volume
Agar–Agar	6.4 g
Pepton from Casein	0.9 g
NaCl	1.1 g

The components are dissolved and the solution autoclaved (121 °C, 15 min). To cool down to 60 °C, the NGM agar is stored in a water bath. After reaching the desired temperature, the following components are added:

$CaCl_2$ (1 M)	375 µL
Cholesterol (5 mg/mL in Ethanol)	375 µL
Carbenicillin (25 mg/mL)	375 µL
$MgSO_4$ (1 M)	375 µL
KH_2PO_4 (1 M, pH=6,0)	9,375 mL
Nystatin-Suspension	9,375 mL

The NGM agar was then filled into Petri dishes (92 x 16 mm) in a suit of 9 mL each. After the NGM agar hardened, it was stored at 4 °C. The maximum storage time of the NGM agar is 3 months. The maximum storage time of the NGM agar is 3 months.

Coating of the NGM agar plates with OP50

A total of 600 µL of an E. coli OP50 day culture was spread on each NGM agar plate using a pipette. Using a disposable L-shaped spatula, this bacterial suspension is evenly distributed on the agar. These plates are dried under a fume hood for approx. 1 hour. The OP50-NGM agar plates were then stored at room temperature for a maximum of one week. The cultivation of Op-50 is described below.

M9 buffer

Table 5-31 M9-buffer solution.

Component	**Weighing-in for 400 mL total volume**
KH_2PO_4	1.2 g
Na2HPO4	2.4 g
NaCl	2.0 g
dd H_2O	ad 400 mL
The salts are shaken until they have dissolved. The solution is then autoclaved (121 °C, 15 min). After cooling the buffer, the following ingredient is added under semisterile conditions:	
$MgSO_4$ (1 M)	4 mL

M9-TWEEN® 20-buffer

Table 5-32 M9-TWEEN® 20-buffer.

Component	Weighing-in for 400 mL total volume
M9-buffer	400 mL
TWEEN® 20	4 mL

The substance TWEEN® 20 is added to the M9 buffer under semisterile conditions using a serological pipette. The M9-TWEEN® 20 buffer was stored at room temperature.

Tris buffer (20 mM)

Table 5-33 Tris buffer.

Component	Weighing-in for 500 mL total volume
Tris	1.2 g
dd H_2O	ad 500 mL

Isolation buffer

Table 5-34 Isolation buffer.

Component	Weighing-in for 500 mL total volume
Sucrose	51.4 g
TES	0.573 g
EGTA	0.389 g
dd H_2O	400 – 480 mL
The substances are completely dissolved in a 500 mL Schott bottle with a stirring fish on the magnetic stirrer. The pH value of the solution is adjusted to 7.2 using KOH (5 N). The solution is then transferred to a volumetric flask.	
dd H_2O	ad 500 mL

5.1.9 Software

Table 5-35 Software used.

Name/Version	Supplier
CLARIOstar	BMG LABTECH GmbH
CLARIOstar MARS	BMG LABTECH GmbH
GraphPad Prism	Statcon GmbH
OROBOROS® DatLab	OROBOROS Instruments GmbH
R 3.6.1	
Bio-Rad CFX Manager 3.1	Bio-Rad Laboratories Inc.
Bio-Render	https://biorender.com/
FIJI (ImageJ 1.53c)	NCBI
Simple Neurite Tracer 3.1.4	NCBI
PyMOL v2.4+	PyMOL by Schrödinger
AutoDock Vina v.1.2.0.	Center for Computational Structural Biology (CCSB)
LigPlot+ v.4.5.3	Thornton Group; European Bioinformatics Institute

5.2 Methods

5.2.1 Strain maintenance

For strain maintenance, agar plates were inoculated with *Hericium erinaceus*. Here, malt extract agar plates were used. The agar plates were each inoculated with approximately 1 cm^2 piece of agar well covered with mycelium, and the lid was sealed with parafilm. After a growth phase of 12 days in the incubator at 24 °C, the plates were stored at 4 °C in the refrigerator. *Hericium erinaceus* (FU70034, isolated from basidiocarp tissue) was obtained from InterMed Discovery (IMD) Natural Solutions, Dortmund, Germany.

5.2.2 Preculture inoculation

Basidiomycetes were cultured submerged in YM6.3 medium (Table 5-7). A well-grown agar piece (approximately 1 cm^2) was transferred to a 250 mL Erlenmeyer flask containing 100 mL of culture medium. The cultures were then homogenised with an Ultra-Turrax for approximately 15 s at $10 \cdot 10^3$ $U\text{-}min^{-1}$ and incubated on a shaker at 24 °C and 150 rpm in darkness.

After a growth period of seven days, these cultures were homogenised and used to inoculate the main cultures.

5.2.3 Main cultures inoculation

The precultures were homogenised with an Ultra-Turrax for approximately 15 s at $10 \bullet 10^3$ U-min^{-1}. The main culture medium ($ZM^{1/2}$ medium) (40 % of the total filling volume of an Erlenmeyer flask) was inoculated with the corresponding preculture (1 mL preculture per 10 mL main culture medium), and the flasks were cultivated on the shaker at 24 °C and 150 rpm under exclusion of light for 9 days.

5.2.4 Checking for contamination

Contamination was routinely checked by observing the growth of the culture and the appearance of the medium. Contamination by yeasts and/or bacteria would have resulted in turbidity of the culture medium. In addition, a microscopic check was carried out.

5.2.5 Extraction of the fungal culture

Samples, comprising mycelium and growth medium (median 32.8 g/400 mL), were homogenized using an agitator bead mill for 10 minutes at 3500 rpm. The fungal culture was extracted once with ethyl acetate in a 1:1 ratio. The organic phase was decanted and dried over sodium sulphate. If the samples were freeze-dried, 20 g were mixed with 100 mL ethyl acetate and stirred for two hours and filtered. It was then transferred to a 50 mL round bottom flask and concentrated to dryness using a rotary evaporator at 240 mbar and a bath temperature of 40 °C. The residue was taken up by careful resuspension in 1 mL acetonitrile. Prior to HPLC analysis, the extract of the culture supernatant was membrane filtered with a syringe filter (Chromafil® PET-45/15 MS, pore size 0.45 µm, Macherey-Nagel, Düren). For the ethanolic mycelium extract, 20 g of freeze-dried sample was mixed with 200 mL 70 % ethanol, stirred for 24 h on a magnetic stirrer, super sonicated for 2 h and filtered. It was then transferred to a 50 mL round bottom flask and concentrated to dryness using a rotary evaporator at 40 mbar and a bath temperature of 50 °C and then freeze-dried. Ethanolic mycelium extracts of *Hericium erinaceus* are used for research due to their ability to efficiently extract and preserve bioactive compounds, their solubility, ease of use, and safety. These factors make them ideal for studying the therapeutic potential of *Hericium erinaceus* in various health conditions, such as neurodegenerative

diseases and cognitive decline. Moreover, it has been reported that ethanolic extracts are effective in extracting erinacines (Chang et al., 2016; Friedman, 2015; Kawagishi et al., 1994; K.-F. Lee et al., 2014).

5.2.6 HPLC

High-performance liquid chromatography (HPLC) is a widely used analytical technique that separates and quantifies individual components within a mixture. The basic principle of HPLC involves passing a liquid sample through a column packed with a stationary phase (typically a porous solid material) under high pressure. A mobile phase (solvent) is used to facilitate the flow of the sample through the column. The different components in the sample interact differently with the stationary phase, which leads to their separation based on their physicochemical properties, such as polarity, size, or charge (Neue, 2006).

The first step in HPLC analysis is acquiring a chromatogram that represents the detector's response over time, with peaks corresponding to separated compounds. Baseline correction algorithms are then applied to eliminate drift or noise, enhancing the accuracy of the signal. Next, algorithms are used to identify and integrate peaks in the chromatogram, and the area under each peak is calculated, which is proportional to the compound concentration. To identify the compounds, their retention times are compared to known reference standards are used.

The HPLC parameters used for the analysis of erinacine C (MERCK HPLC) is listed in Table 5-36. Table 5-37 shows the gradient used.

Table 5-36 HPLC method parameters.

Component	**Model/Parameter**
Guard column	CC 8/3 Nucleosil® 100-5 C18, Macherey-Nagel
Columns	CC 125/3 Nucleosil® 100-5 C18, Macherey-Nagel
Injection volume	10 µL
Eluent A	ACN
Eluent B	dd H_2O
Flow rate	0,6 mL min^{-1}
Data aquisition	D-7000 HSM
Wave length	210 nm with DAD

Table 5-37 HPLC Gradient for the separation

time [min]	A [%]	B [%]
0	30	70
15	50	50
16	50	50
23	100	0
38	100	0
43	30	70
47	30	70

5.2.7 Preparative HPLC

Preparative HPLC is focused on the separation and purification of compounds from complex mixtures at a larger scale. This method utilizes larger column dimensions and higher flow rates, enabling the collection of larger quantities of purified compounds for further analysis or use. Preparative HPLC is often employed in pharmaceutical development, natural product isolation, and chemical synthesis to obtain sufficient amounts of pure compounds for structural characterization (Guiochon et al., 2006). The principles of separation in both HPLC and preparative HPLC are comparable. The preparative HPLC method used for the isolation of erinacine C is listed in Table 5-38. Table 5-39 shows the gradient used. The retention time for collecting erinacine C was determined based on previous experiments aimed at achieving a clear separation.

Table 5-38 Method parameters for preparative HPLC.

Component	Model/Parameter
Guard column	CC 50/20 mm Nucleosil®, 100 C18, 7 µm
Columns	CC 250/20 Nucleosil® 100-7 C18, Macherey-Nagel
Eluent A	ACN
Eluent B	dd H_2O
Flow rate	10 mL min^{-1}
Temperature	Room temperature
Wave length	210 nm

Table 5-39 Gradient for preparative HPLC for separation.

Time [min]	A [%]	B [%]
0	30	70
15	50	50
22.5	95	5
47	95	5

5.2.8 Nuclear magnetic resonance spectroscopy (NMR)

Nuclear Magnetic Resonance (NMR) spectroscopy is a powerful analytical technique used to study the structure and dynamics of molecules. NMR is based on the interaction of atomic nuclei with an external magnetic field, and it is commonly employed in various fields such as chemistry, biochemistry, pharmaceuticals, and materials science.

The underlying principle of NMR involves the absorption and re-emission of electromagnetic radiation by atomic nuclei in a strong magnetic field. When placed in a magnetic field, certain nuclei (e.g., ^{1}H, ^{13}C) with a non-zero spin can absorb energy at specific frequencies, causing them to transition between energy levels. The energy absorbed and the resulting NMR signals depend on the chemical environment of the nuclei, which provides information about the molecular structure and interactions (Keeler, 2010).

Thirty milligrams of the evaporated sample were dissolved in $CDCl_3$ and transferred into an NMR tube. NMR spectra were recorded on a Bruker Avance III 400 MHz NMR spectrometer. The data were collected and processed by TOPSPIN software (Bruker) running on a PC with Microsoft Windows 10. The NMR experiments were performed using Bruker standard pulse sequences and parameters. Chemical shifts are reported in ppm (δ scale) using the solvent signal as the standard and coupling constants (J) in Hz. Chloroform-d_1 + 0.03 % TMS was purchased from Acros Organics, Geel, Belgium. The NMR spectra were evaluated with help of Prof. Tatiana Zhuk and Prof. Andre Fokin.

5.2.9 High-resolution mass spectrometry (HR-MS)

High-resolution mass spectrometry (HR-MS) is an analytical technique used to accurately measure the mass-to-charge ratio (m/z) of ions derived from molecules in a sample. HR-MS is

widely employed in various fields such as proteomics, metabolomics, pharmaceuticals, environmental analysis, and forensics, due to its high sensitivity, selectivity, and resolving power. HR-MS operates by ionizing the molecules in a sample and measuring the time it takes for the ions to travel through a mass analyser, which separates them based on their m/z values. High-resolution mass spectrometers can differentiate ions with very similar m/z values, enabling the precise determination of molecular formulas and the identification of unknown compounds(Watson & Sparkman, 2008).

High-resolution mass spectrometry was carried out using an ESI-MS Micro-TOF by Bruker. The sample was dissolved in acetonitrile and injected into the device. Parameters for measuring were adjusted as follows: Voltage TOF 2400 V; Ion Polarity: positive; dry temperature: 180 °C; Nebuliser 0.4 bar; dry gas 4 l/min. The measurement was carried out by Steffen Wagner from the OC-Analytics platform. The results were analysed with Brucker Daltonics Data Analysis 3.4.

5.2.10 Cell lines

The SH-SY5Y cell line was used for the experiments. This was originally provided by A. Eckert (Basel, Switzerland). Two variants of SH-SY5Y were used in this work: control cells without specifically increased APP and Aβ production (SH-SY5Y MOCK) and a model of AD in which the synthesis of these proteins is increased (SH-SY5Y APP_{695}). The subtypes show similarities in morphology but show differences due to the additionally transfected coding region of human AβPP (AβPP_{695}) or a corresponding empty vector (pCEP4).

5.2.10.1 Thawing cells

The cells, which were frozen at -80 °C, were carefully thawed in a water bath at 37 °C. The cells were then resuspended in medium in a 50 mL Falcon tube and centrifuged (750× *g*, 5 min). After discarding the supernatant, the pellet was dissolved in 11 mL of full medium. The cell suspension was transferred to a cell culture flask and rinsed multiple times. The culture was then incubated for at least 24 hours (37 °C, 5% CO_2) until the first passage of the cells could be performed.

5.2.10.2 Cultivation and splitting of cells

The cultivation of SH-SY5Y cells was carried out in cell culture flasks under sterile conditions (37 °C, 5% CO_2). To optimise the growth conditions, the flasks were split approximately twice

a week to achieve a maximum of 80% growth. The cells were used for experiments in splits four to 15, and then a new unit of cells was taken into culture. For splitting, medium and PBS were heated to 37 °C in a water bath. The cell culture flask was transferred from the incubator to the sterile workbench. The full medium was aspirated using a glass pipette after the cells were washed with 10 mL of warm PBS for a maximum of one minute. One mL of trypsin-EDTA was used to detach the cells from the bottom of the flask. For this purpose, the bottle was carefully swivelled to distribute the protease on the cell lawn. As soon as cells were visible in solution, 9 mL of fresh full medium was added to stop the protease activity. To separate the cells, the cell suspension was then rinsed eight times. The suspension was diluted according to the planned cultivation period by transferring an appropriate amount of the suspension into fresh cell culture flasks in which 12 mL of the complete medium had previously been placed (ratio 1:2 to 1:8). Then, cultivation was carried out for the planned period (37 °C, 5 % CO_2).

5.2.10.3 Determination of the cell count

To determine a uniform and appropriate cell count for the experimental application, the cells of an approximately 80% overgrown cell culture flask were counted in a Neubauer counting chamber using the dye trypan blue. Trypan blue penetrates dead cells and stains them blue, whereas vital cells have an intact membrane barrier. Due to the toxicity of the dye, counting of the cells was performed immediately after mixing with the cells. After the cells were washed in PBS and detached with trypsin, medium according to the experimental approach was used for resuspension. After rinsing, the cell suspension was centrifuged in a 50 mL cell culture tube (750× *g*, 5 min). The supernatant was discarded, and the pellet was resuspended in 1 mL of medium. Ten microliters of the suspension was transferred to a reaction tube containing 90 µL of preprepared trypan blue. Subsequently, ten microliters of this cell-trypan blue suspension was injected into the covered Neubauer counting chamber. All four counting chambers, each with 16 segments, were counted under a light microscope, and the mean value was determined. When calculating the cell count, both the total dilution ($1:10^3$) and the chamber factor ($1:10^4$) were taken into account. The cell count was set to 10^6 cells per millilitre.

5.2.11 Cell treatment

Cells were incubated with concentrations from 0.01 µM to 1000 µM erinacine C or with a 0.01 µg – 100 µg/mL ethanolic *Hericium erinaceus* mycelium extract (both dissolved in DMSO) for 24 h after they reached confluence of 80 %. DMSO (1 %) was used as a control for erinacine C and the ethanolic extract.

5.2.12 Cell culture assay

In the following section, the principle and experimental stages of the assays used are described.

5.2.12.1 MTT Assay

Incubation of the cells

The cultivation and harvesting of the cells were carried out as described in section 5.2.10. After the cell count was set to 10^6 cells/mL, the cell suspension was diluted again at a ratio of 1:5 with reduced medium (adjusted cell number: 2 x 10^5). One hundred microliters of the cell suspension was applied to a 96-well microtitre plate. The plate was then incubated for 24 hours (37 °C, 5 % CO_2). After the incubation period, 1 µL of the effector was applied. The treatment was carried out with the ethanolic extracts of *Hericium erinaceus* and pure erinacine C.

Measurement

After another 24 hours, the plate was centrifuged (750× *g*, 5 min, RT), and the supernatant was carefully aspirated. Subsequently, 100 µL of the MTT solution (5 mg/mL in PBS) diluted 1:10 with reduced medium was applied per well, and the plate was incubated for 4 hours (37 °C, 5 % CO_2). Then, 75 µL of the solution was removed and discarded. The formed formazan crystals were dissolved in 50 µL of DMSO, and the plate was incubated for another 10 min (37 °C, 5 % CO_2). Afterwards, the absorbance of the MTT formazan at 540 nm and 37 °C could be determined in the plate reader.

5.2.12.2 Mitochondrial membrane potential (MMP) determination

Incubation of the cells

After harvesting the cells and adjusting the cell count to 10^6 cells/mL as described in section 5.2.10, the cells were seeded in a 24-well plate. For this purpose, 395 µL of reduced medium was provided, and 100 µL of the cell suspension was applied to each well. The plate was then incubated for 24 hours (37 °C, 5 % CO_2). One day after seeding, 5 µL of the effectors were applied for each group. One hour after the application of the effectors, 5 µL rotenone was added to each of the designated wells. Rotenone inhibits complex I of the respiratory chain, resulting in blocked ATP synthesis and reduced MMP (Perry, Norman, Barbieri, Brown, Harris, et al., 2011). In the columns in which no rotenone or effector was applied, the volume was balanced by the application of reduced medium.

Measurement

On day two after seeding, the plate could be prepared for MMP measurement. First, HBSS was heated in a water bath to 37 °C, the pH was adjusted to 7.4. The salt solution was sterile filtered

through a tip filter. R123 was mixed with sterile filtered HBSS 1:100, diluted again 1:50 and stored in the absence of light. Per well, 10 µL of diluted R123 was applied (0.4 µM), and the plate was incubated for 15 min (37 °C, 5 % CO_2). The cells were then washed with 500 µL HBSS and centrifuged (750× *g*, 5 min). The supernatant was aspirated and discarded. The remaining cells were carefully resuspended in 500 µL fresh HBSS. Subsequently, the actual measurement could be carried out in the plate reader at an excitation wavelength of 490 nm and an emission wavelength of 535 nm (Stockburger et al., 2014).

5.2.12.3 ATP Assay

Incubation of the cells

The cultivation and harvesting of the cells were carried out as described in section 5.2.10. After the cells were counted and the cell count was set to 10^6 cells/mL, the cell suspension was diluted again in a new 50 mL Falcon tube at a ratio of 1:5 with reduced medium (set cell count: 2 x 10^5). One hundred microliters of the cell suspension were applied to each 96-well microtiter plate, and columns were left out for the ATP standard. The plate was then incubated for 24 hours (37 °C, 5 % CO_2).

One day after seeding, the cells could be treated with 1 µL of the effector. One hour later, 1 µL rotenone was applied. The volume was adjusted in cells without treatment with reduced medium. Twenty-four hours after application of the effectors, the ATP levels could be determined.

Measurement

Fifteen minutes before the end of the incubation period, the plate was removed from the incubator and cooled to room temperature under the exclusion of light. After application of the ATP standards, all wells loaded with cells were processed with the ATPlite Luminescence Assay System. For this purpose, 50 µL of the lysis reagent was applied per well using a multichannel pipette, and the plate was incubated in the dark (RT, 5 min). Subsequently, 50 µL of the monitoring solution was added, air bubbles were removed, and the plate was incubated for an additional 40 minutes (RT, 15 min) until the ATP levels could be determined by bioluminescence in the BMGLabtech Clariostar plate reader (λabs = 490 nm, λem = 535 nm).

5.2.12.4 Real-Time Reverse Transcription quantitative PCR (Real-Time RT–qPCR)

Principle

Reverse transcription quantitative polymerase chain reaction (RT–qPCR) enables the quantification of nucleic acids. This method is used for the real-time detection and measurement of products that are exponentially generated in each PCR cycle run and are proportional to the amount of initial DNA (template) before the process (Arya et al., 2005). Through the use of

temperature change effects, a cycle is composed of the following three phases: denaturation (94 °C), annealing (55 °C) and elongation (72 °C). In a cycle, the strands of the template are first separated in this way, the primers are hybridised, and the chain is elongated with the help of the polymerase. At the end of a cycle, two identical copies are present (Mülhardt, 2013). For detection and quantification the double-strand intercalating dye SYBR® Green was used (Arya et al., 2005). Finally, a melting curve analysis is used to ensure that only the target sequence has been amplified.

Incubation

In a 6-well plate, 1 mL of medium was added. The concentration of the cell suspension was adjusted to 10^6 cells/mL, and 1 mL was added to each well. The plate was then incubated for 48 hours (37 °C, 5 % CO_2). After 48 hours, the cells were treated with the effectors. First, the existing medium was removed by suction and replaced by 1980 µL of fresh complete medium and 20 µL of the effector. The plate was then incubated for an additional 24 hours (37 °C, 5 % CO_2). On day 3, the cells were harvested. The cells were rinsed off in the well, and duplicates were combined and transferred to a 15 mL Falcon tube. The cell suspension was centrifuged (750× *g*, 5 min, 4 °C), and the supernatant was aspirated. The remaining cell pellet was resuspended in 300 µL RNA protect and transferred to a 1.5 mL reaction vial, and the cells were immediately chilled with nitrogen. The cells were stored at -80 °C.

Isolation of mRNA from cells

Isolation of mRNA from SH-SY5Y cells was performed using the RNeasy Mini Kit (Qiagen, Hilden, Germany), and the mRNA was stored in RNAprotect® Cell Reagent at -80 °C until processing. After thawing, the cells were centrifuged for 10 min at 300× *g*. The supernatant was then removed, and the cells were homogenised in 350 µL RLT buffer (+ 10 % *β*-mercaptoethanol) using a cannula to rupture the cell structure. After the addition of 350 µL ethanol (70%), the suspension was pipetted onto a RNeasy column and centrifuged for 30 s at 300× *g*. The flow-through was discarded, and a wash step was performed in which 700 µL of RW1 buffer was applied to the RNeasy column. After centrifugation for 35 s at 300× *g*, the flow-through was discarded again, and two more washing steps with 500 µL RPE buffer each followed. After the last wash step, the column was dry centrifuged at 300× *g* for 2 min. The collection tube was discarded, and the column was placed in a fresh 1.5 mL reaction tube. To elute the mRNA, 50 µL RNase-free water was added to the filter and centrifuged at 300× *g* for 1 min. The concentration and purity of the isolated RNA (1 µL undiluted) was determined with a NanoDrop One (Thermo-Scientific) at 260 nm and 280 nm. The purity of the RNA was controlled by the quotients A260/A280 (1.8-2.0) and A260/A230 (> 1.5).

To exclude contamination with genomic DNA, an additional DNase digestion was carried out with the Turbo DNA-free™ Kit. For this, 5 µL of 10x TURBO DNAse buffer and 1 µL TURBO DNAse were added to 50 µL RNA (< 200 µg/mL). This was followed by incubation at 37 °C for 25 min. At the end of the incubation period, 5 µL of DNAse Inactivation Reagent was added and incubated at room temperature for 5 min. This stopped the reaction. The samples were then centrifuged at 300× *g* at RT for 90 s. The supernatant was removed, and the RNA concentration was determined again on a NanoDrop One as described above. The mRNA was aliquoted according to the determined concentration for cDNA synthesis (0.5 µg RNA per synthesis preparation) and stored at -80 °C.

5.2.12.4.1 cDNA production

The cDNA was synthesised using the iScript™ cDNA Synthesis Kit (Bio-Rad, Munich). To prepare the cDNA, the RNA aliquots were thawed and filled to 10 µL with RNAse-free H_2O. Ten microliters of master mix (5 µL RNase-free H_2O, 4 µL 5x iScriptase Reaction Mix and 1 µL iScript Reverse Transcriptase) was then added to each sample. Incubation was then performed in the T100TM thermal cycler (Bio-Rad) (5 min at 25 °C, 20 min at 46 °C and 1 min at 95 °C, lid temperature 105 °C). The finished cDNA was stored in aliquots at -80 °C until further use.

5.2.12.4.2 Real-time quantitative PCR measurement

mRNA expression (gene expression) was measured by quantitative real-time PCR (qPCR) using target-specific primers on the CFX ConnectTM Real-Time System (Bio-Rad, Munich). For this purpose, cDNA aliquots were diluted 1:10 with RNase-free H_2O after thawing. Eight microliters of the master mix (5 µL SYBR Green Supermix, 1 µL diluted Primer Stock (2 or 4 µM), 2 µL RNase-free H_2O) was pipetted per well into a 96-well PCR plate (hard-shell). The diluted cDNA was then added in a volume of 2 µL per well in triplicate. RNase-free H_2O served as a control. The PCR plate was sealed with adhesive foil and incubated in the thermal cycler. The cycling conditions for RT–qPCR are summarised in Table 5-40.

Table 5-40 Cycle conditions for RT–qPCR.

Cycle phase	Temperature [°C]	Time
1. Initial denaturation	95	3 min
2. Denaturation	95	10 s
3. Annealing	56-58	30 s/45 s
4. Elongation	72	29 s
Number of cycles	45	

Depending on the primer used, the primer concentration, annealing time and temperature may vary. The relative quantification was followed by a melting curve analysis to detect primer dimers or nonspecific annealing of the primers. The melting curve was recorded at a temperature increase from 65 °C to 95 °C with a heating rate of 0.5 °C/5 s over a period of 5 min.
The evaluation was carried out by means of the 2-ΔΔCq method using Bio-Rad CFX Manager (Bio-Rad, Munich).

Table 5-41 Primer sequence, size, and concentration.

Primer	Sequence	Manufacture	Product size (bp)	Concentration [nM]
β-Actin (ACTB)	Fwd: 5′-GGACTTCGAGCAAGAGATGG-3′ Rvs: 5′-AGCACTGTGTTGGCGTACAG-3′	Biomol Hamburg,Germany	234	200
ATP-synthase delta-subunit (ATP5D)	Fwd: 5′-GGAAGCTCCTCCTCAGCTTT-3′ Rvs: 5′-CAGGCTTCCGGGTCTTTAAT-3′	Biomol Hamburg, Germany	198	200
cAMP-responsive element-binding protein 1 (CREB1)	Fwd: 5'-TGGAGTTGTTATGGCATCCT-3' Rvs: 5'-ATTTTCAAGCACTGCCACTC-3'	Biomol Hamburg, Germany	169	100
Nuclear Respiratory Factor 1 (NRF1)	Fwd: 5'-GTAACCCTGATGGCACTGTC-3' Rvs: 5'TCTGGATGGTCATCTCACCT-3'	Biomol Hamburg, Germany	183	200
Transcription factor A (TFAM)	Fwd: 5'-TCCCCCTTCAGTTTTGTGTA-3' Rvs: 5'-ATCAGGAAGTTCCCTCCAAC-3'	Biomol Hamburg, Germany	189	200
Glyceraldehyde-3-phosphate dehydrogenase (GAPDH)	Fwd: 5′-CTTTGCCAACTTCCTTCTGC-3′ Rvs: 5′-TTGATTTTGGAGGGATCTCG-3′	Biomol Hamburg, Germany	238	200
Phosphoglycerate kinase 1 (PGK1)	Fwd: 5′-CTGTGGGGGTATTTGAATGG-3′ Rvs: 5′-CTTCCAGGAGCTCCAAA-3′	Biomol Hamburg, Germany	198	200
NAD-dependent deacetylase sirtuin-1 (SIRT1)	Fwd: 5'-TGTGGTAGAGCTTGCATTGA-3' Rvs: 5'-GCCTGTTGCTCTCCTCATTA-3'	Biomol Hamburg, Germany	183	200

5.2.12.5 Measurement of mitochondrial respiration

Principle

Mitochondrial respiration was investigated using the Oxygraph-2k system (Oroboros Instruments, Innsbruck, Austria). The Oxygraph consists of two independent chambers with a Clark-type polarographic sensor where a membrane permeable to oxygen covers an electrode which is reducing oxygen. Oxygen concentration can be determined by the current that ensues. Substrates and inhibitors of the individual complexes of the mitochondrial respiratory chain are added selectively to measure the respiration of the complexes. This allows a statement about the functionality of the complexes and the integrity of the respiratory chain in the cell. (Dieter et al., 2022)

Incubation

Cell culture flasks with a confluence of 60-70 % were incubated with the respective substance (by replacing the old cell culture medium with 9.9 mL of new cell culture medium (37 °C) and adding 100 µL of the respective substance or the solvent control). Cells were placed in the incubator for 24 hours.

Measurement

Before the measurement, 2.4 mL MIR05 (37 °C) was added to each chamber and equilibrated for approx. 30 min. For the measurement, MIR05 was completely removed and replaced by 2.4 mL cell suspension ($4x10^6$ cells/mL MIR05) and equilibrated (endogenous respiration). Ultimately, there were 8 $x10^6$ cells in each chamber.

After stabilising the endogenous respiration, the cells were permeabilised by the addition of digitonin to make the membrane permeable to the substrates and inhibitors. This is followed by the addition of the complex I substrates glutamate (10 mM) and malate (2 mM) (leak respiration without ADP, leak (P/M)). The subsequent addition of ADP (2 mM) allowed the acquisition of complex I activity (KI). The capacity of oxidative phosphorylation (OXPHOS), i.e., the total respiration of complexes I and II is determined by the addition of succinate, a substrate of complex II. The addition of FCCP to saturation (0.5 µM steps) results in uncoupling of the respiratory chain from substrate addition, degradation of the MMP and restoration of the proton gradient with full respiration of the respiratory chain by complex I to complex IV. In this way, the maximum activity of the electron transfer system (ETS) can be recorded. Subsequently, rotenone (0.5 µM), a complex I inhibitor, was administered to differentiate the respiration of complex I from that of complex II. At this stage, uncoupled complex II activity can be detected. By adding the ATP synthase inhibitor oligomycin (2 µg/mL), the proton gradient through the proton leak is slowed down. Complex III is subsequently inhibited by antimycin A (2.5 µM) and

thus enables the measurement of residual oxygen consumption (ROX), oxygen consumption without the involvement of mitochondrial respiration. Finally, cytochrome c oxidase (complex IV) activity is measured by the administration of tetramethylphenylenediamine (TMPD) (0.5 mM), an artificial complex IV substrate, and ascorbate (2 mM) to obtain TMPD in the reduced state. The addition of sodium azide (> 100 mM) inhibits the entire respiratory chain. The oxygen concentration measured hereafter must be subtracted from the complex IV respiration, as these values no longer originate from the activity of the respiratory chain. Furthermore, ROX was subtracted from all respiratory activities. To ensure a sufficient supply of oxygen during the measurement, the chambers were opened briefly in between. This was usually done after adding oligomycin and ascorbate/TMPD. Figure 5-1 displays the above described steps.

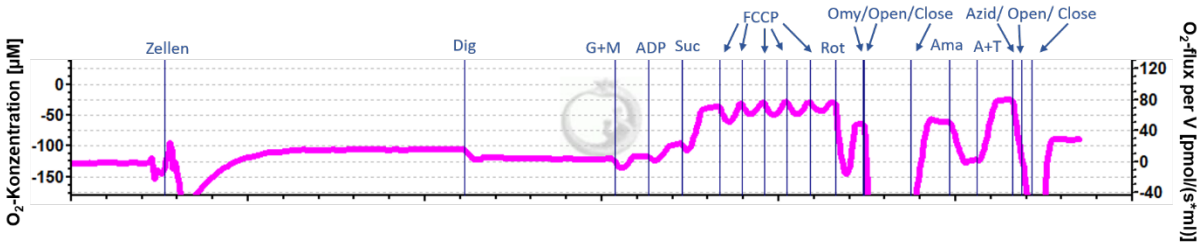

Figure 5-1 Example of respiratory measurement (Oxygraph-2k). Oxygen consumption is shown in pink. Dig= Digitonin; G+M= Glutamate and malate; ADP= Adenosine diphosphate; Suc=Succinate; Red=Rotenone; Omy= Oligomycin; Ama=Antimycin; A+T= Ascorbate + Tetramethylphenylenedia.

5.2.12.6 Citrate synthase (CS) activity measurement

Principle

Citrate synthase (CS) is localised in the mitochondrial matrix but is encoded in the nucleus. Therefore, CS is commonly used as a quantitative marker for the content of intact mitochondria. The CS assay is based on the irreversible conversion of DTNB with CoA-SH to TNB and CoA-S-S-TNB, catalysed by the CS. The resulting TNB can be detected spectrophotometrically at 412 nm. The absorbance is recorded over 200 s in the spectrometer and increases linearly with time. Plotting the absorbance against the measurement time allows the citrate synthase activity to be determined. This in turn can be used to infer the number of intact mitochondria, making CS activity a marker for mitochondrial mass (Larsen et al., 2012).

Incubation and Measurement

For the measurement, an aliquot of the solution for the respiratory measurements was used. The solution was stored at -80 °C until the CS experiment.

Reaction mix:

Table 5-42 Reaction mix and starting reagent for citrate synthase.

Chemical	Volume for 1-well
ddH_2O	80 µL
DTNB-solution	20 µL
Triton-X-100	5 µL
Acetyl-CoA	5 µL
Total	110 µL

Starting reagent:

Chemical	Volume for 1-well
ddH_2O	40 µL
Oxalacetat	10 µL
Total	50 µL

CS was determined in the cells as follows: From the thawed samples, 40 µL was pipetted in triplicate into a 96-well plate. Then, 110 µL of the reaction mix was added to each sample, and the plate was incubated for 5 min at 30 °C in the plate reader. The starting reagent was also tempered to 30 °C in a water bath at the same time. After 5 minutes, 50 µL of the starting reagent was added to each sample, and then the plate was measured at an absorption wavelength of 412 nm in the plate reader. ddH_2O was used as a blank. The mean values of the triplets were calculated. The specific activity was calculated with the following formula:

$$v = \frac{r_A}{l \cdot \varepsilon_B \cdot v_B} \cdot \frac{V_{well}}{V_{sample} \cdot \rho}$$

v= Specific citrate synthase activity [µmol/min/10^6 cells]; r_A= Change in absorption rate per min; εB= Extinction coefficient of TNB at 412 nm and pH 8.1 [= 13,6 mM-1 cm-1]; v_B= Stoichiometric equivalent of TNB in the reaction (=1); $V_{Küvette}$= Volume of the reaction mixture in the well (=200 µL); V_{Sample}= Volume of the sample in the well (40 µL); ρ= Mass concentration or density of the cells in the sample (Protein concentration in mg/cm3, Cell density 10^6x cm3).

5.2.12.7 Determination of neuronal outgrowth

Principle

Testing neuritogenesis or neuronal outgrowth is an assay for assessing the neuroplasticity effects of cells. Neuroplasticity is degrading in the brains of Alzheimer's patients. For this assay, neuronal outgrowth was excited with retinoic acid. Eventually, the neuronal cells are stained and photographed, and the length of the neurons is assessed. To assess the effect of erinacine C

on neurite growth in SH-SY5Y cells, hematoxylin-eosin staining of previously fixed cells was performed. Haematoxylin has a deep blue–violet colour and stains nucleic acids. Eosin, on the other hand, is pink and specifically stains proteins. In a typical tissue, nuclei thus appear blue, while the cytoplasm and extracellular matrix are stained pink to varying degrees (Cardiff et al., 2014).

Incubation of the cells

Cells were harvested from a Greiner flask and counted with a Neubauer counting chamber. The cell suspension was diluted to yield 10^5 cells/mL. Cells were then seeded in transparent 6-well plates with 1 mL DMEM and a microscopy cover slip coated with poly-L-lysine. After 24 hours, the medium was exchanged for reduced DMEM (3% FBS and other supplements identical to the cultivation medium). Furthermore, 10 µM retinoic acid was added to start the differentiation of cells. After 5 days, the medium was changed to unsupplemented DMEM for the remaining cultivation. Additionally, cells were treated with effectors or control solvent.

Measurement

After a total of 10 days, the medium was removed, and the cells were washed with 2 mL PBS (1x). Cells were treated with 1 mL ROTI-Histofix ECO plus (Carl Roth, Germany, Karlsruhe) for 20 min before being washed with 1 mL H_2O. After this, cells were stained in 1 mL of acidified haematoxylin solution for 1 min. Cover slips were removed from the well plate and rinsed with tap water for 15 min. Cover slips were then dipped into eosin solution for 10 seconds before being passed through several washing steps in the following order: H_2O, 70 % EtOH, 90 % EtOH, 100 % EtOH, 100 % isopropanol and 100 % xylol. Finally, one drop of highly viscous Permount (Carl Roth, Germany, Karlsruhe) was placed on a microscopy slide, and the coverslip, cells facing down, was placed on top to completely embed cells within the mounting solution. After preparation, slides were dried overnight at room temperature before analysis via microscopy (Microscope: Axiphot, Zeiss, Camera and Objective, Software: LAS V4.6 (Leica Application Suite).

Pictures were taken from moderately full areas of the sample to include at least 10 cells. From these cells, the number and length of the longest neurite was determined using Mark Longair's Simple Neurite Tracer 3.1.4 plugin for ImageJ. If neurites linked two cells together, the complete neurite length was used.

5.2.12.8 Molecular modelling

Molecular modelling is a computational technique used to study the structure, properties, and behaviour of molecules and molecular systems. It plays a crucial role in various fields such as drug design, materials science, and biochemistry. Molecular modelling is used in drug design to predict the binding affinity and pose of small molecules (ligands) to their target proteins, enabling the identification of potential drug candidates (Höltje et al., 2008).

For modelling, the structure of TrkB was downloaded from the RCBS Protein Data Bank (https://www.rcsb.org). Here, the crystal structure of TrkB of Bertrand et al. was used (Bertrand et al., 2012). The 3D structure of erinacine C was obtained from PubChem (PubChem CID: 10252378; url: https://pubchem.ncbi.nlm.nih.gov/compound/Erinacine-C) (S. Kim et al., 2021). For modelling, AutoDock Vina was used. AutoDock Vina allows the modelling and scoring of protein–ligand interactions (Trott & Olson, 2009). To display the protein–ligand complex, PyMOL was used (Schrödinger LLC, 2015). To visualise the interactions of erinacine C within the cavity of the TrkB-receptor, LigPlot+ was used (Wallace et al., 1995).

5.2.12.9 RNAseq

RNA sequencing (RNAseq) is a high-throughput method that enables the study of the transcriptome, which represents the complete set of RNA molecules within a cell or tissue at a given time. It provides insights into gene expression levels, alternative splicing, novel transcripts, and non-coding RNA identification. RNAseq has become a powerful tool for investigating gene expression changes, understanding regulatory mechanisms, and exploring disease pathogenesis (Z. Wang et al., 2009).

The cells were treated the same way as for real-time RT–qPCR. However, the process was stopped after DNase digestion. The samples were measured by Dr. Stefan Günther at the Department of CPI - DNA & RNA Technologies at the Max Planck Institute for Heart and Lung Research in Bad Nauheim. The kit used is displayed in Table 5-43.

Table 5-43 RNAseq Kit.

Kits	Name
Illumina Kit	
	NextSeq™ 500 High Output Kit (75 cycles)
	GX24 DNA 5k/RNA/CZE LabChip CLS138949
	GX24 pico RNA Reagent Kit CLS960012
	VAHTS Stranded mRNA-seq Library Prep Kit for Illumina
	AmPure Beads XP
	GX24 DNA X-Mark LabChip CLS145331
	GX24 DNA NGS 3K Reagent Kit CLS960013

5.2.12.10 Amyloid beta measurement

Principle

The determination of Aβ levels was based on the HTRF (Homogeneous Time Resolved Fluorescence)) method and the HTRF-Amyloid-Beta 1-40 kit (Cisbio, Codolet, France). Two antibodies that distinguish Aβ are used for this assay. One antibody is linked to a donor and the other to the acceptor. When the two antibodies recognise the analyte, the donor emits fluorescence upon excitation, and the energy is transferred to the nearby acceptor, resulting in specific delayed acceptor fluorescence. The donor fluorescence is also measured and related to the acceptor fluorescence. The cells were incubated in a cell culture flask with erinacine C for 24 h.

Measurement

The measurement followed the method published by Babylon et al. (Babylon et al., 2021). After incubation for 24 h, the cells were collected and rinsed with PBS. Then, the cell suspension was centrifuged (220× g, 5 min). The supernatant was discarded, and the cell pellet was resuspended in 1.5 mL of PBS and protease inhibitor cocktail (Merck, Darmstadt, Germany). The suspension was then centrifuged at 112× g for 5 min, and the supernatant was discarded. The cell pellet was collected, and 600 µL of cell extraction buffer (Thermo Fisher Scientific, Waltham, MA,

USA) was added and incubated for 30 min. The solution was then centrifuged at 13,000× g for 10 min. The supernatant was transferred to a new tube and stored at -80 °C. The supernatant was thawed on ice and pipetted onto a 384-well plate (Greiner Bio-One, Kremsmünster, Austria). An HTRF-Amyloid-Beta 1-40 kit (Cisbio, Codolet, France) was used to measure amyloid *β*-protein concentration, and samples were processed according to the manufacturer's instructions. Optical density was then measured in the plate reader at emission wavelengths of 665 and 622 nm. A*β* concentrations were normalised against protein content.

5.2.13 Caenorhabditis elegans

The strains CL2120 and GMC 101 were purchased from the Caenorhabditis Genetics Center (CGC).

5.2.13.1 *Escherichia coli* OP 50 cultivation

E. coli OP50 serves as a food source for the nematodes. In the following, the storage and cultivation of the bacteria is described.

5.2.13.2 *Escherichia coli OP50* overnight culture

Overnight culture of *E. coli* OP50 was prepared by inoculating 3 mL of 2x YT medium with 20 µL of E. coli OP50 glycerol culture in a cell culture tube under sterile conditions. The cell culture tube was then cultured for 18 to 20 h at 37 °C and 30 rpm in a shaking incubator.

5.2.13.3 *Escherichia coli* OP50 Day culture

Two hundred millilitres of 2x YT medium was inoculated with an overnight culture containing 0.5 mL. The tubes were shaken for approximately 6 h at 37 °C and 300 rpm. Subsequently, the day culture was divided into 50 mL centrifuge tubes, centrifuged at 3210× g for 8 min and resuspended in 5 mL YT medium. Storage is at 4 °C for a maximum of one week.

5.2.13.4 Glycerol culture of *Escherichia coli* OP50

Glycerol cultures are used for the long-term storage of bacterial strains. Therefore, 200 µL glycerol was mixed with 800 µL of the overnight culture under sterile conditions. The suspension was then thoroughly mixed and aliquoted into reaction tubes of 20 µL each and stored at -80 °C in the freezer.

5.2.13.5 Culture of *C. elegans*

The cultivation of *C. elegans* was performed on OP50-NGM agar plates. The plates were stored in a thermal cabinet at 20 °C protected from light. NGM agar, as well as the spread *E. coli* OP50 lawn, served as food sources. To maintain the culture, agar pieces containing nematodes are cut from the plate and transferred to new OP50-NGM agar plates.

5.2.13.6 Age synchronisation of *C. elegans*

To ensure equal age of nematodes, they are synchronised by egg preparation. Using M9 buffer, nematodes are washed from well-grown plates and transferred to a 15 mL centrifuge tube. The nematodes were centrifuged twice at 440x g for 2 minutes at room temperature. The supernatant was discarded, and the pellet was resuspended. Then, 1.5 mL of the bleach solution was added. The tube was shaken until all nematodes had dissolved.
To separate bleach solution containing nematode residues from eggs, the suspension was centrifuged at 3210x g for 2 min at room temperature, and the supernatant was discarded. The pellet was resuspended in 10 mL of M9 buffer. Ten microliters of cholesterol (5 mg/mL in EtOH) were added to this suspension. Finally, the suspension was placed in an overhead shaker and incubated at 25 rpm and 20 °C overnight.

5.2.13.7 Separation of adult nematodes from larvae

For the separation of large quantities of adult nematodes (from 3000 nematodes), nylon nets with a defined mesh size of 30 µm were used. The nematodes were placed on nylon nets in a plastic frame, which was placed in a glass funnel on a 50 mL centrifuge tube. M9-TWEEN® 20 buffer was used to rinse the nylon net to separate the adult nematodes from the young ones. The filter was transferred to a new 15 mL centrifuge tube, and the plastic holder was turned so that the nematodes were on the lower side of the nylon net. The adult nematodes separated from the larvae are then rinsed into the centrifuge tube with 15 mL M9-TWEEN® 20 buffer.

5.2.13.8 Adjusting the number of larvae

The larval suspension was centrifuged in two washes at 1,200x g for 2 minutes at RT, and the supernatant was discarded. The larval suspension was adjusted to a concentration of 10 larvae/10 µL with M9 using a counting chamber.

5.2.13.9 Cultivation of *Caenorhabditis elegans* in OP50-NGM liquid medium.

For the NGM-OP50 liquid medium, the OP50 day culture was adjusted to an OD_{600} on the photometer of 1.0 ± 0.1 with the NGM liquid medium.

5.2.13.10 Effector application and incubation

Effectors are applied on day four upon reaching the young-adult stage. The used effectors are added to 10 % volume in the cell culture flasks by dispenser or serological pipette. The flasks were incubated for 48 h in the dark at 20 °C and 150 rpm. The flasks were then used for the respective experiments.

5.2.14 Assays for Caenorhabditis elegans experiments

5.2.14.1 Heat stress assay for lifespan measurement

SYTOX™ Green was used to measure heat stress. The fluorescent dye cannot pass through the membrane of the nematodes and is only measurable when it intercalates with nucleic acids from the cell nucleus. With the death of the nematodes, the dye can intercalate through the natural apoptosis process. The time of death can be determined via the maximum fluorescence signal. A population comparison was made using the Kaplan–Meier curve.

5.2.14.2 ATP Assay

No intact mitochondria are necessary for the measurement of the ATP concentration. Therefore, the Balch homogeniser is set with a clearance of 8 µm. After the homogenisation step, the homogenate can be measured directly or stored intermediately at - 20 °C. The ATPlite Luminescence Assay System was used for ATP measurement. After preparing the standard series, thawing the samples and preparing the AMR, the 96-well assay can be loaded. The plate was then incubated for 5 minutes in the dark. ATP levels were determined by bioluminescence in a BMGLabtech Clariostar plate reader (λabs = 490 nm, λem = 535 nm).

5.2.14.3 Measurement of protein concentration

In this experiment, the measuring principle is based on the reduction of Cu^{2+} ions to Cu^{+} ions by proteins. This reaction is called the Biuret reaction. Here, the Cu^{+} ions react with bicinchoninic acid (BCA) to form a dark purple complex. At a wavelength of 562 nm, the absorption behaves linearly to the protein concentration over a wide concentration range. The measurement of the protein concentration was repeated until two measured values showed a difference below

0.01 mg/mL. The arithmetic mean is formed from these two values and is then used to normalise the measurement results of the ATP concentration.

5.2.14.4 Quantification of ROS using fluorescent dyes

Loss of mitochondrial membrane potential and increased production of ROS are characteristics of mitochondrial dysfunction that can be studied in live C. elegans nematodes using cationic lipophilic fluorescent dyes, such as MitoTracker™ Red CM-H_2Xros (Jonkman et al., 2020; Nicholls & Ward, 2000; Perry, Norman, Barbieri, Brown, & Gelbard, 2011). The nematodes were cultivated according to a standard protocol. One day before the planned experimental evaluation, the MitoTracker red (MTR) stock solution (1 mM in 100% DMSO) was diluted 1:100 with sterile M9 buffer to an MTR working solution (10 µM in 1% DMSO). The working solution was pipetted into the wells at a 1:10 ratio. The nematodes are incubated for 24 h together with the effector. The experiment took place the following day. The fluorescence microscope is used to select the experimental group that is expected to have the highest level of reactive oxygen species (ROS) or the highest mitochondrial membrane potential, and thus the highest fluorescence intensity. Pictures were taken with Δ 531/593 nm. To paralyse the nematodes after washing and filtering, 200 µL of 20 mM levamisole was added, and the solution was shaken. Images were taken of at least 30 nematodes. The experiments were repeated on three different days to control for statistical variation. The semiautomatic interactive analysis was performed with the open source program FIJI (Fiji Is Just ImageJ). The mean RFP fluorescence intensities were subsequently evaluated statistically.

5.3 Statistical evaluation

The statistical evaluation was performed using GraphPad Prism version 9.0.1 and R statistical software version 3.6.0. The data are mostly presented as boxplots, displaying median values along with whiskers that indicate the minimum and maximum values for each plot. Kaplan-Meier survival curves were used for visualizing and summarizing the survival experience of *C. elegans*. By comparing the entire survival between the groups, the Mantel-Cox test was used to evaluate the difference of survival distributions. Before applying parametric tests, the normality of the data distribution was assessed using the Shapiro-Wilk test and visual inspection of Q-Q plots. To test for differences between two measurement groups, an unpaired two-tailed t-test

was employed for normally distributed data, while the non-parametric Mann-Whitney U test was used for non-normally distributed data. For differences among more than two groups, a one-way ANOVA with Dunnett's Multiple Comparison Test or False Discovery Rate (FDR) adjustment was utilized. The significance level used for hypothesis testing was set at $p < 0.05$.

6 References

Abdullah, N., Ismail, S. M., Aminudin, N., Shuib, A. S., & Lau, B. F. (2012). Evaluation of selected culinary-medicinal mushrooms for antioxidant and ACE inhibitory activities. *Evidence-Based Complementary and Alternative Medicine*, *2012*. https://doi.org/10.1155/2012/464238

Ainsworth, G. C. (Geoffrey C., Bisby, G. R., Kirk, P. M., & CABI Bioscience. (2008). *Ainsworth & Bisby's dictionary of the fungi*. 771.

Akama, K. T., & Van Eldik, L. J. (2000). Beta-amyloid stimulation of inducible nitric-oxide synthase in astrocytes is interleukin-1beta- and tumor necrosis factor-alpha (TNFalpha)-dependent, and involves a TNFalpha receptor-associated factor- and NFkappaB-inducing kinase-dependent signaling mechanism. *The Journal of Biological Chemistry*, *275*(11), 7918–7924. https://doi.org/10.1074/JBC.275.11.7918

Akiyama, H., Barger, S., Barnum, S., Bradt, B., Bauer, J., Cole, G. M., Cooper, N. R., Eikelenboom, P., Emmerling, M., Fiebich, B. L., Finch, C. E., Frautschy, S., Griffin, W. S. T., Hampel, H., Hull, M., Landreth, G., Lue, L. F., Mrak, R., MacKenzie, I. R., … Wyss-Coray, T. (2000). Inflammation and Alzheimer's disease. *Neurobiology of Aging*, *21*(3), 383–421. https://doi.org/10.1016/S0197-4580(00)00124-X

Amara, I., Scuto, M., Zappalà, A., Ontario, M. L., Petralia, A., Abid-Essefi, S., Maiolino, L., Signorile, A., Trovato Salinaro, A., & Calabrese, V. (2020). Hericium Erinaceus Prevents DEHP-Induced Mitochondrial Dysfunction and Apoptosis in PC12 Cells. *International Journal of Molecular Sciences*, *21*(6), 2138. https://doi.org/10.3390/ijms21062138

Anandatheerthavarada, H. K., & Devi, L. (2007). Mitochondrial translocation of amyloid precursor protein and its cleaved products: relevance to mitochondrial dysfunction in Alzheimer's disease. *Reviews in the Neurosciences*, *18*(5), 343–354. https://doi.org/10.1515/REVNEURO.2007.18.5.343

Arnsten, A. F. T., Datta, D., Del Tredici, K., & Braak, H. (2021). Hypothesis: Tau pathology is an initiating factor in sporadic Alzheimer's disease. *Alzheimer's & Dementia*, *17*(1), 115–124. https://doi.org/10.1002/ALZ.12192

Arya, M., Shergill, I. S., Williamson, M., Gommersall, L., Arya, N., & Patel, H. R. H. (2005). Basic principles of real-time quantitative PCR. *Expert Review of Molecular Diagnostics*, *5*(2), 209–219. https://doi.org/10.1586/14737159.5.2.209

Atlante, A., Amadoro, G., Bobba, A., de Bari, L., Corsetti, V., Pappalardo, G., Marra, E., Calissano, P., & Passarella, S. (2008). A peptide containing residues 26–44 of tau protein impairs mitochondrial oxidative phosphorylation acting at the level of the adenine nucleotide translocator. *Biochimica et Biophysica Acta (BBA) - Bioenergetics*, *1777*(10), 1289–1300. https://doi.org/10.1016/J.BBABIO.2008.07.004

Autiero, I., Costantini, S., & Colonna, G. (2009). Human Sirt-1: Molecular Modeling and Structure-Function Relationships of an Unordered Protein. *PLoS ONE*, *4*(10). https://doi.org/10.1371/journal.pone.0007350

Babylon, L., Grewal, R., Stahr, P. L., Eckert, R. W., Keck, C. M., & Eckert, G. P. (2021). Hesperetin Nanocrystals Improve Mitochondrial Function in a Cell Model of Early Alzheimer Disease. *Antioxidants (Basel, Switzerland)*, *10*(7). https://doi.org/10.3390/ANTIOX10071003

Bailly, C., & Gao, J. M. (2020). Erinacine A and related cyathane diterpenoids: Molecular diversity and mechanisms underlying their neuroprotection and anticancer activities. In *Pharmacological Research* (Vol. 159, p. 104953). Academic Press. https://doi.org/10.1016/j.phrs.2020.104953

Baldini, L., Lenci, E., Bianchini, F., & Trabocchi, A. (2022). Identification of a Common Pharmacophore for Binding to MMP2 and RGD Integrin: Towards a Multitarget Approach to Inhibit Cancer Angiogenesis and Metastasis. *Molecules*, *27*(4). https://doi.org/10.3390/molecules27041249

Bayrhuber, M., Meins, T., Habeck, M., Becker, S., Giller, K., Villinger, S., Vonrhein, C., Griesinger, C., Zweckstetter, M., & Zeth, K. (2008). Structure of the human voltage-dependent anion channel. *Proceedings of the National Academy of Sciences of the United States of America*, *105*(40), 15370–15375. https://doi.org/10.1073/PNAS.0808115105/SUPPL_FILE/0808115105SI.PDF

Bertrand, T., Kothe, M., Liu, J., Dupuy, A., Rak, A., Berne, P. F., Davis, S., Gladysheva, T., Valtre, C., Crenne, J. Y., & Mathieu, M. (2012). The crystal structures of TrkA and TrkB suggest key regions for achieving selective inhibition. *Journal of Molecular Biology*, *423*(3), 439–453. https://doi.org/10.1016/j.jmb.2012.08.002

Bhandari, D. R., Shen, T., Römpp, A., Zorn, H., & Spengler, B. (2014). Analysis of cyathane-type diterpenoids from Cyathus striatus and Hericium erinaceus by high-resolution

MALDI MS imaging. *Analytical and Bioanalytical Chemistry*, *406*(3), 695–704. https://doi.org/10.1007/s00216-013-7496-7

Borodina, I., Kenny, L. C., Mccarthy, C. M., Paramasivan, K., Pretorius, E., Roberts, T. J., Van Der Hoek, S. A., & Kell, D. B. (2020). *The biology of ergothioneine, an antioxidant nutraceutical*. https://doi.org/10.1017/S0954422419000301

Brenner, S. (1974). The genetics of Caenorhabditis elegans. *Genetics*, *77*(1), 71–94. https://doi.org/10.1093/genetics/77.1.71

Bürger, M., & Chory, J. (2019). Stressed Out About Hormones: How Plants Orchestrate Immunity. In *Cell Host and Microbe* (Vol. 26, Issue 2, pp. 163–172). Cell Press. https://doi.org/10.1016/j.chom.2019.07.006

Busciglio, J., Pelsman, A., Wong, C., Pigino, G., Yuan, M., Mori, H., & Yankner, B. A. (2002). Altered Metabolism of the Amyloid β Precursor Protein Is Associated with Mitochondrial Dysfunction in Down's Syndrome. *Neuron*, *33*(5), 677–688. https://doi.org/10.1016/S0896-6273(02)00604-9

Cam, J. A., & Bu, G. (2006). Modulation of β-amyloid precursor protein trafficking and processing by the low density lipoprotein receptor family. *Molecular Neurodegeneration*, *1*(1), 8. https://doi.org/10.1186/1750-1326-1-8

Cardiff, R. D., Miller, C. H., & Munn, R. J. (2014). Manual hematoxylin and eosin staining of mouse tissue sections. *Cold Spring Harbor Protocols*, *2014*(6), 655–658. https://doi.org/10.1101/PDB.PROT073411

CC, T., JT, Y., HF, W., MS, T., XF, M., C, W., T, J., XC, Z., & L, T. (2014). Efficacy and safety of donepezil, galantamine, rivastigmine, and memantine for the treatment of Alzheimer's disease: a systematic review and meta-analysis. *Journal of Alzheimer's Disease : JAD*, *41*(2), 615–631. https://doi.org/10.3233/JAD-132690

Cenini, G., Lloret, A., & Cascella, R. (2019). Oxidative Stress in Neurodegenerative Diseases: From a Mitochondrial Point of View. *Oxidative Medicine and Cellular Longevity*, *2019*, 2105607. https://doi.org/10.1155/2019/2105607

Chang, C. H., Chen, Y., Yew, X. X., Chen, H. X., Kim, J. X., Chang, C. C., Peng, C. C., & Peng, R. Y. (2016). Improvement of erinacine A productivity in Hericium erinaceus mycelia and its neuroprotective bioactivity against the glutamate-insulted apoptosis. *LWT - Food Science and Technology*, *65*, 1100–1108. https://doi.org/10.1016/J.LWT.2015.08.014

Chaturvedi, V. K., Agarwal, S., Gupta, K. K., Ramteke, P. W., & Singh, M. P. (2018). Medicinal mushroom: boon for therapeutic applications. *3 Biotech*, *8*(8), 334. https://doi.org/10.1007/S13205-018-1358-0

Cheah, I. K., Ng, L.-T., Ng, L.-F., Lam, V. Y., Gruber, J., Huang, C. Y. W., Goh, F.-Q., Lim, K. H. C., Halliwell, B., & De La Rosa, M. (2019). Inhibition of amyloid-induced toxicity by ergothioneine in a transgenic Caenorhabditis elegans model. *FEBS Letters*, *593*, 2139–2150. https://doi.org/10.1002/1873-3468.13497

Cheah, I. K., Tang, R. M. Y., Yew, T. S. Z., Lim, K. H. C., & Halliwell, B. (2017). Administration of Pure Ergothioneine to Healthy Human Subjects: Uptake, Metabolism, and Effects on Biomarkers of Oxidative Damage and Inflammation. *Antioxidants & Redox Signaling*, *26*(5), 193–206. https://doi.org/10.1089/ars.2016.6778

Chen, J., Zeng, X., Yang, Y. L., Xing, Y. M., Zhang, Q., Li, J. M., Ma, K., Liu, H. W., & Guo, S. X. (2017). Genomic and transcriptomic analyses reveal differential regulation of diverse terpenoid and polyketides secondary metabolites in Hericium erinaceus. *Scientific Reports*, *7*(1), 10151. https://doi.org/10.1038/s41598-017-10376-0

Chen, L., Duan, Y., Wei, H., Ning, H., Bi, C., Zhao, Y., Qin, Y., & Li, Y. (2019). Acetyl-CoA carboxylase (ACC) as a therapeutic target for metabolic syndrome and recent developments in ACC1/2 inhibitors. In *Expert Opinion on Investigational Drugs* (Vol. 28, Issue 10, pp. 917–930). Taylor and Francis Ltd. https://doi.org/10.1080/13543784.2019.1657825

Chen, W., Gamache, E., Rosenman, D. J., Xie, J., Lopez, M. M., Li, Y. M., & Wang, C. (2014). Familial Alzheimer's mutations within APPTM increase Aβ42 production by enhancing accessibility of ε-cleavage site. *Nature Communications*, *5*. https://doi.org/10.1038/NCOMMS4037

Chen, Z., & Zhong, C. (2014). Oxidative stress in Alzheimer's disease. In *Neuroscience Bulletin* (Vol. 30, Issue 2, pp. 271–281). Science Press. https://doi.org/10.1007/s12264-013-1423-y

Cheng, D., Chu, C. H., Chen, L., Feder, J. N., Mintier, G. A., Wu, Y., Cook, J. W., Harpel, M. R., Locke, G. A., An, Y., & Tamura, J. K. (2007). Expression, purification, and characterization of human and rat acetyl cfenzyme A carboxylase (ACC) isozymes. *Protein Expression and Purification*, *51*(1), 11–21. https://doi.org/10.1016/j.pep.2006.06.005

Chiu, C. H., Chyau, C. C., Chen, C. C., Lee, L. Y., Chen, W. P., Liu, J. L., Lin, W. H., & Mong, M. C. (2018). Erinacine A-Enriched Hericium erinaceus Mycelium Produces Antidepressant-Like Effects through Modulating BDNF/PI3K/Akt/GSK-3β Signaling in Mice.

International Journal of Molecular Sciences, *19*(2), 341. https://doi.org/10.3390/ijms19020341

Chuang, M.-H., Chiou, S.-H., Huang, C.-H., Yang, W.-B., & Wong, C.-H. (2009). The lifespan-promoting effect of acetic acid and Reishi polysaccharide. *Bioorganic & Medicinal Chemistry*, *17*(22), 7831–7840. https://doi.org/10.1016/j.bmc.2009.09.002

Cohen, N., Cohen, J., Asatiani, M. D., Varshney, V. K., Yu, H.-T., Yang, Y.-C., Li, Y.-H., Mau, J.-L., & Wasser, S. P. (2014). Chemical Composition and Nutritional and Medicinal Value of Fruit Bodies and Submerged Cultured Mycelia of Culinary-Medicinal Higher Basidiomycetes Mushrooms. *International Journal of Medicinal Mushrooms*, *16*(3), 273–291. https://doi.org/10.1615/IntJMedMushr.v16.i3.80

Colbert, C. L., Kim, C. W., Moon, Y. A., Henry, L., Palnitkar, M., McKean, W. B., Fitzgerald, K., Deisenhofer, J., Horton, J. D., & Kwon, H. J. (2010). Crystal structure of Spot 14, a modulator of fatty acid synthesis. *Proceedings of the National Academy of Sciences of the United States of America*, *107*(44), 18820–18825. https://doi.org/10.1073/pnas.1012736107

Combs, C. K., Johnson, D. E., Karlo, J. C., Cannady, S. B., & Landreth, G. E. (2000). Inflammatory mechanisms in Alzheimer's disease: inhibition of beta-amyloid-stimulated proinflammatory responses and neurotoxicity by PPARgamma agonists. *The Journal of Neuroscience : The Official Journal of the Society for Neuroscience*, *20*(2), 558–567. https://doi.org/10.1523/JNEUROSCI.20-02-00558.2000

Connolly, N. M. C., Theurey, P., Adam-Vizi, V., Bazan, N. G., Bernardi, P., Bolaños, J. P., Culmsee, C., Dawson, V. L., Deshmukh, M., Duchen, M. R., Düssmann, H., Fiskum, G., Galindo, M. F., Hardingham, G. E., Hardwick, J. M., Jekabsons, M. B., Jonas, E. A., Jordán, J., Lipton, S. A., … Prehn, J. H. M. (2018). Guidelines on experimental methods to assess mitochondrial dysfunction in cellular models of neurodegenerative diseases. *Cell Death and Differentiation*, *25*(3), 542–572. https://doi.org/10.1038/s41418-017-0020-4

Cordaro, M., Salinaro, A. T., Siracusa, R., D'amico, R., Impellizzeri, D., Scuto, M., Ontario, M. L., Cuzzocrea, S., Di Paola, R., Fusco, R., & Calabrese, V. (2021). Key Mechanisms and Potential Implications of Hericium erinaceus in NLRP3 Inflammasome Activation by Reactive Oxygen Species during Alzheimer's Disease. *Antioxidants 2021, Vol. 10, Page 1664*, *10*(11), 1664. https://doi.org/10.3390/ANTIOX10111664

Cummings, J., Lee, G., Ritter, A., Sabbagh, M., & Zhong, K. (2019). Alzheimer's disease drug development pipeline: 2019. *Alzheimer's & Dementia: Translational Research & Clinical Interventions*, *5*(1), 272–293. https://doi.org/10.1016/J.TRCI.2019.05.008

Das Sarma, J. (2014). Microglia-mediated neuroinflammation is an amplifier of virus-induced neuropathology. *Journal of NeuroVirology*, *20*(2), 122–136. https://doi.org/10.1007/S13365-013-0188-4/FIGURES/3

David, D. C., Hauptmann, S., Scherping, I., Schuessel, K., Keil, U., Rizzu, P., Ravid, R., Dröse, S., Brandt, U., Müller, W. E., Eckert, A., & Götz, J. (2005). Proteomic and Functional Analyses Reveal a Mitochondrial Dysfunction in P301L Tau Transgenic Mice *. *Journal of Biological Chemistry*, *280*(25), 23802–23814. https://doi.org/10.1074/JBC.M500356200

Davies, P., & Maloney, A. J. F. (1976). SELECTIVE LOSS OF CENTRAL CHOLINERGIC NEURONS IN ALZHEIMER'S DISEASE. *The Lancet*, *308*(8000), 1403. https://doi.org/10.1016/S0140-6736(76)91936-X

De Jonghe, C., Esselens, C., Kumar-Singh, S., Craessaerts, K., Serneels, S., Checler, F., Annaert, W., Van Broeckhoven, C., & De Strooper, B. (2001). Pathogenic APP mutations near the gamma-secretase cleavage site differentially affect Abeta secretion and APP C-terminal fragment stability. *Human Molecular Genetics*, *10*(16), 1665–1671. https://doi.org/10.1093/HMG/10.16.1665

Decker, J. M., Krüger, L., Sydow, A., Zhao, S., Frotscher, M., Mandelkow, E., & Mandelkow, E. M. (2015). Pro-aggregant Tau impairs mossy fiber plasticity due to structural changes and Ca(++) dysregulation. *Acta Neuropathologica Communications*, *3*, 23. https://doi.org/10.1186/S40478-015-0193-3

Dieter, F., Esselun, C., & Eckert, G. P. (2022). *Redox Active α-Lipoic Acid Differentially Improves Mitochondrial Dysfunction in a Cellular Model of Alzheimer and Its Control Cells*. https://doi.org/10.3390/ijms23169186

Diling, C., Chaoqun, Z., Jian, Y., Jian, L., Jiyan, S., Yizhen, X., & Guoxiao, L. (2017). Immunomodulatory activities of a fungal protein extracted from Hericium erinaceus through regulating the gut microbiota. *Frontiers in Immunology*, *8*(JUN). https://doi.org/10.3389/fimmu.2017.00666

Drummond, E., & Wisniewski, T. (2017). Alzheimer's Disease: Experimental Models and Reality. *Acta Neuropathologica*, *133*(2), 155. https://doi.org/10.1007/S00401-016-1662-X

Eckert, A., Schmitt, K., & Götz, J. (2011). Mitochondrial dysfunction - The beginning of the end in Alzheimer's disease? Separate and synergistic modes of tau and amyloid-toxicity. *Alzheimer's Research and Therapy*, *3*(3), 1–11. https://doi.org/10.1186/ALZRT74/FIGURES/5

Eckert, G. P., Renner, K., Eckert, S. H., Eckmann, J., Hagl, S., Abdel-Kader, R. M., Kurz, C., Leuner, K., & Muller, W. E. (2012). Mitochondrial Dysfunction—A Pharmacological Target in Alzheimer's Disease. *Molecular Neurobiology*, *46*(1), 136–150. https://doi.org/10.1007/s12035-012-8271-z

Elkhateeb, W. A., Daba, G. M., Thomas, P. W., & Wen, T.-C. (2019). Medicinal mushrooms as a new source of natural therapeutic bioactive compounds. *Egyptian Pharmaceutical Journal*, *18*(2), 88. https://doi.org/10.4103/EPJ.EPJ_17_19

EMA. (2022). *Aduhelm: Withdrawn application | European Medicines Agency*. https://www.ema.europa.eu/en/medicines/human/withdrawn-applications/aduhelm

Ernster, L., & Schatz, G. (1981). Mitochondria: a historical review. *Journal of Cell Biology*, *91*(3), 227s–255s. https://doi.org/10.1083/JCB.91.3.227S

FDA. (2023). *FDA Grants Accelerated Approval for Alzheimer's Disease Treatment*. Press Announcements. https://www.fda.gov/news-events/press-announcements/fda-grants-accelerated-approval-alzheimers-disease-treatment

FDA. (2021). *FDA Grants Accelerated Approval for Alzheimer's Drug*. FDA News Release. https://www.fda.gov/news-events/press-announcements/fda-grants-accelerated-approval-alzheimers-drug

Feinstein, S. C., & Wilson, L. (2005). Inability of tau to properly regulate neuronal microtubule dynamics: a loss-of-function mechanism by which tau might mediate neuronal cell death. *Biochimica et Biophysica Acta (BBA) - Molecular Basis of Disease*, *1739*(2–3), 268–279. https://doi.org/10.1016/J.BBADIS.2004.07.002

Fernandez-Vizarra, E., & Zeviani, M. (2021). Mitochondrial disorders of the OXPHOS system. In *FEBS Letters* (Vol. 595, Issue 8, pp. 1062–1106). John Wiley and Sons Inc. https://doi.org/10.1002/1873-3468.13995

Ferreira, D., Westman, E., Eyjolfsdottir, H., Almqvist, P., Lind, G., Linderoth, B., Seiger, Å., Blennow, K., Karami, A., Darreh-Shori, T., Wiberg, M., Simmons, A., Wahlund, L. O., Wahlberg, L., & Eriksdotter, M. (2015). Brain Changes in Alzheimer's Disease Patients with Implanted Encapsulated Cells Releasing Nerve Growth Factor. *Journal of Alzheimer's Disease*, *43*(3), 1059–1072. https://doi.org/10.3233/JAD-141068

Forster, J. I., Köglsberger, S., Trefois, C., Boyd, O., Baumuratov, A. S., Buck, L., Balling, R., & Antony, P. M. A. (2016). Characterization of differentiated SH-SY5Y as neuronal screening model reveals increased oxidative vulnerability. *Journal of Biomolecular Screening*, *21*(5), 496–509. https://doi.org/10.1177/1087057115625190

Francis, P. T., Palmer, A. M., Snape, M., & Wilcock, G. K. (1999). The cholinergic hypothesis of Alzheimer's disease: a review of progress. *J Neurol Neurosurg Psychiatry*, *66*, 137–147. https://doi.org/10.1136/jnnp.66.2.137

François, J. M. (2007). A simple method for quantitative determination of polysaccharides in fungal cell walls. *Nature Protocols 2007 1:6*, *1*(6), 2995–3000. https://doi.org/10.1038/nprot.2006.457

Frandemiche, M. L., De Seranno, S., Rush, T., Borel, E., Elie, A., Arnal, I., Lanté, F., & Buisson, A. (2014). Activity-Dependent Tau Protein Translocation to Excitatory Synapse Is Disrupted by Exposure to Amyloid-Beta Oligomers. *Journal of Neuroscience*, *34*(17), 6084–6097. https://doi.org/10.1523/JNEUROSCI.4261-13.2014

Frazier, A. E., Kiu, C., Stojanovski, D., Hoogenraad, N. J., & Ryan, M. T. (2006). Mitochondrial morphology and distribution in mammalian cells. *Biological Chemistry*, *387*(12), 1551–1558. https://doi.org/10.1515/BC.2006.193

Friedman, M. (2015). Chemistry, Nutrition, and Health-Promoting Properties of Hericium erinaceus (Lion's Mane) Mushroom Fruiting Bodies and Mycelia and Their Bioactive Compounds. *Journal of Agricultural and Food Chemistry*, *63*(32), 7108–7123. https://doi.org/10.1021/acs.jafc.5b02914

Frozza, R. L., Lourenco, M. V., & de Felice, F. G. (2018). Challenges for Alzheimer's disease therapy: Insights from novel mechanisms beyond memory defects. *Frontiers in Neuroscience*, *12*(FEB), 37. https://doi.org/10.3389/FNINS.2018.00037/BIBTEX

Ge, S. X., Jung, D., & Yao, R. (2020). ShinyGO: a graphical gene-set enrichment tool for animals and plants. *Bioinformatics*, *36*(8), 2628–2629. https://doi.org/10.1093/BIOINFORMATICS/BTZ931

Ghasemi, M., Turnbull, T., Sebastian, S., & Kempson, I. (2021). The mtt assay: Utility, limitations, pitfalls, and interpretation in bulk and single-cell analysis. *International Journal of Molecular Sciences*, *22*(23). https://doi.org/10.3390/IJMS222312827/S1

Gibson, G. E., Starkov, A., Blass, J. P., Ratan, R. R., & Beal, M. F. (2010). Cause and consequence: Mitochondrial dysfunction initiates and propagates neuronal dysfunction, neuronal death and behavioral abnormalities in age-associated neurodegenerative diseases. *Biochimica et Biophysica Acta (BBA) - Molecular Basis of Disease*, *1802*(1), 122–134. https://doi.org/10.1016/J.BBADIS.2009.08.010

Glenner, G. G., & Wong, C. W. (1984). Alzheimer's disease: Initial report of the purification and characterization of a novel cerebrovascular amyloid protein. *Biochemical and*

Biophysical Research Communications, *120*(3), 885–890. https://doi.org/10.1016/S0006-291X(84)80190-4

Goate, A., Chartier-Harlin, M. C., Mullan, M., Brown, J., Crawford, F., Fidani, L., Giuffra, L., Haynes, A., Irving, N., James, L., Mant, R., Newton, P., Rooke, K., Roques, P., Talbot, C., Pericak-Vance, M., Roses, A., Williamson, R., Rossor, M., … Hardy, J. (1991). Segregation of a missense mutation in the amyloid precursor protein gene with familial Alzheimer's disease. *Nature*, *349*(6311), 704–706. https://doi.org/10.1038/349704A0

Goldgaber, D., Harris, H. W., Hla, T., Maciag, T., Donnelly, R. J., Jacobsen, J. S., Vitek, M. P., & Carleton Gajdusek, D. (1989). Interleukin 1 regulates synthesis of amyloid beta-protein precursor mRNA in human endothelial cells. *Proceedings of the National Academy of Sciences of the United States of America*, *86*(19), 7606–7610. https://doi.org/10.1073/PNAS.86.19.7606

Golpich, M., Amini, E., Mohamed, Z., Azman Ali, R., Mohamed Ibrahim, N., & Ahmadiani, A. (2017). Mitochondrial Dysfunction and Biogenesis in Neurodegenerative diseases: Pathogenesis and Treatment. *CNS Neuroscience & Therapeutics*, *23*(1), 5–22. https://doi.org/10.1111/CNS.12655

Grewal, R., Reutzel, M., Dilberger, B., Hein, H., Zotzel, J., Marx, S., Tretzel, J., Sarafeddinov, A., Fuchs, C., & Eckert, G. P. (2020). Purified oleocanthal and ligstroside protect against mitochondrial dysfunction in models of early Alzheimer's disease and brain ageing. *Experimental Neurology*, *328*. https://doi.org/10.1016/J.EXPNEUROL.2020.113248

Guiochon, G., Felinger, A., Shirazi, D. G., & Katti, A. M. (2006). *Fundamentals of Preparative Chomatography*. 990.

Gurd, B. J. (2011). Deacetylation of PGC-1α by SIRT1: importance for skeletal muscle function and exercise-induced mitochondrial biogenesis. *Applied Physiology, Nutrition, and Metabolism = Physiologie Appliquee, Nutrition et Metabolisme*, *36*(5), 589–597. https://doi.org/10.1139/H11-070

Haass, C., Lemere, C. A., Capell, A., Citron, M., Seubert, P., Schenk, D., Lannfelt, L., & Selkoe, D. J. (1995). The Swedish mutation causes early-onset Alzheimer's disease by β-secretase cleavage within the secretory pathway. *Nature Medicine 1995 1:12*, *1*(12), 1291–1296. https://doi.org/10.1038/nm1295-1291

Hagl, S., Grewal, R., Ciobanu, I., Helal, A., Khayyal, M. T., Muller, W. E., & Eckert, G. P. (2015). Rice bran extract compensates mitochondrial dysfunction in a cellular model of early Alzheimer's disease. *Journal of Alzheimer's Disease*, *43*(3), 927–938. https://doi.org/10.3233/JAD-132084

Han, Z. H., Ye, J. M., & Wang, G. F. (2013). Evaluation of in vivo antioxidant activity of Hericium erinaceus polysaccharides. *International Journal of Biological Macromolecules*, *52*(1), 66–71. https://doi.org/10.1016/J.IJBIOMAC.2012.09.009

Hansen, R. A., Gartlehner, G., Webb, A. P., Morgan, L. C., Moore, C. G., & Jonas, D. E. (2008). Efficacy and safety of donepezil, galantamine, and rivastigmine for the treatment of Alzheimer's disease: A systematic review and meta-analysis. *Clinical Interventions in Aging*, *3*(2), 211. /pmc/articles/PMC2546466/

Hickman, S. E., Allison, E. K., & El Khoury, J. (2008). Microglial dysfunction and defective beta-amyloid clearance pathways in aging Alzheimer's disease mice. *The Journal of Neuroscience : The Official Journal of the Society for Neuroscience*, *28*(33), 8354–8360. https://doi.org/10.1523/JNEUROSCI.0616-08.2008

Hirai, K., Aliev, G., Nunomura, A., Fujioka, H., Russell, R. L., Atwood, C. S., Johnson, A. B., Kress, Y., Vinters, H. V., Tabaton, M., Shimohama, S., Cash, A. D., Siedlak, S. L., Harris, P. L. R., Jones, P. K., Petersen, R. B., Perry, G., & Smith, M. A. (2001). Mitochondrial abnormalities in Alzheimer's disease. *Journal of Neuroscience*, *21*(9), 3017–3023. https://doi.org/10.1523/jneurosci.21-09-03017.2001

Höltje, H.-D., Sippl, W., Rognan, D., & Folkers, G. (2008). Virtual Screening and Docking. In *Molecular Modeling* (Third). Wiley-VCH Verlag GmbH & Co.

Hoover, B. R., Reed, M. N., Su, J., Penrod, R. D., Kotilinek, L. A., Grant, M. K., Pitstick, R., Carlson, G. A., Lanier, L. M., Yuan, L. L., Ashe, K. H., & Liao, D. (2010). Tau Mislocalization to Dendritic Spines Mediates Synaptic Dysfunction Independently of Neurodegeneration. *Neuron*, *68*(6), 1067–1081. https://doi.org/10.1016/J.NEURON.2010.11.030/ATTACHMENT/D85EC27F-8172-4999-B2D3-40B2FE0B5967/MMC1.PDF

Hoyer, S. (1991). Abnormalities of Glucose Metabolism in Alzheimer's Disease. *Annals of the New York Academy of Sciences*, *640*(1), 53–58. https://doi.org/10.1111/J.1749-6632.1991.TB00190.X

Hu, J. H., Li, I. C., Lin, T. W., Chen, W. P., Lee, L. Y., Chen, C. C., & Kuo, C. F. (2019). Absolute bioavailability, tissue distribution, and excretion of erinacine S in hericium erinaceus mycelia. *Molecules*, *24*(8), 1624. https://doi.org/10.3390/molecules24081624

Hu, M., Zhang, P., Wang, R., Zhou, M., Pang, N., Cui, X., Ge, X., Liu, X., Huang, X. F., & Yu, Y. (2022). Three Different Types of β-Glucans Enhance Cognition: The Role of the Gut-Brain Axis. *Frontiers in Nutrition*, *9*, 312. https://doi.org/10.3389/FNUT.2022.848930/BIBTEX

Huang, H.-T., Ho, C.-H., Sung, H.-Y., Lee, L.-Y., Chen, W.-P., Chen, Y.-W., Chen, C.-C., Yang, C.-S., & Tzeng, S.-F. (2021). Hericium erinaceus mycelium and its small bioactive compounds promote oligodendrocyte maturation with an increase in myelin basic protein. *Scientific Reports*, *11*(1), 6551. https://doi.org/10.1038/s41598-021-85972-2

Huang, J., Chen, S., Hu, L., Niu, H., Sun, Q., Li, W., Tan, G., Li, J., Jin, L. J., Lyu, J., & Zhou, H. (2018). Mitoferrin-1 is Involved in the Progression of Alzheimer's Disease Through Targeting Mitochondrial Iron Metabolism in a Caenorhabditis elegans Model of Alzheimer's Disease. *Neuroscience*, *385*, 90–101. https://doi.org/10.1016/J.NEUROSCIENCE.2018.06.011

Huang, Y.-J., Lin, C.-H., Lane, H.-Y., & E. Tsaid, G. (2012). NMDA Neurotransmission Dysfunction in Behavioral and Psychological Symptoms of Alzheimer's Disease. *Current Neuropharmacology*, *10*(3), 272–285. https://doi.org/10.2174/157015912803217288

Hyde, K. D., Xu, J., Rapior, S., Jeewon, R., Lumyong, S., Niego, A. G. T., Abeywickrama, P. D., Aluthmuhandiram, J. V. S., Brahamanage, R. S., Brooks, S., Chaiyasen, A., Chethana, K. W. T., Chomnunti, P., Chepkirui, C., Chuankid, B., de Silva, N. I., Doilom, M., Faulds, C., Gentekaki, E., … Stadler, M. (2019). The amazing potential of fungi: 50 ways we can exploit fungi industrially. In *Fungal Diversity* (Vol. 97, Issue 1, pp. 1–136). Springer Netherlands. https://doi.org/10.1007/s13225-019-00430-9

Illescas, M., Peñas, A., Arenas, J., Martín, M. A., & Ugalde, C. (2021). Regulation of Mitochondrial Function by the Actin Cytoskeleton. *Frontiers in Cell and Developmental Biology*, *9*, 3656. https://doi.org/10.3389/FCELL.2021.795838/BIBTEX

Ito, S., Tan, L. J., Andoh, D., Narita, T., Seki, M., Hirano, Y., Narita, K., Kuraoka, I., Hiraoka, Y., & Tanaka, K. (2010). MMXD, a TFIIH-Independent XPD-MMS19 Protein Complex Involved in Chromosome Segregation. *Molecular Cell*, *39*(4), 632–640. https://doi.org/10.1016/j.molcel.2010.07.029

Ittner, L. M., Ke, Y. D., Delerue, F., Bi, M., Gladbach, A., van Eersel, J., Wölfing, H., Chieng, B. C., Christie, M. J., Napier, I. A., Eckert, A., Staufenbiel, M., Hardeman, E., & Götz, J. (2010). Dendritic function of tau mediates amyloid-beta toxicity in Alzheimer's disease mouse models. *Cell*, *142*(3), 387–397. https://doi.org/10.1016/J.CELL.2010.06.036

Jack, C. R., Bennett, D. A., Blennow, K., Carrillo, M. C., Dunn, B., Haeberlein, S. B., Holtzman, D. M., Jagust, W., Jessen, F., Karlawish, J., Liu, E., Molinuevo, J. L., Montine, T., Phelps, C., Rankin, K. P., Rowe, C. C., Scheltens, P., Siemers, E., Snyder, H. M., … Silverberg, N. (2018). 2018 National Institute on Aging-Alzheimer's Association (NIA-AA) Research Framework NIA-AA Research Framework: Toward a biological definition

of Alzheimer's disease. *Alzheimer's & Dementia*. https://doi.org/10.1016/j.jalz.2018.02.018

Jonkman, J., Brown, C. M., Wright, G. D., Anderson, K. I., & North, A. J. (2020). Tutorial: guidance for quantitative confocal microscopy. In *Nature Protocols* (Vol. 15, Issue 5, pp. 1585–1611). Nature Research. https://doi.org/10.1038/s41596-020-0313-9

Kahle, P. J., & De Strooper, B. (2003). Attack on amyloid. *EMBO Reports*, *4*(8), 747–752. https://doi.org/10.1038/SJ.EMBOR.EMBOR905

Kang, I., Chu, C. T., & Kaufman, B. A. (2018). The mitochondrial transcription factor TFAM in neurodegeneration: emerging evidence and mechanisms. *FEBS Letters*, *592*(5), 793–811. https://doi.org/10.1002/1873-3468.12989

Kaushik, V. K., Kavana, M., Volz, J. M., Weldon, S. C., Hanrahan, S., Xu, J., Caplan, S. L., & Hubbard, B. K. (2009). Characterization of recombinant human acetyl-CoA carboxylase-2 steady-state kinetics. *Biochimica et Biophysica Acta - Proteins and Proteomics*, *1794*(6), 961–967. https://doi.org/10.1016/j.bbapap.2009.02.004

Kawagishi, H. (2021). Chemical studies on bioactive compounds related to higher fungi. In *Bioscience, Biotechnology and Biochemistry* (Vol. 85, Issue 1, pp. 1–7). Oxford University Press. https://doi.org/10.1093/bbb/zbaa072

Kawagishi, H., Shimada, A., Hosokawa, S., Mori, H., Sakamoto, H., Ishiguro, Y., Sakemi, S., Bordner, J., Kojima, N., & Furukawa, S. (1996). Erinacines E, F, and G, stimulators of nerve growth factor (NGF)-synthesis, from the mycelia of Hericium erinaceum. *Tetrahedron Letters*, *37*(41), 7399–7402. https://doi.org/10.1016/0040-4039(96)01687-5

Kawagishi, H., Shimada, A., Shirai, R., Okamoto, K., Ojima, F., Sakamoto, H., Ishiguro, Y., & Furukawa, S. (1994). Erinacines A, B and C, strong stimulators of nerve growth factor (NGF)-synthesis, from the mycelia of Hericium erinaceum. *Tetrahedron Letters*, *35*(10), 1569–1572. https://doi.org/10.1016/S0040-4039(00)76760-8

Kawagishi, H., & Zhuang, C. (2008). Compounds for dementia from Hericium erinaceum. *Drugs of the Future*, *33*(2), 149. https://doi.org/10.1358/dof.2008.033.02.1173290

Keeler, James. (2010). *Understanding NMR spectroscopy*. John Wiley and Sons.

Khan, Md. A., Tania, M., Liu, R., & Rahman, M. M. (2013). Hericium erinaceus: An edible mushroom with medicinal values. *Journal of Complementary and Integrative Medicine*, *10*(1), 253–258. https://doi.org/10.1515/jcim-2013-0001

Khanna, G., Bhandari, R., & Kuhad, A. (2022). Aducanumab. *Drugs of the Future*, *44*(2), 115–121. https://doi.org/10.1358/dof.2019.44.2.2895649

Kim, C. W., Moon, Y. A., Park, S. W., Cheng, D., Kwon, H. J., & Horton, J. D. (2010). Induced polymerization of mammalian acetyl-CoA carboxylase by MIG12 provides a tertiary level of regulation of fatty acid synthesis. *Proceedings of the National Academy of Sciences of the United States of America*, *107*(21), 9626–9631. https://doi.org/10.1073/pnas.1001292107

Kim, S., Chen, J., Cheng, T., Gindulyte, A., He, J., He, S., Li, Q., Shoemaker, B. A., Thiessen, P. A., Yu, B., Zaslavsky, L., Zhang, J., & Bolton, E. E. (2021). PubChem in 2021: New data content and improved web interfaces. *Nucleic Acids Research*, *49*(D1), D1388–D1395. https://doi.org/10.1093/nar/gkaa971

Kim, Y. S., & Joh, T. H. (2006). Microglia, major player in the brain inflammation: their roles in the pathogenesis of Parkinson's disease. *Experimental & Molecular Medicine 2006 38:4*, *38*(4), 333–347. https://doi.org/10.1038/emm.2006.40

Kinney, J. W., Bemiller, S. M., Murtishaw, A. S., Leisgang, A. M., Salazar, A. M., & Lamb, B. T. (2018). Inflammation as a central mechanism in Alzheimer's disease. *Alzheimer's & Dementia: Translational Research & Clinical Interventions*, *4*(1), 575–590. https://doi.org/10.1016/J.TRCI.2018.06.014

Kiyama, T., Chen, C. K., Wang, S. W., Pan, P., Ju, Z., Wang, J., Takada, S., Klein, W. H., & Mao, C. A. (2018). Essential roles of mitochondrial biogenesis regulator Nrf1 in retinal development and homeostasis. *Molecular Neurodegeneration*, *13*(1). https://doi.org/10.1186/S13024-018-0287-Z

Kopach, O., Pavlov, A. M., Sindeeva, O. A., Sukhorukov, G. B., & Rusakov, D. A. (2020). Biodegradable Microcapsules Loaded with Nerve Growth Factor Enable Neurite Guidance and Synapse Formation. *Pharmaceutics 2021, Vol. 13, Page 25*, *13*(1), 25. https://doi.org/10.3390/PHARMACEUTICS13010025

Koppenol, W. H., Bounds, P. L., & Dang, C. V. (2011). Otto Warburg's contributions to current concepts of cancer metabolism. *Nature Reviews. Cancer*, *11*(5), 325–337. https://doi.org/10.1038/NRC3038

Koseki, K., Yamamoto, A., Tanimoto, K., Okamoto, N., Teng, F., Bito, T., Yabuta, Y., Kawano, T., & Watanabe, F. (2021). Dityrosine Crosslinking of Collagen and Amyloid-β Peptides Is Formed by Vitamin B 12 Deficiency-Generated Oxidative Stress in Caenorhabditis elegans. *International Journal of Molecular Sciences*, *22*(23). https://doi.org/10.3390/IJMS222312959

Kovalevich, J., & Langford, D. (2013). Considerations for the use of SH-SY5Y neuroblastoma cells in neurobiology. *Methods in Molecular Biology (Clifton, N.J.)*, *1078*, 9–21. https://doi.org/10.1007/978-1-62703-640-5_2

Krishna, A., Biryukov, M., Trefois, C., Antony, P. M. A., Hussong, R., Lin, J., Heinäniemi, M., Glusman, G., Köglsberger, S., Boyd, O., van den Berg, B. H. J., Linke, D., Huang, D., Wang, K., Hood, L., Tholey, A., Schneider, R., Galas, D. J., Balling, R., & May, P. (2014). Systems genomics evaluation of the SH-SY5Y neuroblastoma cell line as a model for Parkinson's disease. *BMC Genomics*, *15*(1), 1–21. https://doi.org/10.1186/1471-2164-15-1154/TABLES/6

Ku, Y.-S., Sintaha, M., Cheung, M.-Y., & Lam, H.-M. (2018). Plant Hormone Signaling Crosstalks between Biotic and Abiotic Stress Responses. *International Journal of Molecular Sciences*, *19*(10), 3206. https://doi.org/10.3390/ijms19103206

Kushairi, N., Phan, C. W., Sabaratnam, V., David, P., & Naidu, M. (2019). Lion's Mane Mushroom, Hericium erinaceus (Bull.: Fr.) Pers. Suppresses H2O2-Induced Oxidative Damage and LPS-Induced Inflammation in HT22 Hippocampal Neurons and BV2 Microglia. *Antioxidants*, *8*(8), 261. https://doi.org/10.3390/antiox8080261

Lan, F., Cacicedo, J. M., Ruderman, N., & Ido, Y. (2008). SIRT1 modulation of the acetylation status, cytosolic localization, and activity of LKB1: Possible role in AMP-activated protein kinase activation. *Journal of Biological Chemistry*, *283*(41), 27628–27635. https://doi.org/10.1074/JBC.M805711200/ATTACHMENT/77FBE8DB-3C8D-46C0-B912-8B49EE6EFC6D/MMC1.PDF

Lane, C. A., Hardy, J., & Schott, J. M. (2018). Alzheimer's disease. In *European Journal of Neurology* (Vol. 25, Issue 1, pp. 59–70). Blackwell Publishing Ltd. https://doi.org/10.1111/ene.13439

Larsen, S., Nielsen, J., Hansen, C. N., Nielsen, L. B., Wibrand, F., Stride, N., Schroder, H. D., Boushel, R., Helge, J. W., Dela, F., & Hey-Mogensen, M. (2012). Biomarkers of mitochondrial content in skeletal muscle of healthy young human subjects. *The Journal of Physiology*, *590*(Pt 14), 3349. https://doi.org/10.1113/JPHYSIOL.2012.230185

Lee, J., Kim, C. H., Simon, D. K., Aminova, L. R., Andreyev, A. Y., Kushnareva, Y. E., Murphy, A. N., Lonze, B. E., Kim, K. S., Ginty, D. D., Ferrante, R. J., Ryu, H., & Ratan, R. R. (2005). Mitochondrial cyclic AMP response element-binding protein (CREB) mediates mitochondrial gene expression and neuronal survival. *Journal of Biological Chemistry*, *280*(49), 40398–40401. https://doi.org/10.1074/jbc.C500140200

Lee, J. S., & Hong, E. K. (2010). Hericium erinaceus enhances doxorubicin-induced apoptosis in human hepatocellular carcinoma cells. *Cancer Letters*, *297*(2), 144–154. https://doi.org/10.1016/J.CANLET.2010.05.006

Lee, K.-F., Chen, J.-H., Teng, C.-C., Shen, C.-H., Hsieh, M.-C., Lu, C.-C., Lee, K.-C., Lee, L.-Y., Chen, W.-P., Chen, C.-C., Huang, W.-S., & Kuo, H.-C. (2014). Protective Effects of Hericium erinaceus Mycelium and Its Isolated Erinacine A against Ischemia-Injury-Induced Neuronal Cell Death via the Inhibition of iNOS/p38 MAPK and Nitrotyrosine. *International Journal of Molecular Sciences*, *15*(9), 15073–15089. https://doi.org/10.3390/ijms150915073

Lee, K.-F., Tung, S.-Y., Teng, C.-C., Shen, C.-H., Hsieh, M. C., Huang, C.-Y., Lee, K.-C., Lee, L.-Y., Chen, W.-P., Chen, C.-C., Huang, W.-S., & Kuo, H.-C. (2020). Post-Treatment with Erinacine A, a Derived Diterpenoid of H. erinaceus, Attenuates Neurotoxicity in MPTP Model of Parkinson's Disease. *Antioxidants*, *9*(2), 137. https://doi.org/10.3390/antiox9020137

Lee, W. S., Lee, H. J., Yang, J. Y., Shin, H. L., Choi, S. W., Kim, J. K., Seo, W. D., & Kim, E. H. (2022). The Potential Neuroprotective Effects of Extracts from Oat Seedlings against Alzheimer’s Disease. *Nutrients 2022, Vol. 14, Page 4103*, *14*(19), 4103. https://doi.org/10.3390/NU14194103

Levi-Montalcini, R., Skaper, S. D., Dal Toso, R., Petrelli, L., & Leon, A. (1996). Nerve growth factor: from neurotrophin to neurokine. *Trends in Neurosciences*, *19*(11), 514–520. https://doi.org/10.1016/S0166-2236(96)10058-8

Lewin, M. J. M. (1999). Cellular mechanisms and inhibitors of gastric acid secretion. *Drugs of Today (Barcelona, Spain : 1998)*, *35*(10), 743–752. https://doi.org/10.1358/DOT.1999.35.10.561693

Li, I.-C., Chang, H.-H., Lin, C.-H., Chen, W.-P., Lu, T.-H., Lee, L.-Y., Chen, Y.-W., Chen, Y.-P., Chen, C.-C., & Lin, D. P.-C. (2020). Prevention of Early Alzheimer's Disease by Erinacine A-Enriched Hericium erinaceus Mycelia Pilot Double-Blind Placebo-Controlled Study. *Frontiers in Aging Neuroscience*, *12*, 155. https://doi.org/10.3389/fnagi.2020.00155

Li, I.-C., Lee, L.-Y., Chen, Y.-J., Chou, M.-Y., Wang, M.-F., Chen, W.-P., Chen, Y.-P., & Chen, C.-C. (2019). Erinacine A-enriched Hericium erinaceus mycelia promotes longevity in Drosophila melanogaster and aged mice. *PLOS ONE*, *14*(5), e0217226. https://doi.org/10.1371/journal.pone.0217226

Li, I.-C., Lee, L.-Y., Tzeng, T.-T., Chen, W.-P., Chen, Y.-P., Shiao, Y.-J., & Chen, C.-C. (2018). Neurohealth Properties of Hericium erinaceus Mycelia Enriched with Erinacines. *Behavioural Neurology*, *2018*, 5802634. https://doi.org/10.1155/2018/5802634

Li, X. C., Hu, Y., Wang, Z. H., Luo, Y., Zhang, Y., Liu, X. P., Feng, Q., Wang, Q., Ye, K., Liu, G. P., & Wang, J. Z. (2016). Human wild-type full-length tau accumulation disrupts mitochondrial dynamics and the functions via increasing mitofusins. *Scientific Reports 2016 6:1*, *6*(1), 1–10. https://doi.org/10.1038/srep24756

Lin, E. S., & Chen, Y. H. (2007). Factors affecting mycelial biomass and exopolysaccharide production in submerged cultivation of Antrodia cinnamomea using complex media. *Bioresource Technology*, *98*(13), 2511–2517. https://doi.org/10.1016/j.biortech.2006.09.008

Liu, J., Chang, L., Song, Y., Li, H., & Wu, Y. (2019). The role of NMDA receptors in Alzheimer's disease. *Frontiers in Neuroscience*, *13*(FEB), 43. https://doi.org/10.3389/FNINS.2019.00043/BIBTEX

Ma, B. J., Yu, H. Y., Shen, J. W., Ruan, Y., Zhao, X., Zhou, H., & Wu, T. T. (2010). Cytotoxic aromatic compounds from Hericium erinaceum. *The Journal of Antibiotics 2010 63:12*, *63*(12), 713–715. https://doi.org/10.1038/ja.2010.112

Maden, M. (2007). Retinoic acid in the development, regeneration and maintenance of the nervous system. *Nature Reviews Neuroscience 2007 8:10*, *8*(10), 755–765. https://doi.org/10.1038/nrn2212

Majeed, Y., Halabi, N., Madani, A. Y., Engelke, R., Bhagwat, A. M., Abdesselem, H., Agha, M. V., Vakayil, M., Courjaret, R., Goswami, N., Hamidane, H. Ben, Elrayess, M. A., Rafii, A., Graumann, J., Schmidt, F., & Mazloum, N. A. (2021). SIRT1 promotes lipid metabolism and mitochondrial biogenesis in adipocytes and coordinates adipogenesis by targeting key enzymatic pathways. *Scientific Reports 2021 11:1*, *11*(1), 1–19. https://doi.org/10.1038/s41598-021-87759-x

Malinowska, E., Krzyczkowski, W., Herold, F., Łapienis, G., Ślusarczyk, J., Suchocki, P., Kuraś, M., & Turło, J. (2009). Biosynthesis of selenium-containing polysaccharides with antioxidant activity in liquid culture of Hericium erinaceum. *Enzyme and Microbial Technology*, *44*(5), 334–343. https://doi.org/10.1016/J.ENZMICTEC.2008.12.003

Manczak, M., Calkins, M. J., & Reddy, P. H. (2011). Impaired mitochondrial dynamics and abnormal interaction of amyloid beta with mitochondrial protein Drp1 in neurons from patients with Alzheimer's disease: implications for neuronal damage. *Human Molecular Genetics*, *20*(13), 2495–2509. https://doi.org/10.1093/HMG/DDR139

Mandelkow, E. M., & Mandelkow, E. (2012). Biochemistry and Cell Biology of Tau Protein in Neurofibrillary Degeneration. *Cold Spring Harbor Perspectives in Medicine*, *2*(7), a006247. https://doi.org/10.1101/CSHPERSPECT.A006247

Martin Prince, A., Wimo, A., Guerchet, M., Gemma-Claire Ali, M., Wu, Y.-T., Prina, M., Yee Chan, K., & Xia, Z. (2015). *World Alzheimer Report 2015 The Global Impact of Dementia AN ANALYSIS OF PREVALENCE,INIDENCE, COST AND TRENDS*. www.alz.co.uk/worldreport2015corrections

Martínez-Mármol, R., Chai, Y. J., Conroy, J. N., Khan, Z., Hong, S. M., Kim, S. B., Gormal, R. S., Lee, D. H., Lee, J. K., Coulson, E. J., Lee, M. K., Kim, S. Y., & Meunier, F. A. (2023). Hericerin derivatives activates a pan-neurotrophic pathway in central hippocampal neurons converging to ERK1/2 signaling enhancing spatial memory. *Journal of Neurochemistry*, *00*, 1–18. https://doi.org/10.1111/JNC.15767

Matrone, C., Ciotti, M. T., Mercanti, D., Marolda, R., & Calissano, P. (2008). NGF and BDNF signaling control amyloidogenic route and Abeta production in hippocampal neurons. *Proceedings of the National Academy of Sciences of the United States of America*, *105*(35), 13139–13144. https://doi.org/10.1073/PNAS.0806133105

McBride, H. M., Neuspiel, M., & Wasiak, S. (2006). Mitochondria: More Than Just a Powerhouse. *Current Biology*, *16*(14), R551–R560. https://doi.org/10.1016/J.CUB.2006.06.054/ATTACHMENT/08AB04CF-A679-4917-AC88-0025E554D812/MMC1.PDF

Mehta, D., Jackson, R., Paul, G., Shi, J., & Sabbagh, M. (2017). Why do trials for Alzheimer's disease drugs keep failing? A discontinued drug perspective for 2010-2015. *Https://Doi.Org/10.1080/13543784.2017.1323868*, *26*(6), 735–739. https://doi.org/10.1080/13543784.2017.1323868

Mergenthaler, P., Lindauer, U., Dienel, G. A., & Meisel, A. (2013). Sugar for the brain: the role of glucose in physiological and pathological brain function. *Trends in Neurosciences*, *36*(10), 587. https://doi.org/10.1016/J.TINS.2013.07.001

Mitchell, P., & Moyle, J. (1965). Stoichiometry of Proton Translocation through the Respiratory Chain and Adenosine Triphosphatase Systems of Rat Liver Mitochondria. *Nature 1965 208:5006*, *208*(5006), 147–151. https://doi.org/10.1038/208147a0

Mizuno, T., Wasa, T., Ito, H., Suzuki, C., & Ukai, N. (1992). Antitumor-active polysaccharides isolated from the fruiting body of Hericium erinaceum, an edible and medicinal mushroom called yamabushitake or houtou. *Bioscience, Biotechnology, and Biochemistry*, *56*(2), 347–348. https://doi.org/10.1271/BBB.56.347

Mori, K., Inatomi, S., Ouchi, K., Azumi, Y., & Tuchida, T. (2009). Improving effects of the mushroom Yamabushitake (Hericium erinaceus) on mild cognitive impairment: a double-blind placebo-controlled clinical trial. *Phytotherapy Research*, *23*(3), 367–372. https://doi.org/10.1002/ptr.2634

Mori, K., Obara, Y., Hirota, M., Azumi, Y., Kinugasa, S., Inatomi, S., & Nakahata, N. (2008). Nerve Growth Factor-Inducing Activity of Hericium erinaceus in 1321N1 Human Astrocytoma Cells. *Biological & Pharmaceutical Bulletin*, *31*(9), 1727–1732. https://doi.org/10.1248/bpb.31.1727

Mosconi, L., Berti, V., Glodzik, L., Pupi, A., De Santi, S., & De Leon, M. J. (2010). Pre-Clinical Detection of Alzheimer's Disease Using FDG-PET, with or without Amyloid Imaging. *Journal of Alzheimer's Disease*, *20*(3), 843–854. https://doi.org/10.3233/JAD-2010-091504

Mufson, E. J., Counts, S. E., Ginsberg, S. D., Mahady, L., Perez, S. E., Massa, S. M., Longo, F. M., & Ikonomovic, M. D. (2019). Nerve growth factor pathobiology during the progression of Alzheimer's disease. In *Frontiers in Neuroscience* (Vol. 13, Issue JUL, p. 533). Frontiers Media S.A. https://doi.org/10.3389/fnins.2019.00533

Mülhardt, C. (2013). Der Experimentator Molekularbiologie/Genomics. *Der Experimentator Molekularbiologie/Genomics*. https://doi.org/10.1007/978-3-642-34636-1

Müller, U. C., Deller, T., & Korte, M. (2017). Not just amyloid: physiological functions of the amyloid precursor protein family. *Nature Reviews Neuroscience 2017 18:5*, *18*(5), 281–298. https://doi.org/10.1038/nrn.2017.29

Müller, W. E., Eckert, A., Kurz, C., Eckert, G. P., & Leuner, K. (2010). Mitochondrial Dysfunction: Common Final Pathway in Brain Aging and Alzheimer's Disease—Therapeutic Aspects. *Molecular Neurobiology*, *41*(2–3), 159–171. https://doi.org/10.1007/s12035-010-8141-5

Murphy, M. P. (2009). How mitochondria produce reactive oxygen species. In *Biochemical Journal* (Vol. 417, Issue 1, pp. 1–13). Portland Press Ltd. https://doi.org/10.1042/BJ20081386

Nagano, M., Shimizu, K., Kondo, R., Hayashi, C., Sato, D., Kitagawa, K., & Ohnuki, K. (2010). Reduction of depression and anxiety by 4 weeks Hericium erinaceus intake. *Biomedical Research*, *31*(4), 231–237. https://doi.org/10.2220/biomedres.31.231

Namba, T., Dóczi, J., Pinson, A., Xing, L., Kalebic, N., Wilsch-Bräuninger, M., Long, K. R., Vaid, S., Lauer, J., Bogdanova, A., Borgonovo, B., Shevchenko, A., Keller, P., Drechsel, D., Kurzchalia, T., Wimberger, P., Chinopoulos, C., & Huttner, W. B. (2020). Human-

Specific ARHGAP11B Acts in Mitochondria to Expand Neocortical Progenitors by Glutaminolysis. *Neuron*, *105*(5), 867-881.e9. https://doi.org/10.1016/j.neuron.2019.11.027

Napolitano, G., Fasciolo, G., & Venditti, P. (2021). Mitochondrial Management of Reactive Oxygen Species. *Antioxidants 2021, Vol. 10, Page 1824*, *10*(11), 1824. https://doi.org/10.3390/ANTIOX10111824

Neue, U. D. (2006). HPLC Columns, Theory, Technology, and Practice. *Http://Dx.Doi.Org/10.1080/10739149808001913*, *26*(4), 439–440. https://doi.org/10.1080/10739149808001913

Nhan, H. S., Chiang, K., & Koo, E. H. (2015). The multifaceted nature of amyloid precursor protein and its proteolytic fragments: friends and foes. *Acta Neuropathologica*, *129*(1), 1–19. https://doi.org/10.1007/S00401-014-1347-2/FIGURES/3

Nicholls, D. G., & Ward, M. W. (2000). Mitochondrial membrane potential and neuronal glutamate excitotoxicity: Mortality and millivolts. In *Trends in Neurosciences* (Vol. 23, Issue 4, pp. 166–174). Trends Neurosci. https://doi.org/10.1016/S0166-2236(99)01534-9

Nickel, A., Kohlhaas, M., & Maack, C. (2014). Mitochondrial reactive oxygen species production and elimination. *Journal of Molecular and Cellular Cardiology*, *73*, 26–33. https://doi.org/10.1016/J.YJMCC.2014.03.011

Nirody, J. A., Budin, I., & Rangamani, P. (2020). ATP synthase: Evolution, energetics, and membrane interactions. *Journal of General Physiology*, *152*(11). https://doi.org/10.1085/JGP.201912475

Nunnari, J., & Suomalainen, A. (2012). Mitochondria: in sickness and in health. *Cell*, *148*(6), 1145–1159. https://doi.org/10.1016/j.cell.2012.02.035

Oláhová, M., Yoon, W. H., Thompson, K., Jangam, S., Fernandez, L., Davidson, J. M., Kyle, J. E., Grove, M. E., Fisk, D. G., Kohler, J. N., Holmes, M., Dries, A. M., Huang, Y., Zhao, C., Contrepois, K., Zappala, Z., Frésard, L., Waggott, D., Zink, E. M., … Cowan, T. (2018). Biallelic Mutations in ATP5F1D, which Encodes a Subunit of ATP Synthase, Cause a Metabolic Disorder. *American Journal of Human Genetics*, *102*(3), 494–504. https://doi.org/10.1016/J.AJHG.2018.01.020

Oliver, D. M. A., & Reddy, P. H. (2019). Molecular Basis of Alzheimer's Disease: Focus on Mitochondria. *Journal of Alzheimer's Disease*, *Preprint*(Preprint), 1–22. https://doi.org/10.3233/JAD-190048

Olsson, F., Schmidt, S., Althoff, V., Munter, L. M., Jin, S., Rosqvist, S., Lendahl, U., Multhaup, G., & Lundkvist, J. (2013). Characterization of intermediate steps in amyloid beta (Aβ)

production under near-native conditions. *The Journal of Biological Chemistry*, *289*(3), 1540–1550. https://doi.org/10.1074/JBC.M113.498246

Ötzkan, S., Muller, W. E., Gibson Wood, W., & Eckert, G. P. (2021). Effects of 7,8-Dihydroxyflavone on Lipid Isoprenoid and Rho Protein Levels in Brains of Aged C57BL/6 Mice. *NeuroMolecular Medicine*, *23*(1), 130–139. https://doi.org/10.1007/s12017-020-08640-0

Paspalas, C. D., Carlyle, B. C., Leslie, S., Preuss, T. M., Crimins, J. L., Huttner, A. J., van Dyck, C. H., Rosene, D. L., Nairn, A. C., & Arnsten, A. F. T. (2018). The aged rhesus macaque manifests Braak stage III/IV Alzheimer's-like pathology. *Alzheimer's & Dementia*, *14*(5), 680–691. https://doi.org/10.1016/J.JALZ.2017.11.005

Paul, B. D., & Snyder, S. H. (2009). The unusual amino acid L-ergothioneine is a physiologic cytoprotectant. *Cell Death & Differentiation 2010 17:7*, *17*(7), 1134–1140. https://doi.org/10.1038/cdd.2009.163

Peraus, G. C., Masters, C. L., & Beyreuther, K. (1997). Late compartments of amyloid precursor protein transport in SY5Y cells are involved in beta-amyloid secretion. *The Journal of Neuroscience : The Official Journal of the Society for Neuroscience*, *17*(20), 7714–7724. https://doi.org/10.1523/JNEUROSCI.17-20-07714.1997

Perl, D. P. (2010). Neuropathology of Alzheimer's Disease. *Mount Sinai Journal of Medicine: A Journal of Translational and Personalized Medicine*, *77*(1), 32–42. https://doi.org/10.1002/MSJ.20157

Perry, S. W., Norman, J. P., Barbieri, J., Brown, E. B., & Gelbard, H. A. (2011). Mitochondrial membrane potential probes and the proton gradient: A practical usage guide. In *BioTechniques* (Vol. 50, Issue 2, pp. 98–115). Future Science Ltd London, UK . https://doi.org/10.2144/000113610

Perry, S. W., Norman, J. P., Barbieri, J., Brown, E. B., Harris, A., & Gelbard, H. A. (2011). Mitochondrial membrane potential probes and the proton gradient: a practical usage guide. *Biotechniques*, *50*(2), 98–115. https://doi.org/10.2144/000113610.Mitochondrial

Peters, I., Igbavboa, U., Schütt, T., Haidari, S., Hartig, U., Rosello, X., Böttner, S., Copanaki, E., Deller, T., Kögel, D., Wood, W. G., Müller, W. E., & Eckert, G. P. (2009). The interaction of beta-amyloid protein with cellular membranes stimulates its own production. *Biochimica et Biophysica Acta*, *1788*(5), 964–972. https://doi.org/10.1016/J.BBAMEM.2009.01.012

Phan, C. W., David, P., & Sabaratnam, V. (2017). Edible and Medicinal Mushrooms: Emerging Brain Food for the Mitigation of Neurodegenerative Diseases. *Https://Home.Liebertpub.Com/Jmf*, *20*(1), 1–10. https://doi.org/10.1089/JMF.2016.3740

Piguet, O., Double, K. L., Kril, J. J., Harasty, J., Macdonald, V., McRitchie, D. A., & Halliday, G. M. (2009). White matter loss in healthy ageing: a postmortem analysis. *Neurobiology of Aging*, *30*(8), 1288–1295. https://doi.org/10.1016/J.NEUROBIOLAGING.2007.10.015

Ploumi, C., Daskalaki, I., & Tavernarakis, N. (2017). Mitochondrial biogenesis and clearance: a balancing act. *The FEBS Journal*, *284*(2), 183–195. https://doi.org/10.1111/FEBS.13820

Polanco, J. C., Li, C., Bodea, L. G., Martinez-Marmol, R., Meunier, F. A., & Götz, J. (2018). Amyloid-β and tau complexity - towards improved biomarkers and targeted therapies. *Nature Reviews. Neurology*, *14*(1), 22–40. https://doi.org/10.1038/NRNEUROL.2017.162

Portelius, E., Bogdanovic, N., Gustavsson, M. K., Volkmann, I., Brinkmalm, G., Zetterberg, H., Winblad, B., & Blennow, K. (2010). Mass spectrometric characterization of brain amyloid beta isoform signatures in familial and sporadic Alzheimer's disease. *Acta Neuropathologica*, *120*(2), 185–193. https://doi.org/10.1007/S00401-010-0690-1

Pugazhenthi, S., Wang, M., Pham, S., Sze, C. I., & Eckman, C. B. (2011). Downregulation of CREB expression in Alzheimer's brain and in Aβ-treated rat hippocampal neurons. *Molecular Neurodegeneration*, *6*(1), 1–16. https://doi.org/10.1186/1750-1326-6-60/FIGURES/8

Quintanilla, R. A., Orellana, D. I., González-Billault, C., & Maccioni, R. B. (2004). Interleukin-6 induces Alzheimer-type phosphorylation of tau protein by deregulating the cdk5/p35 pathway. *Experimental Cell Research*, *295*(1), 245–257. https://doi.org/10.1016/J.YEXCR.2004.01.002

Rami, L., Sala-Llonch, R., Solé-Padullés, C., Fortea, J., Olives, J., Lladó, A., Pea-Gómez, C., Balasa, M., Bosch, B., Antonell, A., Sanchez-Valle, R., Bartrés-Faz, D., & Molinuevo, J. L. (2012). Distinct functional activity of the precuneus and posterior cingulate cortex during encoding in the preclinical stage of Alzheimer's disease. *Journal of Alzheimer's Disease : JAD*, *31*(3), 517–526. https://doi.org/10.3233/JAD-2012-120223

Rascher, M., Wittstein, K., Winter, B., Rupcic, Z., Wolf-Asseburg, A., Stadler, M., & Köster, R. W. (2020). Erinacine C Activates Transcription from a Consensus ETS DNA Binding

Site in Astrocytic Cells in Addition to NGF Induction. *Biomolecules*, *10*(10), 1440. https://doi.org/10.3390/biom10101440

Reddy, P. H., Yin, X. L., Manczak, M., Kumar, S., Pradeepkiran, J. A., Vijayan, M., & Reddy, A. P. (2018). Mutant APP and amyloid beta-induced defective autophagy, mitophagy, mitochondrial structural and functional changes and synaptic damage in hippocampal neurons from Alzheimer's disease. *Human Molecular Genetics*, *27*(14), 2502–2516. https://doi.org/10.1093/hmg/ddy154

Ren, Y., Geng, Y., Du, Y., Li, W., Lu, Z.-M., Xu, H.-Y., Xu, G.-H., Shi, J.-S., & Xu, Z.-H. (2018). Polysaccharide of Hericium erinaceus attenuates colitis in C57BL/6 mice via regulation of oxidative stress, inflammation-related signaling pathways and modulating the composition of the gut microbiota. *The Journal of Nutritional Biochemistry*, *57*, 67–76. https://doi.org/10.1016/J.JNUTBIO.2018.03.005

Rhein, V., Baysang, G., Rao, S., Meier, F., Bonert, A., Müller-Spahn, F., & Eckert, A. (2009). Amyloid-beta leads to impaired cellular respiration, energy production and mitochondrial electron chain complex activities in human neuroblastoma cells. *Cellular and Molecular Neurobiology*, *29*(6–7), 1063–1071. https://doi.org/10.1007/S10571-009-9398-Y

Roberson, E. D., Scearce-Levie, K., Palop, J. J., Yan, F., Cheng, I. H., Wu, T., Gerstein, H., Yu, G. Q., & Mucke, L. (2007). Reducing endogenous tau ameliorates amyloid β-induced deficits in an Alzheimer's disease mouse model. *Science*, *316*(5825), 750–754. https://doi.org/10.1126/SCIENCE.1141736/SUPPL_FILE/ROBERSON.SOM.PDF

Roda, E., Priori, E. C., Ratto, D., De Luca, F., Di Iorio, C., Angelone, P., Locatelli, C. A., Desiderio, A., Goppa, L., Savino, E., Bottone, M. G., Rossi, P., & Angeloni, C. (2021). *Neuroprotective Metabolites of Hericium erinaceus Promote Neuro-Healthy Aging*. https://doi.org/10.3390/ijms22126379

Ryan, N. S., Rossor, M. N., & Fox, N. C. (2015). Alzheimer's disease in the 100 years since Alzheimer's death. *Brain : A Journal of Neurology*, *138*(Pt 12), 3816–3821. https://doi.org/10.1093/BRAIN/AWV316

Sagan, L. (1967). On the origin of mitosing cells. *Journal of Theoretical Biology*, *14*(3), 225-IN6. https://doi.org/10.1016/0022-5193(67)90079-3

Saitsu, Y., Nishide, A., Kikushima, K., Shimizu, K., & Ohnuki, K. (2019). Improvement of cognitive functions by oral intake of Hericium erinaceus. *Biomedical Research*, *40*(4), 125–131. https://doi.org/10.2220/BIOMEDRES.40.125

Sakamuru, S., Attene-Ramos, M. S., & Xia, M. (2016). Mitochondrial membrane potential assay. *Methods in Molecular Biology*, *1473*, 17–22. https://doi.org/10.1007/978-1-4939-6346-1_2

Scheuner, D., Eckman, C., Jensen, M., Song, X., Citron, M., Suzuki, N., Bird, T. D., Hardy, J., Hutton, M., Kukull, W., Larson, E., Levy-Lahad, E., Viitanen, M., Peskind, E., Poorkaj, P., Schellenberg, G., Tanzi, R., Wasco, W., Lannfelt, L., … Younkin, S. (1996). Secreted amyloid β–protein similar to that in the senile plaques of Alzheimer's disease is increased in vivo by the presenilin 1 and 2 and APP mutations linked to familial Alzheimer's disease. *Nature Medicine 1996 2:8*, *2*(8), 864–870. https://doi.org/10.1038/nm0896-864

Schrödinger LLC. (2015). *The PyMOL Molecular Graphics System, Version~1.8*.

Selkoe, D. J. (2001). Alzheimer's disease: Genes, proteins, and therapy. *Physiological Reviews*, *81*(2), 741–766. https://doi.org/10.1152/PHYSREV.2001.81.2.741/ASSET/IMAGES/LARGE/9J0210134004.JPEG

Sharma, K. (2019). Cholinesterase inhibitors as Alzheimer's therapeutics (Review). *Molecular Medicine Reports*, *20*(2), 1479–1487. https://doi.org/10.3892/MMR.2019.10374/HTML

Sharma, P., Kumar, A., & Singh, D. (2019). Dietary Flavonoids Interaction with CREB-BDNF Pathway: An Unconventional Approach for Comprehensive Management of Epilepsy. *Current Neuropharmacology*, *17*(12), 1158–1175. https://doi.org/10.2174/1570159X17666190809165549

Shaye, D. D., & Greenwald, I. (2011). OrthoList: a compendium of C. elegans genes with human orthologs. *PloS One*, *6*(5). https://doi.org/10.1371/JOURNAL.PONE.0020085

Shen, T. (2013). *Biotechnologische Gewinnung von Cyathan-Diterpenoiden.*

Shen, T., Hof, L. M., Hausmann, H., Stadler, M., & Zorn, H. (2014). Development of an enzyme linked immunosorbent assay for detection of cyathane diterpenoids. *BMC Biotechnology*, *14*(1), 98. https://doi.org/10.1186/s12896-014-0098-4

Shen, T., Morlock, G., & Zorn, H. (2015). Production of cyathane type secondary metabolites by submerged cultures of Hericium erinaceus and evaluation of their antibacterial activity by direct bioautography. *Fungal Biology and Biotechnology*, *2*(1), 8. https://doi.org/10.1186/s40694-015-0018-y

Sheng, B., Wang, X., Su, B., Lee, H., Casadesus, G., Perry, G., & Zhu, X. (2012). Impaired mitochondrial biogenesis contributes to mitochondrial dysfunction in Alzheimer's disease. *Journal of Neurochemistry*, *120*(3), 419–429. https://doi.org/10.1111/j.1471-4159.2011.07581.x

Shi, H., Yu, Y., Lin, D., Zheng, P., Zhang, P., Hu, M., Wang, Q., Pan, W., Yang, X., Hu, T., Li, Q., Tang, R., Zhou, F., Zheng, K., & Huang, X. F. (2020). β-glucan attenuates cognitive impairment via the gut-brain axis in diet-induced obese mice. *Microbiome*, *8*(1), 1–21. https://doi.org/10.1186/S40168-020-00920-Y/FIGURES/8

Shimada, S., Shinzawa-Itoh, K., Baba, J., Aoe, S., Shimada, A., Yamashita, E., Kang, J., Tateno, M., Yoshikawa, S., & Tsukihara, T. (2017). Complex structure of cytochrome c–cytochrome c oxidase reveals a novel protein–protein interaction mode. *The EMBO Journal*, *36*(3), 291–300. https://doi.org/10.15252/EMBJ.201695021

Shimbo, M., Kawagishi, H., & Yokogoshi, H. (2005). Erinacine A increases catecholamine and nerve growth factor content in the central nervous system of rats. *Nutrition Research*, *25*(6), 617–623. https://doi.org/10.1016/J.NUTRES.2005.06.001

Song, T.-Y., Lin, H.-C., Chen, C.-L., Wu, J.-H., Liao, J.-W., & Hu, M.-L. (2014). Ergothioneine and melatonin attenuate oxidative stress and protect against learning and memory deficits in C57BL/6J mice treated with D-galactose. *Free Radical Research*, *48*(9), 1049–1060. https://doi.org/10.3109/10715762.2014.920954

Sorrentino, V., Romani, M., Mouchiroud, L., Beck, J. S., Zhang, H., D'Amico, D., Moullan, N., Potenza, F., Schmid, A. W., Rietsch, S., Counts, S. E., & Auwerx, J. (2017). Enhancing mitochondrial proteostasis reduces amyloid-β proteotoxicity. *Nature 2017 552:7684*, *552*(7684), 187–193. https://doi.org/10.1038/nature25143

Stamets, P. (2000). *Growing gourmet & medicinal mushrooms : a companion guide to The Mushroom cultivator*. 614. https://books.google.fr/books?id=M9Mz99pAdXMC

Stockburger, C., Eckert, S., Eckert, G. P., Friedland, K., & Müller, W. E. (2018). Mitochondrial Function, Dynamics, and Permeability Transition: A Complex Love Triangle as A Possible Target for the Treatment of Brain Aging and Alzheimer's Disease. *Journal of Alzheimer's Disease*, *64*(s1), S455–S467. https://doi.org/10.3233/JAD-179915

Stockburger, C., Gold, V. a M., Pallas, T., Kolesova, N., Miano, D., Leuner, K., & Müller, W. E. (2014). A Cell Model for the Initial Phase of Sporadic Alzheimer's Disease. *Journal of Alzheimer's Disease : JAD*, *42*, 395–411. https://doi.org/10.3233/JAD-140381

Stockert, J. C., Horobin, R. W., Colombo, L. L., & Blázquez-Castro, A. (2018). Tetrazolium salts and formazan products in Cell Biology: Viability assessment, fluorescence imaging, and labeling perspectives. *Acta Histochemica*, *120*(3), 159–167. https://doi.org/10.1016/J.ACTHIS.2018.02.005

Sulston, J. E., & Horvitz, H. R. (1977). Post-embryonic cell lineages of the nematode, Caenorhabditis elegans. *Developmental Biology*, *56*(1), 110–156. https://doi.org/10.1016/0012-1606(77)90158-0

Sultan, A., Nesslany, F., Violet, M., Bégard, S., Loyens, A., Talahari, S., Mansuroglu, Z., Marzin, D., Sergeant, N., Humez, S., Colin, M., Bonnefoy, E., Buée, L., & Galas, M. C. (2011). Nuclear Tau, a key player in neuronal DNA protection. *Journal of Biological Chemistry*, *286*(6), 4566–4575. https://doi.org/10.1074/JBC.M110.199976/ATTACHMENT/BDA2FD46-E925-4B19-BF36-5DF0FC6149A7/MMC1.PDF

Sun, S. K., Ho, C. Y., Yen, W. Y., & Chen, S. Der. (2021). Effect of Water and Ethanol Extracts from Hericium erinaceus Solid-State Fermented Wheat Product on the Protection and Repair of Brain Cells in Zebrafish Embryos. *Molecules 2021, Vol. 26, Page 3297*, *26*(11), 3297. https://doi.org/10.3390/MOLECULES26113297

Svitkina, T. (2018). The Actin Cytoskeleton and Actin-Based Motility. *Cold Spring Harbor Perspectives in Biology*, *10*(1), a018267. https://doi.org/10.1101/CSHPERSPECT.A018267

Swerdlow, R. H. (2020). The Mitochondrial Hypothesis: Dysfunction, Bioenergetic Defects, and the Metabolic Link to Alzheimer's Disease. *International Review of Neurobiology*, *154*, 207. https://doi.org/10.1016/BS.IRN.2020.01.008

Swerdlow, R. H., Parks, J. K., Cassarino, D. S., Maguire, D. J., Maguire, R. S., Bennett, J. P., Davis, R. E., & Parker, W. D. (1997). Cybrids in Alzheimer's disease: A cellular model of the disease? *Neurology*, *49*(4), 918–925. https://doi.org/10.1212/WNL.49.4.918

Takami, M., Nagashima, Y., Sano, Y., Ishihara, S., Morishima-Kawashima, M., Funamoto, S., & Ihara, Y. (2009). gamma-Secretase: successive tripeptide and tetrapeptide release from the transmembrane domain of beta-carboxyl terminal fragment. *The Journal of Neuroscience : The Official Journal of the Society for Neuroscience*, *29*(41), 13042–13052. https://doi.org/10.1523/JNEUROSCI.2362-09.2009

The C. elegans Sequencing Consortium. (1998). Genome sequence of the nematode C. elegans: A platform for investigating biology. *Science*, *282*(5396), 2012–2018. https://doi.org/10.1126/SCIENCE.282.5396.2012/SUPPL_FILE/C-ELEGANS.XHTML

Thies, E., & Mandelkow, E. M. (2007). Missorting of tau in neurons causes degeneration of synapses that can be rescued by the kinase MARK2/Par-1. *The Journal of Neuroscience : The Official Journal of the Society for Neuroscience*, *27*(11), 2896–2907. https://doi.org/10.1523/JNEUROSCI.4674-06.2007

Toledo, J. B., Arnold, M., Kastenmüller, G., Chang, R., Baillie, R. A., Han, X., Thambisetty, M., Tenenbaum, J. D., Suhre, K., Thompson, J. W., John-Williams, L. S., Mahmoudian-Dehkordi, S., Rotroff, D. M., Jack, J. R., Motsinger-Reif, A., Risacher, S. L., Blach, C., Lucas, J. E., Massaro, T., … Kaddurah-Daouk, R. (2017). Metabolic network failures in Alzheimer's disease: A biochemical road map. *Alzheimer's & Dementia*, *13*(9), 965–984. https://doi.org/10.1016/J.JALZ.2017.01.020

Toyama, Y., Kano, H., Mase, Y., Yokogawa, M., Osawa, M., & Shimada, I. (2017). Dynamic regulation of GDP binding to G proteins revealed by magnetic field-dependent NMR relaxation analyses. *Nature Communications*, *8*. https://doi.org/10.1038/ncomms14523

Trott, O., & Olson, A. J. (2009). AutoDock Vina: Improving the speed and accuracy of docking with a new scoring function, efficient optimization, and multithreading. *Journal of Computational Chemistry*, *31*(2), NA-NA. https://doi.org/10.1002/jcc.21334

Trovato, A., Siracusa, R., Di Paola, R., Scuto, M., Ontario, M. L., Bua, O., Di Mauro, P., Toscano, M. A., Petralia, C. C. T., Maiolino, L., Serra, A., Cuzzocrea, S., & Calabrese, V. (2016). Redox modulation of cellular stress response and lipoxin A4 expression by Hericium Erinaceus in rat brain: Relevance to Alzheimer's disease pathogenesis. *Immunity and Ageing*, *13*(1). https://doi.org/10.1186/s12979-016-0078-8

Tsai-Teng, T., Chin-Chu, C., Li-Ya, L., Wan-Ping, C., Chung-Kuang, L., Chien-Chang, S., Chi-Ying, H. F., Chien-Chih, C., & Shiao, Y. J. (2016). Erinacine A-enriched Hericium erinaceus mycelium ameliorates Alzheimer's disease-related pathologies in APPswe/PS1dE9 transgenic mice. *Journal of Biomedical Science*. https://doi.org/10.1186/s12929-016-0266-z

Tuszynski, M. H., Yang, J. H., Barba, D., Hoi-Sang, U., Bakay, R. A. E., Pay, M. M., Masliah, E., Conner, J. M., Kobalka, P., Roy, S., & Nagahara, A. H. (2015). Nerve Growth Factor Gene Therapy: Activation of Neuronal Responses in Alzheimer Disease. *JAMA Neurology*, *72*(10), 1139–1147. https://doi.org/10.1001/JAMANEUROL.2015.1807

Tzeng, T.-T., Chen, C.-C., Chen, C.-C., Tsay, H.-J., Lee, L.-Y., Chen, W.-P., Shen, C.-C., Shiao, Y.-J., Tzeng, T.-T., Chen, C.-C., Chen, C.-C., Tsay, H.-J., Lee, L.-Y., Chen, W.-P., Shen, C.-C., & Shiao, Y.-J. (2018). The Cyanthin Diterpenoid and Sesterterpene Constituents of Hericium erinaceus Mycelium Ameliorate Alzheimer's Disease-Related Pathologies in APP/PS1 Transgenic Mice. *International Journal of Molecular Sciences*, *19*(2), 598. https://doi.org/10.3390/ijms19020598

Uittenbogaard, M., & Chiaramello, A. (2014). Mitochondrial Biogenesis: A Therapeutic Target for Neurodevelopmental Disorders and Neurodegenerative Diseases. *Current*

Pharmaceutical Design, *20*(35), 5574–5593. https://doi.org/10.2174/1381612820666140305224906

Valu, M. V., Soare, L. C., Ducu, C., Moga, S., Negrea, D., Vamanu, E., Balseanu, T. A., Carradori, S., Hritcu, L., & Boiangiu, R. S. (2021). Hericium erinaceus (Bull.) Pers. Ethanolic Extract with Antioxidant Properties on Scopolamine-Induced Memory Deficits in a Zebrafish Model of Cognitive Impairment. *Journal of Fungi (Basel, Switzerland)*, *7*(6). https://doi.org/10.3390/JOF7060477

van Dyck, C., Swanson, C., Aisen, P., Bateman, R., Chen, C., Gee, M., Kanekiyo, M., Li, D., Reyderman, L., Cohen, S., Froelich, L., Katayama, S., Sabbagh, M., Vellas, B., Watson, D., Dhadda, S., Irizarry, M., Kramer, L., & Iwatsubo, T. (2023). Lecanemab in Early Alzheimer's Disease. *The New England Journal of Medicine*, *388*(1), 142–143. https://doi.org/10.1056/NEJMOA2212948

Venturella, G., Ferraro, V., Cirlincione, F., & Gargano, M. L. (2021). Medicinal Mushrooms: Bioactive Compounds, Use, and Clinical Trials. *International Journal of Molecular Sciences*, *22*(2), 1–31. https://doi.org/10.3390/IJMS22020634

Wallace, A. C., Laskowski, R. A., & Thornton, J. M. (1995). Ligplot: A program to generate schematic diagrams of protein-ligand interactions. *Protein Engineering, Design and Selection*, *8*(2), 127–134. https://doi.org/10.1093/protein/8.2.127

Wang, D., Zhang, Y., Yang, S., Zhao, D., & Wang, M. (2019). A polysaccharide from cultured mycelium of Hericium erinaceus relieves ulcerative colitis by counteracting oxidative stress and improving mitochondrial function. *International Journal of Biological Macromolecules*, *125*, 572–579. https://doi.org/10.1016/J.IJBIOMAC.2018.12.092

Wang, H., Xu, J., Lazarovici, P., Quirion, R., & Zheng, W. (2018). cAMP Response Element-Binding Protein (CREB): A Possible Signaling Molecule Link in the Pathophysiology of Schizophrenia. *Pathophysiology of Schizophrenia. Front. Mol. Neurosci*, *11*, 255. https://doi.org/10.3389/fnmol.2018.00255

Wang, J. L., Tong, C. W., Chang, W. T., & Huang, A. M. (2013). Novel genes FAM134C, C3orf10 and ENOX1 are regulated by NRF-1 and differentially regulate neurite outgrowth in neuroblastoma cells and hippocampal neurons. *Gene*, *529*(1), 7–15. https://doi.org/10.1016/J.GENE.2013.08.006

Wang, L.-Y., Huang, C.-S., Chen, Y.-H., Chen, C.-C., Chen, C.-C., & Chuang, C.-H. (2019). Anti-Inflammatory Effect of Erinacine C on NO Production Through Down-Regulation of NF-κB and Activation of Nrf2-Mediated HO-1 in BV2 Microglial Cells Treated with LPS. *Molecules*, *24*(18), 3317. https://doi.org/10.3390/molecules24183317

Wang, S. H., Liao, X. M., Liu, D., Hu, J., Yin, Y. Y., Wang, J. Z., & Zhu, L. Q. (2012). NGF promotes long-term memory formation by activating poly(ADP-ribose)polymerase-1. *Neuropharmacology*, *63*(6), 1085–1092. https://doi.org/10.1016/J.NEUROPHARM.2012.06.050

Wang, X., Wang, W., Li, L., Perry, G., Lee, H. gon, & Zhu, X. (2014). Oxidative stress and mitochondrial dysfunction in Alzheimer's disease. In *Biochimica et Biophysica Acta - Molecular Basis of Disease* (Vol. 1842, Issue 8, pp. 1240–1247). Elsevier. https://doi.org/10.1016/j.bbadis.2013.10.015

Wang, Z., Gerstein, M., & Snyder, M. (2009). RNA-Seq: a revolutionary tool for transcriptomics. *Nature Reviews Genetics 2008 10:1*, *10*(1), 57–63. https://doi.org/10.1038/nrg2484

Wang, Z. X., Tan, L., Liu, J., & Yu, J. T. (2016). The Essential Role of Soluble Aβ Oligomers in Alzheimer's Disease. *Molecular Neurobiology*, *53*(3), 1905–1924. https://doi.org/10.1007/S12035-015-9143-0

Watanabe, R., & Noji, H. (2013). Chemomechanical coupling mechanism of F1-ATPase: Catalysis and torque generation. In *FEBS Letters* (Vol. 587, Issue 8, pp. 1030–1035). FEBS Lett. https://doi.org/10.1016/j.febslet.2013.01.063

Watson, J. T., & Sparkman, O. D. (2008). Introduction to Mass Spectrometry: Instrumentation, Applications and Strategies for Data Interpretation: Fourth Edition. In *Introduction to Mass Spectrometry: Instrumentation, Applications and Strategies for Data Interpretation: Fourth Edition*. John Wiley and Sons. https://doi.org/10.1002/9780470516898

Weingarten, M. D., Lockwood, A. H., Hwo, S. Y., & Kirschner, M. W. (1975). A protein factor essential for microtubule assembly. *Proceedings of the National Academy of Sciences of the United States of America*, *72*(5), 1858–1862. https://doi.org/10.1073/PNAS.72.5.1858

Wiemerslage, L., & Lee, D. (2016). Quantification of mitochondrial morphology in neurites of dopaminergic neurons using multiple parameters. *Journal of Neuroscience Methods*, *262*, 56–65. https://doi.org/10.1016/J.JNEUMETH.2016.01.008

Williams, B. S., & Buvanendran, A. (2021). Memantine. *The Essence of Analgesia and Analgesics*, 319–321. https://doi.org/10.1017/CBO9780511841378.077

Wilson, C., Muñoz-Palma, E., & González-Billault, C. (2018). From birth to death: A role for reactive oxygen species in neuronal development. *Seminars in Cell & Developmental Biology*, *80*, 43–49. https://doi.org/10.1016/J.SEMCDB.2017.09.012

Wolters, N., Schembecker, G., & Merz, J. (2015). Erinacine C: A novel approach to produce the secondary metabolite by submerged cultivation of Hericium erinaceus. *Fungal Biology*, *119*(12), 1334–1344. https://doi.org/10.1016/J.FUNBIO.2015.10.005

Wu, R.-C., Qin, J., Hashimoto, Y., Wong, J., Xu, J., Tsai, S. Y., Tsai, M.-J., & O'Malley, B. W. (2002). Regulation of SRC-3 (pCIP/ACTR/AIB-1/RAC-3/TRAM-1) Coactivator Activity by IκB Kinase. *Molecular and Cellular Biology*, *22*(10), 3549–3561. https://doi.org/10.1128/mcb.22.10.3549-3561.2002

Yang, P. P., Chueh, S. H., Shie, H. L., Chen, C. C., Lee, L. Y., Chen, W. P., Chen, Y. W., Shiu, L. Y., & Liu, P. S. (2020). Effects of Hericium erinaceus Mycelium Extracts on the Functional Activity of Purinoceptors and Neuropathic Pain in Mice with L5 Spinal Nerve Ligation. *Evidence-Based Complementary and Alternative Medicine*, *2020*. https://doi.org/10.1155/2020/2890194

Yang, Y. L., Zhang, S., Ma, K., Xu, Y., Tao, Q., Chen, Y., Chen, J., Guo, S., Ren, J., Wang, W., Tao, Y., Yin, W. B., & Liu, H. (2017). Discovery and Characterization of a New Family of Diterpene Cyclases in Bacteria and Fungi. *Angewandte Chemie - International Edition*, *56*(17), 4749–4752. https://doi.org/10.1002/anie.201700565

Yanshree, Yu, W. S., Fung, M. L., Lee, C. W., Lim, L. W., & Wong, K. H. (2022). The Monkey Head Mushroom and Memory Enhancement in Alzheimer’s Disease. *Cells 2022, Vol. 11, Page 2284*, *11*(15), 2284. https://doi.org/10.3390/CELLS11152284

Yi, Z., Shao-Long, Y., Wang, A.-H., Zhi-Chun, S., Ya-Fen, Z., Ye-Ting, X., & Yu-Ling, H. (2015). *Protective Effect of Ethanol Extracts of Hericium erinaceus on Alloxan-Induced Diabetic Neuropathic Pain in Rats*. https://doi.org/10.1155/2015/595480

Ying, J. X. M. (1987). *Icones of medicinal fungi from China*. China. Science.

Yoshii, S. R., & Mizushima, N. (2015). Autophagy machinery in the context of mammalian mitophagy. *Biochimica et Biophysica Acta (BBA) - Molecular Cell Research*, *1853*(10), 2797–2801. https://doi.org/10.1016/J.BBAMCR.2015.01.013

Young, J. C., Hoogenraad, N. J., & Hartl, F. U. (2003). Molecular chaperones Hsp90 and Hsp70 deliver preproteins to the mitochondrial import receptor Tom70. *Cell*, *112*(1), 41–50. https://doi.org/10.1016/S0092-8674(02)01250-3

Yutaro, O., & Norimichi, N. (2002). The Signaling Pathway of Neurotrophic Factor Biosynthesis. *Drug News & Perspectives*, *15*(5), 290–298. https://doi.org/10.1358/DNP.2002.15.5.840042

Zhang, C.-C., Cao, C.-Y., Kubo, M., Harada, K., Yan, X.-T., Fukuyama, Y., & Gao, J.-M. (2017). Chemical Constituents from Hericium erinaceus Promote Neuronal Survival and Potentiate Neurite Outgrowth via the TrkA/Erk1/2 Pathway. *International Journal of Molecular Sciences*, *18*(8). https://doi.org/10.3390/ijms18081659

Zhang, Q., Zhao, W., Hou, Y., Song, X., Yu, H., Tan, J., Zhou, Y., & Zhang, H.-T. (2023). β-Glucan attenuates cognitive impairment of APP/PS1 mice via regulating intestinal flora and its metabolites. *CNS Neuroscience & Therapeutics*. https://doi.org/10.1111/CNS.14132

Zhang, Y. W., Thompson, R., Zhang, H., & Xu, H. (2011). APP processing in Alzheimer's disease. *Molecular Brain*, *4*(1), 1–13. https://doi.org/10.1186/1756-6606-4-3/FIGURES/1

Zhang, Z., Lv, G., Pan, H., Pandey, A., He, W., & Fan, L. (2012). Antioxidant and hepatoprotective potential of endo-polysaccharides from Hericium erinaceus grown on tofu whey. *International Journal of Biological Macromolecules*, *51*(5), 1140–1146. https://doi.org/10.1016/J.IJBIOMAC.2012.09.002

Zhao, J., Liu, X., Xia, W., Zhang, Y., & Wang, C. (2020). Targeting Amyloidogenic Processing of APP in Alzheimer's Disease. *Frontiers in Molecular Neuroscience*, *13*, 137. https://doi.org/10.3389/FNMOL.2020.00137/BIBTEX

Zhao, M., Wang, Y., Li, L., Liu, S., Wang, C., Yuan, Y., Yang, G., Chen, Y., Cheng, J., Lu, Y., & Liu, J. (2021). Mitochondrial ROS promote mitochondrial dysfunction and inflammation in ischemic acute kidney injury by disrupting TFAM-mediated mtDNA maintenance. *Theranostics*, *11*(4), 1845–1863. https://doi.org/10.7150/thno.50905

Zhao, Y., Sivaji, S., Chiang, M. C., Ali, H., Zukowski, M., Ali, S., Kennedy, B., Sklyar, A., Cheng, A., Guo, Z., Reed, A. K., Kodali, R., Borowski, J., Frost, G., Beukema, P., & Wills, Z. P. (2017). Amyloid Beta Peptides Block New Synapse Assembly by Nogo Receptor-Mediated Inhibition of T-Type Calcium Channels. *Neuron*, *96*(2), 355-372.e6. https://doi.org/10.1016/J.NEURON.2017.09.041

Zhou, L. J., Mo, Y. B., Bu, X., Wang, J. J., Bai, J., Zhang, J. W., Cheng, A. Bin, Ma, J. H., Wang, Y. W., & Xie, Y. X. (2018). Erinacine Facilitates the Opening of the Mitochondrial Permeability Transition Pore Through the Inhibition of the PI3K/ Akt/GSK-3β Signaling Pathway in Human Hepatocellular Carcinoma. *Cellular Physiology and Biochemistry*, *50*(3), 851–867. https://doi.org/10.1159/000494472

7 Acknowledgments

On my PhD-journey I had many people who supporting me in the small and big steps of my thesis. I am standing on the shoulders of giants. I want to thank you by heart for that!

First of all, I want to thank my supervisors Prof. Dr. Gunter Eckert and Prof. Dr. Holger Zorn for developing such a marvellous PhD topic. I grew through writing this thesis to love fungi and I am super thankful for channelling my curiosity on the topic of *Hericium erinaceus*. I am looking forward to seeing the world of fungi growing in all aspects of life. Fungi are future. Furthermore, I want to thank the Horst Görtz Foundation for supporting the topic financially.

A special thanks goes to my "scientific mum's" and friends Dr. Alejandra Omarini and Prof Dr. Tetiana Zhuk, who adopted me. You were always so patient with me, you acted as a role model when I needed it the most, you taught me patience, hope and perseverance in times of deepest stress and biggest fear. From you I learned about the noblest form of science and where to find it – at the intersection of science and art. You watered me emotionally and intellectually; through you I grew a as a person and scientist.

Wendell, Parviz, Philipp, Daniel, Fabian, Hazal, Eric, Philipp, Karl and Daniel thank you very much for leisure time activities during break times and the fascinating discussions about life, philosophy, science, coffee, tea, food, books, politics, economics and all other stupidities. And a special thank goes to Wendell, who had always lend me an ear and supported me in so many ways.

My dear former colleague Carsten Apache Kampf-Helikopter Stufe 2 Esselun, Paladin Stufe 32 what can I say more. You are the best! Touchdown!

Thank you Dr. Victor Hernandez-Olmos for helping me performing my first preparative HPLC run to isolate erinacine C. It felt like heaven having isolated erinacine C in my hands for the first time. Dr. Chase Beathard, Dr. Regan Nelly and Renee Davis thank you for your time and discussing so many aspects of *Hericium erinaceus* and erinacine C with me. A special thanks

goes to Chase who helped me tinkering with the RNAseq analysis. You opened uncountable doors of my work.

A special thanks goes to the four master students I had the honour of supervising: Katharina Apple, Lea Schüssler, Leonie Wach and Nathalie Grimm. Your contribution and engagement helped me substantially in this work. Otherwise, it would have not been possible for me to present that body of research.

My dear parents thank you for supporting me so many years of my life emotionally and financially. Through your support I achieved more than I ever dreamed of. You know, a thousand and one words say more than a thousand words. The world is open now.

My dear friend Philipp, I will miss you. Your friendship was very special to me. Although our earthly time together was short, it was incredibly meaningful. I wish I had understood your pain better.

“Have no fear of perfection - you'll never reach it.

– Salvador Dalí

8 Supplementary Information

8.1 Annotated KEGG PATHWAYS

The following figures show annotated KEGG PATHWAYS of SH-SY5Y-MOCK cells after treatment with 1 µM erinacine C. This is to support the hormone-like effect hypothesis of erinacine C visually.

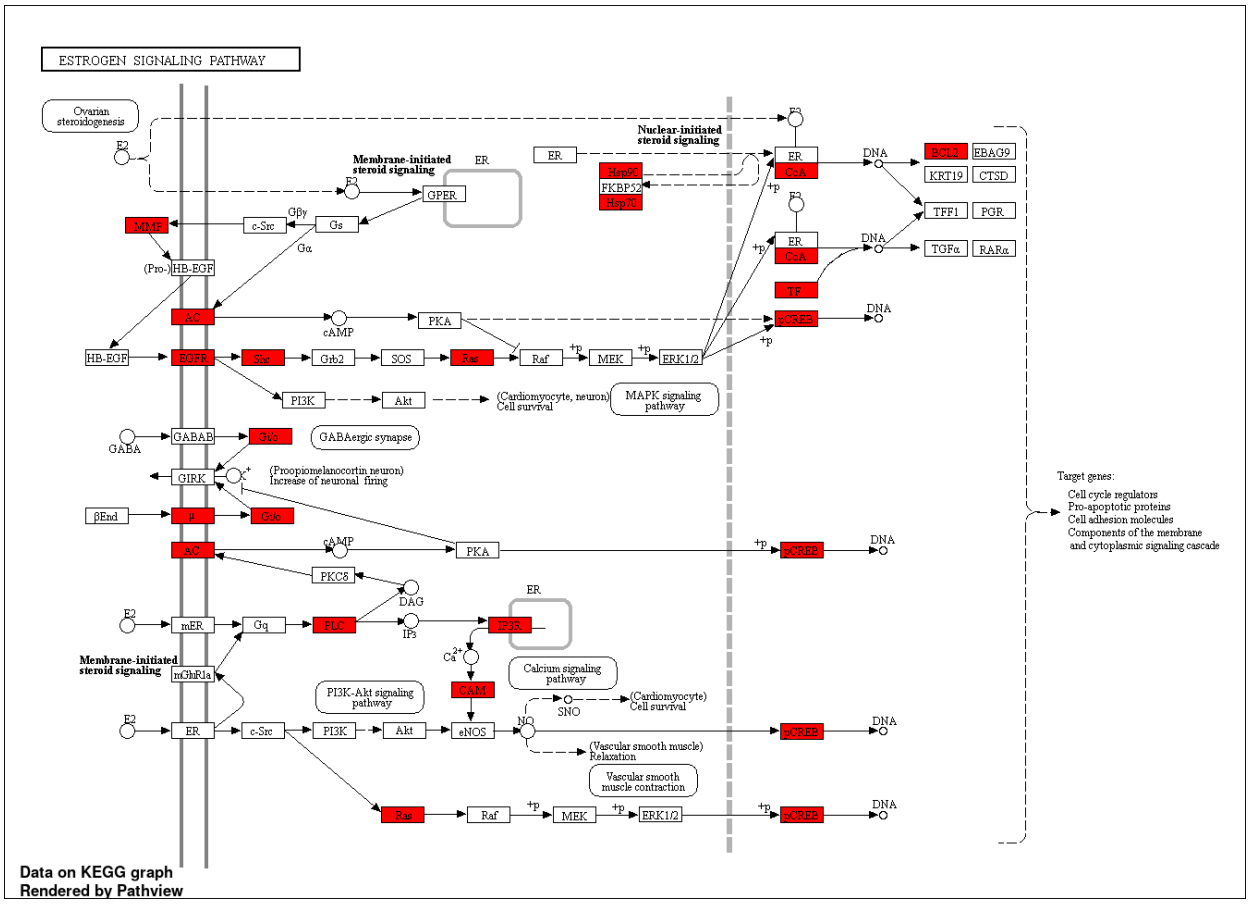

Figure 8-1 Annotated ESTROGEN SIGNALLING PATHWAY in KEGG in SH-SY5Y-MOCK cells after treatment with 1 µM erinacine C. The regulated genes are highlighted in red.

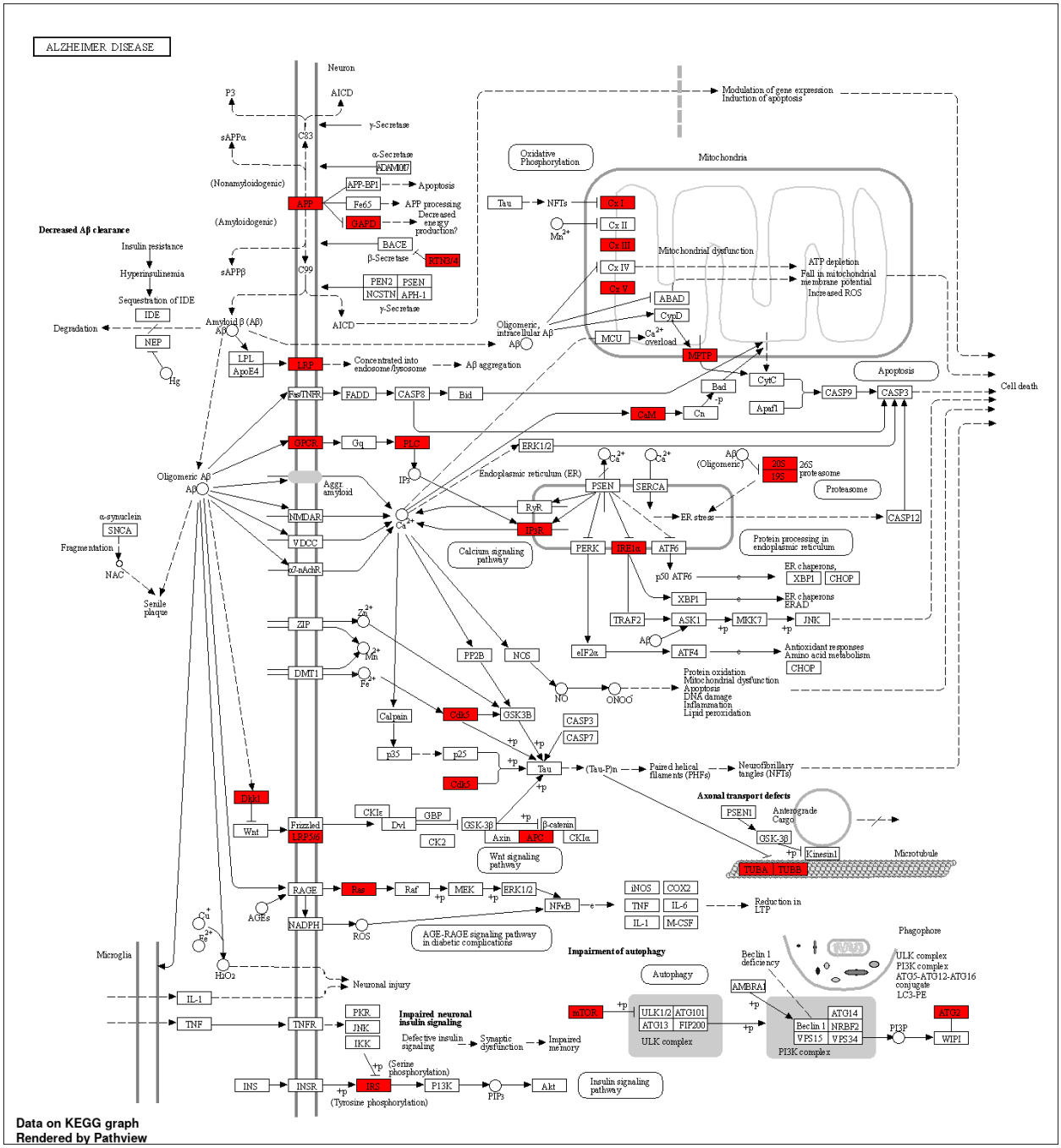

Figure 8-2 Annotated ALZHEIMER'S DISEASE PATHWAY in KEGG in SH-SY5Y-MOCK cells after treatment with 1 μM erinacine C. The regulated genes are highlighted in red.

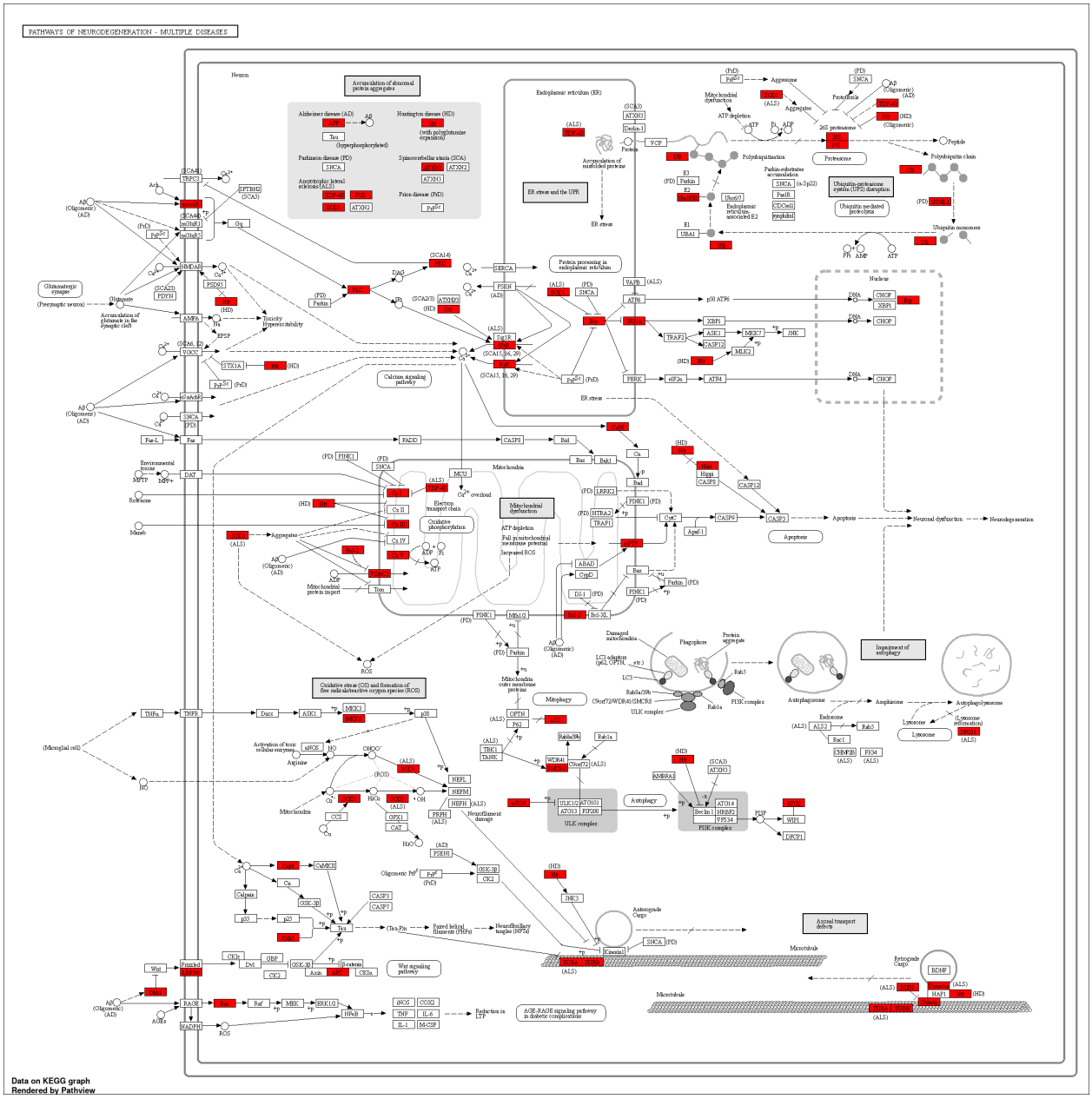

Figure 8-3 Annotated PATHWAYS OF NEURODEGNERATIVE DISEASES in KEGG in SH-SY5Y-MOCK cells after treatment with 1 μM erinacine C. The regulated genes are highlighted in red.

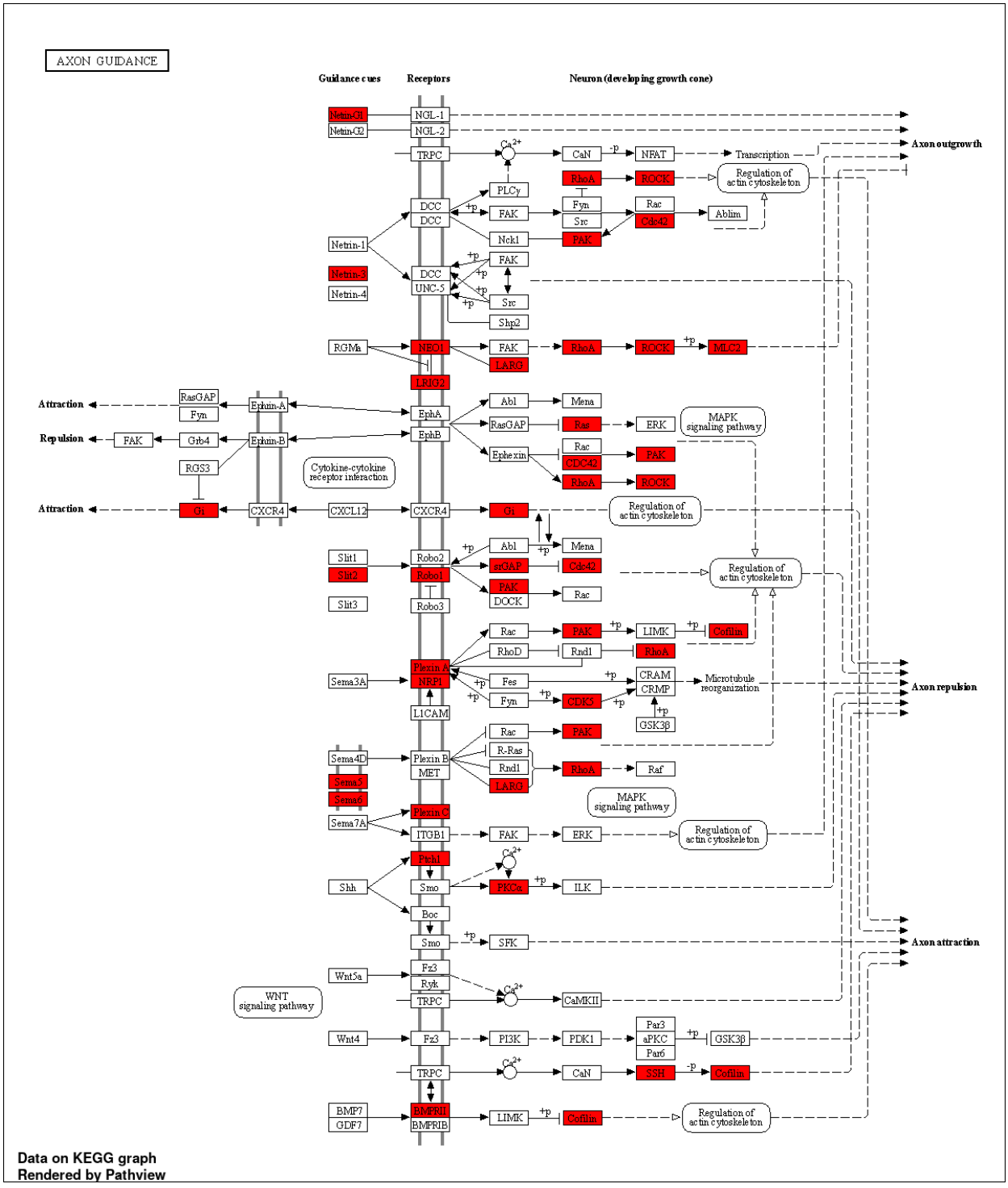

Figure 8-4 Annotated AXON GUIDACE PATHWAYS in KEGG in SH-SY5Y-MOCK cells after treatment with 1 μM erinacine C. The regulated genes are highlighted in red.

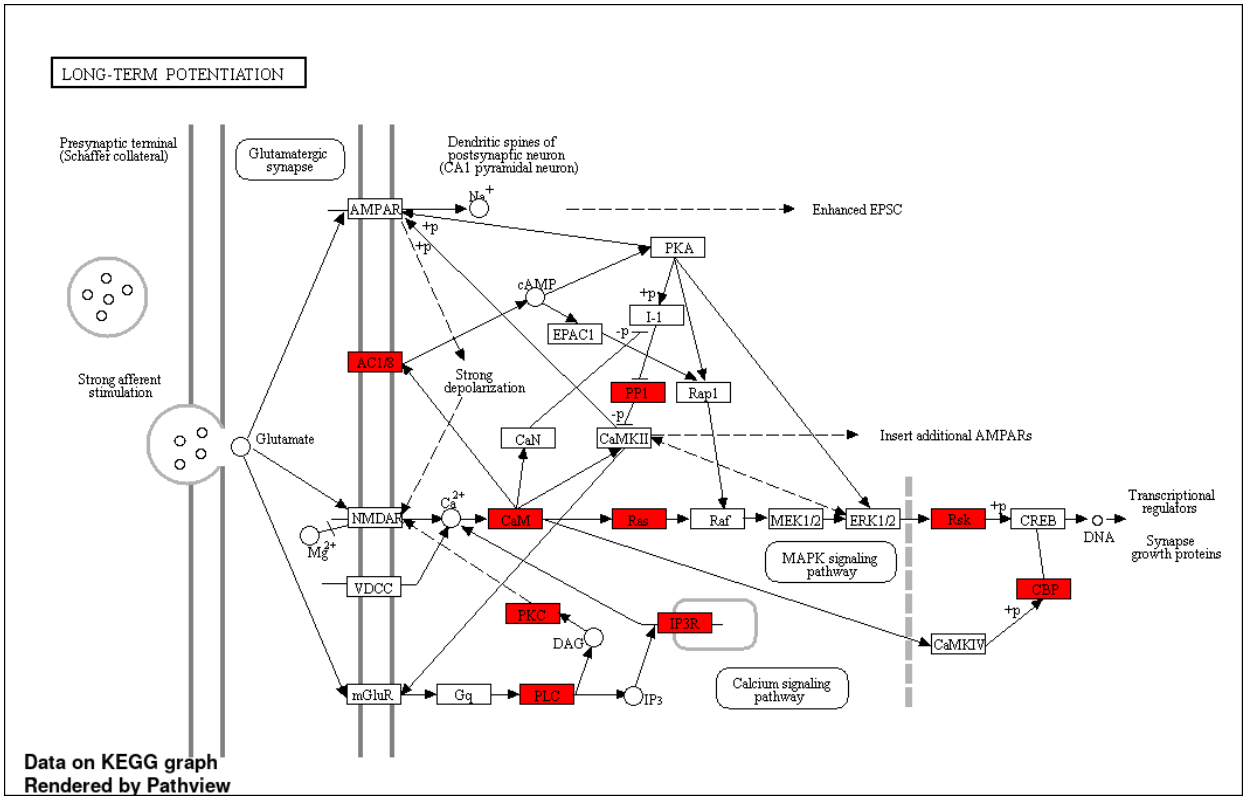

Figure 8-5 Annotated LONG-TERM POTENTATION PATHWAYS in KEGG in SH-SY5Y-MOCK cells after treatment with 1 μM erinacine C. The regulated genes are highlighted in red.

8.2 HPLC Chromatogram of ethanolic *Hericium erinaceus* extract

The chromatogram presented displays the ethanolic extract of *Hericium erinaceus* used in this study. The analysis was conducted using the same parameters for erinacine C, as described in chapter 5.2.6. Regrettably, erinacine C was not detected in the HPLC-DAD analysis.

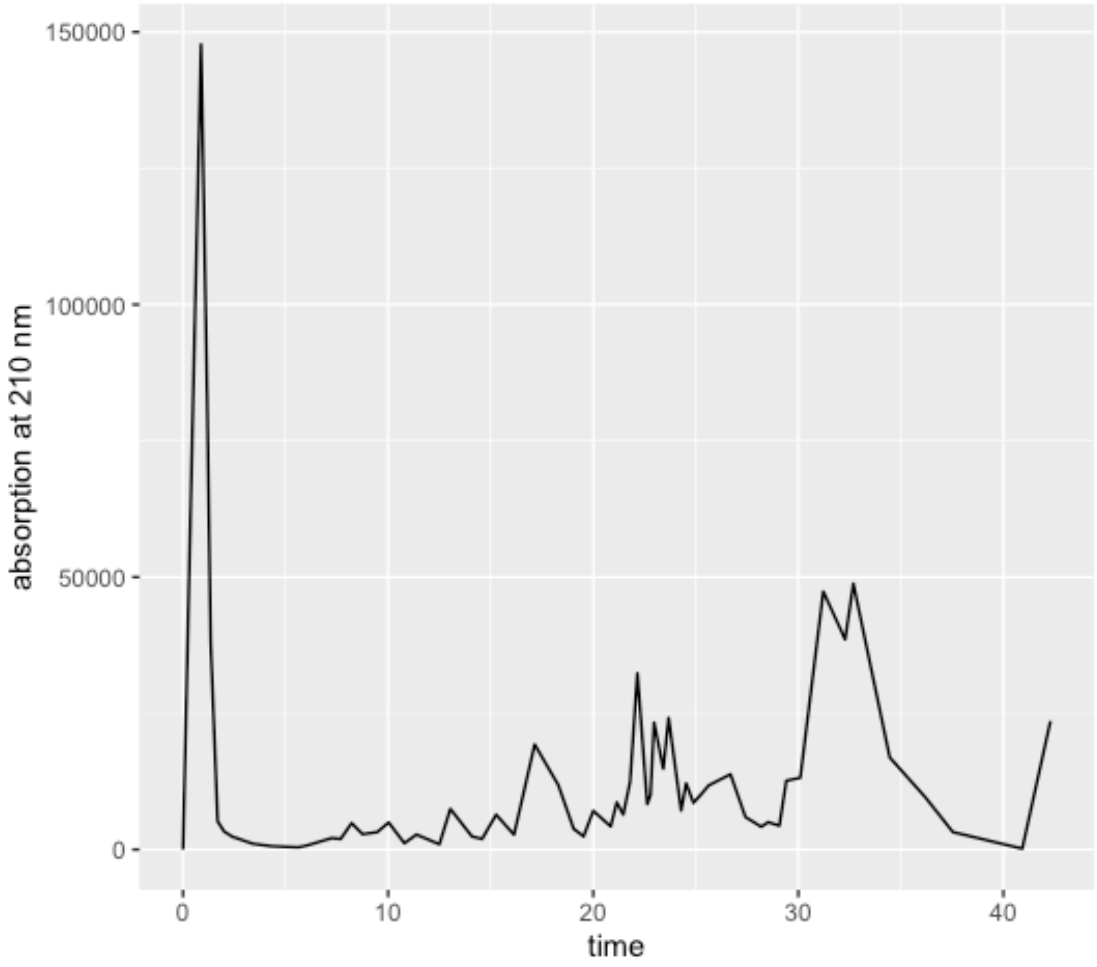

Figure 8-6 Showing the ethanolic Hericium erinacues extract on an analytical HPLC-DAD.
MERCK HPLC (guard column: CC 8/3 Nucleosil® 100-5 C18; column: CC 125/3 Nucleosil® 100-5 C18) at 210 nm with the solvents acetonitrile and water and elution time of 21 minutes (left) after extraction without lyophilization, (right) after extraction with lyophilization. The extraction was carried out using 70% ethanol. Detailed parameters are found in chapter 5.2.6

8.3 Collaborative Efforts with Master's Students in Conducting Experiments

The experiments in this thesis were made possible by the collaboration of four master's students who each contributed their time, energy, patience, and curiosity to the project. The following list provides the names of the students and the specific experiments they were involved in.

Table 8-1 Overview of Experiments Conducted with the Assistance of Master's Students. Highlighting High-Level Titles only.

Name	Chapters and Experiments
Katharina Appel (01/20 – 09/20)	Assisted in establishing the cultivation of HER and HPLC analysis.
Lea Schüssler (11/20 – 02/22)	2.2 Effects of erinacine C on metabolic activity in SH-SY5Y cells 2.3 Effects of erinacine C on mitochondrial membrane potential in SH-SY5Y cells 2.4 Effects of erinacine C on ATP levels in SH-SY5Y cells 2.7 Effects of erinacine C on mRNA Expression in SH-SY5Y cells 2.8 Effects of erinacine C on neurite growth in SH-SY5Y cells
Nathalie Grimm (04/21 – 12/22)	2.12 Effects of ethanolic mycelium extract in *Caenorhabditis elegans* 2.13 Comparative Analysis of ATP levels in CL2122 and GMC101 2.14 Comparative Analysis of ROS levels in CL2122 and GMC101 2.15 Effects of ethanolic mycelium extract on ROS levels in GMC101

Leonie Wach (04/21 – 09/22)	2.5 Effects of erinacine C on mitochondrial respiration 2.6 Oxidative stress in SH-SY5Y cells 2.9 Effects of erinacine C on Aβ1-40 levels 2.16 Effects of ethanolic mycelium extract on viability in SH-SY5Y cells 2.17 Effects of ethanolic mycelium extract on ATP levels in SH-SY5Y cells

Published work

Publication list

Ghezellou P, Dillenberger M, Kazemi SM, Jestrzemski D, **Hellmann B**, Spengler B. Comparative Venom Proteomics of Iranian, *Macrovipera lebetina cernovi*, and Cypriot, *Macrovipera lebetina lebetina*, Giant Vipers. Toxins (Basel). 2022 Oct 20;14(10):716. doi: 10.3390/toxins14100716. PMID: 36287984; PMCID: PMC9609362.

Drobny A, Meloh H, Wächtershäuser E, **Hellmann B**, Mueller AS, van der Klis JD, Fitzenberger E, Wenzel U. Betaine-rich sugar beet molasses protects from homocysteine-induced reduction of survival in Caenorhabditis elegans. Eur J Nutr. 2020 Mar;59(2):779-786. doi: 10.1007/s00394-019-01944-3. Epub 2019 Mar 12. PMID: 30863895.

Chen, Y., Huang, C., **Hellmann, B.**, Jin, Z., Xu, X., & Xiao, G. (2020). A new HPTLC platformed luminescent biosensor system for facile screening of captan residue in fruits. *Food chemistry*, *309*, 125691.

Chen, Y., Huang, C., **Hellmann, B.**, & Xu, X. (2020). HPTLC-densitometry determination of riboflavin fortified in rice noodle: Confirmed by SERS-fingerprint. *Food Analytical Methods*, *13*(3), 718-725.

Wang, P., Chen, Y., Xu, X., **Hellmann, B.**, Huang, C., Bai, Y., & Jin, Z. (2019). HPTLC screening of folic acid in food: In situ derivatization with ozone-induced fluorescence. *Food Analytical Methods*, *12*(2), 431-439.

Wang, L., Chen, Y., Ye, Z., **Hellmann, B.**, Xu, X., Jin, Z., Jin, Y. (2018). Screening of phenolic antioxidants in edible oils by HPTLC-DPPH assay and MS confirmation. *Food Analytical Methods*, *11*(11), 3170-3178.

Declaration of Authorship

I declare: I have prepared the submitted dissertation independently and without unauthorized outside help and only with the help that I have indicated in the dissertation. All text passages taken verbatim or in spirit from published writings and all information based on oral information are marked as such. In the research conducted by me and mentioned in the dissertation, I have complied with the principles of good scientific practice as laid down in the "Statutes of the Justus Liebig University of Giessen for Ensuring Good Scientific Practice".

_____ _____

city, date signature